THÈSE

En vue de l'obtention du

DOCTORAT DE L'UNIVERSITÉ DE TOULOUSE

Délivré par :

Institut National Polytechnique de Toulouse (INP Toulouse)

Discipline ou spécialité :

ENERGETIQUE ET TRANSFERTS

Présentée et soutenue par :

Younes CHHITI

Le: lundi 5 septembre 2011

Titre:

Non catalytic steam gasification of wood bio-oil

JURY

Pr. W.P.M. van Swaaij, Université de Twente, Pays Bas - Rapporteur
Pr. J. Arauzo Pérez, Université de Zaragoza, Espagne - Rapporteur
Dr. F. Marias, ENSGTI, Pau, France - Membre
Dr. F. Broust, CIRAD, Montpellier, France - Membre
Dr. J-M. Commandré, ENSTIMAC, Albi, France - Membre
Dr. C. Dupont, CEA, Grenoble, France – Invité
Pr. Sylvain SALVADOR, EMAC, Albi, France – Directeur de thèse

---

Ecole doctorale :

Mécanique, Energétique, Génie civil et Procédés (MEGeP)

Unité de recherche :

Ecole des Mines d'Albi-Carmaux

Directeur de Thèse :

Pr. Sylvain SALVADOR

Non catalytic steam gasification of wood bio-oil

Vapogazéification non catalytique des huiles de pyrolyse de bois

Résumé: Vapogazéification non catalytique des huiles de pyrolyse de bois

La production d'énergie à partir de biomasse ligno-cellulosique via la technologie de gazéification est une option intéressante dans le contexte énergétique actuel. La combinaison d'une pyrolyse rapide décentralisée de la biomasse pour produire les bio-huiles, suivie par le transport et le vaporeformage dans des bio-raffineries, est apparue comme l'une des méthodes économiquement les plus viables pour la production de gaz de synthèse (H_2+CO). L'objectif de ce travail est de combler le manque de connaissances concernant les processus de transformation physicochimique de l'huile de pyrolyse en gaz de synthèse utilisant la gazéification non catalytique dans des réacteurs à flux entrainé. Il s'agit d'un processus complexe, mettant en œuvre la vaporisation, les réactions de craquage thermique avec formation de gaz, de tars et de deux résidus solides : le char et les suies, qui sont des produits indésirables. Ceci est suivi par le reformage des gaz et des tars, ainsi que la conversion du char et des suies. Pour mieux comprendre le processus, la première étape de la gazéification (la pyrolyse), et par la suite l'ensemble du processus (pyrolyse + gazéification) ont été étudiés. L'étude de la pyrolyse est focalisée sur l'influence de la vitesse de chauffe, de la température ainsi que de la teneur en cendres dans la bio-huile, sur les rendements en char, tars et gaz. A très grande vitesse de chauffe le rendement en char est inferieur à 1%. Les cendres semblent favoriser les réactions de polymérisation et provoquent la diminution du rendement en gaz. Concernant la gazéification, l'effet de la température sur le rendement et la composition du gaz de synthèse a été étudié. Une augmentation de la température de réaction implique une augmentation du rendement en hydrogène et une conversion très élevée du carbone solide. Un calcul d'équilibre thermodynamique a montré que l'équilibre a été atteint à 1400°C. Finalement les mécanismes de formation et d'oxydation des suies ont été étudiés expérimentalement sous différentes atmosphères : inerte (pyrolyse), riche en vapeur d'eau (gazéification) et en présence d'oxygène (oxydation partielle). Un modèle semi empirique est proposé et validé. Il est fondé sur la chimie détaillée pour décrire les réactions en phase gaz, une seule réaction basée sur la concentration de C_2H_2 pour décrire la formation des suies et principalement une réaction hétérogène pour décrire l'oxydation des suies.

Mots clés : bio-huile, gaz de synthèse, gazéification non catalytique, pyrolyse, oxydation partielle, suies.

Abstract: Non catalytic steam gasification of wood bio-oil

Energy production from ligno-cellulosic biomass via gasification technology appears as an attractive option in the current energy context. The combination of decentralized fast pyrolysis of biomass to produce bio-oil, followed by transportation and gasification of bio-oil in bio-refinery has appeared as one of the most economically viable methods for syngas (H_2+CO) production. The objective of this work is to bridge the lack of knowledge concerning the physicochemical transformation of bio-oil into syngas using non catalytic steam gasification in entrained flow reactors. This complex process involves vaporization, thermal cracking reactions with formation of gas, tars and two solid residues - char and soot - that are considered as undesirable products. This is followed by steam reforming of gas and tars, together with char and soot conversion. To better understand the process, the first step of gasification (pyrolysis) and thereafter the whole process (pyrolysis + gasification) were studied. The pyrolysis study focused on the influence of the heating rate, the final pyrolysis temperature and the ash content of bio-oil on char, tars and gas yields. At the higher heating rate char yield is smaller than 1%. In addition, ash seems to promote polymerization reactions and causes a decrease of gas yield. Concerning gasification, the effect of temperature on syngas yield and composition was studied. An increase in the reaction temperature implies higher hydrogen yield and higher solid carbon conversion. A thermodynamic equilibrium calculation showed that equilibrium was reached at 1400°C. Finally, the soot formation and oxidation mechanisms were investigated through experiments in three different atmospheres: inert (pyrolysis), rich in steam (gasification) and in the presence of oxygen (partial oxidation). A semi-empirical model was proposed and validated. It is based on detailed chemistry to describe gas phase reactions, a single reaction using C_2H_2 concentration to describe soot formation and one main heterogeneous reaction to describe soot oxidation.

Key words: bio-oil, syngas, non catalytic gasification, pyrolysis, partial oxidation, soot.

ACKNOWLEDGEMENTS

In this moment I am thinking back to the people who accompanied me and to the episodes which occurred during these years: if I had to list all of them, I should probably write another book! However, someone once said that one book per time is enough, when it is not too much, then I will just greet and thank the people who were important during the PhD period and who helped me reach this further goal, starting from the university teaching staff who bore me again after my bachelor and master degrees.

First and foremost, I would like to express my sincere gratitude and appreciation to my supervisor ***Pr. Sylvain Salvador****, for its knowledge and guidance to my research. Over the past three years,* ***Pr. Sylvain Salvador*** *has been providing me strong continuous support both scientifically and personally. This thesis would have been impossible without its great efforts, encouragement, trust, and patience.*

I also greatly appreciate ***Pr. W.P.M. van Swaaij*** *and* ***Pr. Jesús Arauzo Pérez*** *for reviewing this thesis, and for their insightful and valuable suggestions. My special thanks go to the remaining members of my advisory committee* ***Pr. Frederic Marias, Dr. François Broust, Dr. Jean-Michel Commandré*** *and* ***Dr. Capucine Dupont****. Their expertise, feedback and guidance were crucial to the completion of my thesis. Also I want to thank* ***CIRAD****-Montpellier for the very successful collaboration with* ***Dr. François Broust*** *and* ***Dr. Jean-Michel Commandré****, and also with* ***CEA****-Grenoble for the successful collaboration with* ***Dr. Marine Péyrot*** *and* ***Dr. Capucine Dupont****.*

I express My gratitude to ***Mr. Bernard Auduc*** *technician in Ecole des Mines d'Albi-Carmaux for his technical assistance, and contribution to device design and operation.*
I acknowledge gratefully the financial support from ***EnerBio Program*** *of Fondation Tuck France.*

Many thanks go to my friends (in Morocco, Marseille, and Albi) for their understanding, cooperation and support.

Finally, I would like to express my most sincere gratitude to my dear ***parents****, my sisters (****Fatima-zahra and Kaoutar****), brothers (****Mohamed, Redouane and Jawad****), all my family, my brother-in-law* ***Mr. Ezziani****, my fiancée* ***Kenza*** *and family* ***Charafeddine,*** *for their unconditional encouragement, inspiration and support to my research. Their love and support is the foundation for all that I am, do, and that to which I aspire.*

TABLE OF CONTENTS

ABBREVIATIONS

AD	Anaerobic Digestion
BCO	Bio Crude Oil
BDO	Biomass-Derived Oil
BFB	Bubbling Fluidized Bed
CIRAD	Centre de coopération Internationale en Recherche Agronomique pour le Développement
CFB	Circulating Fluidized Bed
EC	Extinction Coefficient
EU	European Union
FTIR	Fourier Transform InfraRed
GaSPar	Gasification of Solid Particles
GHG	Greenhouse Gas
HACA	H_2 abstraction, C_2H_2 addition
HHV	High Heating Value
HTR	Horizontal Tubular Reactor
HTU	Hydrothermal Upgrading
HT-EFR	High Temperature Entrained Flow Reactor
IC	Internal Combustion
ICP-OES	Inductively Coupled Plasma Optical Emission Spectrometry
IEA	International Energy Agency
LHV	Low Heating Value
MHV	Medium Heating Value
NA	Not Available
NDIR	Non-Dispersive InfraRed
NPOX	Non-Catalytic Partial Oxidation
NREL	Renewable Energy Laboratory
O/C	Oxygen to Carbon
ODE	Ordinary Differential Equations
OSR	Oxidative steam reforming
PAH	Polycyclic Aromatic Hydrocarbon
POX	Partial oxidation
ppb	parts per billion
RAPSODEE	Research in Albi on Particulate Solids, Energy and the Environment
S/C	Steam to Carbon
S/F	Steam to Fuel
SNG	Synthetic Natural Gas
SR	Steam reforming
SWBR	Softwood Bark Residues
TCD	Thermal Conductivity Detector
TEM	Transmission Electron Microscopy
TGA	Thermogravimetric Analysis
TGA-DSC	Thermogravimetry-Differential Scanning Calorimeter
µGC	micro-Chromatograph Gas

CHAPTER 1: INTRODUCTION

1- Research Motivation

Energy and environmental issues are two common concerns of modern society. Energy is a central part of every human being‘s daily life. In all its forms, such as chemical energy (food), thermal energy (heat), or electricity, energy has the ability to transform the daily lives of humans across the world by easing workloads, boosting economies and generally increasing the comfort of our lives. Worldwide energy consumption has been increasing rapidly. This has been accelerated by the improvement of the quality of life that almost directly relates to the amount of energy consumed. At present, fossil fuels based energy resources, such as coal, gas, and oil supply the majority of the total world energy requirement. According to the statistical data from the International Energy Agency (IEA), total world energy consumption without any structural intervention is expected to grow constantly in the next decades (Figure 1).

Energy needs are mainly met by the combustion of fossil fuels: their incidence is nowadays 81% in terms of total primary energy (Figure 2) and 67% for electricity production **[EIA 09].**

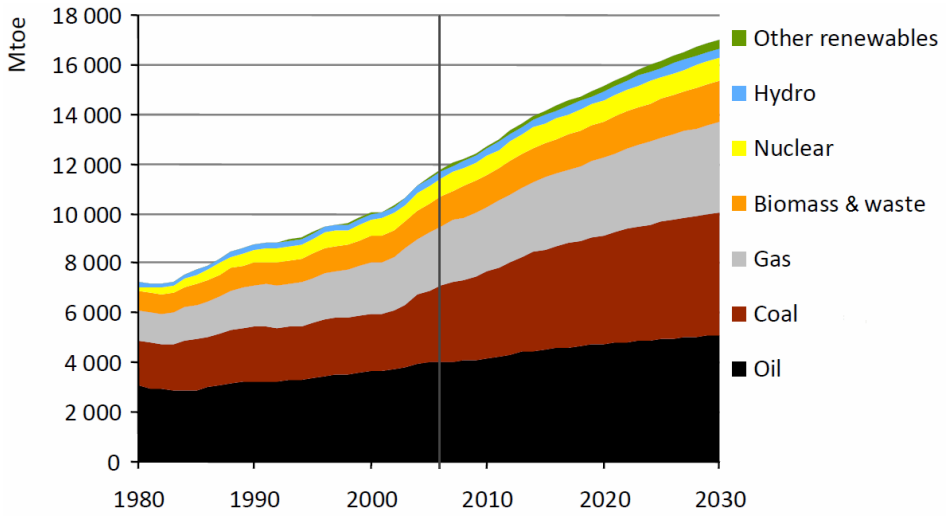

Figure 1. World primary energy demand by fuel **[EIA 08]**

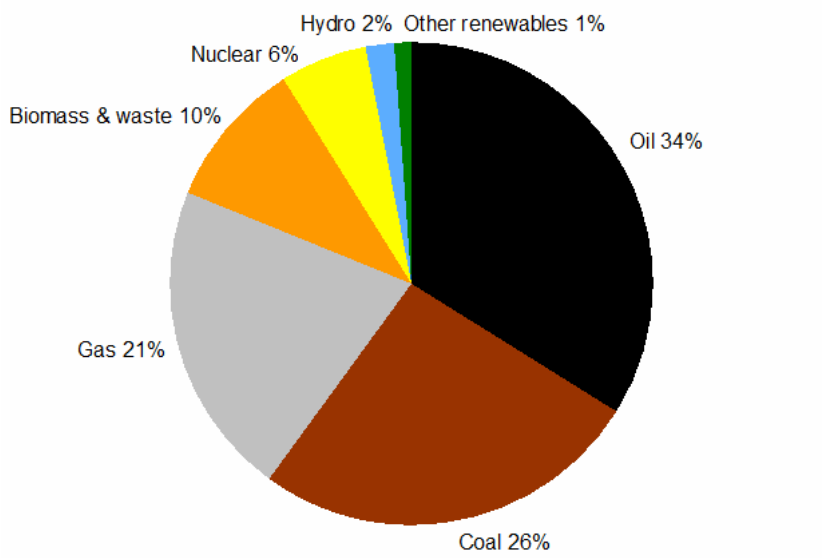

Figure 2. World primary energy consumption by fuel (adapted from **[EIA 09]**)

The global warming owing to the emissions of greenhouse gas is the most drastic consequence of the use of fossil fuels. According to experts in the field, global warming can disturb the natural equilibrium of the Earth‘s ecosystem. If CO_2 emissions are not regulated, global warming can have severe consequences for environment. These consequences, although some of them are not fully corroborated, are increasing sea and ocean levels, ocean acidification, change in rainfall patterns, hurricanes, volcanic eruptions, earthquakes and plant or animal extinctions, among others. Hence, new conversion technology should address this increasing concern. Therefore, the reduction of energy-related CO_2 emissions is the industrial societies greatest challenge at the beginning of the 21st century. A reduction of at least 1% per year is postulated to be necessary. However, with the present use of energy fuels, a steady annual increase of 2% is expected if there will not be a major change in energy and climate policies **[Jochem 00]**.

There are several strategies in order to fight the consequences from the use of fossil fuels as major primary energy sources. Besides strategies for energy saving, i.e. a reduction of the energy consumption and an increase of the exergy of an energy carrier, the use of renewable energy sources is the most logical solution for the energy problem. According to the World Energy Outlook **[EIA 00]**, waste and renewable like (direct) solar, wind, tide, wave energy and biomass are expected to be the fastest growing primary energy sources, with an annual growth rate averaging 2.8% over the outlook period.

Among the renewable sources of energy, substantial focus of research is currently on the use of biomass. Besides being a renewable source of energy, there are many other advantages associated to the use of biomass. It is available abundantly in the world. Its use does not increase the net amount of CO_2 in the atmosphere. Indeed the CO_2 released from processing biomass originally came from the atmosphere itself, and was captured by the vegetation during the photosynthesis process, so that by thermally processing biomass, we are simply promoting the CO_2 cycle at short time scale.

2- Background

Biomass gasification is a promising technology, which can contribute to develop future energy systems which are efficient and environmentally friendly in order to increase the share of renewable energy for heating, electricity, transport fuels and higher applications.
The process of gasification to produce combustible gas also known as syngas or producer gas from organic feeds was used in blast furnaces over 180 years ago. The possibility of using this gas for heating and power generation was soon realized and then emerged in Europe producer gas systems, which used charcoal and peat as feed material. At the turn of the century petroleum gained wider use as a fuel, but during both world wars and particularly World War II, shortage in petroleum supplies led to widespread re-introduction of gasification. By 1945 the gas was being used to power trucks, buses and agricultural and industrial machines. It is estimated that there were close to 9000,000 vehicles running on producer gas all over the world **[Breag 79]**.

After World War II the lack of strategic impetus and the availability of cheap fossil fuels led to general decline in the producer gas industry. However Sweden continued to work on producer gas technology. A decision was then made to include gasifiers in Swedish strategic emergency plans.
The contemporary interest in small scale gasifier R&D, for most part dates from 1973 oil crisis.

The gasification of carbon-containing materials to produce combustible gas is an established technology. Biomass gasification is a thermochemical process that produces relatively clean and combustible gas through pyrolytic and reforming reactions. The syngas generated can be an important resource suitable for direct combustion, application in prime movers such as

engines and turbines, or for the production of synthetic natural gas (SNG) and transportation fuels e.g. Fischer-Tropsch diesel.

For energy production, the major concerns about syngas are its heating value, composition, and possible contamination **[Wei 05]**. The proportion of the combustible gas hydrogen (H_2), methane (CH_4), carbon monoxide (CO), and moisture determines the heating value of the gas. The composition of syngas depends on the biomass properties and gasifier operating conditions. For a specific gasification system, operating conditions play a vital role in all aspects of biomass gasification. These include carbon conversion, syngas composition, tars and soot formation and oxidation **[Devi 03]**.

The main hurdles for large-scale implementation of energy production from solid biomass are the nature of biomass - non uniform, low-energy density, sometimes large ash content - together with the usual inconsistency between the local availability of biomass and the demand for biomass related products: heat, electricity, fuels and chemicals. Usually, import/transport of fossil fuels is cheaper.

Pyrolysis may be a process to overcome these hurdles: biomass is transformed into a versatile liquid called bio-oil, easy to handle and to transport. This bio-oil would then be transported to centralized air/steam gasification units. Bio-oil is an intermediate product which is produced from relatively dry biomass via fast pyrolysis process. It is a liquid with similar elemental composition to its original feedstock and with high bulk and energy density.

The high bulk and energy density of bio-oil can reduce transportation costs to large scale centralized gasification plants; these costs have been a detrimental factor in large scale use of solid biomass resource. Bio-oil can be produced where the biomass is available and then be transported over long distances to central processing units of similar scales as the current petrochemical industry. Besides technical and logistic advantages, this conversion chain may also give incentives for economic development and job creation especially in rural areas.
At the industrial level, one of the major issues in biomass gasification is the soot formed during the process which influences syngas purity. Soot are solid particles that also clog engine parts and thus affect the ability of engines to run smoothly and have also serious environmental effects.

3- Objectives

The chemistry of bio-oil gasification is very complex. Biomass gasification proceeds via a two-step process, pyrolysis followed by gasification that includes gas and tars reforming plus char and soot conversion, as illustrated in Figure 3. Pyrolysis is the decomposition of the bio-oil by heat. This step, also known as devolatilization, is endothermic and produces mainly volatile materials in the form of gaseous and condensable hydrocarbons called tars. The remaining nonvolatile material, containing mainly the carbon material, is referred to as char. The volatile hydrocarbons and char are subsequently converted to syngas in the presence of steam in the second step called gasification.

The overall purpose of this research is to investigate the feasibility of a whole bio-oil non catalytic steam gasification process for the production of high quality syngas.
The objectives of this work are as follows:

- To better understand the first step of gasification i.e. pyrolysis, and investigate the effect of operating conditions, in particularly the influence of temperature and heat flux density on the pyrolysis products yield;
- Thereafter, to study the whole process (pyrolysis+gasification), and to determine the syngas yield and its composition versus operating conditions notably temperature.

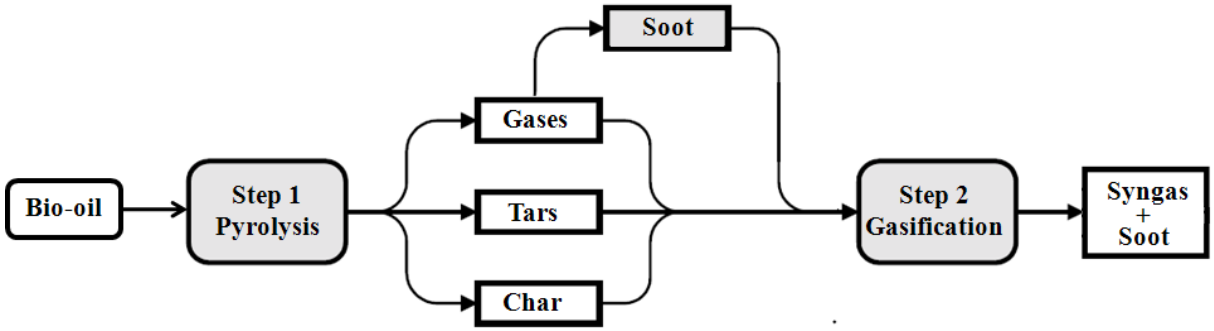

Figure 3. Scheme of the non catalytic gasification of wood bio-oil

- In addition of pyrolysis of bio-oil product (gases, tars and char), the process may lead to emissions of soot (solid carbonaceous material). In this thesis we are also interested in the soot formation and oxidation behavior. This research all together is expected to produce a reliable model to support the design of future large scale plants for non catalytic gasification of bio-oil.

4- Scope of the Thesis

This introduction is considered as **Chapter 1.**

Chapter 2 gives an overview based on literature review of biomass sources, physical and chemical characteristics of lignocellulosic biomass, biomass conversion, gasifier types, bio-oil characteristics and applications and finally a review of literature on soot formation and oxidation during thermochemical conversion of biomass.

Chapter 3 describes in details the different experimental set-ups that were developed and used. Protocols are explained for the bio-oil pyrolysis, gasification and partial oxidation experiments that were carried on. Details are also given about the developed bio-oil pulverization feeder and the soot quantification device.

Chapters 4, 5 and 6 are the core of the thesis. They contain the results obtained from experimental and modeling work in the form of three journal papers. One of the papers have already been accepted and published; others have been submitted and are being reviewed.

The objective of **Chapter 4** is to characterise the pyrolysis step of bio-oil. In particular, it will focus on the influence of the heating rate and the final pyrolysis temperature on the products distribution. Two complementary devices, namely: a Horizontal Tubular Reactor (HTR) and a High Temperature - Entrained Flow Reactor (HT-EFR), were used to study a wide range of heating rates, representative of slow and flash pyrolysis, in the range from 2 to 2000°C.s^{-1} and final temperature from 550 to 1000°C. Finally the catalytic effect of ash on the bio-oil pyrolysis process has also been studied.

Chapter 5 is focused on the non catalytic steam gasification in the absence of O_2 of whole bio-oil in the HT-EFR. The objectives of this work are to determine the syngas yield and composition versus temperature over a wide range from 1000°C to 1400°C. In parallel a thermodynamic equilibrium calculation is performed in order to determine the theoretical temperature at which the thermodynamic equilibrium is reached. Finally the influence of ash on the gasification process has also been studied.

Chapter 6 relates a study on soot formation and oxidation during bio-oil thermal conversion in the HT-EFR. A model is proposed to describe soot formation and oxidation. It is based on the description of bio-oil heating, devolatilization, reforming of gases and gasification of solids (char and soot). To support the model validation, experiments were carried out. The temperature was varied from 1000 to 1400°C. Three thermochemical situations were studied in order to cover possible industrial applications: default of steam, large excess of steam (H_2O/C = 8), and in the presence of oxygen in the range O/C = 0.075 to 0.5.

Finally general conclusions of this research and suggestions for future work are proposed.

REFERENCES

[Breag 79] Breag GR, Chittenden AE. Producer Gas; Its Potential and Applications in Developing countries, Report No. G130, Tropical Products Institute, London, October 1979.

[Devi 03] Devi L, Ptasinski KJ, Janssen FJ.JG. A Review of the Primary Measures for Tar Elimination in Biomass Gasification Processes 2003;24:125-140.

[EIA 09] IEA (International Energy Agency), Key World Energy Statistics, Paris, France, 2009.

[EIA 08] IEA (International Energy Agency), World Energy Outlook, Paris, France, 2008.

[EIA 00] IEA (International Energy Agency), World Energy Outlook 2000 www.IEA.org.

[Jochem 00] Jochem E. Goldemberg J. Challenges and options for future energy policy. Bulletin - Magazine of the Swiss Federal Institute of Technology in Zurich 2000.

[Wei 05] Wei L. Experimental study on the effects of operational parameters of a downdraft gasifier. PhD Thesis, Mississippi State, USA 2005.

CHAPTER 2: LITERATURE REVIEW

In this chapter, a general overview is given of biomass, energy generation processes from biomass, gasifier types, bio-oil characteristics and applications. A literature review is also provided on soot formation and oxidation during themochemical conversion of biomass.

1- BIOMASS

1-1 Definition

The sun provides the majority of energy on earth through solar radiation. Solar energy is a result of nuclear fusion reactions within the sun and this energy radiates to the earth over a range of wavelengths of electromagnetic energy that we know as light and heat. This light energy is naturally harnessed by plants through photosynthesis to create a source of energy in the form of complex carbon, hydrogen, and oxygen.

The word ―biomass" consists of ―bio" + "mass" and originally refers in the field of ecology to amount of animals and plants.

The term biomass is defined as any organic matter that is available on a renewable basis, including dedicated energy crops and trees, agricultural food and feed crop residues, aquatic plants, wood and wood residues, animal wastes and other waste materials **[Kamm 06]**. Lignocellulose is the most abundant renewable biomass. It is constituted of cellulose, hemicelluloses and lignin, as well as other minor components. Both cellulose and hemicelluloses fractions are polymers of sugars.

1-2 Physical and chemical characteristics of lignocellulosic biomass

1-2-1 Composition

Understanding the chemical structure of biomass is extremely important for the development of processes of production of fuels and chemicals from biomass. Biomass has a complex chemical composition, and both organic and inorganic constituents are important for further handling and conversion processes.

The term "lignocellulosic biomass" is used when referring to plants, softwood or hardwood. Figure 1 shows the complete molecular structure of lignocellulosic biomass.

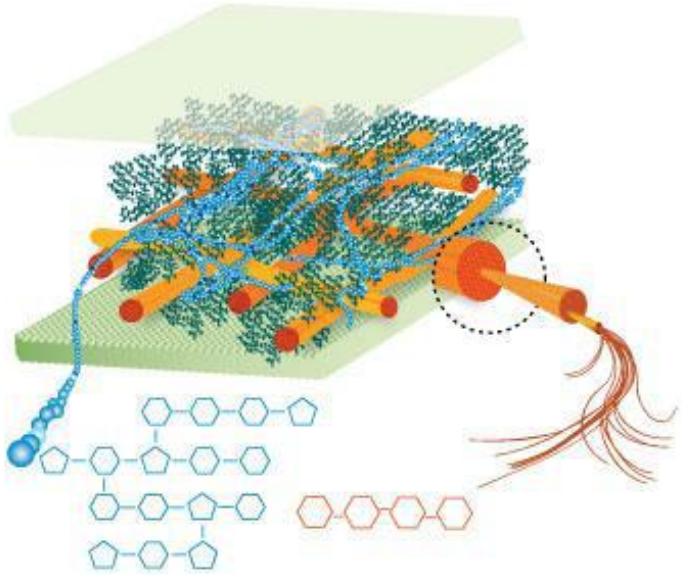

Figure 1. Complete molecular structure of biomass containing the three main components cellulose is shown in orange, hemicelluloses in blue, and lignin in green **[Ceres Biofuels 07]**

- Cellulose is a major structural component of cell walls, and it provides mechanical strength and chemical stability to plants. Solar energy is absorbed through the process of photosynthesis and stored in the form of cellulose **[Raven 92].** It has been estimated that around $7.5x10^{10}$ tonnes of cellulose are consumed and regenerated every year **[Kirk-Otmer 01]**. It is thereby the most abundant organic compound in the world. Cellulose is a linear crystalline polysaccharide, with general formula $(C_6H_{10}O_5)_n$. It serves as the framework substance, making up 40-50% of wood. The polymer is formed from repeating units of cellobiose, a disaccharide of β-linked glucose.
- Hemicelluloses are matrix substances between cellulose microfibrils. They are polysaccharides of variable composition containing both five (including xylose and arabinose) and six carbon monosaccharide units (including galactose, glucose, and mannose). Hemicelluloses constitute 20 to 30% of wood and other biomasses, generally with higher concentrations in hardwoods than softwoods. The most abundant monomeric unit of hemicelluloses is xylan.
- Lignin is a polymer constituted of aromatic compounds produced through a biosynthetic process and forms a protective layer for the plant walls. The lignin is formed of highly branched, substituted, mononuclear polymers of phenylpropane units, derived from coniferyl, sinapyl, and p-coumaryl alcohols. It is often bounding to adjacent cellulose fibers to form a lignocellulosic complex. The structure varies among different plants. Softwood lignin is mainly composed of guaiacyl units

stemming from the precursor trans-coniferyl alcohol. Hardwood lignin is mostly composed of guaiacyl and syringyl units derived from trans-coniferyl and trans-sinapyl alcohols. Grass lignin contains p-hydroxyphenyl units deriving from trans-p-coumaryl alcohol. Almost all plants contain all three guaiacyl, syringyl, and p-hydroxyphenyl units in lignin.

Apart from the three basic chemical compounds, water is also present in the complex forming biomass. Furthermore, minor amounts of proteins, minerals and other components can be found in the lignocellulose composition as well.

The composition of lignocellulose highly depends on its source. There is a significant variation of the lignin and (hemi) cellulose content in lignocellulose depending on whether it is derived from hardwood, softwood, or grass. Table 1 summarizes the composition of lignocellulose encountered in the most common sources of biomass.

Table 1. Composition of lignocellulose in several sources on dry basis **[Sun 02]**

Lignocellulosic materials	**Cellulose (%)**	**Hemicelluloses (%)**	**Lignin (%)**
Hardwoods stems	40–55	24–40	18–25
Softwood stems	45–50	25–35	25–35
Nut shells	25–30	25–30	30–40
Corn cobs	45	35	15
Grasses	25–40	35–50	10–30
Paper	85–99	0	0–15
Wheat straw	30	50	15
Sorted refuse	60	20	20
Leaves	15–20	80–85	0
Cotton seed hairs	80–95	5–20	0
Newspaper	40–55	25–40	18–30
Waste papers from chemical pulps	60–70	10–20	5–10
Primary wastewater solids	8–15	NA	24–29
Swine waste	6.0	28	NA
Solid cattle manure	1.6–4.7	1.4–3.3	2.7–5.7
Coastal Bermuda grass	25	35.7	6.4
Switchgrass	45	31.4	12.0

1-2-2 Internal structure – physical properties

Lignocellulosic biomass has a complex internal structure. It is formed of a number of major components that have, in their turn, also complex structures. To obtain a clear picture of the material, a more detailed analysis of the structure of each main component is made in this section, as well as a description of the structure of lignocellulose itself. The physical properties of each of the components are also addressed, and how each of these components contributes to the behaviour of the complex structure as a whole.

a- Cellulose

Cellulose is a high molecular-weight (10^6 g or more) linear polymer of β-(1→4)-D-glucopyranose units in the $^4C_1$ conformation. The fully equatorial conformation of β-linked glucopyranose residues stabilizes the chair structure, minimizing flexibility. Glucose anhydride, which is formed via the removal of water from each glucose unit, is polymerized into long cellulose chains. The basic repeating unit of the cellulose polymer consists of two glucose anhydride units, which form a cellobiose unit.

The chemical formula of cellulose is $(C_6H_{10}O_5)_n$ and the structure of one chain of the polymer is shown in Figure 2.

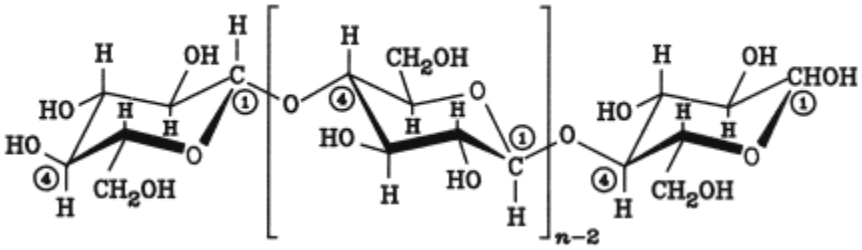

Figure 2. Structure of cellulose molecule

Many properties of cellulose depend on its degree of polymerization (DP), i.e. the number of glucose units that make up one polymer molecule. The DP of cellulose can extend to a value of 17,000, even though more commonly a number of 800-10,000 units is encountered **[Kirk-Otmer 01]**.

The nature of the bond between the glucose molecules (β-1,4 glucosidic) allows the polymer to be arranged in long straight chains. The latter arrangement of the molecule, together with the fact that the hydroxides are evenly distributed on both sides of the monomers, allows the formation of hydrogen bonds between the molecules of cellulose. The hydrogen bonds result in the formation of a compound that is constituted of several parallel chains which are attached to each other **[Faulon 94]**.

An illustration of the arrangement of the cellulose molecules in parallel chains and of the accompanying hydrogen bonding is given in Figure 3.

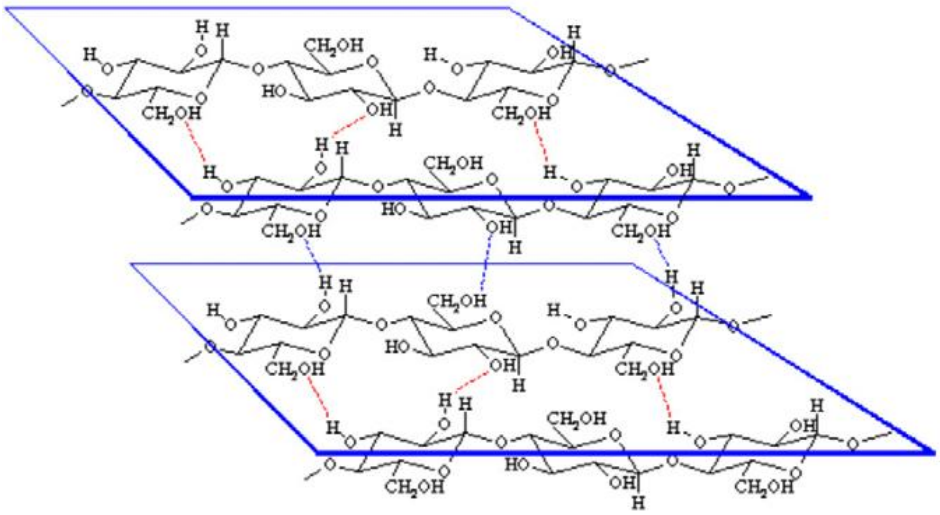

Figure 3. Illustration of the arrangement of the cellulose molecules in parallel chains and of the accompanying hydrogen bonding

Cellulose is found both in crystalline and non-crystalline structure. The coalescence of several polymer chains leads to the formation of microfibrils, which in turn are united to form fibres. In this way cellulose can obtain a crystalline structure. Figure 4 illustrates structure as well as placement of cellulose in the cell wall.

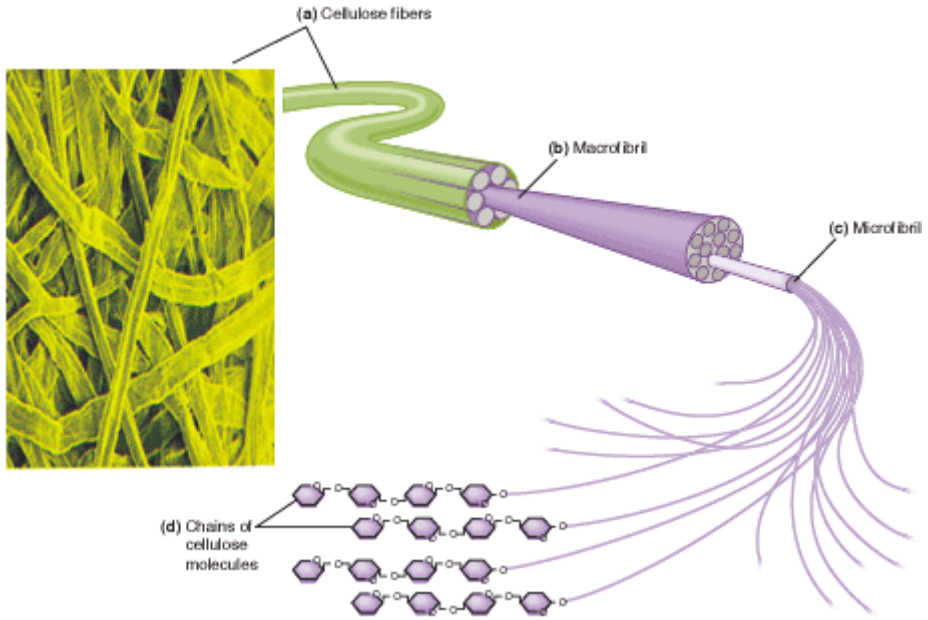

Figure 4. Formation of micro- and macrofibrils (fibres) of cellulose and their position in the wall

Cellulose degradation occurs at 240-350°C to produce anhydrocellulose and levoglucosan. When cellulose is pyrolyzed at a heating rate of 12°C/min under helium gas, endothermic reaction is observed at 335°C (temperature of maximum weight loss). The reaction is completed at 360°C **[Mohan 06]**.

b- Hemicelluloses

Hemicelluloses are a mixture of various polymerized monosaccharides such as glucose, mannose, galactose, xylose, arabinose, 4-*O*-methyl glucuronic acid and galacturonic acid residues. Hemicelluloses extracted from plants have a high degree of polydispersity, polydiversity and polymolecularity (a broad range of size, shape and mass characteristics). Hemicelluloses exhibit lower molecular weights than cellulose. The number of repeating saccharide monomers is only ~150, compared to the number in cellulose ~800-10,000.

Figure 5 shows the molecule of xylan, which is the main component of hemicelluloses. It is based on 1-4 linkages of xylopyranosyl units with α-(4-O)-methyl-D-glucuronopyranosyl units attached to anhydroxylose units. The result is a branched polymer chain that is mainly composed of five carbon sugar monomers, xylose, and to a lesser extent six carbon sugar monomers such as glucose.

Important aspects of the structure and composition of hemicelluloses are the lack of crystalline structure, mainly due to the highly branched structure, and the presence of acetyl groups connected to the polymer chain **[Kirk-Otmer 01]**.

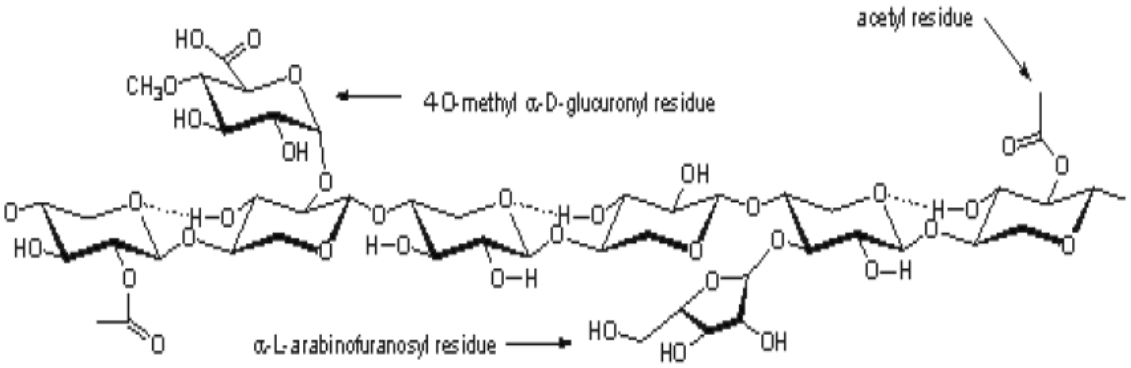

Figure 5. A schematic representation of the hemicelluloses backbone of arborescent plants

The onset of hemicelluloses thermal decomposition occurs at low temperatures. The mass loss of hemicelluloses occur in slow pyrolysis of wood in the temperature range of 130-194°C, with most of this loss occurring above 180°C. However, the relevance of this more rapid

decomposition of hemicelluloses versus cellulose does not appear to be relevant during fast pyrolysis, which is completed in a few seconds at a rapid heating rate **[Runkel 51]**.

c- Lignin

Lignin is the most abundant polymeric aromatic organic substance in the plants. It is an amorphous three-dimensional polymer with phenylpropane units as predominant building blocks. P-coumaryl alcohol, coniferyl alcohol and sinapyl alcohol units (Figure 6) are the most commonly encountered units.

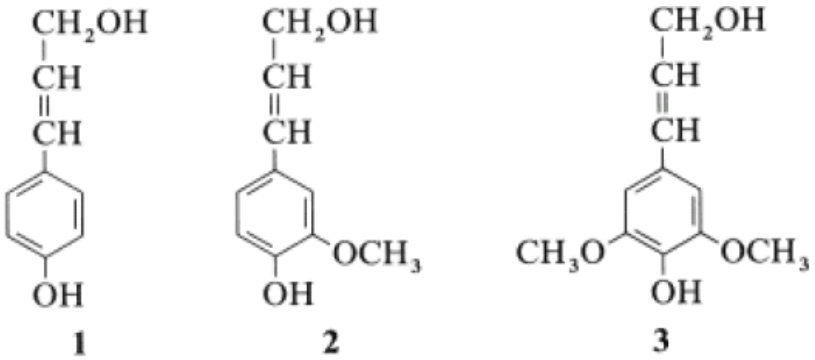

Figure 6. P-coumaryl- , coniferyl- and sinapyl alcohol: dominant building blocks of the three-dimensional polymer lignin

The property of polydispersity, just as with hemicelluloses, characterizes lignin as well. Different branching and bonding in similar molecules are encountered **[Lin 02]**. Figure 7 shows a model structure of softwood lignin.

Lignin in wood behaves as an insoluble three-dimensional network. It plays an important role in the cell endurance and development, as it affects the transport of water, nutrients and metabolites in the plant cell. It acts as binder between cells and creates a composite material that has a remarkable resistance to impact, compression and bending.

Lignin decomposes when heated at 280-500 ºC. Lignin pyrolysis produces more residual char than does the pyrolysis of cellulose **[Mohan 06]**.

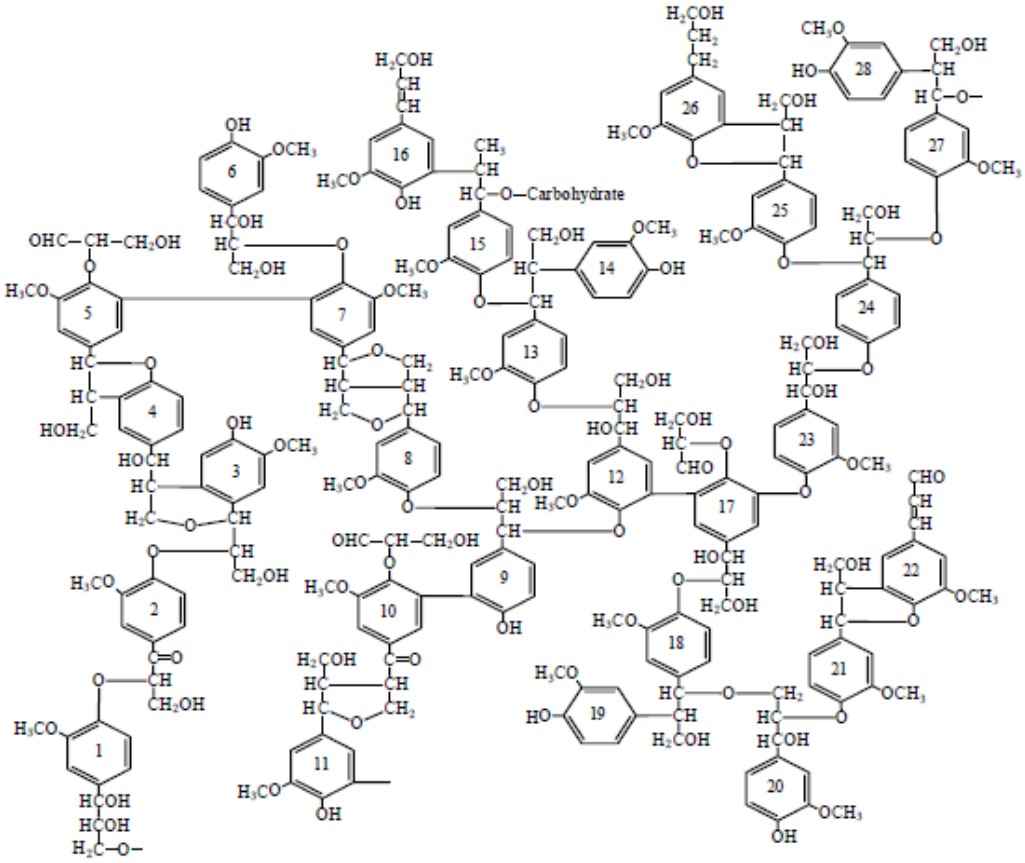

Figure 7. A model of chemical structure of softwood lignin **[Northey 98]**

d- Water

The amount of water in biomass, that is its moisture content, significantly varies from one feedstock to another and may vary between different samples of the same feedstock. Values ranging between 5 and 50% are classically encountered. Moisture content depends on the location of the raw biological material, its surroundings and the season of harvesting. High moisture in feedstock is undesirable for process so that biomass generally passes trhough a stage of drying before conversion.

e- Ash and other components

Ash is the name given to the non-aqueous residual components of biomass that remain after it is burnt. It mainly consists of metal oxides or salts, with 25-45% of the ash being composed of calcium carbonate. The ash component of biomass is non-reactive and cannot be converted into biofuels. Mass fraction of 0.1 to 10% is classically encountered.

Extractives are constituted of the compounds that may be extracted by solvent. They are not integral part of the cellular structure and can be either simple fats, amino acids, chlorophyll or

tannin for instance. The type and quantity of extractives found in a given feedstock vary widely from one sample to another **[Fengel 89]**.

1-2-3 Chemical interaction between components

There are four main types of bonds identified in the lignocellulose complex. Those are ether type of bonds, ester bonds, carbon-to-carbon bonds and hydrogen bonds. These four bonds are the main types of bonds that provide linkages within the individual components of lignocellulose (intrapolymer linkages), and connect the different components to form the complex (interpolymer linkages). The position and bonding function of the latter linkages is summarized in Table 2 **[Faulon 94]**.

Table 2. Overview of linkages between the monomer units that form the individual polymers lignin, cellulose and hemicelluloses, and between the polymers to form lignocelluloses

Bonds within different components (intrapolymer linkages)	
Ether bond	Lignin, (hemi)cellulose
Carbon to carbon	Lignin
Hydrogen bond	Cellulose
Ester bond	Hemicelluloses
Bonds connecting different components (interpolymer linkages)	
Ether bond	Cellulose-Lignin
	Hemicelluloses lignin
Ester bond	Hemicelluloses-lignin
Hydrogen bond	Cellulose-hemicelluloses
	Hemicelluloses-Lignin
	Cellulose-Lignin

a- Intrapolymer linkages

The main types of bonds that connect the building molecules within the lignin polymer are ether bonds and carbon-to-carbon bonds (Table 2). Ether bonds may appear between allylic and aryl carbon atoms, or between aryl and aryl carbon atoms, or even between two allylic carbon atoms. The total fraction of ether type bonds in the lignin molecule is around 70% of the total bonds between the monomer units. The carbon-to-carbon linkages form the remaining 30% of the total bonds between the units. They can also appear between two aryl carbon atoms or two allylic carbon atoms, or between one aryl and one allylic carbon atom **[5 Kirk-Otmer 01]**.

The polymer of cellulose is formed on the basis of two main linkages:

- The glucosidic linkage is the one that forms the initial polymer chain. More specifically, it is a 1-4 β D-glucosidic bond that connects the glucose units together. The glucosidic bond can also be considered as an ether bond, since it is in fact the connection of two carbon atoms with an elementary oxygen interfering **[Solomon 88]**.

- The hydrogen bond is considered to be responsible of the crystalline fibrous structure of cellulose. The arrangement of the polymer in long straight parallel chains together with the fact that the hydroxyl groups are evenly distributed in both sides of the glucose monomer, allow the formation of hydrogen bond between two hydroxyl groups of different polymer chains **[Faulon 94]**.

It has been identified that carboxyl groups are also present in cellulose in a fraction of 1 carboxyl per 100 or 1,000 monomer units of glucose **[Krassig 02]**.

As already mentioned, hemicelluloses consist of polysaccharides other than cellulose. Their structure (Figure 2) reveals that ether type of bonds, such as the fructosic and glucosidic bonds, is the main type of bonds in these molecules. The main difference with cellulose is that the hydrogen bonds are absent and that there is significant amount of carboxyl groups. The carboxyl groups can be present as carboxyl or as esters or even as salts in the molecule **[Kirk-Otmer 01]**.

b- Interpolymer linkages

In order to determine the linkages that connect the different polymers of the lignocellulose complex, lignocellulose is broken down and the individual components are separated. However, their separation is commonly achieved by methods that result in alteration of their original structure. As a consequence, the conclusions on the connecting linkages between the polymers remain questionable.

However, it has been identified that there are hydrogen bonds connecting lignin with cellulose and with hemicelluloses, respectively. Furthermore, the existence of covalent bonds between lignin and polysaccharides is identified. More specifically, it is certain that hemicelluloses connect to lignin via ester bonds. It is also known that there are ether bonds between lignin and the polysaccharides. It is still not clear though whether the ether bonds are formed between lignin and cellulose, or hemicelluloses.

Hydrogen bonding between hemicelluloses and cellulose is also identified. However, this linkage is not expected to be strong due to the fact that hemicelluloses lack of primary alcohol functional group external to the pyranoside ring **[Faulon 94]**.

2- LIGNOCELLULOSIC BIOMASS RESOURCES

Up to the 19th century, biomass in the form of firewood and charcoal was the main source of energy, but then it was replaced by coal and oil in the 20th century. In the 21st century, however, there is interest on biomass again because of the following characteristics: it is renewable, it is storable and substitutive, it is abundant worldwide, and it is carbon neutral.

There is no established way of classification of biomass, which is defined differently according to the field; categorization depends on the purpose and application. Generally there are two ways to categorize biomass: one is biological categorization based on types of existing biomass in nature (such as categorization according to ecology or type of vegetation), and the other is based on the use or application as feedstock. The latter is highly significant in terms of making effective use of energy sources.

Biomass can be found in various forms, each of which has specific properties, uses and advantages. The main sources of lignocellulosic biomass are wood from conventional and short-rotation forestry, other energy crops, residues from forestry and agricultural production, and by-products and wastes from industrial and municipal processes.

An example of biomass categorization appears in Table 3. In this categorization, biomass includes not only the conventional products and wastes from agriculture, forestry, and fisheries, but also plantation biomass.

Table 3. Examples of biomass resources

Category	Examples
Dedicated plantations	Short-rotation forestry (eucalyptus willow)
	Perennial crops (miscanthus)
	Arable crops (rapeseed, sugarcane, sugarbeet)
Residues	Wood from forestry thinning
	Wood felling residues
	Straw from cereals
	Other residues from food and industrial crops (sugarcane, tea, coffee, rubber trees, oil and coconut palms)
By-products and wastes	Sawmill waste
	Manure
	Sewage sludge
	Organic fraction of municipal waste
	Used vegetable oils and fats

3- BIOMASS CONVERSION

Although it is a common source of energy (especially in developing countries), biomass is not an ~~–i~~deal" fuel due to its fibrous nature, low density and low heating value. Indeed, the energy that can be obtained from a particular resource depends on its chemical composition and moisture content. Except when straightforward combustion is appropriate, it is not usually possible to directly use biomass raw materials. Therefore biomass is treated in various processes to create products which can be more efficiently and economically be used in modern energy equipments. This conversion is generally achieved by some type of biological or thermal processes as shown in Figure 8.

Fermentation and digestion are examples of biological processes. They use microbial or enzymatic activity to convert sugars from biomass into ethanol, or biomass into solid fuels or biogas.

Combustion, gasification and pyrolysis are examples of thermal processes. We are focused on this type of process in this research work and will therefore describe them in more detail in the following sections. They produce either direct heat or gas or bio-oil. The gas can be used

to drive a motor or a fuel cell or be converted into liquid or gaseous fuels. The bio-oil can be further transformed into gaseous and upgraded liquid fuels.

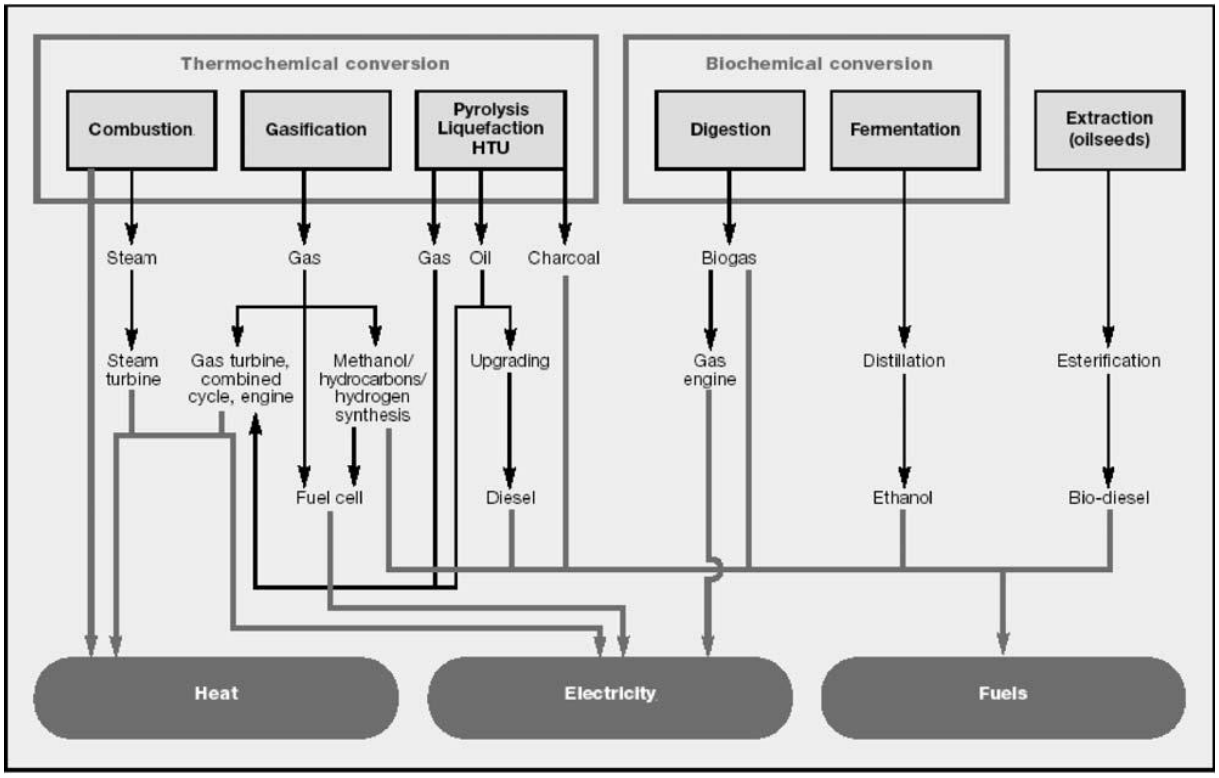

Figure 8. Main conversion options for biomass to secondary energy carriers **[Turkenburg00]**

3-1 Pyrolysis

Pyrolysis is the thermal degradation at temperatures of 300-600°C of carbonaceous material in the absence of an externally supplied oxidizing agent. The products of pyrolysis are char (solid), tar (liquid at room temperature, therefore often referred to as ~~b~~io-oil" in the context of this process) and gas. The relative yields of the products depend very much on the process conditions, i.e. heating rate, final temperature, pressure and gas residence time in the reactor. The heating rate of the biomass particles is the most important parameter for pyrolysis with regard to the product yield distribution. Slow pyrolysis (heating rates in the order of $10°C.s^{-1}$) is applied for maximum char yields, fast or even flash pyrolysis (heating rates up to $10^{4}°$ $C.s^{-1}$ provide maximum yields of bio-oil.

3-2 Gasification

Gasification is the thermal degradation of carbonaceous material in the presence of an externally supplied oxidizing agent: air, carbon dioxide or steam. The main product of gasification is a mixture of gas mainly constituted of carbon monoxide, hydrogen, carbon dioxide, water, methane, air and nitrogen. The gas may also contain solid particles (ash, soot), oxygenated organics and higher-molecular hydrocarbons, the latter two product classes are commonly referred to as ―tars". The quality of the producer gas depends on the same parameters as in the pyrolysis process.

The main purpose of biomass gasification is the production of low or medium heating value (LHV, MHV) gas which can be used as fuel gas in an internal combustion (IC) engine for power production. Gas turbines, fuel cells, the synthesis of liquid fuels or syngas are other applications of the producer gas. Gasification is the process of interest in this work.

3-3 Combustion

Combustion is the complete oxidation of the biomass feedstock. Contrary to pyrolysis and gasification, which are fuel conversion processes, combustion can provide collectible energy (heat). The hot flue gas is used for heating purposes or for steam production by means of subsequent steam turbine processes. Moreover, the Stirling engine provides a possibility for power production by combustion without steam production. Low NOx processes and particle and aerosol reduction are important subjects of the current biomass combustion research.

3-4 Liquefaction

Liquefaction is the thermochemical conversion of biomass in the liquid phase at low temperatures (250-350°C) and high pressures (100-200 bar), usually with a high hydrogen partial pressure and catalysts to enhance the rate of reaction and/or to improve the selectivity of the process. The main goal is to reach maximum liquid-yields with higher quality than from the pyrolysis process, i.e. the produced fuel has a higher heating value and lower oxygen content. The lower oxygen content makes the fuel chemically more stable and requires less upgrading to hydrocarbon product.

4- PYROLYSIS AND GASIFICATION: LITERATURE REVIEW

4-1 Pyrolysis

As previously said, pyrolysis is a thermal decomposition process that takes place in the absence of oxygen to convert biomass into solid charcoal, liquid (bio-oil), and gas. Pyrolysis is considered to be an industrial realized process for biomass conversion **[IEA 2006] [Maschio 92] [Marsh 07] [Demirbas 01]**.

As mentioned before, each component of lignocellulosic biomass is pyrolysed at different rates by different mechanisms and pathways. Lignin decomposes over a wider temperature range compared to cellulose and hemicelluloses which rapidly degrade over narrower temperature ranges. Hence there is an apparent thermal stability of lignin during pyrolysis. Thermogravimetry analysis (TGA) testing of biomass shows that there are three stages for a typical biomass pyrolysis process **[Maschio 92]**. The first stage, pre-pyrolysis, occurs between 120 and 200°C with a slight weight loss, when some internal rearrangements, such as bond breakage, the appearance of free radicals, and the formation of carbonyl groups take place, with a corresponding release of small amounts of water (H_2O), carbon monoxide (CO), and CO_2. The second-stage is the main pyrolysis process, during which solid decomposition occurs, accompanied by a significant weight loss from the initial biomass. The last stage is the continuous char devolatilization, caused by the further cleavage of C-H and C-O bonds.

Depending on the reaction temperature and residence time, pyrolysis can be classified into slow pyrolysis, intermediate pyrolysis fast pyrolysis, and flash pyrolysis.

4-1-1 Intermediate and slow pyrolysis

Slow pyrolysis has been applied for thousands of years and has been mainly used for the production of charcoal. In slow pyrolysis, biomass was typically heated to ~ 500 ºC at slow heating rates (up to 10-20°C/min). The vapor residence time varies from 5 min to 30 min **[Mohan 06]**. Thus, the components in the vapor phase continue to react with each other, as solid char and liquid are being formed.

The main product, charcoal, can be used in a wide range of areas, from domestic cooking and heating to metallurgical or chemical use as the raw material for production of chemicals, activated carbon, fireworks, absorbents, soil conditioners, and pharmaceuticals **[Karaosmanoglu 99]**. As reported by Mok et al. **[Mok 92]**, a higher yield of charcoal can be obtained from biomass feedstocks with higher lignin contents and lower hemicelluloses

contents. In contrast to fast pyrolysis, slow pyrolysis does not necessarily require fine feedstock particle size (smaller than 1 mm).

4-1-2 Fast pyrolysis

Fast pyrolysis is a process in which very high heat flux are imposed to biomass particles, leading to very high heating rates, in the absence of oxygen. Biomass decomposes to generate vapors, aerosol, and char. After cooling and condensation of the vapors and aerosol, a dark brown mobile liquid is formed which has a heating value of about half of the conventional fuel oil.

Fast pyrolysis process produces 60-75 wt% of liquid bio-oil, 15-25-wt% of solid char, and 10-20-wt% of non condensable gas, depending on the feedstock used. No waste is generated because the bio-oil and solid char can each be used as a fuel and the gas can be recycled back in the process. Fast pyrolysis uses much higher heating rates than slow pyrolysis. While slow pyrolysis is related to the traditional pyrolysis processes for making charcoal, fast pyrolysis is an advanced process which is carefully controlled to give high yields of liquid. Research has shown that maximum liquid yields are obtained with high heating rates, at reaction temperatures around 500°C and with short vapour residence times to minimize secondary reactions.

Very short residence times result in incomplete depolymerization of the lignin due to random bond cleavage and inter-reaction of the lignin macromolecule resulting in a less homogenous liquid product, while longer residence times can cause secondary cracking of the primary products, reducing yield and adversely affecting bio-oil properties **[Bridgewater 99].**

The essential features of fast pyrolysis process are:

- very high heating and heat transfer rates, which usually requires a finely ground biomass feed: <1mm
- carefully controlled pyrolysis reaction temperature of around 500°C in the vapour phase, with short vapour residence times of typically less than 2 s;
- rapid cooling of the pyrolysis vapours to give the bio-oil product.

4-1-3 Flash pyrolysis

Very fast pyrolysis is sometimes referred to as _flash pyrolysis‘ **[Demirbas 02]**, usually in the context of laboratory studies involving rapid movement of substrate through a heated tube under gravity or in a gas flow. Higher temperatures and shorter residence times than fast pyrolysis are used; the main product distributions are similar to fast pyrolysis. The distinction

between flash and fast pyrolysis has largely disappeared and now the term ‗flash' has largely disappeared and is gradually being replaced by a more generalized definition for fast pyrolysis.

4-1-4 Fast pyrolysis reactor configuration

Fast pyrolysis conversion technology has led to design of original reactor systems that provide the essential ingredients of high heating rates, moderate temperatures and short vapour product residence times for liquids. The most commonly used reactors for fast pyrolysis are bubbling fluidized-bed, circulating fluidized-bed, ablative, entrained flow, rotating cone, and vacuum reactors. There are three main methods achieving fast pyrolysis.

1. Ablative pyrolysis, in which heat is transferred by conduction: wood is pressed against a heated surface and rapidly moved during which the wood melts at the heated surface and leaves an oil film behind which evaporates. This process uses large particles of wood and is typically limited by the rate of heat supply to the reactor. It leads to compact and intensive reactors that do not need a carrier gas, but with the penalties of surface area controlled system and moving parts at high temperature.

2. Bubbling fluidized bed and circulating fluidized bed pyrolysis, in which heat is transferred from a heat source to the biomass by a mixture of convection and radiation. The heat transfer limitation is within the particle, thus, requiring very small particles of typically no more than 3 mm to obtain good liquid yields. Substantial carrier gas is needed for fluidisation or transport.

3. Vacuum pyrolysis, which has slow heating rates but removes pyrolysis products as rapidly as in the previous methods, which thus simulates fast pyrolysis. Larger particles can be accepted but the vacuum leads to larger equipment and higher costs. Total liquid yields are typically lower than 60-65% compared to 75-80 wt% with the previous two methods.

4-1-5 Pyrolysis products

a- Char

Char is a porous carbon structure that remains after the hydrogen and oxygen fractions have left the fuel. Char is often defined as the solid residue after pyrolysis. It is often polluted with other components: mineral fractions and after incomplete pyrolysis, large fractions of hydrogen and oxygen, that can still be present in char.

Char is believed to contribute to the formation of polycyclic aromatic hydrocarbon (PAHs) during biomass pyrolysis, particularly at low temperature [Sharma 04]. Char can be used as a

fuel in form of briquettes or as a char-oil, char-water slurry; alternatively char can be upgraded to activated carbon and used in purification processes **[Islam 05]**.

The properties of the char obtained after biomass pyrolysis have a direct influence on the subsequent char oxidation step, since the amount and type of pores determine the gas accessibility to the active surface sites. Properties of char are decisively affected not only by properties of parent material but also by pyrolysis operating conditions, mainly the heating rate, the maximum temperature and the residence time at this temperature.

b- Pyrolysis liquid

The liquid product from biomass pyrolysis is known as bio-oil. Bio-oil is not a product of thermodynamic equilibrium during pyrolysis but, as detailed previously, it is produced with short residence times and rapid cooling or quenching from the pyrolysis temperature. This condensate is not at thermodynamic equilibrium at storage temperatures. Hence the bio-oil chemical composition tends to change toward thermodynamic equilibrium during storage. Details on bio-oil will be given in the following sections.

c- Gas

The third main product from pyrolysis is gas. The gas mainly consists of H_2, CO_2, CO, and CH_4 together with traces of C_2 species. CO_2 and CO are preferentially produced at low temperature, while H_2 is released at high temperature.

4-1-6 Pyrolysis reaction schemes

The exact pyrolysis mechanisms of biomass are still not clear, although substantial literature sources are available on biomass devolatilization kinetics and mechanisms. Many biomass devolatilization models have been developed. One-step global mechanisms and semi-global multi-step mechanisms can be basically distinguished. The simplified approaches define devolatilization rates with single or two-step Arrhenius reaction schemes involving pseudo-species.

The one-step global mechanisms can be shown as:

$$Biomass \xrightarrow{k} Volatiles + Char \quad Or \quad Biomass \xrightarrow{k} Tar\,(Bio\text{-}oil) + Gas + Char \qquad (1)$$

The reaction kinetic rate (k) is expressed in single-step Arrhenius law form as $k = A \exp(-E_a/RT)$, and the devolatilization rate is expressed as:

$$\frac{-dm_p}{dt} = k\left[m_p - (1 - f_{v,0})m_{p,0}\right] \qquad (2)$$

where m_p is the biomass particle mass, $m_{p,0}$ is the initial particle mass, and $f_{v,0}$ is the initial volatile fraction.

For two-step Arrhenius reaction schemes, the kinetic devolatilization rate expressions of the form proposed by Kobayashi **[Kobayashi 76]** are:

$$k_1 = A_1 \exp(-E_a/RT) \quad (3)$$

$$k_2 = A_2 \exp(-E_a/RT) \quad (4)$$

where k_1 and k_2 are competing rates that may control the devolatilization over different temperature ranges.

One-step multi-reaction schemes have been developed by Thunman and Leckner **[Thunman 02]** via three parallel reactions into char, tar and gas and can be shown as follow:

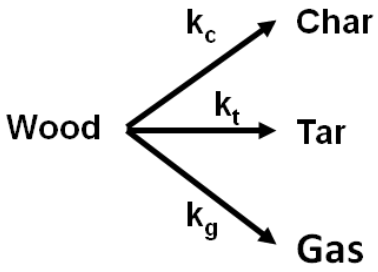

(5)

More recent models are adapted to be able to handle different feedstocks. The composition of the feedstock is represented using three model species. In these models the source species like wood or biomass is replaced by a mixture of cellulose, hemicelluloses and lignin.

Most models are only proposed for cellulose, but several schemes were also proposed for the other biomass main components. The rest of this section describes several other proposed kinetic schemes for cellulose pyrolysis.

Broido and Shavizadeh **[Broido 76]** developed a multistep model. In this scheme cellulose is firstly converted to an active state by an initiation reaction. Hereafter the active cellulose reacts via two competing reactions to produce tar, char and gas.

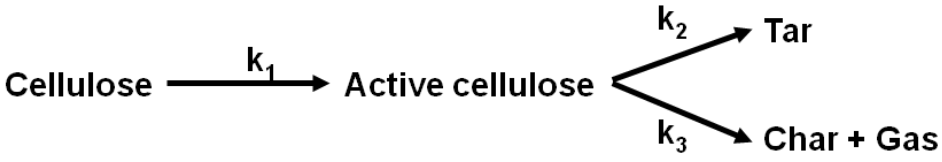

(6)

The two competing reactions represent two pathways that the decomposition of cellulose can follow. The ―char path" is favored at low temperature (200-280°C) whereas the ―tar path" dominates at elevated temperatures (280-340°C).

Over the years the validity of the Broido-Shafizadeh model has been disputed by several authors. The use of the initiation step was disputed by Varegyi and Jakab **[Varhegyi 94]** and by Antal and Varhegyi **[Antal 95]** who claimed that in most cases experimental data could be better modeled without this step.

A different approach was proposed by Alves **[Alves 89 a] [Alves 89 b]** and Shrivastava **[Srivastava 96]**. Their model describes the decomposition by three or two consecutive reactions. This approach requires preset yields for each reaction and therefore lacks of predictive capabilities.

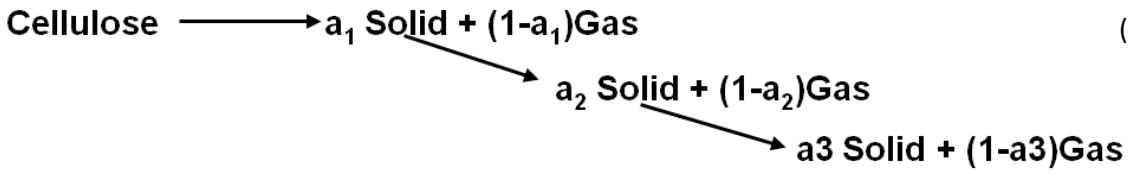

(7)

A third approach was the Di Blasi model **[Di Blasi 96]**. It is similar to the model of Thunman. In this model cellulose decomposes via three competing reactions into gas, char and tar. Consecutively the tar is converted by two secondary reactions into secondary gas and char.

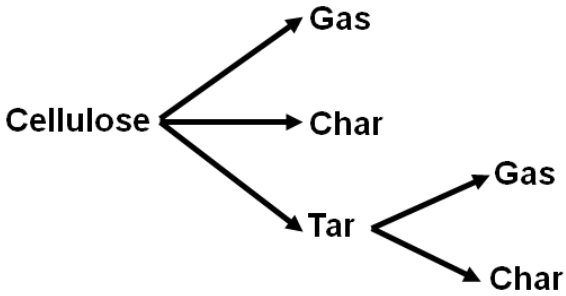

(8)

The last model discussed here is the Miller-Bellan model **[Miller 97]**. This model uses an adapted form of the Broido-Shafizadeh model. It uses three model species to model biomass decomposition and has three sets of kinetic constants for each model component.

(9)

It also uses a secondary reaction for the conversion of tar to smaller gas species. In this reaction no difference is made concerning the origin of the tar.

4-1-7 Secondary reactions

Tars produced during the decomposition of the virgin fuel can decompose further. Several authors suggest a transformation of tar to char and gas following two independent reactions. Tar decomposition is suggested to be catalyzed by the solid matrix of the fuel resulting in char creation on the pore walls.

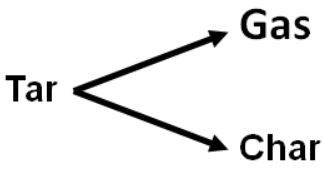

(10)

It is unclear however how this takes place. Among several others Miller and Bellan **[Miller 97]** suggest a single tar reaction with only gas as product species.

(11)

4-2 Gasification

4-2-1 Gasification Chemistry

Gasification can be seen as an extension of pyrolysis; biomass gasification is a complex thermo-chemical process involving numerous different reactions. The biomass gasification process can be divided into two parts: pyrolysis and gasification. Pyrolysis was discussed in the previous section. In the gasification part the gas, tar and char react further. Gasification, as a core technology for the production of chemicals and clean power, refers to a process converting biomass into either fuel gas (containing CH_4 and some N_2 usually) or syngas (containing mainly H_2 and CO).

During gasification several reactions take place. A simplified representation of these reactions is given in equations (12)-(18) **[de Jong 03] [Moulijn 01] [Van den 85]**.

Heterogeneous reactions

$C_{(s)} + O_2 \leftrightarrow CO_2$ $\Delta H_{298}^0 = -394\ \text{kJmol}^{-1}$ (12)

$C_{(s)} + H_2O \leftrightarrow CO + H_2$ $\Delta H_{298}^0 = 131\ \text{kJmol}^{-1}$ (13)

$C_{(s)} + CO_2 \leftrightarrow 2CO$ $\Delta H_{298}^0 = 173\ \text{kJmol}^{-1}$ (14)

$C_{(s)} + 2H_2 \leftrightarrow CH_4$ $\Delta H_{298}^0 = -75\ \text{kJmol}^{-1}$ (15)

Homogeneous reactions

$CO + H_2O \leftrightarrow CO_2 + H_2$ $\Delta H_{298}^0 = -41\ \text{kJmol}^{-1}$ (16)

$CH_4 + H_2O \leftrightarrow CO + 3H_2$ $\Delta H_{298}^0 = 206\ \text{kJmol}^{-1}$ (17)

Cracking reaction

$\text{Tar} \rightarrow aCO + bCH_4 + cC$ (18)

Evans and Milne **[Evans 87]** observed three major reaction regimes during the gasification process identified as primary, secondary, and tertiary regimes as shown in Figure 9.

Biomass is mainly converted into a mixture of hydrogen, carbon monoxide, light hydrocarbons, such as methane, and other non combustible gas such as carbon dioxide, water vapour, and nitrogen. In most cases, the product gas can contain particulates such as char, ash, soot, etc.

Reactor temperature is one of the most important operating conditions which affect both the heating value and producer gas composition.

The gasification process is usually performed with aid of a gasification agent. The gasification agent can be steam, or air, or enriched air, or oxygen, or a combination of steam and an oxygen source, or carbon dioxide. The process is performed at relative high temperature 600-1500°C. There are also small amounts of impurities in the gas: char, soot, tars, alkalis, nitrogen compounds, sulphur compounds, and chlorine compounds.

The composition of the product gas can vary significantly depending on operating conditions (e.g temperature, operating pressure, oxidant agent), type of feed stock, moisture content in the fuel, mode of bringing the reactants into contact inside the gasifier **[Basu 06]**. Moreover, the quality of the product gas is associated with other factors such as the type of gasifier, the residence time, and the heating rate which is usually associated with the type of feed stock, particle size and temperature.

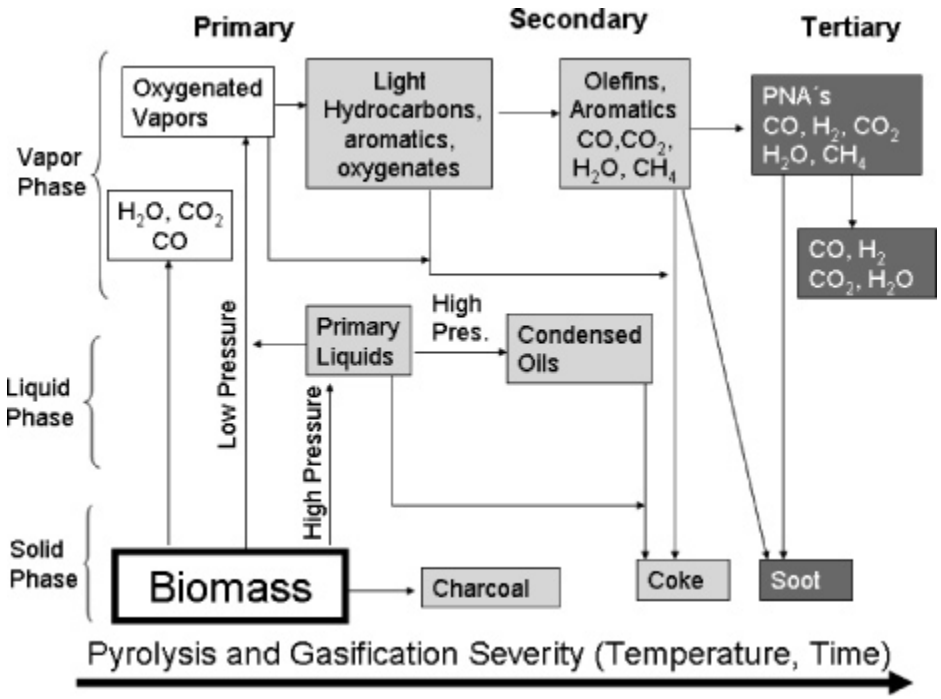

Figure 9. Gasification and pyrolysis reaction pathways adapted from Milne et al **[Milne 97]**

There are hundreds of different types of gasifiers in the patent literature. However, they can be divided into four main types: Updraft gasifier, Downdraft gasifier, Fluidized-bed gasifier and Entrained flow gasifier. In the following sections, the different technologies for biomass gasification are described.

4-2-2 Gasifier types

Until now, most gasifiers have been developed and commercialized for the production of heat and power from syngas. The main differences between gasifiers are:

- The type of injection: biomass is either fed from the top of the gasifier, or from the side and then is moved around either by gravity or air flows;
- The gasification agent used;
- The type of heating: it can be done either by partial combustion of the biomass in the gasifier (directly heated), or from an external source (indirectly heated), such as circulation of an inert material;
- The temperature range;
- The pressure range under which the gasifier is operated.

a- Updraft gasifier

Updraft reactor is the simplest and oldest form of gasifier, also known as counter-current gasifier. Biomass enters at the top of the reactor and air/oxygen/steam enters at the bottom of

the reactor, flows upward, and the product gas leaves at the top. In Figure 10, a schematic representation of an updraft gasifier is given.

Complete combustion of char takes place at the bottom of the bed, liberating CO_2 and H_2O. This hot gas (~1000°C) passes through the bed above, where it is reduced to H_2 and CO and cooled to 750°C. Going up the reactor, the reducing gas (H_2 and CO) pyrolyses the descending dry biomass and finally dries the incoming wet biomass, leaving the reactor at a quite low temperature (~500°C) **[Stultz 92] [Reed 01] [Bridgwater 93]**.

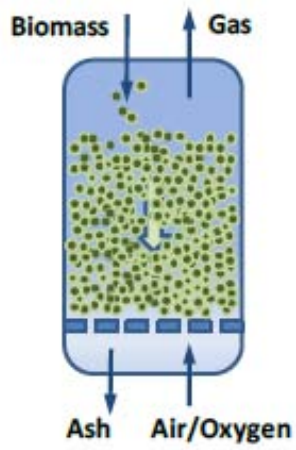

Figure 10. The Updraft gasifier (counter-current reactor) scheme

The advantages of updraft gasifiers are that they are a mature technology for heat production, they can be used for small-scale applications, they can handle feedstocks with high moisture content, and there is very few carbon in the remaining ash. The disadvantages of updraft gasifiers are that they have a feedstocks size limit, high tar yields which implies extensive syngas cleanup before engine, turbine or synthesis applications.

b- Downdraft gasifier

This gasifier was widespread during World War II. It was used to convert biomass or charcoal into fuel for gasoline vehicles in periods of great shortages of transportation fuels. The downdraft gasifier is a co-current reactor, where the fuel and the gasification agent move in the same direction. In Figure 11, a schematic representation of a downdraft gasifier is given.

There are different reaction zones in a downdraft gasifier. In the drying zone, moisture is evaporated from biomass as it slowly moves down towards the pyrolysis zone. In the pyrolysis zone, biomass is converted into char, tars and gas. Some of the pyrolysis products are combusted. Due to the high temperature, tars are cracked. As a result, the produced gas is relatively clean. However, downdraft gasifier has some drawbacks:

The disadvantages of downdraft gasifiers are:

- It requires feedstocks drying to low moisture content;
- Syngas exiting the reactor is at high temperature, requiring secondary heat recovery system.

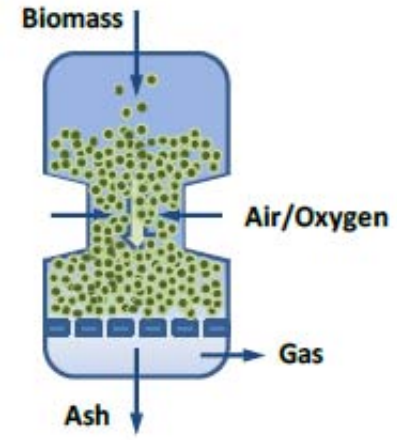

Figure 11. The downdraft gasifier (co-current reactor) scheme

c- Fluidized-bed gasifier

The biomass, which is previously reduced to a fine particle size, and air, steam, or oxygen enter at the bottom of the reactor. An inert or catalytic bed material is used to transport heat and mass through the reactor. The bed is fluidized by blowing the gasification agent through the bed, which lifts the bed against gravity. As a result, the turbulence in the bed creates an even temperature distribution in the bed. In Figure 12, a schematic representation is given of a fluidized-bed gasifier. Therefore, contrary to fixed bed gasifiers there are no different reaction zones in fluidized bed gasifiers. The operating temperature of a fluidized bed is usually of 700-900°C and the pressure range is between 0 and 70 bar. The most common types of fluidized beds are the bubbling fluidized bed (BFB) and the circulating fluidized bed (CFB).

The advantages of fluidized-bed gasifiers are:

- Exhibit a nearly uniform temperature distribution throughout the reactor;
- Provide high rates of heat transfer between inert material, biomass and gas;
- High conversion possible with low tar and low unconverted carbon.

The disadvantages of fluidized-bed gasifiers are:

- The tolerance of high moisture content feedstocks is much more limited.
- The system design is also more complex, requiring blowers to inject the oxidant at the bottom of the fluidized bed.

- Bed sintering when a biomass with high ash content is used. The alkali components in the ash have the tendency to form low-melting eutectics with silica being the most common bed material, which can lead to loss of fluidization.

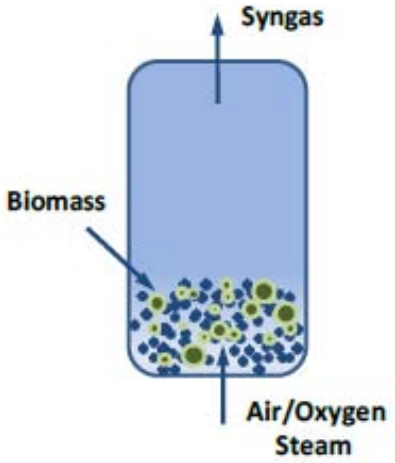

Figure12. Fluidized-bed gasifiers scheme

d- Entrained flow gasifier

This is the type of process of interest in this work. In an entrained flow gasifier, as shown in Figure 13, no inert material is present but a finely reduced feedstock is required. The biomass is present in dust form. Contact surfaces are very high and hence reaction times are very short. The feed and air move co-currently and the reactions occur in a dense cloud of particles at very high temperature >1000°C so that firstly the syngas results almost free from tars and secondly ash melts, being then collected at the bottom of the reactor in the form of slag. Conversion in entrained flow reactors is close to 100%. There is little experience with biomass in such systems.

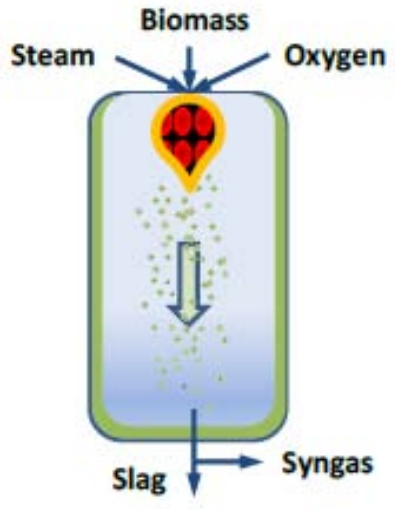

Figure 13. Entrained flow gasifier schematic

4-2-3 Syngas?

Syngas is always confused with the producer gas, however there is a difference between those two terms:

- Producer gas is the mixture of gas produced by the gasification of biomass at relatively low temperatures (700 to 1000ºC). Producer gas is composed of carbon monoxide (CO), hydrogen (H_2), carbon dioxide (CO_2) and typically a range of hydrocarbons such as methane (CH_4). Producer gas can be burned as a fuel gas such as in a boiler for heat or in an internal combustion gas engine for electricity generation or combined heat and power. The composition of the gas can be modified by change in of gasification parameters.

- Syngas (synthesis gas) is a mixture of carbon monoxide (CO) and hydrogen (H_2), which is the product of high temperature steam gasification of biomass. Following clean-up to remove any impurities such as tars, syngas can be used to produce organic molecules such as synthetic natural gas or liquid biofuels such as synthetic diesel or other products as explained below.

There are four main uses of syngas that are currently being explored for production of liquid fuels:

- Fischer-Tropsch synthesis, a chemical catalytic process that has been used since the 1920s to produce liquid fuels from coal-derived syngas and natural gas;
- Mixed alcohols synthesis, a chemical catalytic process that produces a mixture of methanol, ethanol, propanol, butanol and smaller amounts of heavier alcohols;
- Syngas fermentation, a biological process that uses anaerobic microorganisms to ferment the syngas to produce ethanol or other chemicals;
- Methanol synthesis, also a chemical catalytic process currently used to produce methanol.

Figure 14 shows routes for transportation fuels and chemicals production from syngas **[Spath 03]**.

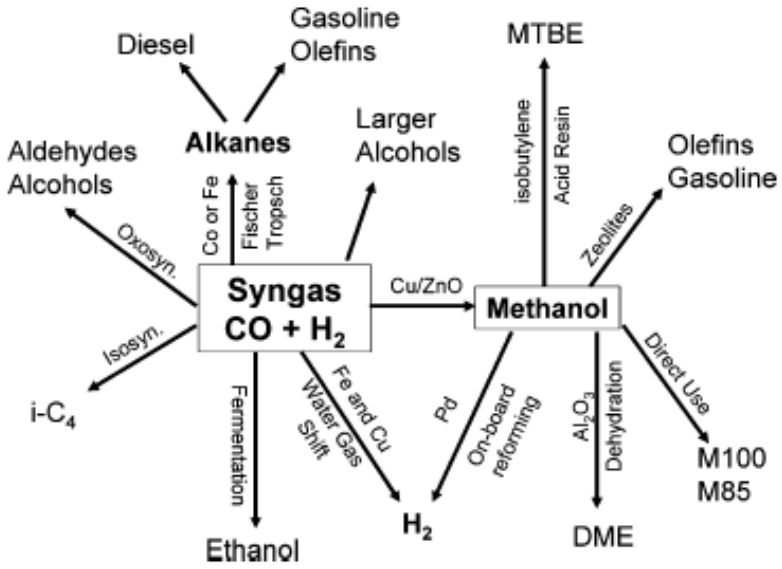

Figure 14. Pathways for fuel production from syngas adapted from Spath and Dayton

For energy production, the major concerns about syngas are its heating value, composition, and possible contamination **[Wei 05]**. The composition of syngas depends on the biomass properties and gasifier operating conditions. The principle contaminants in syngas, as it leaves the gasifier, are:

- soot ;
- ash;
- tars;
- H_2S (hydrogen sulphide) depending on the sulphur content of the feed;

And trace quantities of:

- NH_3 (ammonia), COS (carbonyl sulphide), HCl (hydogen chloride), HCN (hydrogen cyanide), and heavy metals.

5- BIO-OIL

As explained before, bio-oil has several advantages over it original biomass sources, which make it interesting for added value applications:

- The volumetric energy density is increased by roughly twice compared to original solid biomass. This makes transport, especially over long distances, economically more attractive. When large scale biomass utilization is considered, bio-oil can be produced locally from where it is transported to central processing units, thus decoupling the biomass availability and demand.

- Bio-oil makes storage, transport, processing, and pressurization more effective.

- Bio-oil is cleaner than the original feedstock. Because of the relative low process temperature, most the minerals and metals remain in the solid state and are concentrated in the char.

5-1 Definition

Pyrolysis oil is one of humanity‘s oldest manufactured products; it was used in ancient Egypt for embalming the deads **[Koller 03]**. More recently, fast (or flash) pyrolysis has been the subject of R&D as a promising process for the upgrading of biomass to marketable energy products and fuels.

Bio-oil is also referred to as biomass pyrolysis liquid, pyrolysis oil, bio-crude oil (BCO), wood liquids, wood oil, liquid smoke, wood distillates, pyroligneous acid, liquid wood and tar.

Bio-oil is a dark brown coloured free flowing liquid with a distinctive acrid or smoky odor. It has similar elemental composition to the feedstock biomass material **[Bridgewater 99]**. Bio-oil is multi-component mixture of different size molecules derived from depolymerization and fragmentation of cellulose, hemicelluloses and lignin. Therefore, the elemental composition of bio-oil and petroleum derived fuel is different.

The chemical compositions of bio-oil are determined by many factors, such as biomass type, feedstock pretreatment (particle size, moisture and ash contents), reactor type, pyrolysis conditions (temperature, heating rate, residence time, pressure, gaseous environment) as well as vapor filtration and condensation. Generally, bio-oil comprises quite a lot of water, more or less solid particles and hundreds of organic compounds that belong to:

- Acids: Formic, acetic, propanoic, hexanoic, benzoic, etc.
- Esters: Methyl formate, methyl propionate, butyrolactone, methyl n-butyrate, velerolactone, etc.
- Alcohols: Methanol, ethanol, 2-propene-1-ol, isobutanol, etc.
- Ketones: Acetone, 2-butanone, 2-butanone, 2-pentanone, 2-cyclopentanone, 2,3 pentenedione, 2-hexanone, cyclo-hexanone, etc.
- Aldehydes: Formaldehyde, acetaldehyde, 2-butenal, pentanal, ethanedial, etc.
- Phenols: Phenol, methyl substituted phenols.
- Alkenes: 2-methyl propene, dimethylcyclopentene, alpha-pinene, etc., Aromatics: Benzene, toluene, xylenes, nphthalenes, phenanthrene, fluoranthrene, chrysene, etc.
- Nitrogen compounds: Ammonia, methylamine, pyridine, methylpyridine, etc.
- Furans: Furan, 2-methyl furan, 2-furanone, furfural, furfural alcohol, etc.

- Guaiacols: 2-methoxy phenol, 4-methyl guaiacol, ethyl guaiacol, eugenol, etc.
- Syringols: Methyl syringol, 4-ethyl syringol, propyl syringol, etc.
- Sugars: Levoglucosan, glucose, fructose, D-xylose, D-arabinose, etc.
- Miscellaneous oxygenates: Hydroxyacetaldehyde, hydroxyacetone, dimethyl acetal, acetal, methyl cyclopentenolone, etc **[Diebold 00].**

Oligomeric species in bio-oil are mainly derived from lignin, but also cellulose. Oligomer molecular weights from several hundred to as much as 5000 or more can be obtained. This makes a complete chemical characterization of bio-oil almost impossible.

5-2 Composition and physicochemical properties

Water is the most abundant single component in bio-oil. Depending on the original moisture in the feedstock and the product of dehydration during the pyrolysis reaction and storage, the water content of bio-oils usually varies in the range of 15–30 wt% which cannot readily be separated. The presence of water lowers the heating value and may cause phase separation of bio-oils. On the other hand, it helps to reduce viscosity and enhances the fluidity and facilitate atomization, and contributes to the microexplosion of droplets, which ensure good heat transfer. In addition, OH radicals from water can inhibit the formation of soot and can also accelerate its oxidation.

In contrast to petroleum fuels, bio-oil contains large oxygen content, usually 45%-50%. The presence of oxygen is the primary reason for the vast differences in the properties and behavior between hydrocarbon fuels and biomass bio-oil. The bio-oil is immiscible with liquid hydrocarbons because of its high polarity and hydrophilic nature **[Mohan 06]**.

Oxygen is present in almost all organic compounds in bio-oil. The lower heating value (LHV) of bio-oils is typically 14–18 MJ/kg, which is much lower than that of petroleum fuels (41–43 MJ/kg). It is attributable to the high oxygen content. However, the density of bio-oil is about 1.2 g/ml compared with that of petroleum fuels, which is of 0.8–1.0 g/ml.

Bio-oils comprise substantial amounts of carboxylic acids, such as acetic and formic acids, which leads to low pH values of 2–3, which causes corrosion in fuel handling systems. Typical properties of wood pyrolysis bio-oil and heavy fuel oil are presented in Table 4.

Table 4. Typical Properties of Wood Pyrolysis Bio-oil and Heavy Fuel Oil **[Czernik 04]**

Physical properties	Value	
	Bio-oil	heavy fuel oil
moisture content (wt %)	15-30	0.1
pH	2.5	
specific gravity	1.2	0.94
element composition (wt %)		
C	54-58	85
H	5.5-7.0	11
O	35-40	1.0
N	0-0.2	0.3
Ash	0-0.2	0.1
HHV (MJ/kg)	16-19	40
viscosity, at 50°C(cP)	40-100	180
solid (wt %)	0.2-1.0	1
distillation residue	up to 50	1

5-3 Multiphase structure

Bio-oil can be considered as a microemulsion in which the continuous phase is an aqueous solution of holocellulose decomposition products and small molecules from lignin decomposition. The continuous liquid phase stabilizes a discontinuous phase that is largely composed of pyrolytic lignin macromolecules. Microemulsion stabilization is achieved by hydrogen bonding and nanomicelle and micromicelle formation.

Although most bio-oils are macroscopic single phase liquids, in fact, they possess microscopic multiphase structures. Pérez **[Pérez 06]** pointed out that crude bio-oil exhibitdiverse multiphase characteristics depending on the originating biomass feedstock. The presence of waxy materials (e.g., fatty acids, fatty alcohols, sterols, and aliphatic hydrocarbons), the appearance of upper layer (originating from extractive derivatives), the contribution of heavy compound micelles, and the presence of char particles and aqueous droplets are some of the multiphase features that characterize bio-oil. The presence of waxy materials is important because of the tendency of these materials to crystallize. The presence of the network formed of heavy compounds and waxy materials determines the lower temperature at which the bio-oil can be filtered. Such a network plays an important role in the bio-oil phase stability. Char particles are responsible for the plugging of fuel nozzles in fuel applications. The presence of aqueous phase droplets does not seem to be a major problem for fresh oil. However, the separation of aqueous phase in storage tanks can be a serious problem

for aged bio-oil. Bio-oil multiphase structure can be summarized in physical model of the bio-oil, as presented schematically in Figure 15.

Most bio-oils behave as Newtonian fluids at temperatures lower than 80°C. However, some bio-oils rich in extractives may exhibit non-Newtonian fluid behaviors. Ba **[Ba 04 a] [Ba 04 b]** investigated the steady and dynamic rheological properties of the SWBR-derived bio-oil. The steady rheological study discovered a phase-transition temperature of the bio-oil at 46°C. According to these results, it could be concluded that the waxy materials, pyrolytic lignins and solids in the bio-oil formed three-dimensional structures (<46°C). This structure would melt and disappear at higher temperatures. As a result, the bio-oil behaved in a manner similar to that of a Bingham plastic fluid and a Newtonian liquid before and after 46°C, respectively.

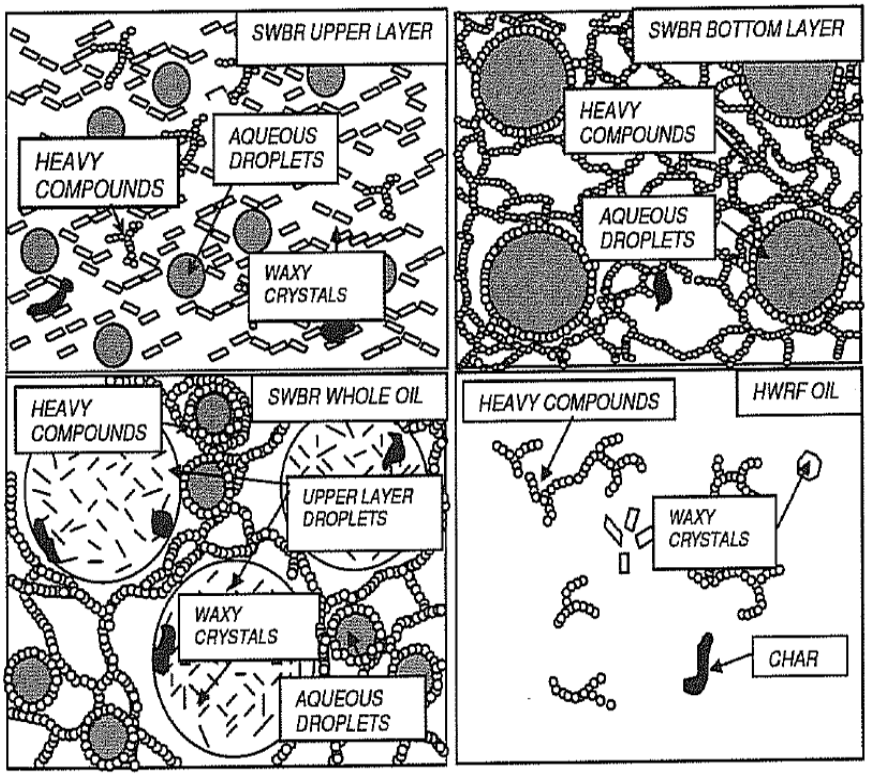

Figure 15. Schematic representation of physical model illustrating bio-oil multiphase structure **[Pérez 06]**

In addition to thermal instability, bio-oil exhibits chemical instability. Many components in it will take part in diverse reactions during storage. Diebold **[Diebold 99]** concluded that the chemical reactions may take place during ageing of bio-oils.

Aldehydes seem to be the most unstable fraction. They can react with water to form hydrates;

- with alcohols to form hemiacetals, acetals and water;
- with phenolics to form resins and water;

- with proteins to form dimers;
- and with one another to form oligomers and resins.

Moreover, acids can react with alcohols to form esters and water; mercaptans will react to form dimers; and olefins will polymerize to form oligomers and polymers. In addition, oxygen in air will oxidize the bio-oil to form more acids and reactive peroxides that catalyze the polymerization of unsaturated compounds. Furthermore, the char particles will act as catalysts to accelerate the ageing reactions. The properties of bio-oils will be changed as a result of these ageing reactions. First, chemical reactions change the polarity of bio-oils. For example, esterification reactions convert highly polar organic acid and alcohol molecules into esters with relatively low polarity and extremely polar water. Second, polymerization reactions generate large molecules that have poor mutual solubility with other compounds in bio-oils. These changes are the primary reason for the increase in water content and viscosity as well as for the phase separation observed during the storage of bio-oils.

5-4 Steam gasification of bio-oil

The pyrolysis bio-oil as such cannot be used for high end applications and therefore has to be upgraded. Three main routes can be identified: direct upgrading of the liquid, extraction of specific components and gasification/steam reforming. In this Thesis, the gasification/steam reforming at relatively high temperatures (1000-1400°C) of bio-oil is investigated.

The general overall stoichiometric reaction for steam reforming of bio-oil can be written as:

$$\boldsymbol{C_k H_j O_m + a\, H_2O/CO_2/O_2 \rightarrow CO_2 + CO + H_2 + H_2O + CH_4 + C_{2+} + Tar + C_S} \quad (19)$$

Steam reforming of fossil fuels is a well-established technology, and steam reforming of bio-oil is an extension of this technology. Catalytic steam reforming reactions occur at high temperature (600-800°C) usually with a Ni-based catalyst.

The research of catalytic steam reforming of bio-oil was initiated by the National Renewable Energy Laboratory (NREL) in the USA. Production of hydrogen from reforming bio-oil was investigated by Wang **[Wang 97] [Wang 98]** extensively, including the reactions in a fixed bed or a fluidized bed and studies of the reforming mechanisms on model compounds.

Owing to bio-oil complex components and unstable properties many research groups have been trying to develop new catalyst formulations using model compounds of bio-oil and the aqueous phase of bio-oil to produce hydrogen/syngas while minimizing coke formation. A

summary of some new research is given in Table 5. Although noble compounds (especially Rh) were found to give high activities and stabilities, Ni is still preferred. Ni is a relatively cheap metal and it is capable to fit both steam and dry reforming and to activate water **[Matas 09]**.

Catalytic steam reforming of bio-oil is a costly process and presents several disadvantages such as carbon deposit and the deactivation of catalysts due to coke or oligomer deposition. For these reasons, there is an interest in developing non catalytic gasification of bio-oil.

Only very few works can be found on the non catalytic reforming of whole bio-oil. Bimbela et al. studied catalytic and non catalytic steam reforming of acetol (bio-oil model compound) in fixed bed at low temperature (550-750°C) in order to highlight the specific role of the catalyst in this process **[Bimbela 09]**. The same study was carried out by Guus van Rossum et al. concerning catalytic and non catalytic gasification of bio-oil in a fluidized bed over a wide temperature range (523-914°C) **[van Rossum 07]**. Marda et al. has developed a system for the volatilization and conversion of a bio-oil mixed with methanol to syngas via non-catalytic partial oxidation (NPOX) using an ultrasonic nozzle to feed the mixture. The effects of both temperature (from 625 to 850°C) and added oxygen (effective O/C ratio from 0.7 to 1.6) on the yields of CO and H_2 have been explored. They obtained hydrogen yield of about 75% of theoretical maximum **[Marda 09]**. Panigrahi et al. gasified biomass-derived oil (BDO) to syngas at 800°C. They obtained syngas (H_2 + CO) yield ranging from 75 to 80 mol % **[Panigrahi 03]**. Henrich et al. gasified lignocellulosic biomass. The first process step is a fast pyrolysis at atmospheric pressure, which produces a large quantity of bio-oil, that was mixed to slurries. The mixture is pumped into a slagging entrained flow gasifier and is atomized and converted to syngas at high operating temperatures and pressures **[Henrich 04]**.

Choren **[Choren 09]** adjusted the process using a three stage gasifier. In the first stage, the biomass is fed to a low temperature pyrolyser/gasifier (~400-500°C) and oxygen is added. The biomass is pyrolysed producing a gas/vapor mixture and char which are separated from each other. The gas vapor stream is fed to the second gasification step where, by adding additional oxygen the temperature is raised above 1400°C resulting in almost total conversion of the gas/vapor mixture to H_2, CO, CO_2 and H_2O. In the third gasification section, the char is contacted with the hot gas mixture and then undergoes endothermic gasification lowering the temperature to ~800°C. In this process concept, the syngas is used for Fischer-Tropsch fuel production. Choren gasification process is presented in Figure 16.

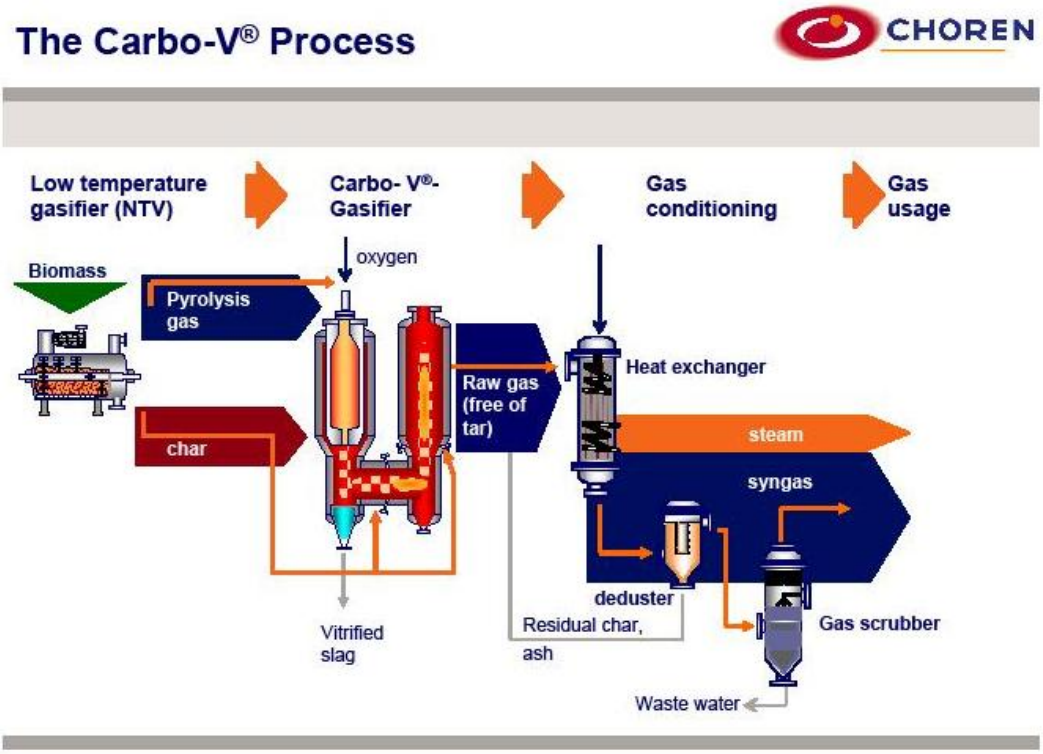

Figure 16. Choren Gasification Process **[Choren 09]**

Table 5. Some works on catalytic steam gasification of bio-oil and model compounds of bio-oil

Feed material	Catalyst	Reactor type	Source
Bio-oil	Ni/MgO-La_2O_3-Al_2O_3 catalyst	Fixed Bed and Fluidized Bed	P. Lan *et al.*, 2010
Methanol	Noble metals (Ag, Au, Au–Ag alloy and Pt) nanoparticles on TiO_2	Photocatalyst bed	Chiarello *et al.*, 2010
Methanol	CuO/ZnO/Al_2O_3	Steam reforming reactor	Abdullah *et al.*, 2010
Bio-oil/methanol mixture (50/50wt%)	Quartz wool	Microreactor,	Marda *et al.*, 2009
Acetic acid	Pt/ZrO_2 or Pt/CeO_2 catalyst	Fixed bed reactor	Güell *et al.*, 2009
Acetol and acetic acid	Mixture of sand and Ni-alumina catalyst	Fluidized bed reactor	Medrano *et al.*, 2009
Acetol and n-butanol	Mixture of Ni-Al catalyst	Fixed bed	Bimbela *et al.*, 2009
Acetic Acid	Ni supported by ZrO_2, K, La	Packed	Matas *et al* 2009
Acetic acid, Pyrolysis oil	Ni supported by Al2O3, K/La_2O_3	Packed	Davidian *et al* 2008
Ethyl Propionate, Ethyl Lactate, Propionic Acid, Lactic Acid	Rh, Pt supported by Al_2O_3, SiO_2, Ce, La	Monolith	Rennard *et al* 2008
Acetic acid and acetone	Ni, Rh or Ir supported by $CaO^{\cdot 2}Al_2O_3$ and $12CaO\cdot^{7}Al_2O_3$	Quartz tube reactor	Vagia *et al*, 2008
Bio-oil (sawdust)	Dolomite, Ni/MgO commercial catalyst	Two-stage fixed bed reactor system,	Wu *et al.*, 2008
Bio-oil	Pt, Rh supported by $Ce0.5Zr0.5O_2$	Packed Monolith	Iojoiu *et al* 2007
Ethylene glycol	Ni supported by Olivine	Fluidized bed	Kechagiopoulos *et al* 2007
Bio-oil	$C_{12}A^{7\cdot}O^{-}$-based catalysts	fixed bed	Zhaoxiang *et al.*, 2007
Phenol	Rh supported by MgO, Mg-Ce-Zr-O	Packed	Polychronopoulou *et al* 2006
Acetic Acid	Pt supported by ZrO_2	Packed	Takanabe 2006
Acetic Acid, Acetol	Ni supported by Al_2O_3, La_2O_3, Co	Fluidized bed	Galdámez 2005

6- SOOT FORMATION AND OXIDATION

Soot is one of the main pollutants generated in biomass thermal conversion processes. In this thesis we are interested also in the soot formation and oxidation. This last part of the literature is dedicated to soot.

6-1 Introduction

Soot formation is a very complex phenomenon involving homogeneous and heterogeneous processes. Soot is a carbon solid that can be produced in combustion systems when the local environment is sufficiently fuel-rich. Soot may represent a problem during operation of engines because it can generate solid deposits, for example, in valve engines **[Bozzano 02]**.
Soot is an important pollutant itself as a low size particle, and therefore breathable, but also because, due to its structure, it may act as a condensation nucleus of polyaromatic hydrocarbons (PAHs) and other organic substances **[Ambrogio 02]**. Apart from the undesired effects of soot, it has also been mentioned to be interesting as a possible NO_x reduction agent **[Bilbao 94]**.

Soot formation can be desirable within the combustion chamber, because it favors heat transfer due to its high radiation capacity and because it may reduce the NO levels, but soot particles should be eliminated before exiting the combustion device. Soot formation has been extensively studied in the past years in different experimental devices, such as flames, shock wave reactors, and flow reactors using different fuels as soot precursors, such as methane and other hydrocarbons and mainly also diesel fuels (e.g. **[Bockhorn 94] [Richte 00] [Skjøth-Rasmussen 02] [kjøth-Rasmussen 04]**), but the literature on soot formation from biomass remains poor. Because of soot formation complexity, a number of uncertainties still remain. While significant progress has been achieved in relation to the determination of its physical and chemical characteristics, significant uncertainty still remains concerning formation, growing and reduction under different conditions. In particular, the formation of soot implies a number of complex physical and chemical processes that control the conversion of gaseous fuel into solid particles that are not well known at present **[Kennedy 97]**. The most accepted theory for soot formation is well described by Haynes and Wagner **[Haynes 81]**, in which the pyrolysis of hydrocarbons produces smaller hydrocarbons, acetylene in particular. The initial step is the formation of the first aromatic species from the aliphatic hydrocarbons, followed by the addition of other aromatic and alkyl species to give higher species, i.e. PAHs. The

continued growing of these PAHs results in the generation of the smallest soot particles with diameters of the order of 1nm and a mass of around 500–2000 uma **[Bozzano 02]**. The formation of PAHs is a key issue and is of huge interest today. It is believed to follow the HACA (H_2 abstraction, C_2H_2 addition) route **[Frenklach 02] [Frenklach 94]**, even though there are some other different theories for PAHs growth and soot formation **[Krestinin 00]**.

During its formation and also once soot is formed, it can react with several gases such as O_2, CO_2 or H_2O and be gasified. The soot reactivity to these gases is directly related to its structure and composition. Properties such as surface area, particle size and crystallinity affect soot particles reactivity. Soot nanostructure depends on its formation conditions, like fuel origin, residence time and temperature. An understanding of these dependences is fundamental to control the physical properties of the soot and therefore, its chemical reactivity **[VanderWal 04] [Murr 05] [Grieco 00] [Grieco 92]**. The following section gets into details about soot formation an oxidation mechanism.

6-2 Soot formation

A significant research effort on PAH and soot has been undertaken during recent years. Although many important details of PAH and soot formation remain poorly understood, there is considerable agreement on the general features of the processes involved, which are schematically summarized in Figure 17 **[Bockhorn 94]**.

a- Formation of molecular precursors of soot

The molecular precursors of soot particles are thought to be heavy PAHs of molecular weight 500–1000 amu. The growth process from small molecules such as benzene to larger and larger PAH appears to involve both the addition of C2, C3 or other small units, among which acetylene has received much attention, to PAH radicals, and reactions among the growing aromatic species, such as PAH–PAH radical recombination and addition reactions.

The presence of hydrogen enables the creation of free radicals. Two free radicals are created whenever a hydrogen atom hops from one carbon site to another. This can happen in a concerted reaction whereby the large energy cost of breaking a C–H bond is offset by the energy gained in making another C–H bond, thereby mitigating the total energy cost and creating two radicals. Free radicals rapidly rearrange the carbon skeletal structure and just as rapidly are eliminated by recombination. Therefore, the presence of hydrogen acts as a sort of a facilitator or catalyst continually supplying free radicals that drive the rearrangement process.

The same hydrogen exchange process that creates the free radicals also produces molecular hydrogen inside the precursor soot matrix that can diffuse out and eventually deplete the particle matrix of hydrogen. This process is called dehydrogenation.

Precursor soot as its name implies is an integral step in the production of mature soot. Conversion of precursor soot into mature soot occurs by rapid loss of hydrogen with concurrent rearrangement of the carbon skeletal structure (the carbonization process). Precursor soot can be formed during the pyrolysis of any hydrocarbon species.

Firstly, the hydrocarbon fuel species pyrolyze to form gas phase polycyclic aromatic hydrocarbons (PAHs) through these the stepwise addition of two and three carbon-containing species **[Bockhorn 94]**. Under the right conditions, the PAHs chemically condense to form three-dimensional nanoparticles with some very unusual properties. The liquid nature of precursor soot permits coalescence of the droplets to form larger singlet particles. This is yet another mechanism for rapid particle growth that helps explain the ability of the precursor soot to grow to observed micrometer sizes on millisecond timescales in flames **[Reilly 00]**.

b- Nucleation or inception of particles from heavy PAH molecules

In this process mass is converted from molecular to particulate systems, i.e. heavy PAH molecules form nascent soot particles with a molecular mass of approximately 2000 amu and an effective diameter of about 1.5 nm. Chemical details of the formation of nascent soot particles are relatively poorly understood, mostly because of experimental difficulties.

c- Mass growth of particles by addition of gas phase molecules

After the formation of the nascent soot particles their mass is increased via the addition of gas phase species such as acetylene and PAH, including PAH radicals. These reactions are believed to involve radical sites on the soot particles in the case of stable reactants such as acetylene and stable PAH but not necessarily in the case of PAH radicals. This process of course does not affect the number of soot particles.

d- Coagulation via reactive particle–particle collisions

Sticking collisions between particles during the mass growth process significantly increases particles size and decreases particle number without changing the total mass of soot present. The continuation of substantial molecular addition of gas phase species after the early

formation of composite particles via sticking particle–particle collisions, partly hides the identity of primary particulate units in electron microscopy images of soot particles.

e- Carbonization of particulate material

At higher residence times under pyrolytic conditions in the postflame zone, the polyaromatic material comprising the yet formed particles undergoes functional group elimination, cyclization, ring condensation and ring fusion attended by dehydrogenation and growth and alignment of polyaromatic layers. This process converts the initially amorphous soot material to a progressively more graphitic carbon material, with some decrease in particle mass but no change in particle number.

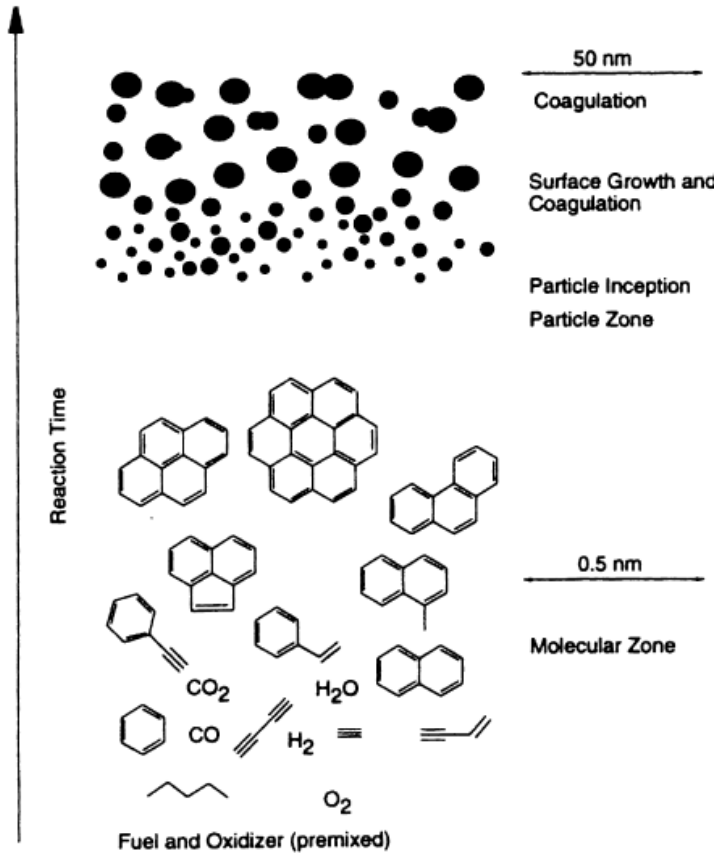

Figure 17. A rough picture for soot formation in homogeneous mixtures **[Bockhorn 94]**

6-3 Composition and structure of soot

The ultimate analyses of typical diesel soot and the same material degassed at 13 mPa for 5h at 150°C **[Marcucilli 94]** are given in Table 6. Carbon is the predominant compound followed by oxygen. The sulphur was apparently present as compound adsorbed onto the surface (as sulphates), whereas the oxygen was strongly bonded.

Table 6. Typical soot analyses **[Neeft 96]**

Element	C	H	N	O	S
Virgin soot	83.5	1.04	0.24	10.5	1.13
Degassed soot	83.8	0.85	0.22	10.7	0.10

FTIR analysis revealed the presence of C=O, C–O–C and C–OH bonds, and some aromatic structures.

Soot as sampled is found to be in the form of agglomerates which are around 100 µm in size. These agglomerates are composed of smaller, very open „particles‘, which are in turn a collection of smaller carbonaceous spherules. The terms agglomerate (100 µm typical size), particle (0.1–1 µm) and spherule (10–50 nm) will be used for these three scales of particulate. Figure 18 is a micrograph of some typical particles, showing the individual spherules.

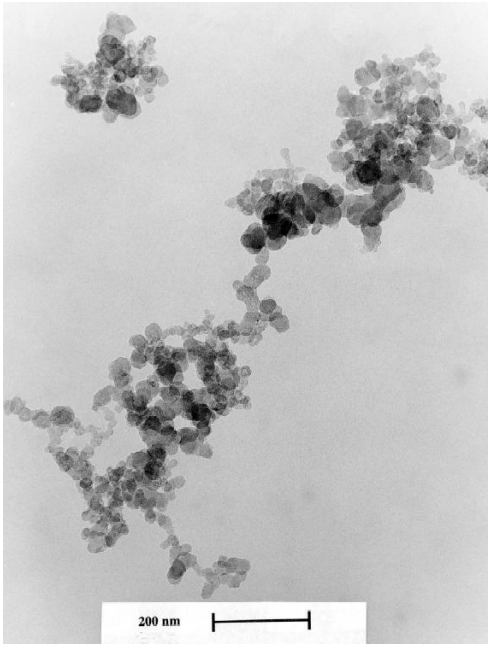

Figure 18. Micrograph of diesel soot, showing particles consisting of clumps of spherules **[Neeft 96]**

Ruiz et al. **[Ruiz 07]** studied the influence of temperature on the properties of the soot formed from C_2H_2 pyrolysis at temperature range of 1000–1200°C pictured in Figure 19. Particle size determination is achieved through transmission electron microscopy (TEM) micrographs analysis. Two particle size ranges can be distinguished: 150–220 nm for the soot samples formed at 1000 and 1050°C, and 75–110 nm for the soot samples formed from 1100 to 1200°C. Therefore, the particle average size decreases when the formation temperature increases. These morphological phenomena are attributed to the shrinkage of the outer shell **[Kim 03] [Richter 00] [Zhu 00]**. This process converts the initially amorphous soot material to a progressively more graphitic carbon material with some decrease in particle size.

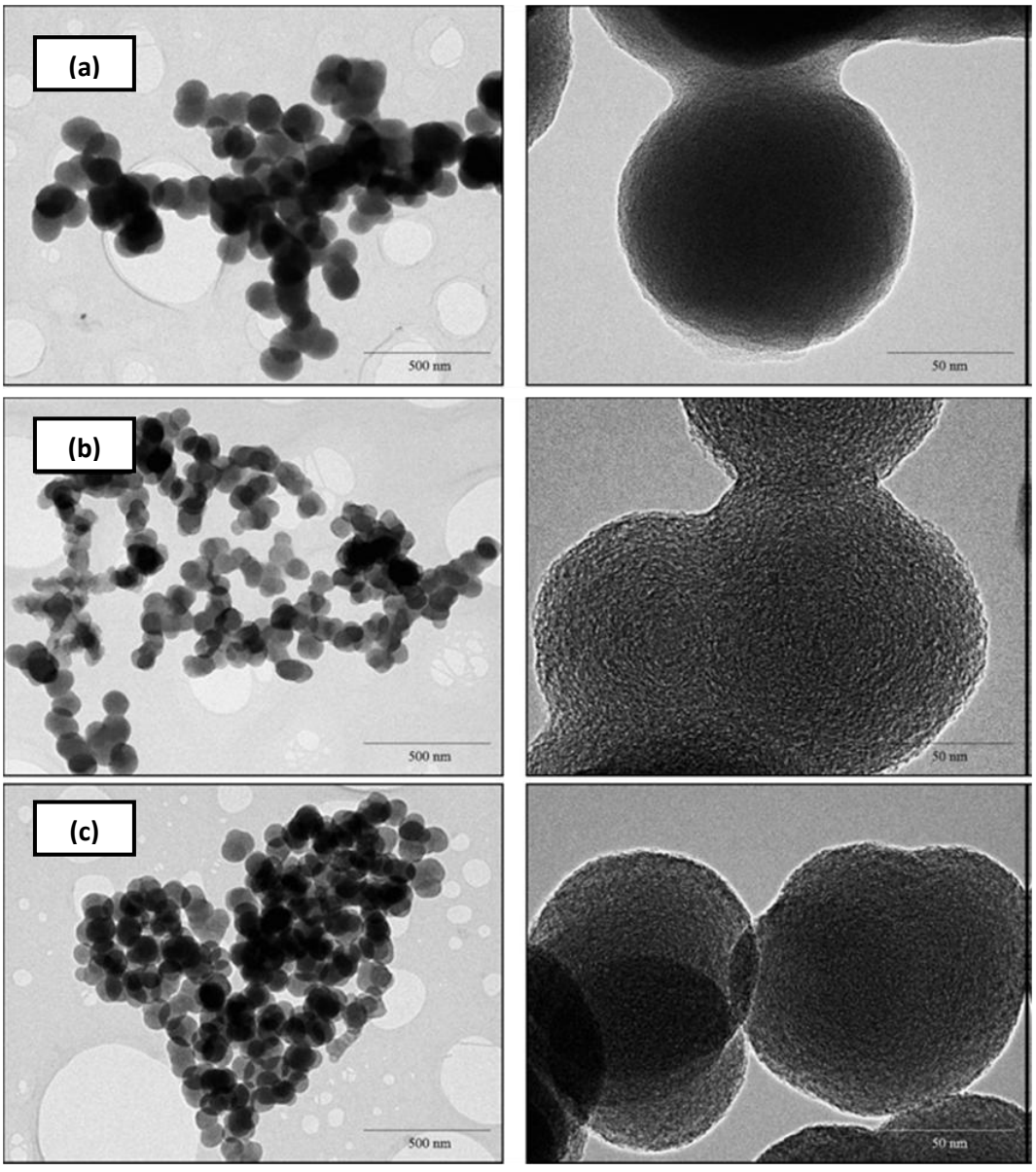

Figure 19. TEM images of the soot samples obtained at different temperatures: (a) 1000°C; (b) 1100°C; (c) 1200°C **[Ruiz 07]**

6-4 Soot gasification

The action of the oxidants O_2, H_2O, CO_2, NO, N_2O and NO_2 involve at least two steps:
(i)- An O-atom is transferred from the gas to form a solid complex;
(ii)- The complex decomposes and a C-atom is lost from the surface. The two-step sequence involves oxidant at each step and produces carbon monoxide. The dominant parameter is oxygen occupancy, which is a function of the oxidant.

a- Oxidation with oxygen (combustion)

Oxidation of PAH and soot particles is a process competing with the formation of these species. It decreases the mass of PAH and soot material through the formation of CO and CO_2. Detailed investigations on carbon oxidation show that molecular O_2 and the O and OH radicals all participate in soot oxidation **[Cavaliere 94]**. OH is particularly effective **[Lee 62] [Roth 90]**. Roth et al. **[Roth 91]** showed that hydrogen peroxide favors soot oxidation at low temperatures, due to the presence of high concentrations of OH radical.

b- Oxidation with steam, carbon dioxide (gasification)

Gasification of soot produced from aromatic and aliphatic hydrocarbons with water vapour and carbon dioxide was studied by de Soete **[de Soete 88]**. There was negligible reaction with H_2O below 800 K and the major product at higher temperatures was CO. Regarding kinetics, the order of reaction with respect to H_2O was close to one. The gasification rates with carbon dioxide were lower than those with water vapour. The reaction order for CO_2 was again one, and the ratio CO/CO_2 was close to 1. De Soete **[de Soete 88]** showed that the trends in the reaction of soot with H_2O and CO_2 are similar to those with oxygen, but at a reduced rate of reaction.

REFERENCES

[Abdullah 10] Abdullah M, Khairurrijal, Noor F A, Marully A R, Sanny M. Design of Steam Reforming Reactor for Converting Methanol into Hydrogen Using an Ultrasonic Nebulizer as Liquid Feeder and Polymer Liquid Processed CuO/ZnO/Al2O3 Particles as Catalyst. Journal of Sustainable Energy & Environment 2010;1:11-15.

[Alves 89 a] Alves S S, Figueiredo J L. Kinetics of cellulose pyrolysis modelled by three consecutive first-order reactions. Journal of Analytical and Applied Pyrolysis 1989;7:37-46.

[Alves 89 b] Alves S S, Figueiredo J L. Interpreting isothermal thermogravimetric data of compex rections: Application to cellulose pyrolysis at low temperature. Journal of Analytical and Applied Pyrolysis 1989;15:347-455.

[Ambrogio 02] Ambrogio M, Saracco G, Specchia V, Gulijk C, Makkee M, Moulijn J A. On the generation of aerosol for diesel particulate filtration studies. Sep. Purif. Technol. 2002;27: 195-209.

[Antal 95] Antal M J J, Gabor V. Cellulose Pyrolysis Kinetics: the Current State of Knowledge. Ind. Eng. Chem. Res 1995;3:703-717.

[Ba 04 a] Ba T, Chaala A, Pérez MG, Rodrigue D, Roy C. Colloidal properties of bio-oils obtained by vacuum pyrolysis of softwood bark. Characterization of watersoluble and water-insoluble fractions. Energy Fuel 2004;18:704-12.

[Ba 04 B] Ba T, Chaala A, Pérez MG, Roy C. Colloidal properties of bio-oils obtained by vacuum pyrolysis of softwood bark, Storage stability. Energy Fuel 2004;18:188–201.

[Basu 06] Basu P. Combustion and gasification in fluidized beds, USA. CRC press Taylor and Francis group 2006.

[Bilbao 94] Bilbao R, Millera A, Alzueta M U. Influence of the Temperature and Oxygen Concentration on NOx Reduction In The Natural Gas Reburning Process. Ind. Eng. Chem. Res. 1994;33:2846–2852.

[Bimbela 09] Bimbela F, Oliva M, Ruiz J, Garcia L, Arauzo J. Catalytic steam reforming of model compounds of biomass pyrolysis liquids in fixed bed: Acetol and n-butanol. J. Anal. Appl. Pyrolysis 2009:85:204-213.

[Bridgwater 93] Bridgwater A V, Evans G D. An Assessment of Thermochemical Conversion Systems For Processing Biomass and Refuse. Energy Technology Support Unit (ETSU) on behalf of the Department of Trade 1993, ETSU B/T1/00207/REP.

[Bridgewater 99] Bridgewater A V, Meier D, Radlein D. An overview of fast pyrolysis of biomass. Org Geochem 1999;30:1479-93.

[Bridgewater 99] Bridgwater A V, Bridgwater S V, Czernik S, Diebold J, Meier D, Oasmaa A, Peacocke C, Piskorz , Radlein D Eds. An introduction to fast pyrolysis of biomass for

fuels and chemicals, in Fast pyrolysis of biomass: a handbook. CPL Press, Newbury, Berkshire 1999;1-13.

[Bockhorn 94] Bockhorn H (Ed.). Soot Formation in Combustion: Mechanisms and Models. Springer Verlag, Heidelberg 1994.

[Bozzano 02] Bozzano G, Dente M, Faravelli T, Ranzi E. Fouling Phenomena in Pyrolysis and Combustion. Processes Appl. Therm. Eng. 2002;22:919-927.

[Broido 76] Broido A. Kinetics of Solid-Phase Cellulose Pyrolysis, Thermal Uses and Properties of Carbohydrates and Lignins, New York. Academic Press 1976;19-35.

[Brown 03] Brown, R. C. (2003). Biorenewable Resources-Engineering New Products from Agriculture, Blackwell Publishing.

[Cavaliere 94] Cavaliere A, Barbella R, Ciajolo A, D'Anna A, Ragucci R. Fuel and soot oxidation in diesel-like conditions. In: Twenty fifth international symposium on combustion, Philadelphia: The Combustion Institute 1994; 67-74.

[Ceres Biofuels 07] Ceres Biofuels. http://www.ceres.net/AboutUs/AboutUs-Biofuels-Carbo.html 2007.

[Chiarello 10] Gian Luca Chiarello, Myriam H Aguirre, Elena Selli. Hydrogen production by photocatalytic steam reforming of methanol on noble metal-modified TiO2. Journal of Catalysis 2010; 273:182-190.

[Choren 09] Choren GmbH. www.choren.com 2009.

[Czernik 04] Czernik S, Bridgwater AV. Overview of applications of biomass fast pyrolysis oil. Energy & Fuels 2004,18:590-598.

[de Jong 03] de Jong W, Unal O, Andries J, Hein K R G. Spliethoff H. Thermochemical conversion of brown coal and biomass in a pressurised fluidised bed gasifier with hot gas filtration using ceramic channel filters: measurements and gasifier modelling. Appl Energy 2003;74:425-437.

[Davidian 08] Davidian T, Guilhaume N, Provendier H, Mirodatos C. Continuous hydrogen production by sequential catalytic cracking of acetic acid Part II. Mechanistic features and characterization of catalysts under redox cycling. Appl. Catal. A 2008;337:111-120.

[de Soete 88] de Soete G. Catalysis of soot combustion by metal oxides. In: Western States section meeting, Salt Lake City, 21–22March, The Combustion Institute 1988.

[Demirbas 01] Demirbas A. Biomass resource facilities and biomass conversion processing for fuels and chemicals. Energy Convers Manage 2001;42:1357-78.

[Demirbas 02] Demirbas A, Arin G. An Overview of Biomass Pyrolysis. Energy Sources 2002;24: 471-482.

[Di Blasi 96] Di Blasi C. Heat, Momentum and Mass Transport through a Shrinking Biomass Particle Exposed to Thermal Radiation. Chemical Engineering Science 1996;51:1121-1132.

[Diebold 00] Diebold J P. A Review of the chemical and physical mechanism of the storage stability of fast pyrolysis biooils. NREL report no. NREL/SP-570-27613, National Renewable Energy Laboratory 2000, Colorado, USA.

[Diebold 99] Diebold J P. A review of the chemical and physical mechanisms of the storage stability of fast pyrolysis bio-oils. NREL/SR-570-27613, subcontractor report 1999.

[Evans 87] Evans R J, Milne T A. Molecular Characterization of the Pyrolysis of Biomass. Energy and Fuels 1987;1,123-137.

[Faaij 06] Faaij A P C. Bioenergy in Europe: Changing Technology Choices. Energy Policy 2006; 34:322-342.

[Faulon 94] Faulon J, Carlson G A. A three-dimensional model for lignocellulose from gymno-spermous wood. Organic Geochemistry 1994; 2:1169-1179.

[Fengel 89] Fengel, Dietrich; Gerd, Wegener. Wood Chemistry, Ultrastructure, and Reactions. Berlin-New York: Walter de Gruyter 1989.

[Frenklach 02] Frenklach M. Phys. Reaction mechanism of soot formation in flames. Chem. Chem. Phys. 2002;4:2028.

[Frenklach 94] Frenklach M, Wang H. Soot Formation in Combustion: Mechanisms and Models, Springer Verlag, Heidelberg 1994;165-192.

[Galdámez 05] Galdámez J R, García L, Bilbao R. Hydrogen Production by Steam Reforming of Bio- Oil Using Coprecipitated Ni-Al Catalysts. Acetic Acid as a Model Compound. Energy & Fuels 2005;19:1133-1142.

[Haynes 81] Haynes B S, Wagner H G. Soot formation. Prog. Energy Combust. Sci. 1981;7:229-273.

[Henrich 04] Henrich E, Weirich F. Pressurized Entrained Flow Gasifiers for Biomass. Environmental Engineering Science 2004;21:53-64.

[Güell 09] Güell B M, Babich I, Nichols K P, Gardeniers J G E, Lefferts K, Seshan K. Design of a stable steam reforming catalyst--A promising route to sustainable hydrogen from biomass oxygenates. Applied Catalysis B: Environmental 2009; 90:38-44.

[Grieco 00] Grieco W J, Howard J B, Rainey L C, Vander Sande J B. Fullerenic carbon in combustion-generated soot, Carbon 2000;38:597-614.

[Grieco 92] Grieco W J, Howard J B, Rainey L C, Vander Sande J B. Spectroscopic and chemical characterisation of ~~–f~~ullerene black", Chem. Phys. Lett. 1992;194:62-66.

[IEA06] IEA (International Energy Agency). IEA bioenergy annual report, http://www.energytech.at/pdf/iea_bereport06. pdf 2006.

[Islam 05] Islam M N, Alam Beg M R, Islam M R. Pyrolytic Oil from Fixed Bed Pyrolysis of Municipal Solid Waste and its Characterization. Journal of Renewable Energy 2005;30:413-420.

[Iojoiu 07] Iojoiu E E, Domine M E, Davidian T, Guilhaume N, Mirodatos C. Hydrogen production by sequential cracking of biomass-derived pyrolysis oil over noble metal catalysts supported on ceria-zirconia. Appl. Catal. A 2007;323:147-161.

[Kamm 06] Kamm B, Kamm M, Gruber PR, Kromus S. Biorefinery systems – an overview. In: Biorefineries – industrial processes and products. Wiley-VCH Verlag Weinheim 2006.

[Karaosmanoglu 99] Karaosmanoglu F, Tetik E. Charcoal from the pyrolysis of rapeseed plant straw-stalk. Energy Source 1999;2:503-510.

[Kechagiopoulos 07] Kechagiopoulos P N, Voutetakis S S, Lemonidou A A, Vasalos I A. Sustainable hydrogen production via reforming of ethylene glycol using a novel spouted bed reactor. Catal. Today 2007;127:246-255.

[Kennedy 97] Kennedy I M. Proc. Combust. Inst. 27 (1997) 1557.

[Kim 03] Kim Y A, Hayashi T A, Osawa K, Dresselhaus M S, Endo M. Annealing effect on disordered multi-wall carbon nanotubes. Chem. Phys. Lett. 2003;380:319-324.

[Kirk-Otmer 01] Kirk-Otmer 4th edition 2001; vol 5, 13, 15, 20.

[30 Kobayashi 76] Kobayashi H, Howard J B, Sarofim A F. Coal devolatilization at high temperatures. In Proc. 16th International Symposium on Combustion 1976.

[Koller 03] Koller et al. Plinius the Elder (Caius Plinius Secundus); Naturalis Historiae. Book II, Nature 2003;77:425:784.

[Krassig 02] Krassig H, Schurz J. Ullmann's Encyclopedia of Industrial Chemistry, Sixth edition, Weinheim, Germany, Wiley-VCH 2002.

[Krestinin 00] Krestinin A V. Detailed Modeling of Soot Formation in Hydrocarbon Pyrolysis. Combust. Flame 2000;121:513-524.

[Lan 2010] Lan P, Xu Q, Zhou M, Lan L, Zhang S, Yan Y. Catalytic Steam Reforming of Fast Pyrolysis Bio-Oil in Fixed Bed and Fluidized Bed Reactors. Chemical Engineering & Technology December 2010;33:2021-2028.

[Lear 90] Lear AE, Brown TC, Haynes BS. Formation of metastable oxide complexes during the oxidation of carbons at low temperatures. In: Twenty-third international symposium on combustion, Pittsburgh: The Combustion Institute 1990;23:1191-1197.

[Lee 62] Lee K B, Thring M W, Bee´r J M. On the rate of combustion of soot in a laminar soot flame. Combust Flame 1962;6:137-45.

[Lin 02] Lin S Y, Lin I S. Ullmann's Encyclopedia of Industrial Chemistry, Sixth edition, Wein-heim, Germany, Wiley-VCH 2002.

[Marsh 07] Marsh R, Hewlett S, Griffiths T, Williams K. Advanced thermal treatment for solid waste - a waste manager‘s guide. Proceeding of the 22nd international conference on solid waste management and technology. Philadelphia (USA) 2007.

[Maschio 92] Maschio G, Koufopanos C, Lucchesi A. Pyrolysis, a promising route for biomass utilization. Bioresour Technol 1992;42:219–31.

[Matas Güell 09] Matas Güell B, Torres da Silva I M, Seshan K, Lefferts L. Sustainable route to hydrogen - Design of stable catalysts for the steam gasification of biomass related oxygenates. Appl. Catal. B 2009; 38:1-2.

[60 Matas 09] Matas Güell B, Torres da Silva I M, Seshan K, Lefferts L. Sustainable route to hydrogen - Design of stable catalysts for the steam gasification of biomass related oxygenates. Appl. Catal. B: Environmental 2009;88:59–65

[Marcucilli 94] Marcucilli F, Gilot P, Stanmore B R, Prado G. Experimental and theoretical study of diesel soot reactivity. In: Twenty fifth international symposium on combustion, Philadelphia: The Combustion Institute 1994;619–26.

[Marda 09] Marda J R, DiBenedetto J, McKibben S, Evans R J, Czernik S, French RJ, Dean A M. Non-catalytic partial oxidation of bio-oil to synthesis gas for distributed hydrogen production. international journal o f hydrogen energy 2009; 34:8519–8534.

[Medrano 09] Medrano J A, Oliva M, Ruiz J, García L, Arauzo J. Catalytic steam reforming of model compounds of biomass pyrolysis liquids in fluidized bed reactor with modified Ni/Al catalysts. Journal of Analytical and Applied Pyrolysis 2009 85;214-225.

[Mille 97] Miller R S, Bellan J. A Generalized Biomass Pyrolysis Model Based on Superimposed Cellulose, Hemicelluloses and Lignin Kinetics. Combust. Sci. and Tech 1997;126: 97-137.

[Milne 97] Milne T A, Agblevor F, Davis M, Deutch S, Johnson D. A review of chemical composition of fast pyrolysis oils. Developments in thermochemical biomass conversion. London: Blackie Academic & Professional 1997;409-424.

[Mohan06] Mohan D, Pittman Jr C U, Steele P H. Pyrolysis of Wood/Biomass for Bio-oil: A Critical Review. Journal of Fuel 2006;20:848-889.

[Mohan 06] Mohan D, Pittman Jr C U, Steele P H. Pyrolysis of Wood/Biomass for Bio-oil: A Critical Review. Journal of Fuel 2006;20:848-889.

[Mok 92] Mok WS-L, Antal Jr MJ, Szabo P, Varhegyi G, Zelei B. Formation of charcoal from biomass in a sealed reactor. Ind Eng Chem Res 1992;31:1116–1162.
[Moulijn 01] Moulijn J A, Makkee M, Van Diepen A. Chemical Process Technology. Chichester: John Wiley and Sons Ltd 200.

[Murr 05] Murr L E, Soto K F. A TEM study of soot, carbon nanotubes, and related fullerene nanopolyhedra in common fuel-gas combustion sources, Mater. Charact. 2005;55:50-65.

[Neeft 96] Neeft J P A, Makkee M, Moulijn J A. Diesel particulate emission control. Fuel Proc Technol 1996;47:1-69.

[Northey 98] Northey, B. Wood Chemistry, http://depts.washington.edu/pse406/40inter.htm 1998.

[Panigrahi 03] Panigrahi S, Dalai A K, Chaudhari S T, Bakhshi N N. Synthesis Gas Production from Steam Gasification of Biomass-Derived Oil. Energy Fuels 2003; 17:637-642.

[Pérez 06] Pérez M G, Chaala A, Pakdel H, Kretschmer D, Rodrigue D, Roy C. Multiphase structure of bio-oils. Energy Fuel 2006;20:364-75.

[Polychronopoulou 06] Polychronopoulou K, Efstathiou A M. Spillover of labile OH, H, and O species in the H2 production by steam reforming of phenol over supported-Rh catalysts. Catal. Today 2006;116;341-347.

[Raven 92] Raven, P.H., R.F. Evert, et al. Biology of plants (6th edition). W.H. Freeman and com-pany/Worth Publishers 1992.

[Rennard 08] Rennard D C, Dauenhauer P J, Tupy S A, Schmidt L D. Autothermal Catalytic Partial Oxidation of Bio-Oil Functional Groups: Esters and Acids. Energy & Fuels 2008;22,1318-1327.

[Reed 01] Reed T B, Siddhartha G. A Survey of Biomass Gasification 2001, 2nd edition

[Reilly 00] Reilly P T A, Gieray R A, Whitten W B, Ramsey J M. Direct observation of the evolution of the soot carbonization process in an acetylene diffusion flame via real-time aerosol mass spectrometry. Combust Flame 2000;122:90-104.

[Richter 00] Richter H, Howard J B. Formation of polycyclic aromatic hydrocarbons and their growth to soot—a review of chemical reaction pathways. Prog. Energy Combust. Sci. 2000;26:565-608.

[Roth 90] Roth P, Brandt O, von Gersum S. High temperature oxidation of suspended soot particles verified by CO and CO2 measurements. In: Twenty-third international symposium on combustion, Pittsburgh: The Combustion Institute 1990;1485-1491.

[Roth 91] Roth P, Eckhardt T, Franz B, Patschull J. H O -assisted regeneration of diesel particulate traps at typical exhaust gas temperatures. Combust Flame 1998;115:28-37.

[108 23 Ruiz 07] Ruiz M P, Guzm´an de Villoria R, Millera A, Alzueta M U, Bilbao R. Influence of the temperature on the properties of the soot formed from C2H2 pyrolysis. Chemical Engineering Journal 2007;127:1-9.

[Runkel 51] Runkel R 0 H, Wilke K D. Thermoplastic properties of wood. Holz als roh und werkstoff. 1951:9;260-270.

[Sharma 04] Sharma R K, Wooten J B, Baliga V L, Lin X, Chan W G, Hajaligol M R. Characterization of Chars from Pyrolysis of Lignin. Journal of Fuel 2004;83:1469-1482.

[Skjøth-Rasmussen 02] Skjøth-Rasmussen M S, Glarborg P, Østberg M, Larsen M B, Sørensen S W, Johnsson J E, Jensen A D, Christensen T S. Proc. Combust. Inst. 2002;29:1329-1336.

[Skjøth-Rasmussen 04] Skjøth-Rasmussen M S, Glarborg P, Østberg M, Johaneessen J T, Livbjerg H, Jensen A D, Christensen T S. Combust. Flame 2004;136:91-128.

[Solomon 88] Solomon T W G. Organic chemistry, 4th edition, John Wiley & Sons 1988.

[Spath 03] Spath P L, Dayton D C. Preliminary Screening - Technical and Economic Assessment of Synthesis Gas to Fuels and Chemicals with Emphasis on the Potential for Biomass-DeriVed Syngas; Report No. NREL/TP-510-34929; National Renewable Energy Laboratory, Golden, CO, 2003; http://www.osti.gov/bridge.

[Sun 02] Sun Y, Cheng J. Hydrolysis of lignocellulosic materials for ethanol production: A review. Bioresource Technology 2002; 83:1-11.

[Srivastava 96] Srivastava V K, Sushil, Jalan R K. Prediction of Concentration in the Pyrolysis of Biomass Materials-II. Energy Conversion and Management 1996;37:473-483.

[Stultz 92] Stultz S C, Kitto J B. Steam: it‘s generation and use. The Babcock & Wilcox Company, Barberton, Ohio USA 1992.

[Takanabe 06] Takanabe K, Aika K, Inazu K, Baba T, Seshan K, Lefferts L. Steam reforming of acetic acid as a biomass derived oxygenate: Bifunctional pathway for hydrogen formation over Pt/ZrO2 catalysts. J. Catal. 2006;243:263-269.

[Turkenburg 00] Turkenburg W C, Faaij A. Renewable Energy Technologies. New York, United Nations Development Programme 2000.

[Thunman 02] Thunman H, Leckner B. Thermal conductivity of wood-models for different stages of combustion. Biomass and Bioenergy 2002;23:47-54.

[Vagia 08] Vagia E C, Lemonidou A A. Hydrogen production via steam reforming of bio-oil components over calcium aluminate supported nickel and noble metal catalysts. Applied Catalysis A: General 2008;351:111-121.

[van Rossum07] van Rossum G, Kersten S R A, van Swaaij W P M. Catalytic and Noncatalytic Gasification of Pyrolysis Oil. Ind. Eng. Chem. Res. 2007;46:3959-3967.

[VanderWal 04] VanderWal R L, Tomasek A J. Soot nanostructure: dependence upon synthesis conditions. Combust. Flame 2004;136:129-140.

[Van den 85] Van den Aarsen F G. Fluidised Bed Wood Gasifier Performance and Modeling. PhD Thesis, TU Twente 1985.

[Varhegyi 94] Varhegyi G, Jakab E, Antal M J. Is the Broido-Shafizadeh Moodel for Cellulose Pyrolysis True? Energy&Fuels 1994;8:1345-1352.

[Wang 97] Wang D, Czernik S, Montane´ D, et al. Biomass to hydrogen via pyrolysis and catalytic steam reforming of the pyrolysis oil and its fractions. Ind Eng Chem Res 1997;36:1507–1518.

[Wang 98] Wang D, Czermik S, Chornet E. Production of hydrogen from biomass by catalytic steam reforming of fast pyrolytic oils. Energy Fuels 1998;12:19-24.

[Wei 05] Wei L. Experimental study on the effects of operational parameters of a downdraft gasifier. PhD Thesis, Mississippi State 2005.

[Wu 08] Wu C, Huang Q, Sui M, Yan Y, Wang F. Hydrogen production via catalytic steam reforming of fast pyrolysis bio-oil in a two-stage fixed bed reactor system. Fuel Processing Technology, Dimethyl Ether Special Section 89 2008; 1306-1316.

[Zhaoxiang 07] Wang Z, Pan Y, Dong T, Zhu X, Kan T, Yuan L, Torimoto Y, Sadakata M, Li Q. Production of hydrogen from catalytic steam reforming of bio-oil using C12A7-O-based catalysts. Applied Catalysis A: General 2007;320:24-34.

[Zhu 00] Ci L, Zhu H, Wei B, Xu C, Liang J, Wu D. Graphitization behavior of carbon nanofibers prepared by the floating catalyst method. Mater. Lett. 2000;43:291-294.

CHAPTER 3: MATERIALS AND METHODS

This chapter exposes the different experimental set-ups that were developed and used. The protocols for bio-oil characterization, pyrolysis and gasification are explained. The feeding device and the sampling probes are described in detail. The developed soot quantification device is presented as well.

Note: This chapter contains more detail than the articles that follow, so the reader can skip these parts in the articles.

1- HORIZONTAL TUBULAR REACTOR

The experiments of fast pyrolysis were carried out in a horizontal tubular reactor HTR (Figures 1 and 2). This device allowed carrying out experiments under heating rate conditions which cannot be obtained in thermobalance.

The reactor consists of a double-walled quartz pipe. The length and inside diameters are of 850 mm and 55 mm respectively for the inner tube, and of 1290 mm and 70 mm respectively for the outer tube. The reactor temperature can reach 1100°C.

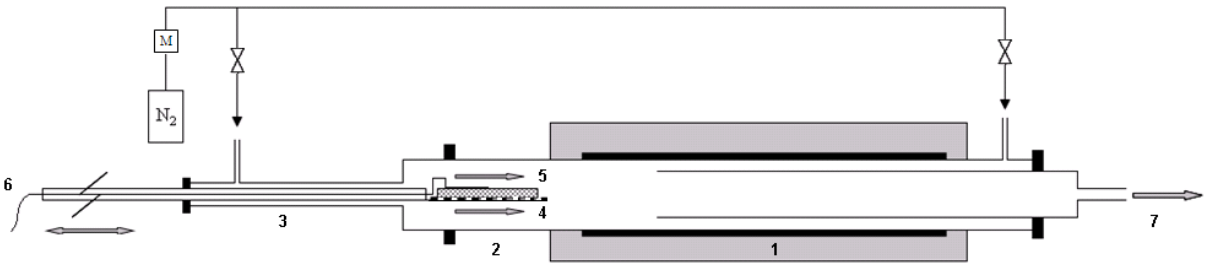

1- Furnace
2- Quartz reactor
3- Movable sample boat
4- Metal grid
5- Refractory wool soaked with 1g of bio-oil
6- Thermocouple
7- Gas outlet
M- Mass flow meters and controllers

Figure 1. Horizontal Tubular Reactor (HTR) ready for sample introduction

Figure 2. Photograph of Horizontal Tubular Reactor

The procedure carried out for an experiment was the following. First, the furnace was heated and the gas flowrate (nitrogen) was adjusted using a mass flow meter/controller. When the temperature was stabilized, the sample was placed on the metal grid at the unheated section of the reactor. This section was swept by half of the total cold nitrogen flow injected, in order to maintain it cold and under inert atmosphere, and therefore avoid its degradation. Meanwhile the second half of the nitrogen flow was preheated through the double-walled annular section of the reactor as shown in Figure 1.

Two sample modalities were selected:

- for studying the effect of temperature and of ash content at low heating rate, 1g of bio-oil was placed inside a crucible of 25mm diameter and 40 mm height;
- to achieve higher heating rates, runs were performed with 1g of bio-oil previously soaked in a refractory wool sample of 100x20 mm length and width and 3 mm thickness. The choice of this sample holder allowed increasing the exchange surface and subsequently obtaining higher heating rates. This wool has no visible catalytic effect on bio-oil pyrolysis under the explored conditions. Indeed, previous bio-oil pyrolysis experiments were carried out first in a crucible, and secondly in the refractory wool. The wool did not induce any change on the products yields.

The reactor outlet was first connected to an O_2 gas analyser to indicate when there is no more oxygen in the reactor. Afterwards, the sample was introduced in the furnace. The sample then remained in the middle of the reactor during a definite time and was then brought back out of the furnace; the solid residue was weighed after cooling.

The reactor outlet was connected to a sampling bag at t = 0 just before sample introduction in the furnace. The gases formed by pyrolysis were collected in the bag. By knowing duration of the experiment the volume of N_2 content in the bag was known accurately. After the experiment the bag was disconnected from HTR, and connected to the micro-chromatograph analyser (μGC). From the total volume of gas in the bag and the measurement of the different gas species concentrations, the mass yield of each gas coulds accurately calculated.
Due to the lack of direct measurement, the tar yield is considered as equal to the difference between the virgin bio-oil and the sum of the yields of gas and of solid residue.

The obtained solid residue in the crucible is a very voluminous porous body. This is due to known phenomena of swelling and micro-explosion which underwent inside the sample of bio-oil during its temperature increase. Figure 3 shows the photograph of the sample before pyrolysis and the solid formed after pyrolysis when using the crucible.

Before pyrolysis After pyrolysis

Figure 3. Bio-oil sample before and after pyrolysis

2- ENTRAINED FLOW REACTOR

A laboratory scale high temperature entrained flow reactor HT-EFR was used in this work. The HT-EFR consists in a vertical tubular reactor electrically heated by a total 18 kW three-zones electrical furnace, and is able to reach 1600°C in a 1m long isothermal reaction zone. Figures 4 and 5 present respectively a schematic representation and a photograph of EFR.

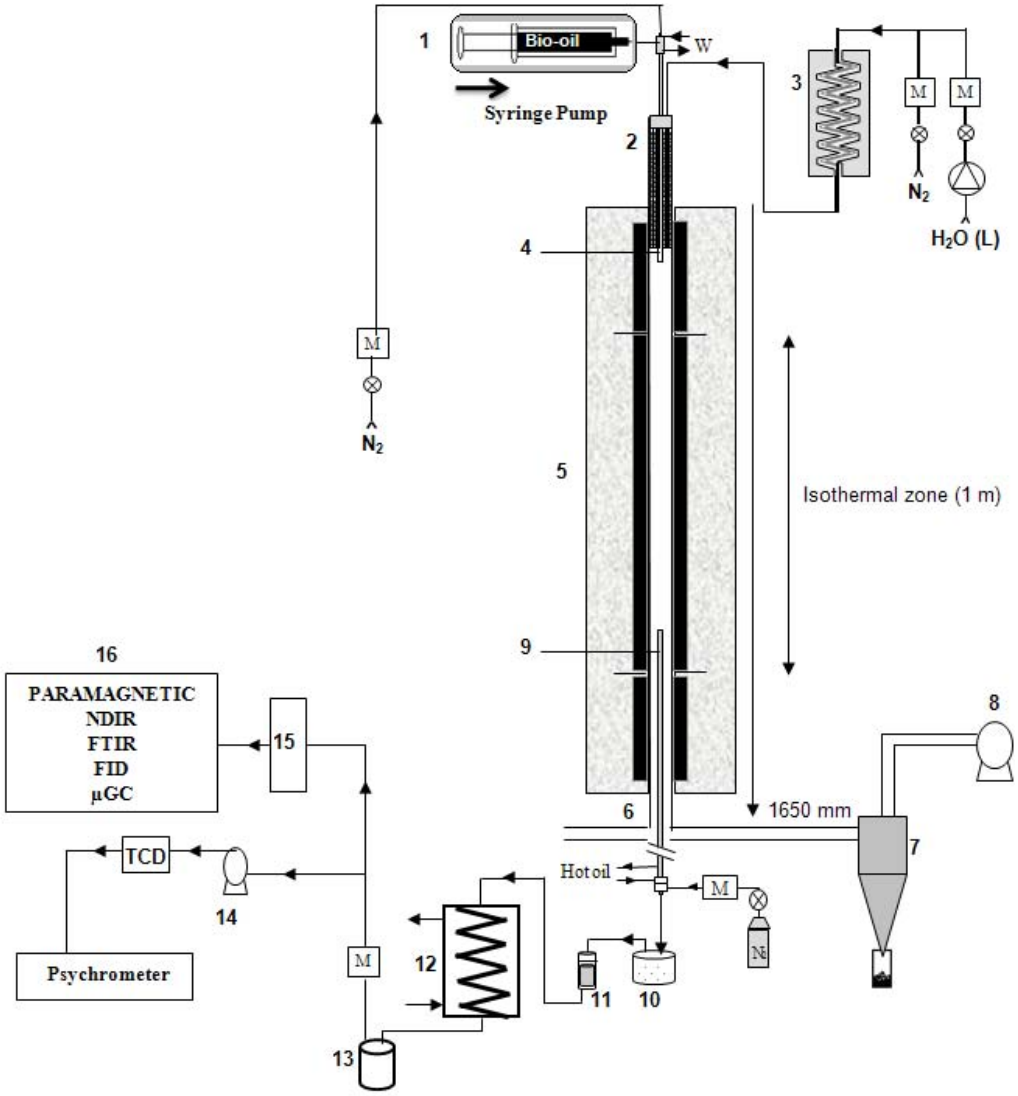

1- Injection system
2- Electrical preheater
3- Steam generator
4- Water cooled feeding probe
5- Three zones electrical furnace
6- 75 mm i.d. alumina reactor
7- Cyclone collector
8- Exhaust fan
9- Water cooled sampling probe
10- Hot settling box
11- Hot particle collector (filter)
12- Water cooler
13- Condensate collector
14- Sampling pump
15- Gas dryer
16- Gas analysers

M - Mass flow meters and controllers
N_2 - Nitrogen
W - Water (probes cooling)

Figure 4. Schematic view of the entrained flow reactor of Ecole des Mines d'Albi

Figure 5. Photograph showing the position of the reactor (HT-EFR) in the facility

The atmosphere gas is generated by feeding the controlled flow of nitrogen in a 2 kW electrical steam generator. This atmosphere gas is then preheated to 900°C using a 2.5 kW electrical battery of heating elements before reaching the isothermal reaction zone. The HT-EFR was initially set up to achieve high heating-rate gasification of solid biomass, and was equipped for the present work with a specially designed bio-oil pulverization feeder, in order to obtain a very constant mass flowrate spray.

The feeder consists of a 1 m long and 14 mm o.d. probe cooled with water at 30°C. At its end a commercial stainless steel nozzle is integrated. This allows uniform distribution with fine atomization. Nozzle type (DELAVAN WDB) is a solid cone, with orifice diameter of 0.46mm and a spray angle of 60°.

The oil is fed with a syringe which is automatically pushed. The expected mass flowrate of 0.3 g/min was too low for direct pulverization. Therefore, a 3.5 $NL.min^{-1}$ N_2 flowrate was used to entrain oil in the feeding probe and to ensure a thin spray of the oil. The spray of droplets is dispersed on the section of a 75 mm i.d. alumina reactor swept by 15 $NL.min^{-1}$ of atmosphere gas. Reactions take place along the reactor during a controlled gas residence time, which was of about 3-4s. The residence time of droplets or solid residue after reaction is

assumed to be similar to that of the gas because of the very small particle size. The gas residence time was calculated as the ratio of the reaction zone length to the average gas velocity in the reactor. At 1650 mm downstream of the injection point, gases and solid residue were sampled by a hot-oil cooled probe at 150°C. Gas and solid residue were separated using a settling box and a filter, both heated to avoid water condensation. The water and potential remaining tars were first condensed in a heat exchanger, and non-condensable gases were forwarded to a micro-chromatograph analyser (μGC) to quantify H_2, CO, CO_2, CH_4, C_2H_2, C_2H_4, C_2H_6, C_3H_8 and C_6H_6. The μGC offers excellent resolutions of all analyze species at higher concentrations with repeatability of ± 2 percent relative standard deviation, the system offers also a minimum detectable quantity of about 10 ppm for most gases species.

Gases were also analyzed by other analyzers that allowed to check the absence of O_2, to confirm the analysis and to control continuously gas production: a Fourier Transform InfraRed (FTIR) analyser, a Non-Dispersive InfraRed (NDIR) analyser coupled with a paramagnetic analyser for O_2 and a Thermal Conductivity Detector (TCD) to quantify H_2.

a- Steam generator

To perform experiments in the presence of steam, a steam generator was installed on the platform. It consists of a spiral tube of 9m in length and 14 mm in diameter. Two electric heaters of 1.8 kW of power heat the tube. The device is thermally insulated, and a control system keeps the steam outlet temperature at 180°C. This generator is shown in Figure 6.

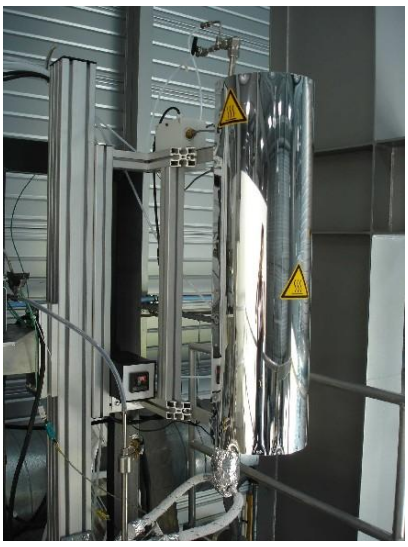

Figure 6. Photograph of steam generator

Steam is then injected into the electric preheater. The bio-oil feeding probe is placed in the axis of the preheater. To prevent coking (formation and deposition of solid carbon) of the bio-

oil, the feeding probe is cooled at 30°C by a thermostatically controlled water bath at 30°C. This device is shown in Figure 7.

Figure 7. Photograph of thermostatically controlled water bath

b- Gas flow preheater

The gas preheater is constituted of 10 spiral resistors of 2.4 kW total power, which are placed in 10 alumina tubes maintained around a central tube. The gas preheating is insured by convective heat exchange. The temperature control is achieved with a thermocouple placed between the tubes and measuring the temperature at the outlet of the preheater. This device is shown in Figure 8.

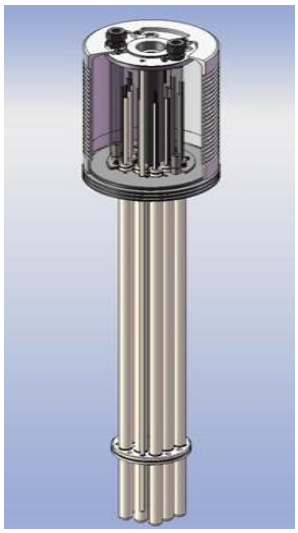

Figure 8. Scheme of gas flow preheater

c- Dosing and injection of oil

The dosing of bio-oil is performed by a programmable syringe pump (Figure 9). We had to equip it with a balancing-jack to compensate the force resulting from the pressure inside the syringe that injects bio-oil into the feeding probe.

The expected mass flowrate of 0.3 g/min was too low for direct pulverization. Therefore, a 3.5 $NL.min^{-1}$ N_2 flowrate was used to entrain oil in the feeding probe and to ensure a thin spray of the oil. This flow of nitrogen also contributes towards the cooling of the nozzle.

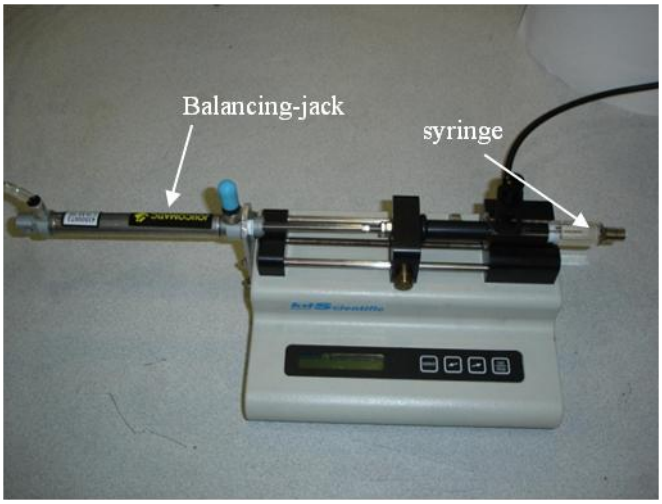

Figure 9. Photograph of programmable syringe pump equipped with a jack-balancing

Before the beginning of the PhD, a first liquid injection system was developed in order to pulverize the liquid and especially pyrolysis bio-oils. A first feeding probe was designed and manufactured for this purpose. It consisted of two coaxial tubes. In the central tube of 4mm inside diameter circulating bio-oil and nitrogen, and in the annular space circulates cooling liquid. At the end of the feeding probe of 1 m long and 14 mm outer diameter is screwed a solid cone stainless steel nozzle (Figure 10).

Figure 10. Photograph of a solid cone stainless steel nozzle

An irregular flow of bio-oil was found at the nozzle exit. In order to have a regular spraying during a long period feeding probe was filled with sand grains of 1 mm diameter in order to minimize dead volumes. A sieve grid was placed between the sand grains and the nozzle to prevent clogging of the nozzle.

The first injection tests have led to the plugging of both the tube filled with sand and the injection nozzle due to the coking process. These problems were attributed to improper cooling of the probe and of the nozzle which is in direct contact with the heated atmosphere.

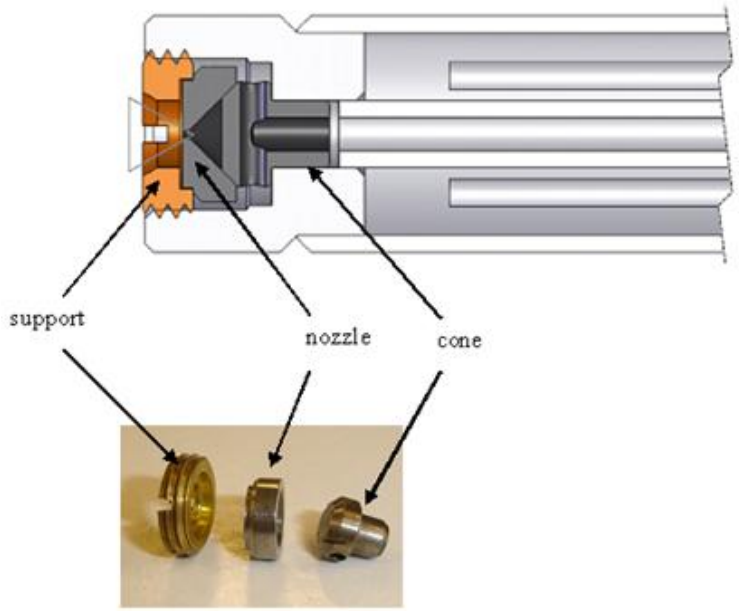

Figure 11. New configuration of the nozzle integrated into the probe

To overcome these problems, the oil bath was replaced by a thermostatically controlled water bath to ensure better cooling of the probe. Indeed, the flow of water (less viscous) was higher, and the specific heat of water is greater than that of oil. In order to limit the heat exchange between the bio-oil and the walls of inner tube, a flexible silicone tube of 4 mm outer diameter and 2 mm internal diameter was placed inside the tube. The temperature of the water bath could be lowered to 30°C. With these improvements on the feeding probe, injection experiments have been conducted, but the nozzle was still plugged during several experiences, and further improvements in nozzle were necessary.

During the first phase of my thesis, a new injection system has been designed to ensure better cooling of the spraying nozzle. On this new feeding probe (1 m long, 14 mm outer diameter) the inside tube has a smaller diameter: 2 mm, and it is not filled with sand. Two small pieces taken from the solid cone stainless steel nozzle, the nozzle and the cone with slots are integrated within the end of the probe (Figure 11)

Cold tests have shown a steady spray of bio-oil with this new configuration of the feeding probe (rod out of the RFE-HT). Figure 12 shows a photograph of the impact of the cold spray of bio-oil on a plane surface that was moved along at a distance of 10 cm from nozzle. The microscopic observation of drops indicates a size ranging between 10 and 100µm. It should be noted that only the larger droplets impacting on the surface because the fine droplets are removed with air.

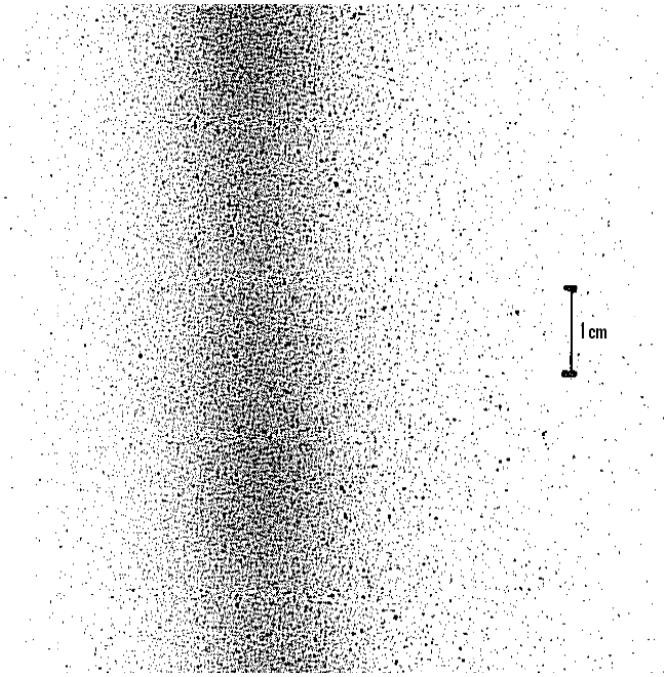

Figure 12. Photograph of the impact of cold spray of bio-oil on a plane surface.

After several injection experiments with unfiltered crude bio-oil, clogging problem appeared again. Two explanations were found:

- clogging due to fine solid particles present in the bio-oil;
- clogging due to carbonization of bio-oil at the nozzle.

Figure 13 shows the nozzle covered by a deposit of carbon formed by carbonization.

Figure 13. Spray nozzle removed after clogging by carbonization

Indeed we were led to the stop the transport nitrogen in order to change the syringe when empty. The nozzle is then less cooled and clogging took place at that time. For further tests, a

valve was placed between the syringe and the needle and enabled to change the syringe without stopping the transport nitrogen. Furthermore, bio-oil was first filtered through a 40µm sieve to remove solid particles.

In addition of the improvements made, cleaning the probe with a solvent after each injection of bio-oil has allowed us to address the problems of clogging.

d- Sampling device

Sampling of gas and solids can be made through two different sampling probes; both are oil-cooled in order to stop the chemical reactions:

- a sampling probe designed specifically to sample the gas at different heights, with a good control of residence time;
- an "exchanger" sampling probe designed specifically to collect solid residue (char and soot).

- **Sampling probe**

The sampling probe shown in Figure 14 is made of stainless steel and measures 1.8 m in length with inner diameter of 12 mm and outer diameter of 34 mm. The cooling oil is supplied at the end of the probe by three tubes of 1 mm internal diameter. The outer shell of the probe is insulated by ceramic wool to avoid the intense exchange heat with the reactor walls.

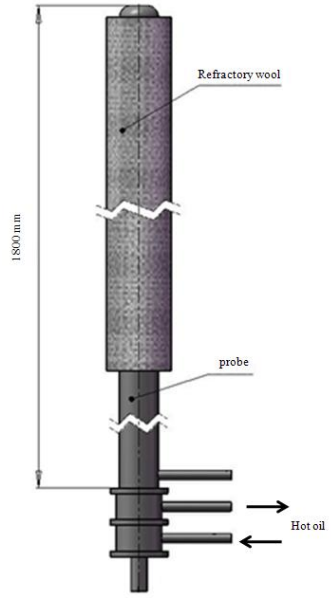

Figure 14. Sampling probe

- **“Exchanger” sampling probe**

The experiments concerning the quantification of solid (char or soot) conducted in the reactor required the collection of the solid products. For that purpose, an "exchanger" sampling probe was used (Figure 15). This probe is composed of an outer cylinder of 60.3 mm diameter and features 19 stainless steel tubes of 8mm internal diameter. Because of its large diameter (similar to that of the reactor) this probe can disrupt the temperature of the reactor. Hence, it was designed for sampling at the reactor outlet only.

Figure 15. “Exchanger” sampling probe

e- Determination of gas residence time

The residence time is defined by:

$$t_g = \frac{h}{v_g} \quad (1)$$

With

t_g gas residence time (s)

h height of the reaction zone (m)

v_g mean velocity of the gas in the reactor (ms^{-1})

The height of the reaction zone is the distance between bio-oil injection and the sampling probe. In the calculation of the mean velocity of gas, two assumptions were made:

- The gas is isothermal and at the reactor temperature;
- For the calculation of the residence time, the change in gas flow rate due to chemical reactions is neglected compared to the atmosphere gas flow rate.

From the ideal gas law, the volumetric flow of the gas atmosphere is fixed in the operating conditions. The volumetric flow of gas into the reactor can be calculated in $m^3.s^1$:

$$Q_{\text{gas vol}} = Q_{\text{N gas vol}} \times \frac{T_{\text{reactor(K)}}}{T_{\text{ref(=273 K)}}} \times \frac{P_{\text{ref}}}{P_{\text{reactor}}} \times \frac{1}{60} \quad (2)$$

With

$Q_{\text{gas vol}}$	volumetric flow of the gas ($m^{3}.s^{-1}$)
$Q_{\text{N gas vol}}$	volumetric flow of the gas ($Nm^{3}.min^{-1}$)
P_{reactor}	pressure in the reactor (Pa)
P_{ref}	reference pressure (10^5Pa)
T_{reactor}	temperature of the reactor (K)

The mean velocity of the gas in the reactor can then be deduced:

$$V_g = \frac{Q_{\text{gas vol}}}{\frac{\pi d_{\text{reactor}}^2}{4}} \quad (3)$$

With d_{reactor} reactor diameter (m)

However, the gas mean velocity in the sampled section is different from the mean velocity of the total flow in the reactor. Indeed, only two thirds of the total flow of the reactor is sampled. This flow is chosen sufficiently large to ensure a good representativity of the sample. A correction factor has been established and taken into account.

Several important points may be highlighted concerning the sampling and measurements:

- The total gas flowrate at the exit of the reactor is calculated based upon the N_2 flowrate fed into the reactor and upon the produced gas species concentrations that are

measured. A mass balance was used to calculate the total flowrate and the mass yield for each gas species.

- Due to the lack of direct measurement, the tar yield is considered as equal to the difference between the virgin bio-oil and the sum of the yields of gas and solid residue.
- Zero O_2 concentration in the outlet gas before bio-oil injection is used to check that there is no air leakage in the reactor.

3- SOOT QUANTIFICATION DEVICE

Laser extinction was used to make quantitative measurements of soot content in the produced gas. The setup is shown in Figure 16 and detailed in Figure 17. For laser extinction, a modulated 50 kHz, 0.5mW, HeNe laser beam (632.8 nm) is passed through sooting region (optical path of 75 mm) and collected by an integrating sphere, narrow band pass filter, and a photodiode. This collection system accounts for beam-steering effects caused by refractive index gradients and minimizes background interference from soot luminosity **[Musculus 02, Pickett 02]**.

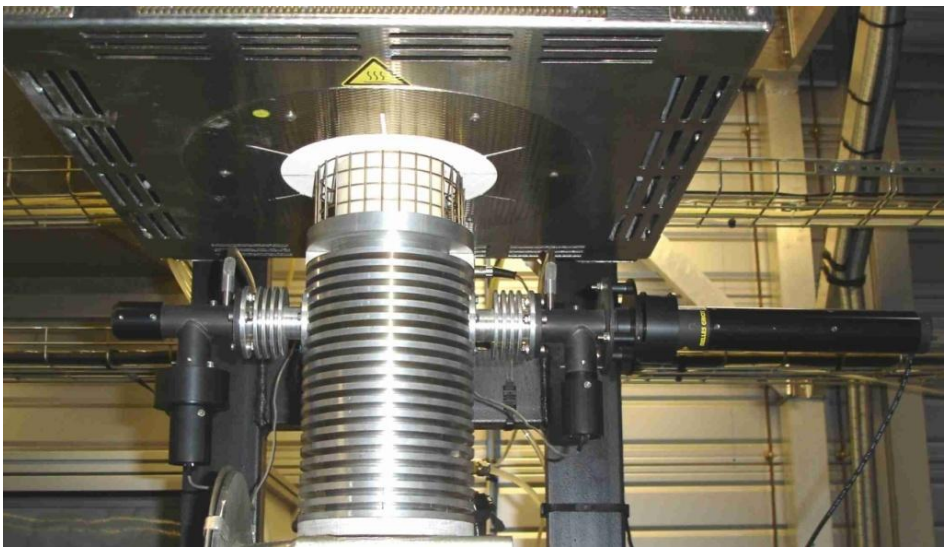

Figure 16. Photograph of the optical setup for soot measurements

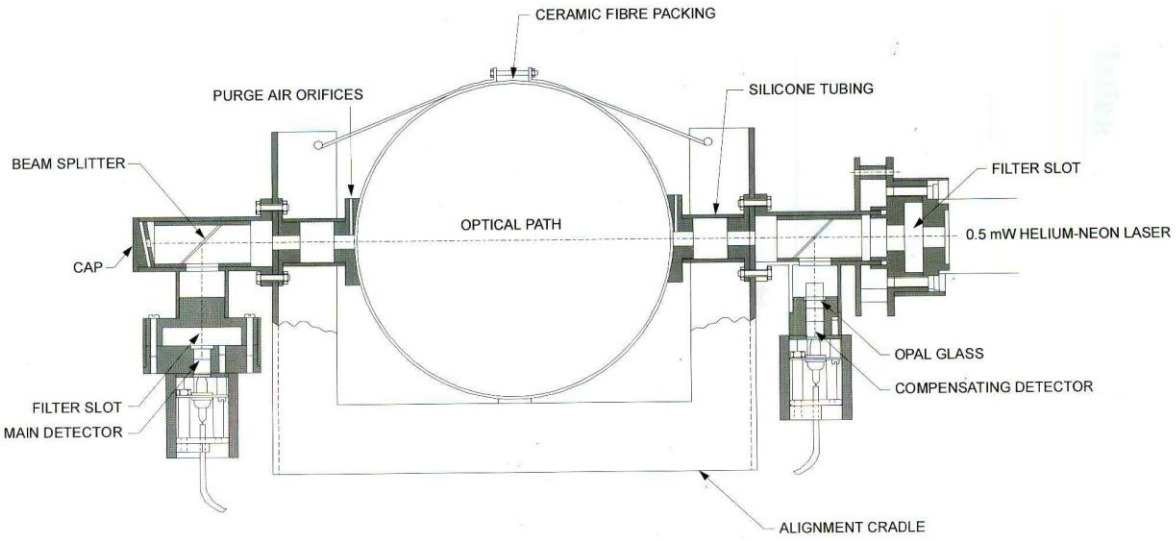

Figure 17. Schematic representation of the optical setup for soot measurements

The laser system is aligned so that the light falls on the photodetector system which has two signal outputs. Transmission is measured by splitting the laser beam at the entrance to instrument (beam splitter shown in Figure 17), and using a first photodetector to serve as a laser power reference. The rest of the beam passes through the sooting region. When light passes through a soot particle, part of the light energy is absorbed by the atoms. The amount of the absorbed light depends on the characteristics of the soot and the sooting region thickness. The transmitted laser intensities I and I_0 with and without soot, respectively, are related to optical thickness L through the relationship:

$$K= \ln (I_0/I)/L \qquad (4)$$

Where K is the extinction coefficient. The above intensities were corrected for background luminosity by turning off the modulated laser.

The optical thickness can be quantitatively related to the soot volumetric fraction through a linear relation **[Pickett 06] [Choi 94] [Cignoli 01] [Coppalle 94]**. The coefficient associated to this relation was experimentally determined, as explained below.

Bio-oil contains a large amount of water (26%), and during pyrolysis, a considerable amount of condensate species (tar+water) is produced. These species tend to condensate on the soot particles and make therefore soot become sticky. Hence the weighing of the soot collected in the sampling probe and in the filter is difficult. To cope with this issue, a calibration of the

measurement was performed with acetone. Acetone is considered as one of the model compounds of bio-oil. Moreover, as shown in the SEM observations of Figure 18, the soot produced by acetone and the ones produced by bio-oil have very similar size in the range of 10 to 50 nm. Chain-like aggregates composed of several tens or more of sub-units, known as monomers or spherules, can be observed in both cases.

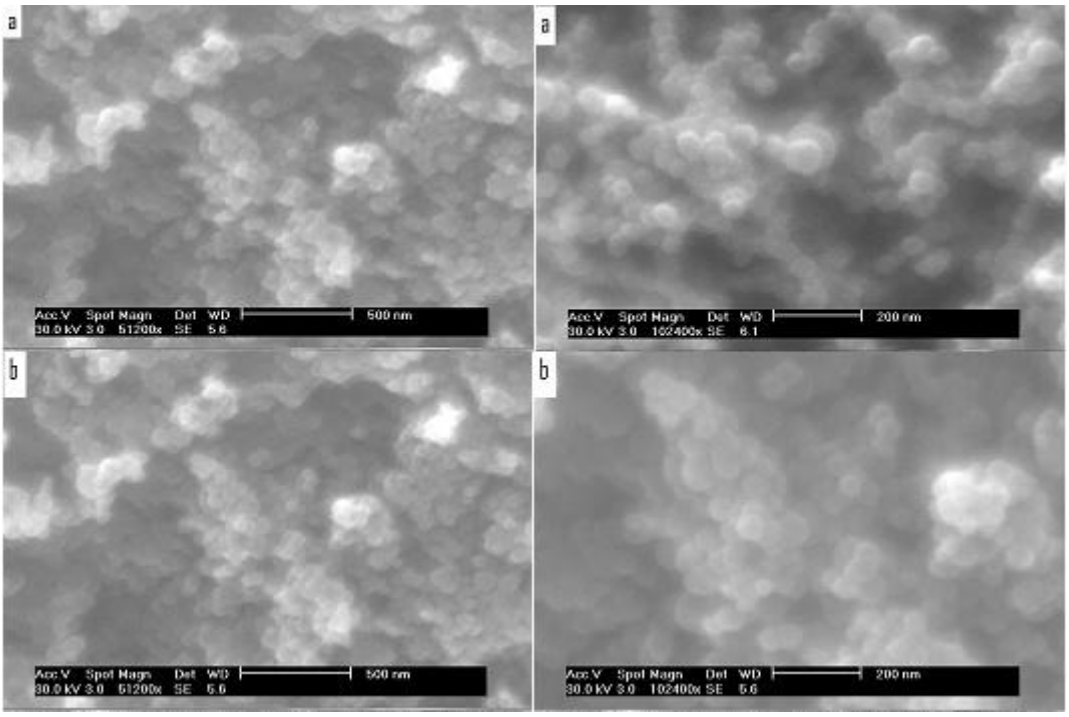

Figure 18. SEM images of the soot samples obtained from acetylene and from bio-oil pyrolysis at 1200°C. **a** - acetone; **b** - bio-oil

The acetone was pyrolyzed at different temperatures ranging from 1000 to 1400°C. Figure 19 shows the extinction coefficient measured at different temperatures. It shows that a maximum of soot is produced at 1200°C. This temperature was chosen for further calibration. Extinction coefficient (EC) values in this sooting condition exceeded 6 m^{-1}. At this temperature, there are black clouds of soot moving and floating along the reactor; the opacity of the clouds makes the nozzle invisible from the bottom of the reactor.

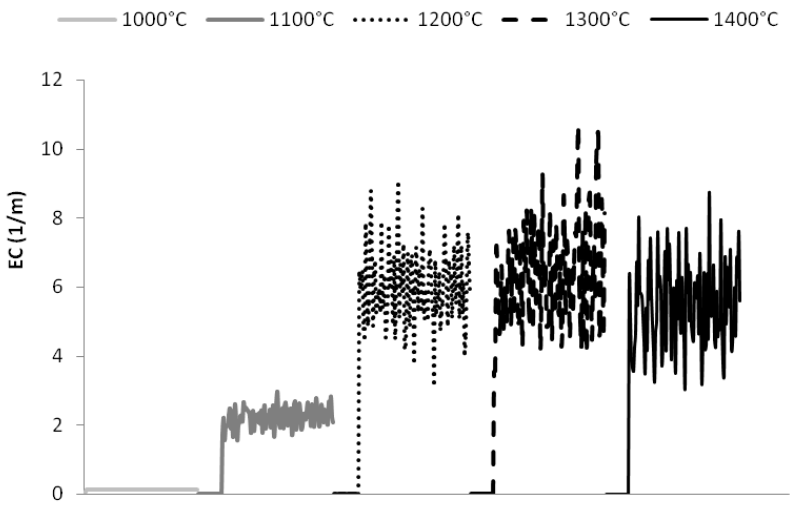

Figure 19. Extinction coefficient versus temperature – acetone pyrolysis

The pyrolysis of acetone was also carried out using different flow rates of acetone: 6, 12 and 18 ml/h. For each experiment the EC was continuously measured, as shown in Figure 20. Each experiment was then repeated with the laser device off and the sampling probe set in. After pyrolysis, soot in the sampling probe, the settling box and in the filter was collected and accurately weighed. The soot volumetric fraction was calculated for each experiment using the relationship.

$$Fv = \frac{\text{Soot volumetric flow rate}}{\text{Total volumetric flow rate}} = \frac{Qm_s/\rho_s}{Qv_g \cdot \frac{T}{273}} \quad (5)$$

With

Fv	Soot volumetric fraction
Qm_s	Soot mass flow rate (g/min) = mass of soot/sampling time
ρ_s	Soot density = 1800 g/l
Qv_g	Nitrogen volume flow rate sweeping the reactor ($NL.min^{-1}$)
T	Temperature (°C)

The total gas flowrate at the exit of the reactor was calculated based only upon the N_2 flowrate fed to the reactor assuming that the fraction of produced gas and soot is negligible.

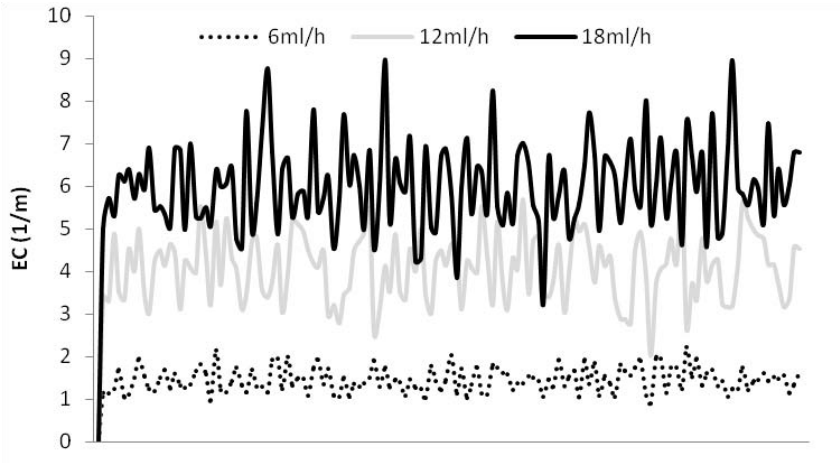

Figure 20. Extinction coefficient during acetone pyrolysis at 1200°C with different acetone flowrates

Figure 21 shows the calculated volumetric fractions (in ppb) versus the measured EC. The obtained calibration curve is a linear function (F_v=s.EC.10^{-9}) with a slope of s=16.89. This factor is subsequently used for all experiments to derive the mass yield of soot following:

$$\text{Yield} = \frac{\text{Qv}_g.\text{T.s.EC.}10^{-9}.\rho}{273.\text{Qm}_{\text{B.O}}} \quad (6)$$

With: $Qm_{B.O}$ bio-oil mass flow rate (g/min).

One should note that the value for ρ_s fixed at 1800g/l is used twice in the calculations and has finally no impact on the calculated soot mass yield.

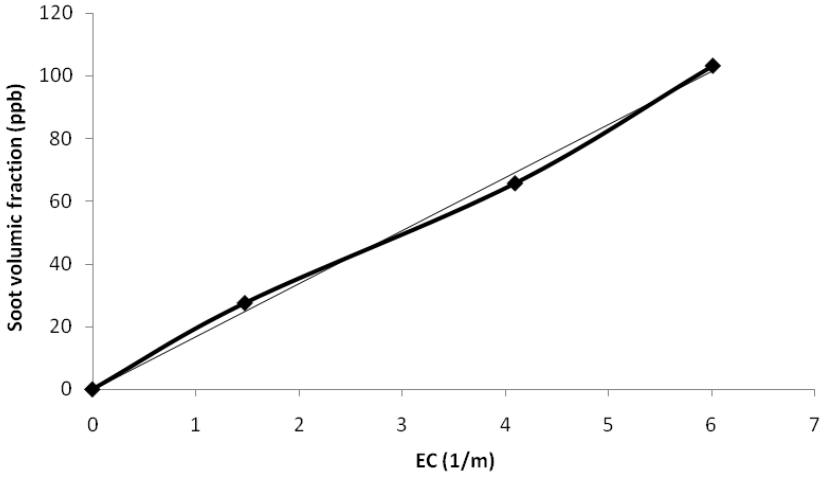

Figure 21. Soot volumetric fraction versus extinction coefficient

Note that the presence of char during the quantification of soot may impact the measurement. Previous studies **[Chhiti 10]**, have shown that the char yield during pyrolysis process is lower than 1% of the initial bio-oil at 1000°C and still lower at higher temperature. At 1000°C, the laser detects almost nothing (yield < 0.1%). This is reassuring for soot measurements in the temperature range of 1000-1400°C explored in this work.

4- FEEDSTOCK

The feedstock used for all experiments was bio-oil produced by fast pyrolysis of mixture of hardwood (oak, maple, ash) in an industrial-scale fluidized bed unit (Dynamotive, West Lorne, Ontario) and provided by CIRAD, France. Its physico-chemical properties have been measured (see Table 1). The water content of the bio-oil measured by Karl Fischer method (ASTM E203) is around 26 wt % which is in agreement with the average values reported in literature. It can be noticed that the solid particles content is rather high (2.3 wt%) while the ash content remains very low (around 0.06 wt %). This confirms that the solid particles mainly consist of high-carbon content char particles. These particles were entrained during bio-oil production by the gas stream to the bio-oil condensers. Ultimate analysis and LHV of the bio-oil are very similar to those of wood. From the ultimate analysis, the chemical formula of the bio-oil can be established as $CH_{1.18}O_{0.48}.0.4H_2O$.

After the production, the bio-oil was stored at 5°C in a fridge. Before experiments, it was filtered on a 30 µm sieve to eliminate largest solid particles which represented less than 0.01 %wt of the oil.

Table 1. Ultimate analysis and physico-chemical properties of bio-oil derived from hardwood fast pyrolysis

Ultimate analysis (wt.%)				**H_2O**	**Ash**	**Solids**	**LHV**	**Kinematic viscosity**
C	H	O	N	(wt.%)	(wt.%)	(wt.%)	(MJ/kg)	at 20°C ($mm^2.s^{-1}$)
42,9	7,1	50,58	< 0,10	26,0	0,057	2,34	14,5	103

5- BIO-OIL CHARACTERIZATION BY TG-DSC

Thermogravimetric analysis (TGA) is a test to determine the mass loss profile as a function of temperature. This type of analysis is widely used to characterize the phenomena of evaporation, thermal decomposition and combustion properties of pyrolysis bio-oil.

We characterized the thermogravimetric behavior of our bio-oil under air and nitrogen. Figure 22 shows the thermal cycle used:

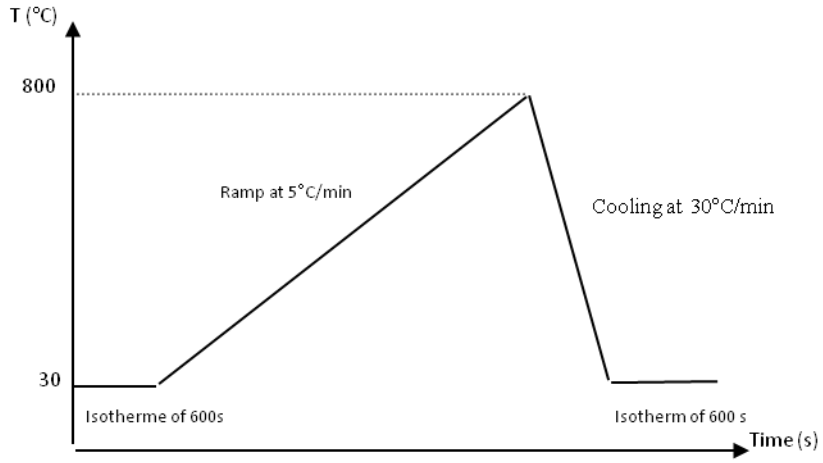

Figure 22. Temperature cycle of TGA experiments

a- Under nitrogen

According to literature, weight loss of bio-oil in inert atmosphere can be divided into two stages:

- evaporation of light volatile (<150-200°C);
- thermal decomposition of unstable heavy compounds (> 350-400°C).

In TG curves presented in Figure 23 the experiment was repeated 3 times. One can observe that, two mass losses are visible; this is in accordance with literature. Each mass loss was recorded at identical temperatures for 3 experiments.

$\Delta m_1 \approx$ - 35,9 % ($\sigma = \pm$ 0,8 %) betwen 30°C and 165°C

$\Delta m_2 \approx$ - 35,2 % ($\sigma = \pm$ 2,0 %) betwen 165°C and around 450°C

A large part of the weight loss takes place at short times and temperatures below 165°C. This is presumably a consequence of the evaporation of the most volatile components of bio-oil (formaldehyde, acetaldehyde, acetone, methanol, ethanol, 2-propanol, formic acid, hydroxypropanone, acetic acid, butanol) and water **[NIST]**.

The second mass loss begins at 165°C. The high temperature range of the weight loss curves can be attributed to the evaporation of carboxylic acids (propionic, acrylic, butyric), lighter furans (furfural), hydroxyacetaldehyde, methoxy and dimethoxyphenols compounds (eugenol, syringol, vanillin and isoeugenol) and presumably to gas release caused by cracking reactions **[Branca 05].**

The thermogravimetric curves cannot give any information about the rate of secondary char formation, as it is not possible to make a distinction between the evolution of species in the liquid or solid phase. It is observed that even at 800°C, the mass of solid residue is not stabilized. It corresponds to about 13–15% of the total initial mass of the liquid. This gives a value of the char yield of bio-oil for low heating rate pyrolysis at 5°C.min^{-1}.

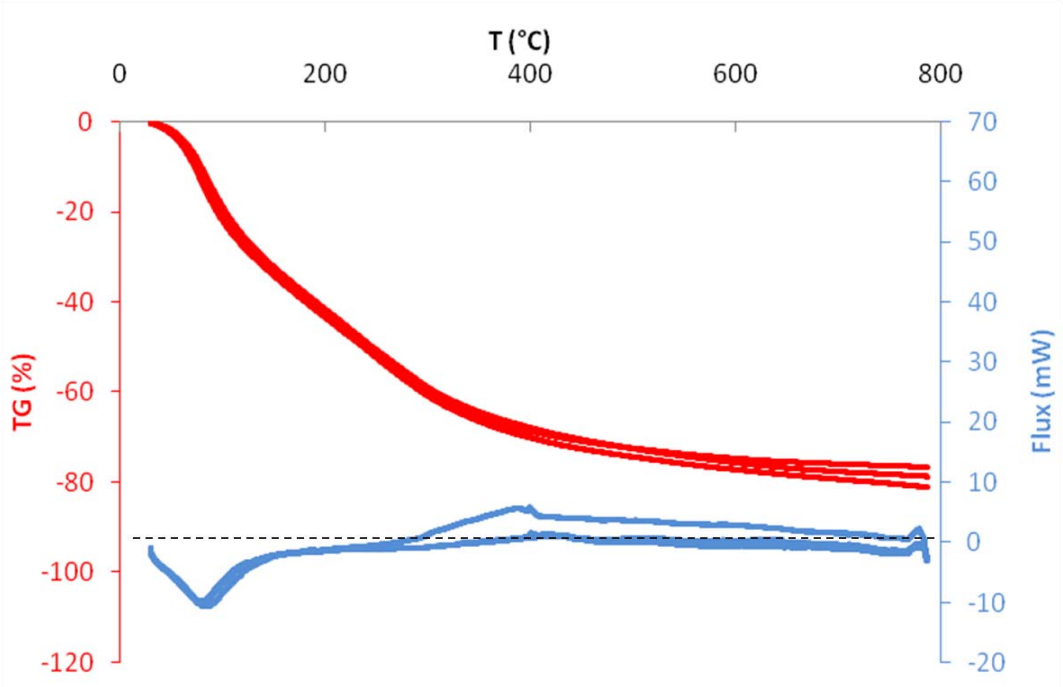

Figure 23. Thermogravimetric behavior of bio-oil pyrolysis under nitrogen

The heat flow curves show that reaction heat of thermal cracking is very low compared to that of evaporation.

b- Under air

According to literature, the weight loss for bio-oil TGA performed under air consists of three stages:

- The first and second stages are similar to TGA under inert atmosphere.
- The third stage is the combustion of the char formed (solid residue) in previous stages; this occurs at a temperature > 400°C. Under air, oxygen participates in the second stage.

In TG curves shown in Figure 24, one can observe that for each analysis performed, three mass losses are visible, in agreement with to literature. Each mass loss was recorded at identical temperatures for the three experiments.

$\Delta m_1 \approx$ - 38.3 % ($\sigma = \pm$ 0,8 %) betwen 30°C and 165°C;

$\Delta m_2 \approx$ - 25,9 % ($\sigma = \pm$ 0,7 %) betwen 165°C and around 360°C;

$\Delta m_3 \approx$ - 31,7 % ($\sigma = \pm$ 0,3 %) betwen 355°C and 555°C.

The measurement of heat flow at the beginning shows an endothermic phenomenon between 30°C and 165°C with a mean enthalpy of 622 J/g comparable to that measured under N_2. Several exothermic fluctuations appear between 300 and 400°C. Then a third strongly exothermic phenomenon appears between 400°C and about 570°C with a mean enthalpy of -7751 J/g.

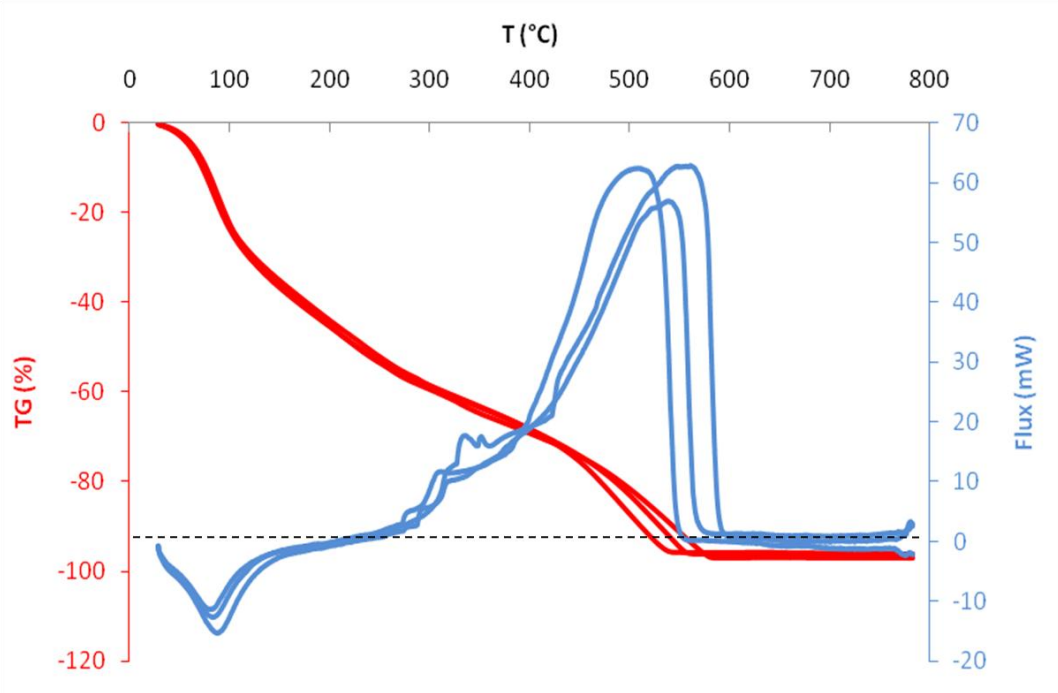

Figure 24. Thermogravimetric behavior of bio-oil degradation under air

Thermogravimetric analysis of bio-oil allows to characterizing different steps of bio-oil degradation. The results obtained during this study will contribute to the interpretation of the different results of this thesis.

REFERENCES

[Branca 05] Branca C, Di Blasi C, Russo C. Devolatilization in the temperature range 300–600 K of liquids derived from wood pyrolysis and gasification. Fuel 2005; 84:37-45.

[Chhiti 10] Chhiti Y, Salvador S, Commandre JM, Broust F. Wood bio-oil pyrolysis: Influence of temperature, heating rate and ash content on char, gas and tar yield. Submitted to Fuel mars 2011.

[Choi 94] Choi MY, Hamins A, Mulholland GW, Kashiwagi T. Simultaneous optical measurements of soot volume fraction and temperature in premixed flames. Combust. Flame 1994;99:174-186.

[Cignoli 01] Cignoli F, DeIuliis S, Manta V, Zizak G. Two dimensional two-wavelength emission technique for soot diagnostics. Appl. Opt. 2001;40:5370-5378.

[Coppalle 94] Coppalle A, Joyeux D. Temperature and soot volume fraction in turbulent diffusion flames: measurements of mean and fluctuating values. Comb. Flame 1994;96:275-285.

[Musculus 02] Musculus MP, Dec JE, a Tree DR. Effects of Fuel Parameters and Diffusion Flame Lift-Off on Soot Formation in a Heavy-Duty Diesel Engine. SAE Paper No. 2002-01-0889.

[NIST] NIST Chemistry WebBook, http://webbook.nist.gov/chemistry.

[Pickett 02] Pickett LM, Siebers DL. An investigation of diesel soot formation processes using micro-orifices. Proc. Combust. Inst. 2002;29:655–662.

[Pickett 06] Pickett L M, Siebers D L. Soot Formation in Diesel Fuel Jets Near the Lift-Off Length. International Journal of Engine Research 2006;7:103-130.

CHAPTER 4: WOOD BIO-OIL PYROLYSIS: INFLUENCE OF TEMPERATURE, HEATING RATE AND ASH CONTENT ON CHAR, GAS AND TAR YIELD

This chapter is submitted as a research paper in an international journal, reference: Chhiti Y, Salvador S, Commandre JM, Broust F. Wood bio-oil pyrolysis: Influence of temperature, heating rate and ash content on char, gas and tar yield. Submitted to Fuel mars 2011.

Keywords: bio-oil, pyrolysis, char, gas, tar.

ABSTRACT

In this study, pyrolysis process of wood bio-oil was studied. The effects of temperature in the range 550-1000°C, heating rate in the range 2-2000°C.s^{-1} and ash content of the bio-oil on char, tar and gas yields were investigated. The main gas species generated are quantified by Micro-GC: H_2, CO, CO_2, CH_4 and trace amounts of C_2H_4 and C_2H_6.

A temperature increase from 550°C to 1000°C enhanced greatly the gas yield, whilst solid and liquid yields decreased significantly. The heating rate was varied in a range covering rapid pyrolysis using the Horizontal Tubular Reactor (HTR) to flash pyrolysis using an Entrained Flow Reactor (EFR). A decrease of char yield from 11 wt.% down to 4 wt.% was observed when heating rate is changed from 2 to 100°C.s^{-1}. In EFR a flash heating rate of 2000°C.s^{-1} led to a char yield as low as 1 wt.%.

Bio-oil with a natural ash contents of 0.05 wt.% and bio-oil added with 3 wt.% of ash were finally pyrolysed. Ash seems to favor re-polymerization reactions that lead to an increase in char yield. A decrease in the amount of gas is observed when ash is added while an increase was a priori expected.

1- INTRODUCTION

Thermochemical processes are the most common route for converting the biomass into energy. Pyrolysis is one of these processes, and is also the first step of any other thermochemical process. During pyrolysis, biomass is thermally decomposed in the absence of oxygen into residual solid called char, liquids also called tar or bio-oil and gases. The yields and the composition of end products of pyrolysis depend on several parameters including temperature, biomass species, heating rate, operating pressure, as well as the extraneous addition of catalysts **[Demirbas 02] [Bridgwater 94]**. Heating rate, temperature and residence time, are three very important parameters **[Dai 00] [Zanzi 02]**, have been widely investigated using solid biomass particles in bench scale reactors including fixed beds **[Actes 05]** and fluidized beds **[Chen 04]**. According to the operating conditions, the pyrolysis process can be sub-divided into:

Slow pyrolysis: Slow pyrolysis is characterized by low heating rates (up to 0.16-0.32°C.s^{-1}). This route favors char production (yields up to 30-40 wt%) and leads to rather low liquid and gas yields. Significant amount of work has been done on this process **[Goyal 08]**.

Fast pyrolysis: Fast pyrolysis is the process in which very high heat flux are imposed to biomass particles, leading to very high heating rates (several hundreds of degrees per minute), at moderate temperature and low gas phase residence time. In such conditions, high yields of high-grade liquids (bio-oils) can be obtained, up to 75 wt%. Fluidized bed reactors are being developed for fast pyrolysis as they offer high heating rate and easy control etc **[Luo 04] [Scott 82]**. Other designs of reactors have also been developed for this aim, such as vacuum pyrolysis **[Parkel 87]**, microwave pyrolysis **[Krieger 94]**, rotating cone reactor **[Wagenaar 94]** and vortex reactor **[Diebold 87]**.

Flash pyrolysis: Flash pyrolysis is characterized by still higher flux densities imposed to biomass particles, leading to heating rates up to several hundreds of degrees per second and reaction characteristic times of only a few seconds. These particular conditions are for instance encountered in entrained flow reactors (EFR) operating at very high temperatures **[Gercel 85]**. Such processes are generally operated under oxidative atmosphere leading to gasification reactions occurring on the primary pyrolysis products.

Fast pyrolysis of biomass to bio-oils has gained particular attention for the last years, due to the uniqueness and the specific properties of bio-oils.

Bio-oils, also referred to as biomass pyrolysis liquids, pyrolysis oils, or bio-crude oils, are dark brown, free flowing liquids with an acrid or smoky odour. They are complex mixtures of compounds that are derived from the depolymerization of cellulose, hemicellulose and lignin. Chemically, they comprise quite a lot of water (15–30 wt% depending on the initial moisture in feedstocks and pyrolysis conditions **[Oasmaa 05]**), and hundreds of organic compounds that include acids, alcohols, ketones, aldehydes, phenols, ethers, esters, sugars, furans, nitrogen compounds and multifunctional compounds **[Milne 97]**. Finally they contain also some residual char particles (0.1 to 3wt%) which sizes usually varies in the range of 1–200 μm with most particles being below 10 μm **[Lu 09]**. This composition depends on many factors, such as biomass type, feedstock pre-treatment (particle size and shape, moisture and ash content), pyrolysis conditions (temperature, heating rate, residence time, pressure…) as well as hot vapor filtration and condensation.

Bio-oil presents some well-known drawbacks such as rather high viscosity, ageing and moderate LHV due to its oxygen content. Bio-oil is also thermally unstable; at elevated temperatures ageing reactions will be accelerated. Four stages can be observed during heating of bio-oils: thickening, phase separation, gummy formation from the pyrolytic lignins, and char/coke formation from the gummy phase at higher temperatures **[Oasmaa 97]**. Boucher et al. **[Boucher 00]** treated a bio-oil sample at 50 and 80°C, respectively, to find out that the whole properties of the bio-oil were significantly altered at 80°C, while no significant variations were observed for the bio-oil kept at 50°C for a week.

However, in spite of these drawbacks bio-oils have been giving rise to increasing interest. Indeed fast pyrolysis allows converting biomass into a more uniform liquid feedstock with much higher energy volume density than that of solid biomass. This is particularly promising due to the high geographic dispersion of biomass which generally leads to high transportation costs. Moreover, bio-oils can easily be stored and transported from scattered gathering stations to a large-scale processing plant.

Bio-oil can have the following potential industrial uses **[Goyal 08]**: combustion for heat and power (boilers, engines or gas turbines), production of chemicals (anhydro-sugars like levoglucosan, resins, liquid smoke, wood preservative), binders for pelletizing and briquetting

of combustible organic waste materials and syngas production via gasification process such as entrained flow reactors. The combination of fast pyrolysis followed by transportation of bio-oil to large steam reforming units also has attracted considerable attention of the research community, as one of the promising viable methods for syngas or hydrogen production. This work is devoted to the characterization of the first step of bio-oil gasification: pyrolysis.

For the high temperature applications such as gasification, steam reforming or even combustion, it is of particular interest to understand the behaviour of bio-oils during the very first step of pyrolysis under various high heat flux densities.

The earliest combustion tests of bio-oil droplets were conducted in Sandia National Laboratory **[Wornat 94] [Shaddix 97]**. Streams of monodispersed droplets were injected into a laminar flow reactor. The experimental conditions were as follows: droplet diameter of about 300 μm, reactor temperature of 1600 K and O_2 concentrations of 14–33%. In-situ video imaging of burning droplets reveals that biomass oil droplets undergo several distinct stages of combustion. Initially biomass oil droplets burn quiescently in a blue flame. The broad range of component volatilities and inefficient mass transfer within the viscous biomass oils bring about an abrupt termination of the quiescent stage, however, causing rapid droplet swelling and distortion, followed by a microexplosion.

Thermogravimetric analysis (TGA) is widely used to characterize the evaporation, thermal decomposition and combustion properties of bio-oils. The weight loss process of bio-oils in inert atmospheres can be divided into two stages: the evaporation of light volatiles (<150-200°C) and the subsequent thermal decomposition of unstable heavier components (<350-400°C). In the case of TGA tests performed in the presence of air, the weight loss of bio-oils can be divided into three stages. The first two stages are similar to those in inert atmospheres and the third stage is the combustion of chars formed in the first two stages (>400°C) **[Ba 04] [Ba 04]**.

Branca et al. **[Branca 05]** studied the devolatilization and heterogeneous combustion of wood fast bio-oil. Weight loss curves of wood fast bio-oil in air have been measured, under controlled thermal conditions, carrying out two separate sets of experiments. The first, which has a final temperature of 600 K, concerns evaporation/cracking of the oil and secondary char formation. A heating rate of 0,08 $C.s^{-1}$ was applied. The yield of secondary char varies from about 25% to 39% (on a total oil basis). After collection and milling, in the second set of

experiments, heterogeneous combustion of the secondary char is carried out to temperatures of 873 K.

In another study, Branca et al. **[Brance 05]** found that thermogravimetric curves of bio-oil in air show two main reaction stages. The first (temperatures ≤ 600 K) concerns evaporation, formation and release of gases and formation of secondary char (coke). Then, at higher temperatures, heterogeneous combustion of secondary char takes place. They found that the pyrolysis temperature does not affect significantly weight loss dynamics and amount of secondary char (approximately equal to 20% of the liquid on a dry basis).
Hallet et al. **[Hallett 06]** established a numerical model for the evaporation and pyrolysis of a single droplet of bio-oil derived from biomass. The model is compared with the results of suspended droplet experiments, and is shown to give good predictions of the times of the major events in the lifetime of a droplet: initial heating, evaporation of volatile species, and pyrolysis of pyrolytic lignin to char.

Guus van Rossum et al. **[Van Rossum 10]** studied the evaporation of bio-oil and product distribution at varying heating rates (~1.5–1.5.10^4°C.s^{-1}) with surrounding temperatures up to 850°C. A total product distribution (gas, vapor, and char) was measured using two atomizers with different droplet sizes. A big difference is seen in char production between the two atomizers where the ultrasonic atomizer gives much less char compared to the needle atomizer, ~8 and 22% (on carbon basis), respectively. Small droplets (88-117µm generated by ultrasonic atomizer, undergoing high heating rate) are much quicker evaporated than larger droplets (~ 1.9 mm, generated by needle atomizer, undergoing low heating rate)

Thus, the objective of this study is to characterize the bio-oil behavior in various pyrolysis conditions. In particular, it will focus on the influence of the heating rate and the final pyrolysis temperature on the product distribution. Two complementary devices were used to study a wide range of heating rates, representative of slow and flash, in the range from 2 to 2000°C.s^{-1} and final temperature from 550 to 1000°C. Finally ash is known for its catalytic effect during thermo-chemical conversion of biomass, as previously approved the works done on solid biomass. In the present work the influence of ash on the bio-oil pyrolysis process has also been evaluated.

2- MATERIALS AND METHODS

2-1 Description of the laboratory device and of the procedure

Bio-oil pyrolysis process was studied at two different reactor configurations: a Horizontal Tubular Reactor (HTR) enabling to ensure heating rates from slow to fast pyrolysis and an Entrained Flow Reactor (EFR) allowing reaching very high heating rates.

2-1-1 Horizontal Tubular Reactor HTR

The experiments of fast pyrolysis were carried out in a HTR (Figure 1). This device allowed carrying out experiments in conditions of fast pyrolysis which is not possible in a thermobalance. The reactor consisted of a double-walled quartz pipe. The length and inside diameters were 850 mm and 55 mm respectively for the inner tube, and 1290 mm and 70 mm respectively for the outer tube. The reactor temperature can reach 1100°C.

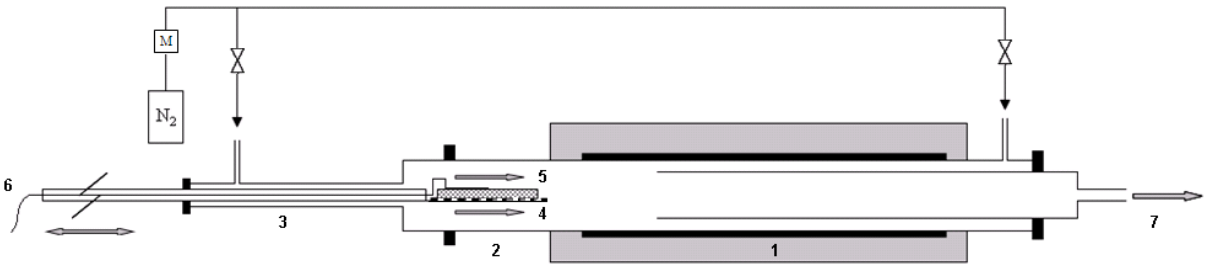

1- Furnace
2- Quartz reactor
3- Movable sample boat
4- Metal grid
5- Refractory wool soaked with 1g of bio-oil
6- Thermocouple
7- Outlet gas
M- Mass flow meters and controllers

Figure 1. Horizontal Tubular Reactor (HTR) ready for sample introduction

The procedure carried out for an experiment was the following. First, the furnace was heated and the gas flowrate (nitrogen) was adjusted using a mass flow meter controller. When the temperature was stabilized, the sample was placed on the metal grid at the unheated section of the reactor. This section was swept by half of the total cold nitrogen flow injected, in order to maintain it cold and under inert atmosphere, and therefore avoid its degradation. Meanwhile the second half of the nitrogen flow was preheated through the double-walled annular section of the reactor as shown in Figure 1. The sample consisted in 1g of bio-oil was placed inside a crucible of 25 mm diameter and 40 mm height for studying the effect of temperature and of ash content. In order to achieve higher heating rates, some runs were performed with 1g of

bio-oil previously soaked in a refractory wool sample of 100x20 mm length and width and 3 mm thickness. The choice of this sample holder allowed increasing the exchange surface and subsequently obtaining larger heating rates. We proved that this wool has no catalytic effect on bio-oil pyrolysis. Indeed, previous bio-oil pyrolysis experiments were carried out first with a single crucible, and secondly in the refractory wool deposited in the crucible. The wool didn‘t induce any change on the products yield.

The reactor outlet was first connected to an O_2 gas analyser to ensure that there is no oxygen in the reactor. Afterwards, a manual insertion enabled to move the sample in the furnace at different velocities, ranging between 0.06 and 30 $cm.s^{-1}$. The sample temperature evolution was measured using a thermocouple placed in the middle of the sample in order to determine a heating rate for each experiment. Variation of the heating rate was obtained by varying the sample introduction through the tubular reactor. Four different durations have been used : 16, 8, 4 and finally 0.03 min resulting in four different heating rates. The sample then remained in the middle of the reactor for a definite time and is brought back out of the furnace; the solid residue was weighed after cooling. Even after several experiments, no char deposit was observed inside the reactor. Only tar deposits were observed in the cold outlet of the reactor. The reactor outlet was connected to a sampling bag at t = 0 just before sample introduction. The gases formed by pyrolysis were collected in the bag. The duration of all experiments was 10 min with a 2 $NL.min^{-1}$ N_2 flowrate which enabled to know accurately the volume of N_2 sampled in the bag. In HTR reactor, the volume of formed gas never exceeded 1% of the volume of N_2 sampled in the bag. After the experiment the bag was disconnected from HTR, and connected to the micro-chromatograph analyser (μGC). From the total volume of gas in the bag and measure of the gas concentration, the quantity of each gas formed by 1g of bio-oil can be precisely calculated.

2-1-2 Entrained Flow Reactor EFR

In order to increase heating rate and reach flash pyrolysis conditions, additional experiments were carried out in a laboratory scale EFR. It consisted in a vertical tubular reactor electrically heated by a total of 18 kW three-zone electrical furnace, and was able to reach 1600°C in a 1m long isothermal reaction zone, as illustrated in Figure 2. The atmosphere gas was generated by feeding the controlled flows of nitrogen in a 2 kW electrical steam generator. This atmosphere gas was then preheated using a 2.5 kW electrical battery of heating elements

before reaching the isothermal reaction zone. EFR was equipped with a specially designed bio-oil spraying feeder, with the aim to obtain a very constant mass flowrate spray **[Chhiti 10]**. The feeder consisted of a 1 m long and 14 mm o.d. probe cooled with water at 30°C. At its extremity a stainless steel nozzle was integrated, which allowed uniform distribution with fine atomization. The microscopic observation of droplets impacted on a surface indicates a size ranging between 10 and 100µm. However, the majority of the droplets were much smaller and not measurable.

The oil was fed with a syringe which is pushed automatically. The expected mass flowrate of0.3 $g.min^{-1}$ was too low for direct spraying. Therefore, a 3.5 $NL.min^{-1}$ N_2 flowrate was used to entrain oil in the feeding probe and to ensure a thin spray of the oil. The spray of droplets was dispersed on the section of a 75 mm i.d. alumina reactor swept by 15 $NL.min^{-1}$ of N_2 atmosphere. At 1760 mm downstream of the injection point, gases and solid residue were sampled by a hot-oil cooled probe. The sampling flowrate is measured accurately using a mass flow meter. The total gas flowrate at the exit of the reactor is calculated based upon the N_2 flowrate fed to the reactor and upon the produced gas species concentrations that are measured. A mass balance was used to calculate the total flowrate for each gas species. Gas and solid residue were separated using a settling box and a filter, both heated to avoid water condensation. The water and potential remaining tars were first condensed in a heat exchanger, and non-condensable gases were forwarded to a micro-chromatograph analyser (µGC) to quantify H_2, CO, CO_2, CH_4, C_2H_2, C_2H_4, C_2H_6, C_3H_8 and C_6H_6.

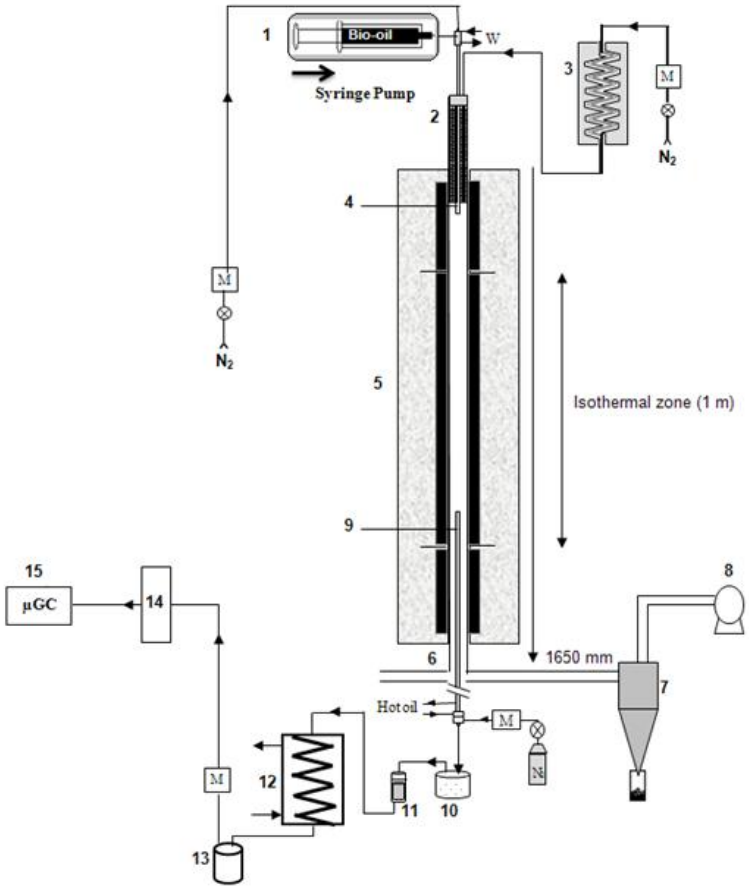

1- Injection system
2- Electrical preheater
3- Steam generator
4- Water cooled feeding probe
5- Three zones electrical furnace
6- 75 mm i.d. alumina reactor
7- Cyclone collector
8- Exhaust fan
9- Oil cooled sampling probe
10- Hot settling box
11- Hot particle collector (filter)
12- Water cooler
13- Condensate collector
14- Gas dryer
15- Gas analyser
M - Mass flow meters and controllers
N_2 - Nitrogen
W - Water (probes cooling)

Figure 2. Scheme of the Entrained Flow Reactor (EFR)

2-2 Feedstock

The feedstock used for all experiments was bio-oil produced by fast pyrolysis of mixture of hardwood (oak, maple, ash) in an industrial-scale fluidized bed unit (Dynamotive, West Lorne, Ontario) and provided by CIRAD, France. Its physico-chemical properties have been measured (see Table 1). The water content of the bio-oil measured by Karl Fischer method (ASTM E203) is around 26 wt % which is in agreement with the average values reported in literature. It can be noticed that the solid particles content is rather high (2.3 wt.%) while the ash content remains very low (around 0.06 wt.%). This confirms that the solid particles mainly consist of high-carbon content char particles. These particles were entrained during bio-oil production by the gas stream to the bio-oil condensers. Ultimate analysis and LHV of

the bio-oil are very similar to those of wood. From the ultimate analysis, the chemical formula of the bio-oil can be established as $CH_{1.18}O_{0.48}.0.4H_2O$.

After the production, the bio-oil was stored at 5°C in a fridge. Before experiments, it was filtered on a 30 µm sieve to eliminate largest solid particles which represented less than 0.01 %wt of the oil.

Table 1. Ultimate analysis and physico-chemical properties of bio-oil derived from hardwood fast pyrolysis

Ultimate analysis (wt.%)				**H_2O**	**Ash**	**Solids**	**LHV**	**Kinematic viscosity**
C	H	O	N	(wt.%)	(wt.%)	(wt.%)	(MJ/kg)	at 20°C ($mm^2.s^{-1}$)
42,9	7,1	50,58	< 0,10	26,0	0,057	2,34	14,5	103

2-3 Method for char/gas/tar yields measurement and interpretation

The yields of char/gas/tar products are interpreted in the following manner. At first, the water contained by bio-oil vaporizes together with light volatile matters. As the temperature of bio-oil continues to increase, pyrolysis occurs, leading to the release of so-called primary volatile matters and to the formation of char. Primary volatile matters may undergo a complex series of cracking reactions giving rise to non-condensable gases as well as secondary and eventually tertiary volatile matters and re-polymerization inside the sample which leading to formation of solid carbon.

At high furnace temperature (above 1000°C), the gas species can also undergo reforming reactions, as steam is present in the gas, leading to much more non-condensable gases (including H_2) generated. The progress of the cracking and reforming reactions is influenced by the temperature of the gas phase, and the vapor residence time which was estimated to several seconds both in the HTR and in the EFR as detailed further.

Finally the collected products are:

- the solid residue, or char;
- permanent gases. The major gas species classically identified during pyrolysis are H_2, CO, CO_2, C_2H_2, C_2H_4;
- tars: the condensable volatile organic compounds;
- water which is originating both from the water initially present in bio-oil and from the pyrolysis reaction.

Thereafter the term –condensate" stands for the mix of tars and water. No condensation system is set up. Therefore, the condensate yield is calculated as the complement to 100 wt.% of the yields in gas and solid residue.

3- RESULTS AND DISCUSSIONS

3-1 Preliminary runs of bio-oil pyrolysis at two final reactor temperatures

Two reactor temperatures were tested in order to evaluate the effect of the final pyrolysis temperature on devolatilization process affecting the yield of gas, condensate and residual solid:

- Moderate temperatures at 550°C;
- High temperature 1000°C to approach the severe conditions of gasification.

The yields of final products are listed in Figure 3. With temperature increasing from 550 to 1000°C, the total gas yield sharply increases from 12.2 to 43.0 wt.%, while condensate (tar + water) decreases from 73.2 to 47.5 wt.%. Varying temperature shows a great influence on the gas composition as well.

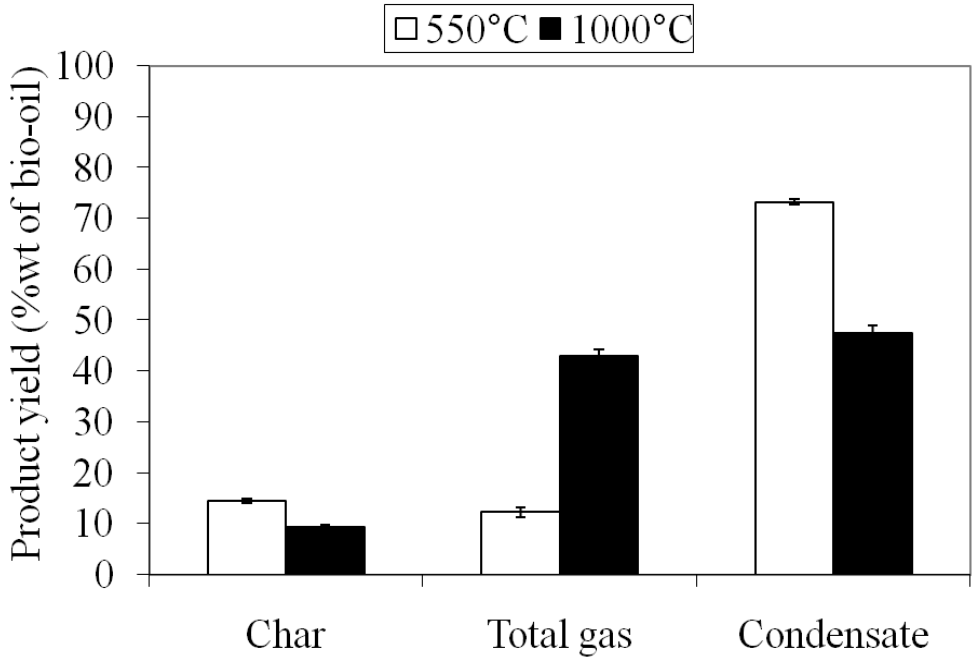

Figure 3. Product yield of bio-oil pyrolysis in HTR – effect of temperature

Figure 4 shows that the main gas products are H_2, CO, CO_2, CH_4 and some C_2 hydrocarbons (C_2H_2, C_2H_4 and C_2H_6). Among them, the H_2 and CO content increased significantly from

0.056 wt.% to 1.65 wt.% and from 5.9 to 23.9 wt.% respectively as temperature increased from 550 to 1000°C. Yields of CH_4 also increased from 1.2 to 5.0 wt.% whilst that of CO_2 increased from 4.2 to 10.8 wt.%. The yields of C_2H_2, C_2H_4 and C_2H_6 are relatively small. The specie C_2H_6 only appears at 550°C while C_2H_2 only appears at 1000°C. The thermal cracking of gas-phase hydrocarbons at high temperature might explain the variation of gas product composition observed.

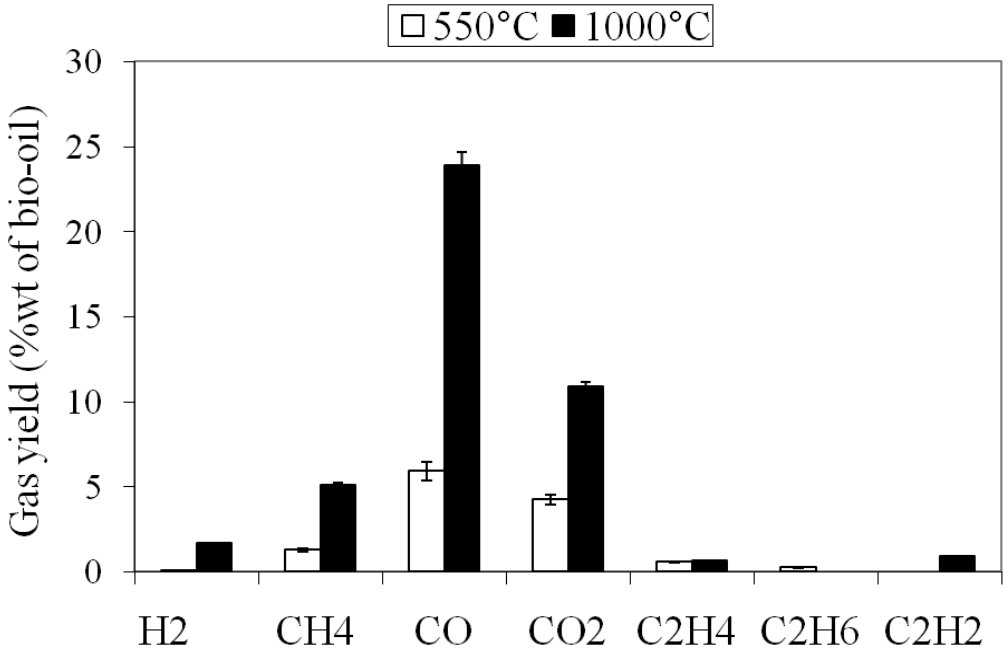

Figure 4. Gas yield of bio-oil pyrolysis in HTR – effect of temperature

Finally, with increasing temperature from 550°C to 1000°C, the char yield decreased significantly from 14.5 to 9.4 wt.%. However changing the reactor temperature implies a change of both the heat flux density imposed to bio-oil (and hence its heating rate) but also the final temperature reached by the char produced. Therefore the later trend observed might be due to two reasons:

- the char formed at 550°C contains residual volatile matters which are released when the temperature increases to 1000°C;
- increasing the heating rate results in the decrease of the char yield. This is actually in good agreement with what is usually observed in the literature from pyrolysis of biomass **[Mani 10] [Ayllón 06] [Haykiri-Acma 06]**.

To check the first assumption, a char first prepared at 550°C was submitted to a second heating step at 1000°C. During this second step, the mass of char did not change, which

excluded the first assumption, and highlighted actually the effect of heating rate. In order to confirm this trend, additional experiments were carried out to separate the effect of these two parameters. This is studied in details in the following section.

3-2 Effect of heating rate and final temperature on the product yields

The temperature profiles obtained in the HTR are illustrated in Figure 5. A calculation of the highest heating rate is then made taking into account only the linear part of curves. Details of the calculated heating rates and products yields obtained from experiments are given in Table 2.

The temperature profiles curves show that the heating rate ranges from 2 to 14°C.s^{-1} at the final pyrolysis temperature of 550°C, and from 2 to 100°C.s^{-1} at the final pyrolysis temperature of 1000°C. The response time of temperature measurement system was characterized by placing the thermocouple alone and the thermocouple placed in the refractory wool without bio-oil sample together inside the reactor in 0.03 min. The results are also plotted in Figure 5. At 1000°C we can notice that the response of the thermocouple and refractory wool does not exceed 100°C.s^{-1}. This means that the actual heating rate for the sample introduced in 0.03min may be still higher than 100°C.s^{-1}. This is further illustrated on Figure 6.

Table 2. Product yield of bio-oil pyrolysis at different temperatures and heating rates

	Duration of sample introduction (min)	**Heating rate of the sample °C.s^{-1}**	**Solid %wt**	**Total gas %wt**	**condensate %wt (by difference)**
Pyrolysis at 550°C	**16**	**2**	**14.4**	**14.1**	**71.4**
	8	**5**	**12.4**	**13.7**	**73.8**
	4	**10**	**11.4**	**13.3**	**75.2**
	0.03	**14**	**10.5**	**13.3**	**76.0**
	flash	**>2000**	**1.2**	**13.6**	**85.1**
Pyrolysis at 1000°C	**16**	**2**	**11.5**	**41.6**	**46.8**
	8	**5**	**10.4**	**41.7**	**47.8**
	4	**14**	**8.6**	**40.9**	**52.2**
	0.03	**100**	**3.8**	**43.8**	**53.4**
	flash	**>2000**	**0.9**	**40.3**	**58.7**

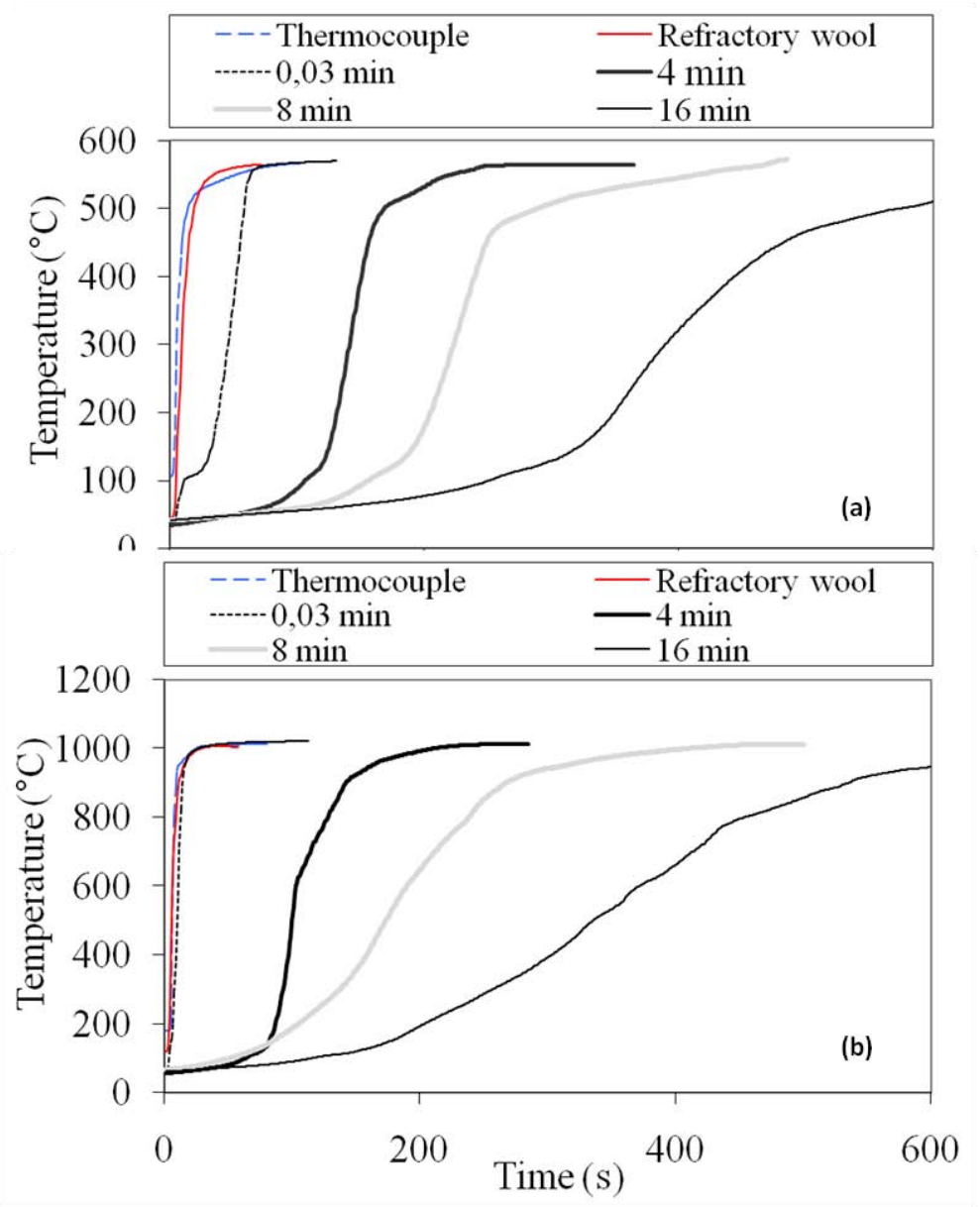

Figure 5. Temperature evolution of the sample during bio-oil pyrolysis in HTR at different heating rates and two final temperatures. **a:** 550°C, **b:** 1000°C

In order to highlight the effect of heating rate and final temperature on the yields of char, they were plotted in figure 6 with the heating rate as the x scale, using a log scale. The low heating rate experiments gave higher yields of char. Char yield then decreased significantly: from 14.4 wt.% down to 10.5 wt.% when heating rate increased from 2 to 14°C.s^{-1} at the final temperature of 550°C, and from 11.5 to 3.8 wt.% when heating rate was increased from 2 to 100°C.s^{-1} at the final temperature of 1000°C.

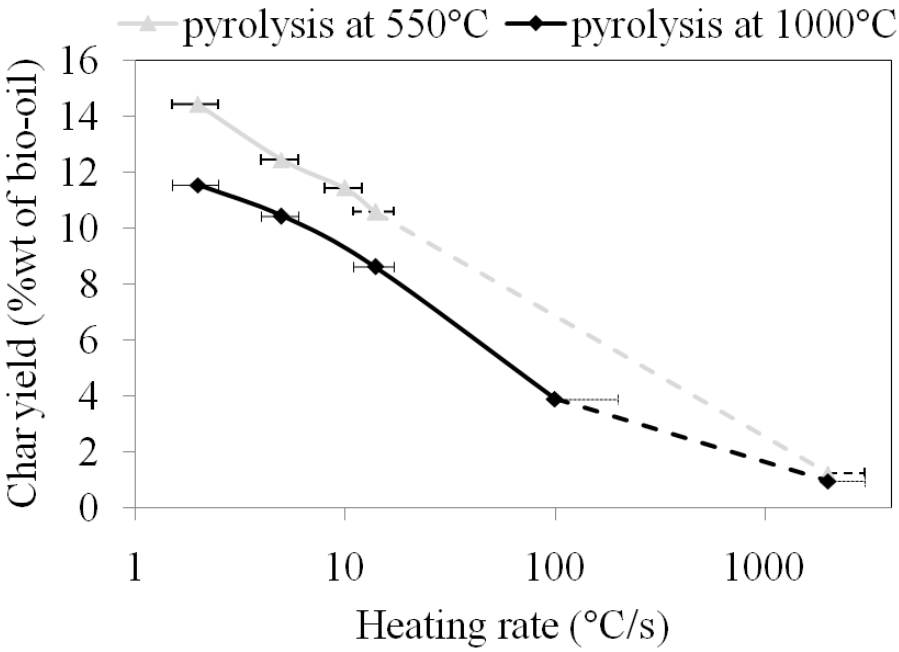

Figure 6. Char yield obtained from pyrolysis of bio-oil at two final temperatures: 550°C and 1000°C - effect of heating rate

In order to increase still the heating rate and reach the flash pyrolysis conditions, we have performed additional experiments in the EFR. This process allows achieving very high heating rate. Indeed it is shown that when a particle or droplet is transported by a cold spraying gas, its heating rate is controlled by mixing of the cold gas with the hot gas in the reactor. CFD modeling was used and derived this order of magnitude. Heating rate was estimated at 2000°C.s^{-1} **[Van de Steene 00]**. Under these conditions, the char yield measured is very low: < 1 wt.%. As can be seen in Figure 6, the char yield obtained with EFR is in rather good agreement with the values obtained in HTR and extrapolated to high heating rates. This result is in agreement with the work carried out by Guus van Rossum et al. **[Van Rossum 10]**. They found that small droplets (undergoing high heating rate) are much quicker evaporated and give fewer char compared to larger droplets (undergoing low heating rate pyrolysis).

Globally from all the data collected, the char yield depends very much on the heating rate, and less on the final temperature, confirming the observation from section 3-1. These results give important information for understanding the pathways occurring during gasification of bio-oil in reactors such as EFR: the amount of char formed by pyrolysis and submitted to subsequent steam-gasification reactions will be very low whereas the main reactions will occur in the gas

phase (reforming, partial oxidation…). Considering that solid gasification is rate-limiting, this might be an advantage of using bio-oil instead of biomass as feedstock for EFR gasification.

Figure 7 shows the effect of heating rate on the product yields at two final pyrolysis temperatures. There is no apparent impact of the heating rate but a drastic influence of the temperature on the total gas yield which remains of about 13–14 wt.% and 40–43 wt.% at 550°C and 1000°C, respectively.

On the other hand, we can notice that the total condensate yield increased when the heating rate increased and when the final temperature decreased. A maximum value of 76 wt.% is obtained at 14°C.s^{-1} and a final temperature of 550°C, which is about 5 wt.% higher than that obtained at 2°C.s^{-1}. In the same manner, at 1000°C the total condensate yield increased with the heating rate, up to 53.4 wt.% at 100°C.s^{-1}. This value was about 6 wt.% higher than that of 2°C.s^{-1}.

All these trends can be summarized and explained as follows.

i) Pyrolysis inside the sample

The volatile matters yield increases with the heating rate of bio-oil, to the detriment of the char yield as reported earlier. The primary volatiles may undergo secondary reactions through two competitive pathways **[Zaror 85] [Seebauer 97]**:

- re-polymerizing to form char;
- cracking to form lighter volatiles which implies less tar repolymerisation.

The re-polymerization pathway is probably favored by lower heating rates. Indeed, low heating rates lead to longer volatiles residence times inside the sample, and favor secondary reactions of re-polymerization to form solid residue. These conditions are known to favor the formation of secondary char from biomass pyrolysis experiments **[Zaror 85]** and apparently, this could be extended to the case of bio-oil pyrolysis.

ii) Gas phase reactions outside the sample

Once the volatiles have escaped from the sample, they can undergo additional secondary gas-phase cracking reactions as previously presented. The conversion rate of this reaction highly increases with the gas temperature, leading to higher gas yields to the detriment of condensates. This result is in agreement with number of pyrolysis works carried out on biomass **[Seebauer 97]**.

Let‘s notice that due to the procedure described, higher heating rate leads to lower residence time of tars in the hot zone because the bio-oil sample is introduced more rapidly to the centre

of the heated zone. The estimate of the gas residence time in the HTR was calculated, from their release at the sample position (which varies with time according to the duration of sample introduction) to the exit of the reactor. It varies from 8 to 16s at 550°C and from 5 to 10s at 1000°C.

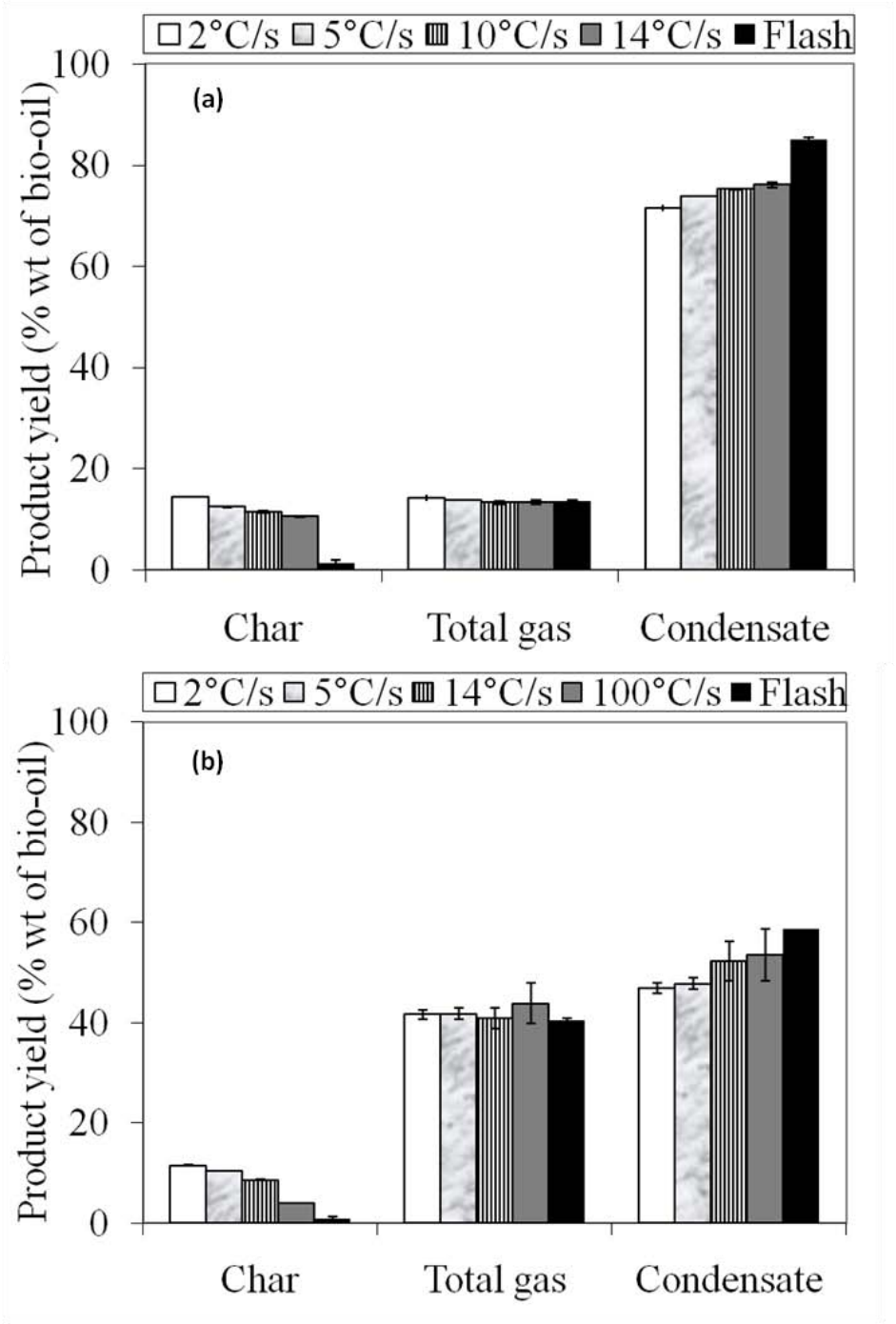

Figure 7. Product yield obtained from bio-oil pyrolysis at two final temperatures. **a:** 550°C, **b:** 1000°C- effect of heating rate

3-3 Effect of ash content

The influence of the presence of mineral matter on yields of final products from solid biomass pyrolysis has been extensively studied. M. Nik-Azar et al. **[Nik-Azar 97]** have studied the effects of cations on the yields of char, tar, and total gas from rapid pyrolysis of beech wood. Raw wood, acid washed wood, and wood impregnated with potassium, sodium, and calcium cations were pyrolyzed in 1 atm pressure of helium at 1000°C.s^{-1} heating rate to a peak temperature of 1000°C. They found that washing wood samples with acid reduces the yields of char and gases. Ming-qiang Chen have investigated catalytic effects of inorganic additives on the pyrolysis of pine wood sawdust by microwave heating at 470°C under nitrogen atmosphere. They found that inorganic additives increased the yield of solid products greatly and decreased the yield of gaseous products more or less. Liquid yield undergoes no dramatic change **[Chen 08]**. The aim of this part was to evaluate whether ash will have the same effect on the pyrolysis of bio-oil.

Crude bio-oil containing 0.05 wt.% of minerals and crude bio-oil with 3 wt.% of added ash were pyrolysed to highlight effect of minerals on pyrolysis process. The added ash are prepared by burning crushed beech wood (particle size of 300-400 µm) in a furnace equipped with 3 drawers at 600°C. The choice of this temperature is designed to perform a « mild » heat treatment in order to preserve the properties of minerals present in biomass and keep the same properties as in the case of the production of bio-oil by pyrolysis of wood. The wood is distributed in the drawers on a thin layer of 1.5 cm thickness to ensure good heat transfer and air diffusion. Air was fed to the reactor at low flow rate, 30 NL.h^{-1}, to avoid ignition and high temperature rapid combustion of wood. The analysis of the elements most cited in literature was performed on the ashes resulting from this combustion, by ICP-OES (Inductively Coupled Plasma Optical Emission Spectrometry). The results of the main elements are presented in Table 3. Logically for biomass ash Ca, K, Mg and Mn are present in high concentrations.

Table 3. Composition of ashes (from combustion of wood) [wt%, dry ashes]

Ca	K	Mn	Mg	P	Ni	Na	Al
11.67	3.80	1.74	1.54	1.01	0.25	0.24	0.10

Products yields obtained in experiments are listed in Figures 8. The results are expressed as a percentage of products on an added ash free basis. At 550°C, we can notice that when the amount of ash is increased in bio-oil, the char yield increased significantly from 14.5 to 18.5 wt.% and both gas and tar yields reduced. The total gas yield decreased from 12.2 to 11.1 wt.% and tar decreased from 73.3 to 70.4 wt .% as can be seen in figure 8a.

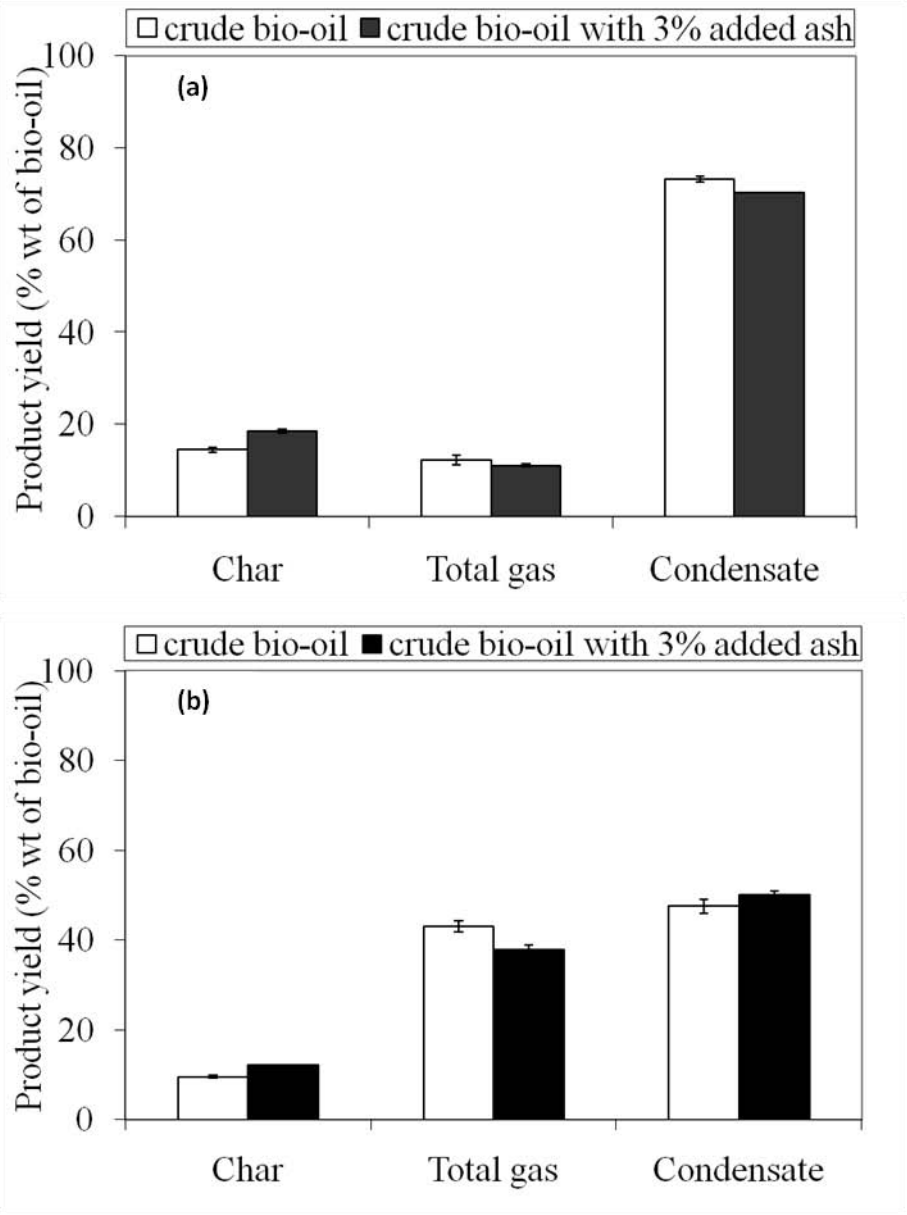

Figure 8. Product yields of bio-oil pyrolysis at two final temperatures. **a:** 550°C **b:** 1000°C – Effect of ash content

Meanwhile, increasing the amount of ash in bio-oil shows a great influence on gas product components as indicated in Figure 9. Among them, CO_2 content increased from 4.2 wt.% to 5.2 wt. while wt.% CO content decreased significantly, from 5.9 wt.% to 4.0 wt.%. Also a

slight decrease of other gases is observed in particular CH_4 and C_2H_4. These phenomena can probably be explained by the catalytic effect of ash, which can favor polymerization reactions. These reactions lead to the formation of larger quantity of solid residue and result in decrease of the amount of gas. The same conclusions are also valid for the case of pyrolysis at 1000°C (figure 8b and 9b).

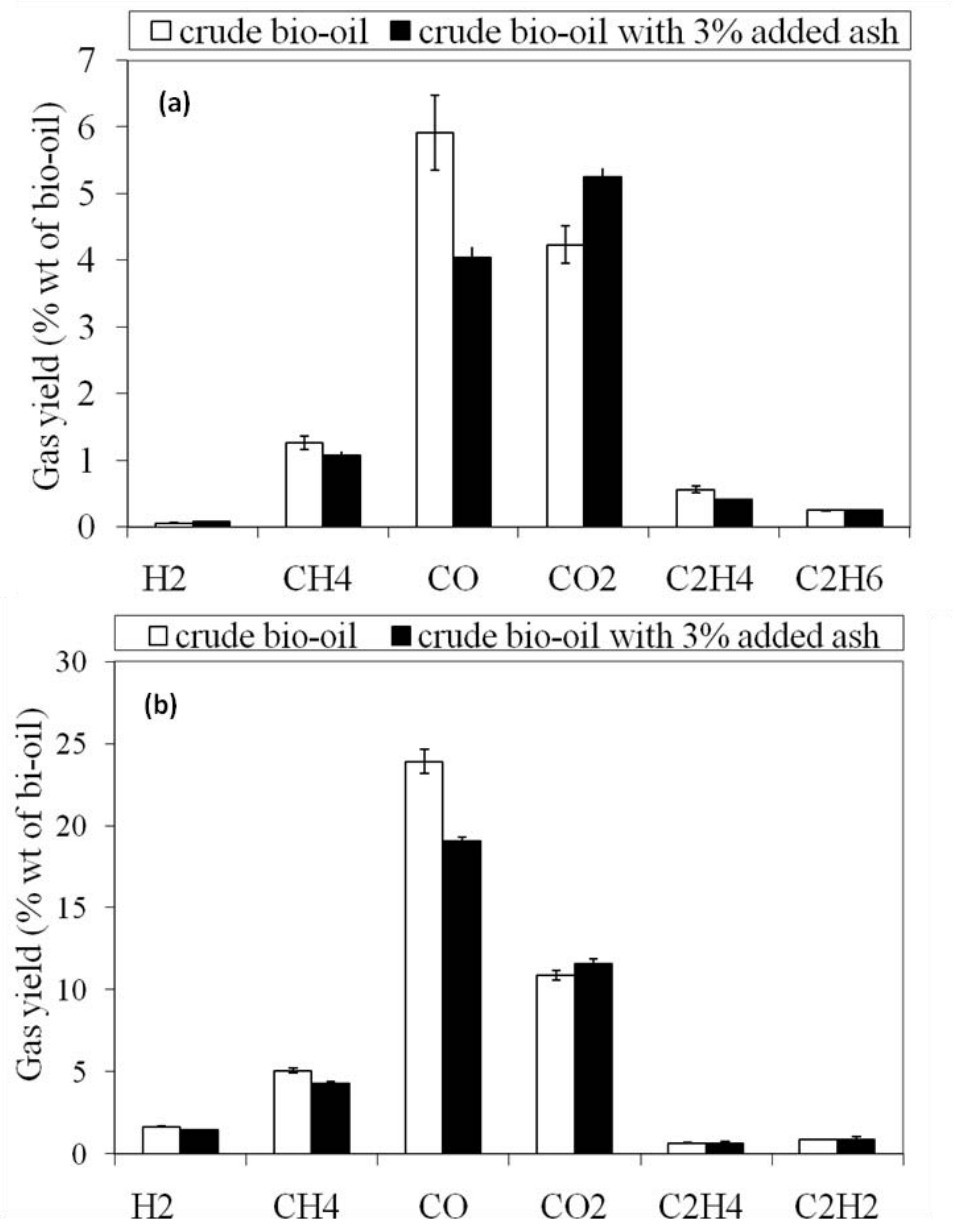

Figure 9. Gas yields of bio-oil pyrolysis at two final temperatures. **a:** 550°C, **b:** 1000°C – Effect of ash content

4- CONCLUSIONS

Experiments of pyrolysis have been carried out on bio-oil at different heating rates and different final temperatures. Two different devices have been used in order to cover a wide range of heating rates.

The yields of gas/condensate/char were determined after pyrolysis. They were 12/73/14 wt.% at 550°C with gas residence time of 8s, and 43/47/9 wt.% at 1000°C with gas residence time of 5s. The composition of the obtained gas was established at the two final temperatures.
The heating rate of bio-oil has little impact on the gas yield, but plays a major role on the char yield. This later decreases from 11 wt.% with a heating rate of $2°C.s^{-1}$ down to 1 wt.% only for flash heating rate of $2000°C.s^{-1}$ at final temperature of 1000°C. At very high heating rate the char yield depends less on the final temperature. These results show that for EFR type gasification process the quantity of formed char is very small, but will require either complete gasification or removal from the gas produced by the gasifier.

Additional pyrolysis runs performed on wood bio-oil added with 3 wt.% of ash gave some interesting results:
(i) Ash increased the yield of solid products greatly and decreased the yield of gaseous products. Liquid yield undergoes no dramatic change. Ash seems to favor polymerization reactions leading to the formation of char.
(ii) Ash clearly affects the gas composition. When ash is added CH_4 and CO yields decrease, while CO_2 yield increases.

Acknowledgements
The authors gratefully acknowledge the financial support from EnerBio Program of Fondation Tuck France, and express their gratitude to Mr. Bernard AUDUC technician in Ecole des Mines d'Albi-Carmaux for his assistance and contribution to device design and operation.

REFERENCES

[Actes 05] Ates F, Putun AE, Putun E. Fixed bed pyrolysis of Euphorbia rigida with different catalysts. Energy Conversion and Management 2005; 46:421–432.

[Ayllón 06] Ayllón M, Aznar M, Sånchez JL, Gea G, Arauzo J. Influence of temperature and heating rate on the fixed bed pyrolysis of meat and bone meal. Chemical Engineering Journal 2006; 121:85–96.

[Ba 04] Ba T, Chaala A, Pérez MG, Rodrigue D, Roy C. Colloidal properties of bio-oils obtained by vacuum pyrolysis of softwood bark. Characterization of watersoluble and water-insoluble fractions. Energy Fuel 2004; 18: 704–12.

[Ba 04] Ba T, Chaala A, Pérez MG, Roy C. Colloidal properties of bio-oils obtained by vacuum pyrolysis of softwood bark. Storage stability. Energy Fuel 2004; 18:188–201.

[Boucher 00] Boucher ME, Chaala A, Pakdel H, Roy C. Bio-oils obtained by vacuum pyrolysis of softwood bark as a liquid fuel for gas turbines. Part II: stability and ageing of bio-oil and its blends with methanol and a pyrolytic aqueous phase. Biomass Bioenergy 2000; 19:351–61.

[Branca 05] Branca C, Di Blasi C, Elefante R. Devolatilization and Heterogeneous Combustion of Wood Fast Pyrolysis Oils. Ind. Eng. Chem. Res 2005; 44:799-810.

[Brance 05] Branca C, Di Blasi C, Russo C. Devolatilization in the temperature range 300–600 K of liquids derived from wood pyrolysis and gasification. Fuel 2005; 84:37–45.

[Bridgwater 94] Bridgwater AV. Catalysis in thermal biomass conversion. Applied Catalysis. A, General 1994; 116:5–47.

[Chen 04] Chen G, Andries J, Spliethoff H, Fang M, van de Enden PJ. Biomass gasification integrated with pyrolysis in a circulating fluidised bed. Solar Energy 2004; 76:345–349.

[Chen 08] Chen M, Wang J, Zhang M, Chen M, Min XZ, Tan Z. Catalytic effects of eight inorganic additives on pyrolysis of pine woodsawdust by microwave heating. J. Anal. Appl. Pyrolysis 2008; 82:145–150.

[Chhiti 10] Chhiti Y, Salvador S, Commandre JM, Broust F, Couhert C. Wood bio-oil non catalytic gasification: influence of temperature, dilution by an alcohol and ash content. Energy and Fuels 2010, Online.

[Dai 00] Dai X, Wu C, Li HB, Chen Y. The fast pyrolysis of biomass in CFB reactor. Energy and Fuels 2000; 14:552–557.

[Demirbas 02] Demirbas A, Arin G. An overview of biomass pyrolysis. Energy Sources 2002; 24:471–482.

[Diebold 87] Diebold J, Scahill. Production of primary oils in a vortex reactor. ACS Preprints (Div. Fuel Chem.) 1987; 32:21–28.

[Gercel 02] Gercel HF. Production and characterization of pyrolysis liquids from sunflower pressed bagasse. Bioresource Technol 2002; 85:113–7.

[Goyal 08] Goyal HB, Diptendu S, Saxena RC. Bio-fuels from thermochemical conversion of renewable resources: A review. Renewable and Sustainable Energy Reviews 2008; 12:504–517.

[Hallett 06] Hallett WLH, Clark NAA. model for the evaporation of biomass pyrolysis oil droplets. Fuel 2006; 85:532–544.

[Haykiri-Acma 06] Haykiri-Acma H, Yaman S, Kucukbayrak S. Effect of heating rate on the pyrolysis yields of rapeseed. Renewable Energy 2006; 31:803–810.

[Krieger 94] Krieger-Bockett. Microwave pyrolysis of biomass. Res. Chem. Intermed. 1994; 20:39–49.

[Lu 09] Lu Qiang, Li Wen-Zhi, Zhu Xi-Feng. Overview of fuel properties of biomass fast pyrolysis oils. Energy Conversion and Management 2009; 50: 1376-1383.

[Luo 04] Luo Z, Wang S, Liao Y, Zhou J, Gu Y, Cen K. Research on biomass fast pyrolysis for liquid fuel. Biomass Bioenergy 2004; 26:455–62.

[Mani 10] Mani T, Murugan P, Abedi J, Mahinpey N. Pyrolysis of wheat straw in a thermogravimetric analyzer: Effect of particle size and heating rate on devolatilization and estimation of global kinetics. Chemical Engineering Research and Design 2010; 88:952-958.

[Milne 97] Milne TA, Agblevor F, Davis M, Deutch S, Johnson DA. review of chemical composition of fast pyrolysis oils. Developments in thermochemical biomass conversion 1997; 409–24.

[Nik-Azar 97] Nik-Azar M, Hajaligol MR, Sohrabi M, Dabir B. Mineral matter effects in rapid pyrolysis of beechwood. Fuel Processing Technology 1997; 51:7- 17.

[Oasmaa 05] Oasmaa A, Meier D. Norms and standards for fast pyrolysis liquids. 1. Round robin test. J Anal Appl Pyrol 2005; 73:323–34.

[Oasmaa 97] Oasmaa A, Leppamaki E, Koponen P, Levander J, Tapola E. Physical characterization of biomass-based pyrolysis liquids. Application of standard fuel oil analyses. Espoo 1997, Technical Research Centre of Finland 1997.

[Parkel 87] Pakdel, Roy C. Chemical characterization of wood oils obtained in a vacuum pyrolysis process development unit. ACS Preprints (Div. Fuel Chem.) 1987; 32:203–214.

[Seebauer 97] Seebauer V, Petek J, Staudinger G. Effects of particle size, heating rate and pressure on measurement of pyrolysis kinetics by thermogravimetric analysis. Fuel 1997; 76:1277-1282.

[Shaddix 97] Shaddix CR, Huey SP. Combustion characteristics of fast pyrolysis oils derived from hybrid poplar. In: Bridgwater AV, editor. Developments in thermochemical biomass conversion. London: Blackie Academic & Professional 1997; 465–80.

[Scott 82] Scott, Piskorz J. The flash pyrolysis of aspen-poplar wood. Can. Eng. 1982; 60:666–674.

[Van de Steene 00] Van de Steene L, Salvador S, Charnay G. Controlling powdered fuel combustion at low temperature in a new entrained flow reactor. Combustion Science and Technology 2000; 159: 255-279.

[Van Rossum 10] Van Rossum G, Güell BM, Balegedde Ramachandran RP, Seshan K, Lefferts L, Van Swaaij WPM, Kersten SRA. Evaporation of pyrolysis oil: Product distribution and residue char analysis. AIChE Journal 2010; 56:2200–2210.

[Wagenaar 94] Wagenaar BM, Prins W, van Swaaij WPM. Pyrolysis of biomass in the rotating cone reactor: modeling and experimental justification. Chem. Eng. Sci. 1994; 49:5109-5126.

[Wornat 94] Wornat M J, Porter BG, Yang NYC. Single droplet combustion of biomass pyrolysis oils. Energy Fuel 1994; 8:1131–42.

[Zanzi 02] Zanzi R, Sjostrom K, Bjornbom E. Rapid pyrolysis of agricultural residues at high temperature. Biomass and Bioenergy 2002; 23:357–366.

[Zaror 85] Zaror CA, Hutchings IS, Pyle DL, Stiles HN, Kandiyoti R. Secondary char formation in the catalytic pyrolysis of biomass. Fuel 1985; 64:990–994.

CHAPTER 5: WOOD BIO-OIL NON CATALYTIC GASIFICATION: INFLUENCE OF TEMPERATURE, DILUTION BY AN ALCOHOL AND ASH CONTENT

This chapter is published as a research paper in an international journal, reference: Chhiti Y, Salvador S, Commandre JM, Broust F, Couhert C. Wood bio-oil non catalytic gasification: influence of temperature, dilution by an alcohol and ash content. Energy and Fuels 2010, Online.

Keywords: bio-oil, gasification, reforming, syngas

ABSTRACT

Biomass gasification is gaining attention as a route for biomass energy production. When large scale units are considered, bio-oil shows lots of advantages compared to solid biomass such as high energy volume density, and easy handling and storing. Syngas (H_2 and CO) can be produced from bio-oil by two gasification processes, also called reforming processes: catalytic reforming at medium temperature and non catalytic reforming at high temperature. In the literature, most of the works focus on the catalytic reforming and mainly concern the aqueous fraction of bio-oil or model compounds. Only very few works can be found on the non catalytic reforming of crude bio-oil. The objectives of this work were to perform experimentally the injection and gasification of non-diluted bio-oil in a lab-scale High Temperature Entrained Flow Reactor (HT-EFR), and to determine the syngas composition and yield.

The influence of temperature on the gasification process has been investigated over a wide range from 1000°C to 1400°C. Hydrogen yield increases with temperature via steam reforming of CH_4 and C_2H_2 and with water gas shift reaction. A thermodynamic equilibrium calculation was conducted. It shows that equilibrium is reached within several second at the temperature of 1400°C.

After that, experiments of gasification were carried out at 1400°C with pure ethanol and with ethanol added bio-oil and in order to study the impact of dilution on the syngas yield.

The influence of ash on the gasification process has also been evaluated. The ash seems to cause a decrease in the total amount of gas produced.

1- INTRODUCTION

The process of obtaining energy from conventional sources causes atmospheric pollution, resulting in problems like global warming, acid rain, etc. The development of non-conventional sources like wind, sunlight, water, biomass, etc., is inevitable. Syngas (H_2 and CO) production from renewable sources such as lignocellulosic biomass can reduce the emissions of SO_2 and NO_x remarkably; the CO_2 neutral energy supply can also be achieved **[Sharma 91]**. Biomass gasification process is one of the main routes to produce either syngas, dedicated to second generation biofuels synthesis, or hydrogen. However, lignocellulosic biomass is a resource with variable composition, wide geographical dispersion and low energy density. These are important drawbacks when large-scale bio-energy production units are considered. In order to minimise the impact of transport, an alternative to the direct upgrading of biomass consists of preconditioning it on decentralised sites before transportation to a centralised bio-energy production unit.

Fast pyrolysis is a thermal decomposition process operated in the absence of oxygen with the aim to convert biomass into liquid products (bio-oil) together with non-condensable gases and solid char as by-products. For a few years, fast pyrolysis is being considered as a promising route for preconditioning biomass into bio-oil as liquid intermediate biofuel before its transport to a gasification unit. Indeed, bio-oil has much higher volume energy density than that of solid biomass and could be easily stored and transported from decentralised production sites to a large-scale processing unit. A lot of works on fast pyrolysis have been reported within the last years **[Meier 99] [Mohan 06]**.

The essential features to obtain high yields of bio-oil (up to 75 wt% on dry basis) are a moderate pyrolysis temperature (500°C), high heating rates (10^3-10^5°C.$^{-1}$), short vapour residence times (<2 s) and rapid quenching of the pyrolysis vapours. A number of pyrolysis reactors have been developed, including bubbling or circulating fluid bed, rotating cone, vacuum pyrolysis reactor, ablative reactor, and twin screw reactor **[Bridgwater 00] [Bridgwater 01] [Bridgwater 04]**. Since 1990, demonstration and pre-commercial units have been developed within EU and North-America.

A lot of works have also been dedicated to bio-oil characterization, upgrading and utilization. Bio-oil is very different compared to petroleum fuels. It is necessary to develop new

technologies for their successful utilization, which requires adequate understanding of their overall fuel properties **[Oasmaa 99]**.

However, the behaviour of these bio-oils within the gasification reactor also called reforming reactor has been hardly studied so far in the literature and the improvement of the scientific knowledge is necessary to the emergence of this route. A number of experimental studies devoted to bio-oil combustion brought some knowledge about the behaviour of a single droplet when heated and submitted to a reactive atmosphere.

Calabria and Alessio carried out lots of studies on the combustion behaviors of fibre-suspended single bio-oil droplets. The droplet size varied between 300 and 1100 μm and the furnace temperature changed in the range of 400–1200°C. The droplets were observed to undergo initial heating, swelling and microexplosion before ignition. During this stage, the temperature–time curves showed two zones with constant temperatures (100 and 450°C), which corresponded to the evaporation of light volatiles and the thermal cracking of unstable components, respectively. The droplets were ignited at around 600°C. The combustion of the droplets started with an enveloping blue flame. Then, the flame developed a yellow tail with its size increasing, which indicated the formation of soot. After that, the flame shrank and extinguished, and the remaining solid carbonaceous residues burned leading to the formation of ash **[Calabria 07] [Allessio 98] [Calabria 00]**.

Various pathways can be used for the production of hydrogen and hydrogen-rich gases from biomass: anaerobic digestion, fermentation, metabolic processing, high pressure supercritical conversion, gasification and pyrolysis **[Milne 02] [Ni 06] [Antonakou 06]**. Among them gasification appear to be the most feasible. The combination of fast pyrolysis of biomass followed by transportation in large units for steam reforming has attracted considerable attention of the research community, as one of the most promising viable methods for hydrogen production.

In air/steam gasification process the essential steps are pyrolysis, partial oxidation, cracking of tar, solid carbon residue gasification, reforming (steam and/or dry), and water gas shift to yield syngas, water, carbon dioxide, and unwanted products like tars, methane and carbon **[Levenspiel 05]**. As a summary, a schematic representation of air/steam gasification of single droplet of bio-oil is proposed in Figure 1.

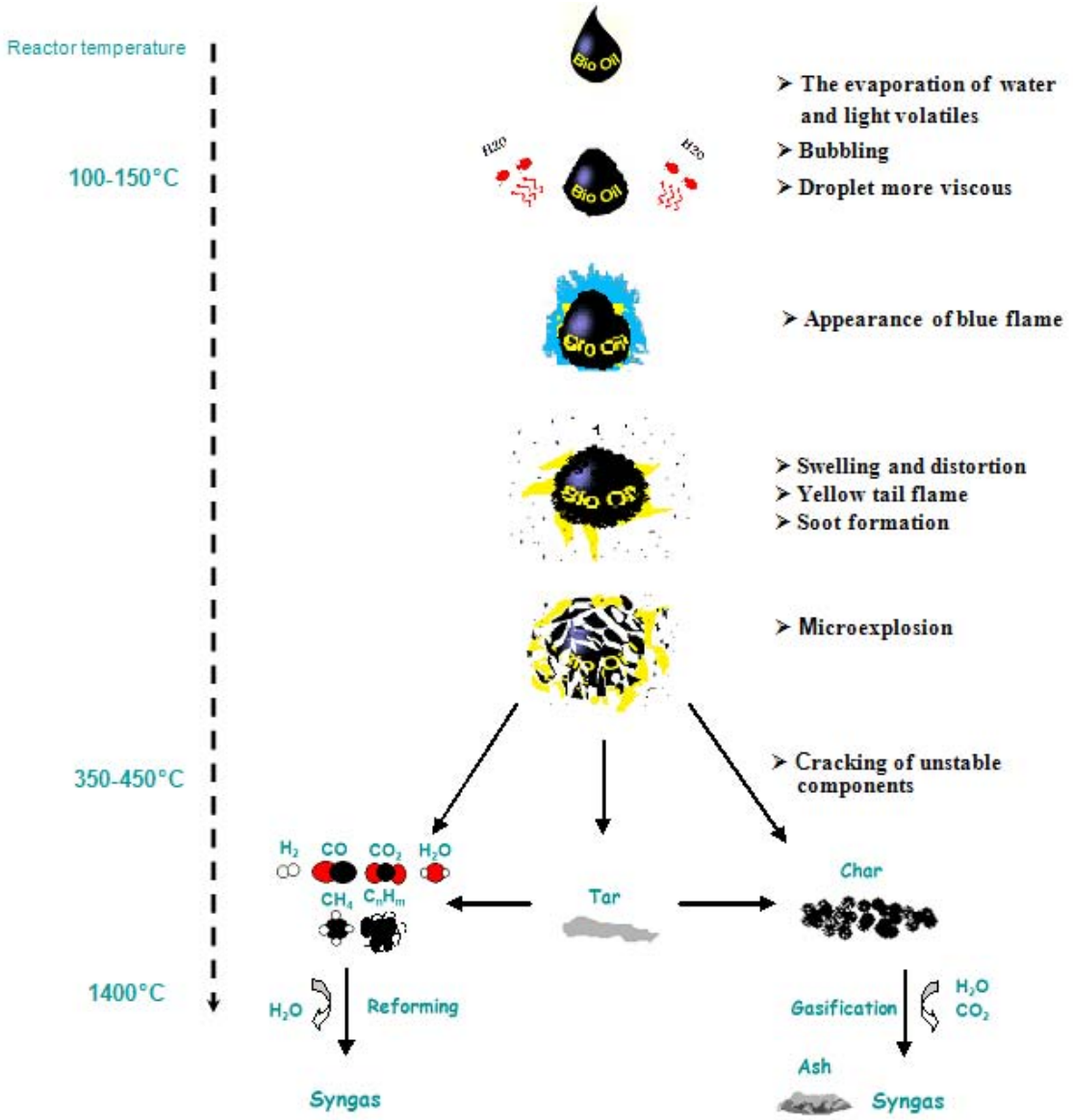

Figure 1. Schematic representation of air steam gasification of bio-oil droplet

1-1 Steam reforming of bio-oil

The steam reforming of the bio-oil can be simplified as the steam reforming of an oxygenated organic compound ($C_nH_mO_k$) following:

$$C_nH_mO_k + (n - k)\, H_2O \leftrightarrow nCO + (n + m/2 - k)\, H_2 \qquad (1)$$

During the last decade, catalytic steam reforming of bio-oil components has been widely studied, focusing on acetic acid as one of the most representative compounds.

Production of hydrogen from catalytic steam reforming of bio-oil was extensively investigated by NREL **[Wang 97] [Wang 98]**. Czernik et al. obtained hydrogen in a fluidized bed reactor from the carbohydrate derived fraction of wood bio-oil with a yield of about 80% of theoretical maximum **[Czernik 02]**. The catalytic steam reforming of the bio-oil or the model oxygenates (e.g., ethanol, acetic acid) has been widely explored via various catalysts, e.g., Ni-based catalysts **[Sakaguchi 10]**, Mg-doped catalysts **[Garcia 00]** and noble metal-loaded catalysts **[Trimm 97] [Rioche 05] [Goula 04]**. A lower steam-to-carbon ratio (S/C) and a lower reforming temperature are essential from the viewpoint of economy. Noble metals (Pt, Ru, Rh) are more effective than the Ni-based catalysts and less carbon depositing. Such catalysts are not common in real applications because of their high cost. Catalytic steam reforming of bio-oil is a costly process and presents several disadvantages such as carbon deposit and the deactivation of catalysts due to coke or oligomer deposition even in the presence of an excess of steam (S/C > 5) **[Trimm 97] [Rostrup-Nielsen 97]**. For these reasons, there is an interest in developing non catalytic gasification of bio-oil, which is the propose of this work.

Only very few works can be found on the non catalytic reforming of whole bio-oil. Bimbela et al. studied catalytic and non catalytic steam reforming of acetol (bio-oil model compound) in fixed bed at low temperature (550-750°C) in order to highlight the specific role of the catalyst in this process**[Bimbela 09]**. The same study is carried out by Guus van Rossum et al. concerning catalytic and non catalytic gasification of bio-oil in a fluidized bed over a wide temperature range (523-914°C) **[van Rossum 07]**. Marda et al. has developed a system for the volatilization and conversion of a bio-oil mixed with methanol to syngas via non-catalytic partial oxidation (NPOX) using an ultrasonic nozzle to feed the mixture. The effects of both temperature (from 625 to 850°C) and added oxygen (effective O/C ratio from 0.7 to 1.6) on the yields of CO and H_2 have been explored. They obtained hydrogen yield of about 75% of theoretical maximum **[Marda 09]**. Panigrahi et al. gasified biomass-derived oil (BDO) to syngas and gaseous fuels at 800°C. They obtained syngas (H_2 + CO) yield ranging from 75 to 80 mol % **[Panigrahi 03]**. Henrich et al. gasified lignocellulosic biomass. The first process step is a fast pyrolysis at atmospheric pressure, which produces large condensate, that was mixed to slurries. The slurries are pumped into a slagging entrained flow gasifier and are atomized and converted to syngas at high operating temperatures and pressures **[Henrich 04]**.

The present study is focused on the non catalytic steam reforming in the absence of O_2 of whole wood bio-oil in a High Temperature Entrained Flow Reactor (HT-EFR). The objectives of this work are to determine the syngas yield and composition as a function of temperature, and to carry in parallel a thermodynamic equilibrium calculation to determine the temperature at which the thermodynamic equilibrium is reached. Moreover, the impact of bio-oil alcohol-dilution on the syngas yield has been investigated. Finally the influence of ash on the reforming process has also been evaluated.

2- MATERIALS AND METHODS

2-1 Description of experimental device

The steam reforming experiments of bio-oils were carried out in a laboratory scale HT-EFR. It consists in a vertical tubular reactor electrically heated by a total 18 kW three-zone electrical furnace, and is able to reach 1600°C in a 1m long isothermal reaction zone, as illustrated in Figure 2. The atmosphere gas is generated by feeding the controlled flows of water and nitrogen in a 2 kW electrical steam generator. This atmosphere gas is then preheated to 900°C using a 2.5 kW electrical battery of heating elements before reaching the isothermal reaction zone. The HT-EFR was initially set up to achieve high heating-rate gasification of solid biomass, and was equipped for the present work with a specially designed bio-oil pulverization feeder, with the aim to obtain a very constant mass flowrate spray **[Couhert 09]**. The feeder consists of a 1 m long and 14 mm o.d. probe cooled with water at 50°C. At its extremity a stainless steel nozzle is integrated. This allows uniform distribution with fine atomization. Nozzle type (DELAVAN WDB) is a solid cone, with orifice diameter of 0.46mm and a spray angle of 60°. The oil is fed with a syringe which is pushed automatically. The expected mass flowrate of 0.3 g/min was too low for direct pulverization. Therefore, a 3.5 $NL.min^{-1}$ N_2 flowrate was used to entrain oil in the feeding probe and to ensure a thin spray of the oil. The spray of droplets is dispersed on the section of a 75 mm i.d. alumina reactor swept by 16 $NL.min^{-1}$ of an atmosphere gas containing 10 vol. % of steam in N_2. The steam to fuel mass ratio (fuel includes inherent water in bio-oil) was S/F=4.5, which equivalent to steam to carbon molar ratio of S/C= 8.3.

Steam reforming takes place along the reactor during a controlled vapour residence time, which was about 3s. The gas residence time is calculated as ratio of the reaction zone to the average gas velocity in the reactor. At 1760 mm downstream of the injection point, gases and solid residue were sampled by a hot-oil cooled probe. Gas and solid residue were separated

using a settling box and a filter, both heated to avoid water condensation. The water and potential remaining tars were first condensed in a heat exchanger, and non-condensable gases were forwarded to a micro-chromatograph analyser (μGC) to quantify H_2, CO, CO_2, CH_4, C_2H_2, C_2H_4, C_2H_6, C_3H_8 and C_6H_6.

Gases were also analyzed by other analyzers that allowed checking the absence of O_2, to confirm the analysis and to control continuously gas production during the gasification: a Fourier Transform InfraRed (FTIR) analyser, a Non-Dispersive InfraRed (NDIR) analyser coupled with a paramagnetic analyser for O_2 and a Thermal Conductivity Detector (TCD) to quantify H_2.

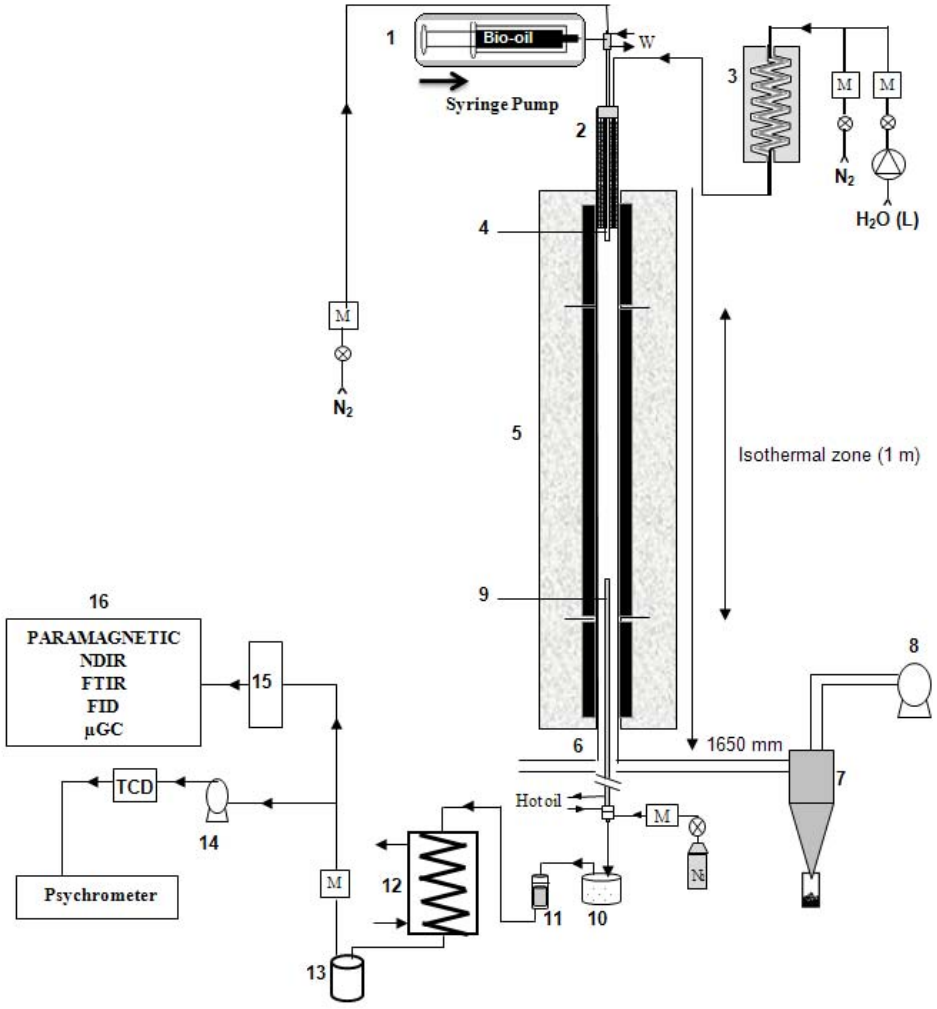

1- Injection system
2- Electrical preheater
3- Steam generator
4- Water cooled feeding probe
5- Three zones electrical furnace
6- 75 mm i.d. alumina reactor
7- Cyclone collector
8- Exhaust fan
9- Water cooled sampling probe
10- Hot settling box
11- Hot particle collector (filter)
12- Water cooler
13- Condensate collector
14- Sampling pump
15- Gas dryer
16- Gas analysers

M - Mass flow meters and controllers
N_2 - Nitrogen
W - Water (probes cooling)

Figure 2. Schematic view of the entrained flow reactor of Ecole des Mines d'Albi

2-2 Feedstock

The feedstock used for all experiments was bio-oil produced by fast pyrolysis of mixture of hardwood (oak, maple, ash) in an industrial-scale fluidized bed unit (Dynamotive, West Lorne, Ontario) and provided by CIRAD, France. Its physico-chemical properties have been measured (see Table 1). The water content of the bio-oil measured by Karl Fischer method (ASTM E203) is around 26 wt % which is in agreement with the average values reported in literature. It can be noticed that the solid particles content is rather high (2.3 wt.%) while the ash content remains very low (around 0.06 wt.%). This confirms that the solid particles mainly consist of high-carbon content char particles. These particles were entrained during bio-oil production by the gas stream to the bio-oil condensers. Ultimate analysis and LHV of the bio-oil are very similar to those of wood. From the ultimate analysis, the chemical formula of the bio-oil can be established as $CH_{1.18}O_{0.48}.0.4H_2O$.

After the production, the bio-oil was stored at 5°C in a fridge. Before experiments, it was filtered on a 30 µm sieve to eliminate largest solid particles which represented less than 0.01 %wt of the oil.

Table 1. Ultimate analysis and physico-chemical properties of bio-oil derived from hardwood fast pyrolysis

Ultimate analysis (wt.%)				**H_2O**	**Ash**	**Solids**	**LHV**	**Kinematic viscosity**
C	H	O	N	(wt.%)	(wt.%)	(wt.%)	(MJ/kg)	at 20°C ($mm^2.s^{-1}$)
42,9	7,1	50,58	< 0,10	26,0	0,057	2,34	14,5	103

3- RESULTS AND DISCUSSIONS

3-1 Effect of temperature

The first objective was to study the influence of temperature - over a wide range - on the syngas yield and composition.

Generally the gas mixture formed from catalytic reforming of bio-oil is composed of hydrogen, carbon monoxide and dioxide, methane, acetylene, unconverted steam, coke (carbon) and soot. Figure 3 presents the mole fraction of the gaseous products from this work (in dry basis and without N_2) as a function of temperature in the range 1000 to 1400°C. Error bars were established by repeating each test 2 or 3 times. The species C_2H_4, C_2H_6, C_3H_8 and C_6H_6 are not detected by chromatograph. Whatever the operating temperature between

1000°C and 1300°C, bio-oil is mainly decomposed to H_2, CO, CO_2, CH_4 and C_2H_2. Above 1300°C C_2H_2 disappears, while CH_4 disappears above 1400°C. As the temperature rises, the fraction of H_2 increases monotonically at the expense of carbon monoxide, methane and acetylene. Above 1300°C the hydrogen content remains almost stable. At 1400°C hydrogen mole fraction reaches the maximum value of 64 mol% of the syngas.

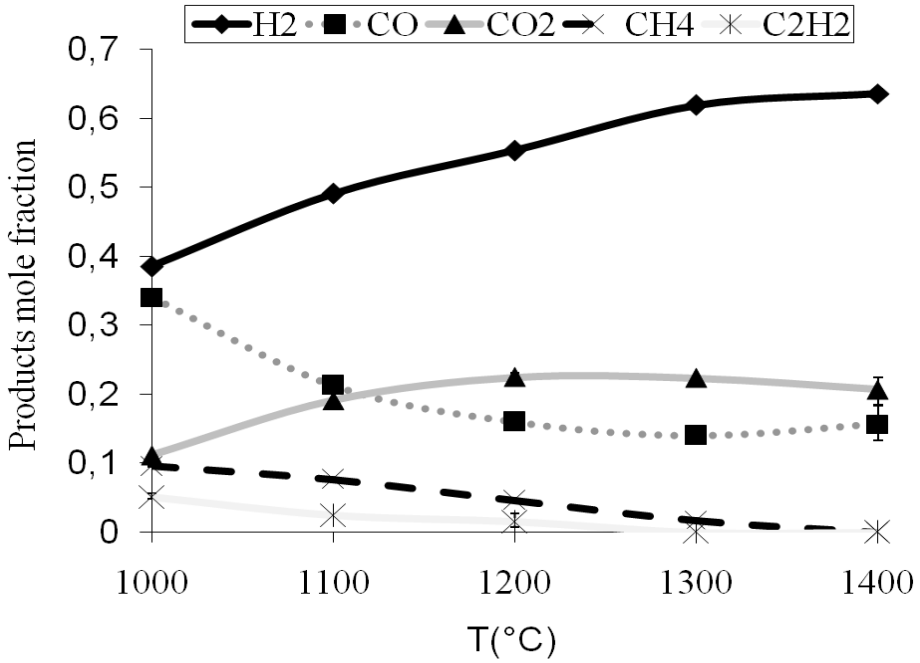

Figure 3. Composition of the produced syngas (dry basis and without N_2) - effect of temperature, at S/F=4.5

The reactions that may explain the increase of hydrogen with temperature are :

- The steam reforming of CH_4 and C_2H_2 into H_2 and CO (2)
- The water gas shift reaction $CO + H_2O \leftrightarrow CO_2 + H_2$ (3)

The water gas shift reaction can also explain the increase of carbon dioxide and the decrease of carbon monoxide between 1000 and 1200°C. Above 1200°C, carbon monoxide slightly increases. This may be explained by steam gasification of the solid carbon residue resulting from the pyrolysis of oil droplets to yield carbon monoxide and hydrogen following the reaction:

$$C + H_2O \leftrightarrow CO + H_2 \quad (4)$$

and potentially following the Boudouard reaction which would explain the slight decrease of CO_2:

$$C + CO_2 \rightarrow 2CO \quad (5)$$

It was observed that as the temperature increases the amount of collected solid decreases significantly above 1000°C. The process allows achieving very high heating rate estimated at 2000°C.s^{-1} **[Van de Steene 00]**. Under these conditions, the char yield measured is very low: < 1 wt.%. At 1400°C more than the 99.9% the bio-oil is converted to gas.

3-2 Equilibrium calculation

The thermodynamic equilibrium calculation is independent of reactor and predicts the yield of final products, based on the minimization of the Gibbs free energy of the system. It was conducted here using FactSage software 5.4 to establish whether the syngas was close or not to equilibrium at the different temperatures. Operating temperature varied from 1000°C to 1400°C; pressure was fixed at 1 atm. The software is not presented in detail in this paper; details of the thermodynamic calculation could be found on FactSage web site **[Factsage 09]**.
The results of prediction are presented in Figure 4, expressed in g of gas produced per g of crude bio-oil injected. As the temperature increases from 1000 to 1400°C the calculated equilibrium yield of H_2 remains approximately constant at 0,11g/g, while the yield of CO increases from 0.3 at 1000°C to 0.45g/g at 1400°C. The CO_2 yield decrease from 1.1 g/g at 1000°C down to 0.9 at 1400°C.
At 1000°C the calculation yields are far away from the experimental results. The deviation from equilibrium at lower temperatures is also reported by Sakaguchi et al **[Sakaguchi 10]**. At 1200°C the thermodynamic equilibrium begins to establish. The calculation nevertheless does not retrieve the presence of CH_4 and C_2H_2. At 1400°C the experimental yields are very close to the equilibrium calculation yields: 0.11 and 0.12 respectively for H_2, 0.45 and 0.45 respectively for CO, and 0.86 and 0.88 respectively for CO_2. It can be concluded that at this temperature the equilibrium is reached.

It is also interesting to compare the obtained experimental yields at 1400°C to the theoretical yields corresponding with complete gasification of oil that would follow:

$$CH_{1.18}O_{0.48}.0.4H_2O + 1.12\ H_2O \rightarrow CO_2 + 2.11\ H_2 \qquad (6)$$

The maximum stoichiometric H_2 yield for this oil would be 0.150g per 1g crude bio-oil while a value of 0.126 g was obtained experimentally. This shows that under our experimental conditions and at 1400°C steam reforming of bio-oil lead to a production of H_2 with a yield of about 84% of theoretical maximum.

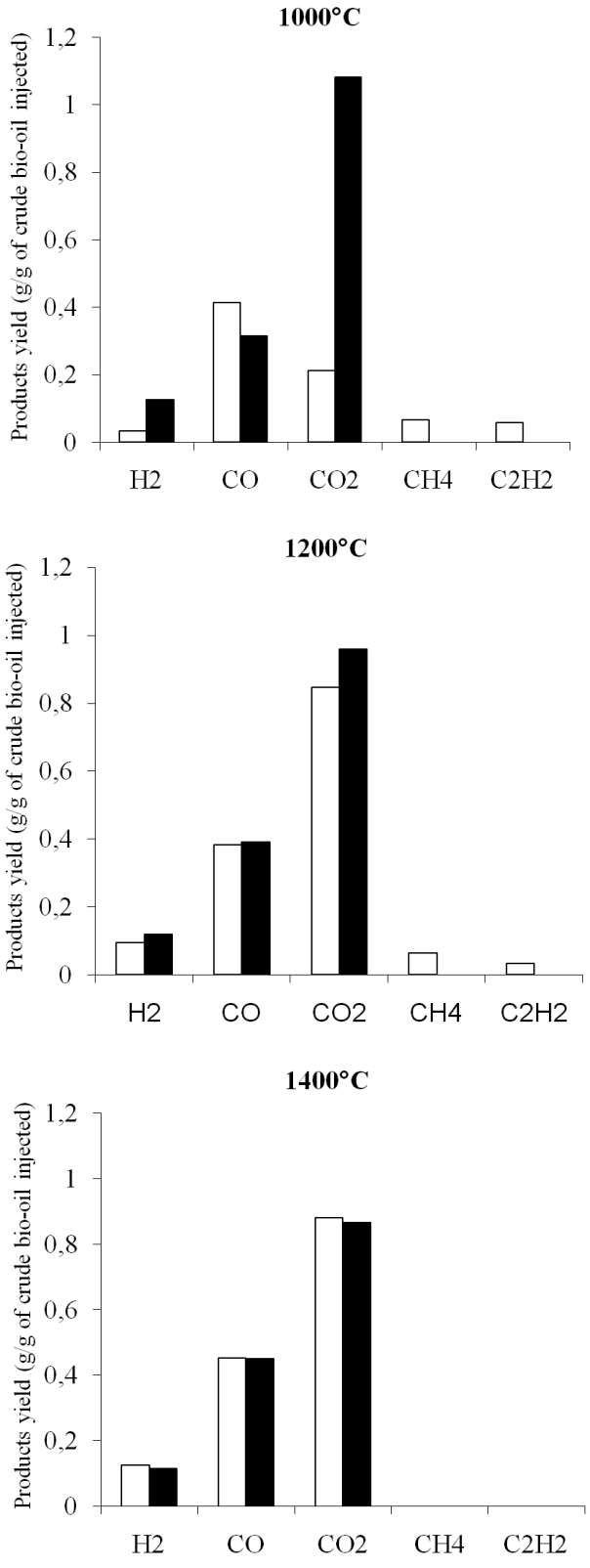

Figure 4. Gas yield from bio-oil reforming at 1000, 1200 and 1400°C, S/F=4.5
□ Experiments
■ Equilibrium calculation

3-3 Effect of dilution by a solvent

Most of the published works of steam reforming concern the aqueous fraction of bio-oil, model compounds or mixture of bio-oil/solvent. This choice is essentially linked to injection problems of the very viscous bio-oil. The injection of a mixture bio-oil/solvent is a classical way to facilitate nebulisation of crude bio-oil and to avoid injection plugging. It was therefore decided in this work to study the gasification of alcohol added bio-oil in order to evaluate the impact of dilution on the syngas yield. Bio-oil and ethanol were simply mixed and agitated in a container. The two components appear to be miscible; no segregation was observed even after storage. Figure 5 shows the gas yields of steam reforming of crude bio-oil, 75/25% bio-oil/ethanol mixture, 50/50% bio-oil/ethanol mixture and pure ethanol at 1400°C.

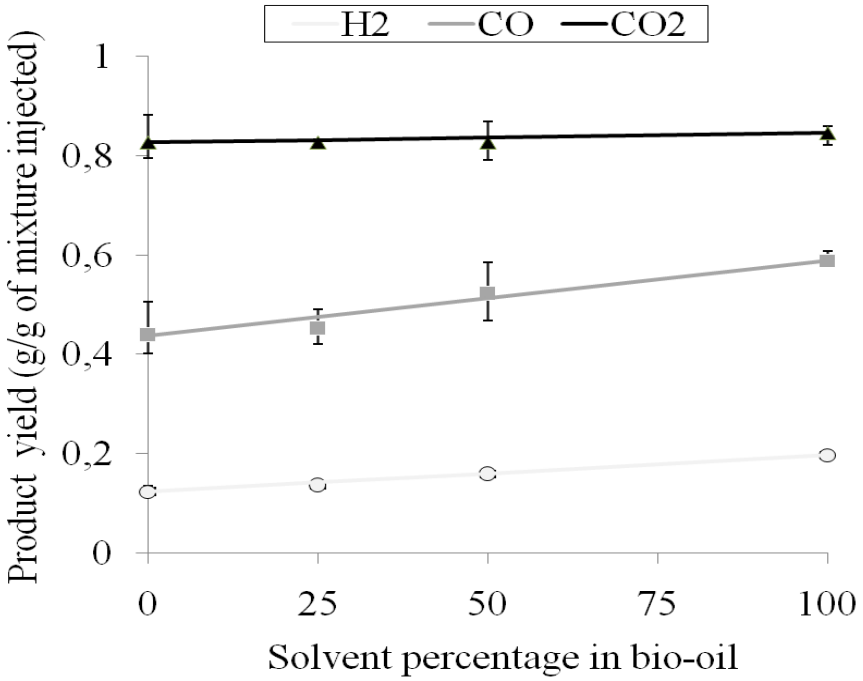

Figure 5. Yield of H_2, CO and CO_2 during gasification at 1400°C and S/F=4.5 of crude bio-oil with different dilutions (CH_4 and C_2H_4 were not present in the produced gas at 1400°C).
- Lines: Theoretical results - **Symbols:** Experimental results

We can notice that the hydrogen and carbon monoxide yield increase when we increase the fraction of ethanol in crude bio-oil, while CO_2 remains more or less constant, CH_4 and C_2H_4 were not present in the produced gas at 1400°C. Considering the yield of pure ethanol and crude bio-oil, we can observe that the H_2 and CO yields seem to follow an additivity law: theoretical yields as calculated from an additivity law fit with experimental yields of gasification products. Some dispersion can be observed concerning CO yields. Nevertheless,

the difference between experimental results and calculated values remain smaller than experimental error bars. This validates an additivity law. The fact that an additivity law is observed cannot be interpreted as a non interaction between bio-oil and the solvent along the primary pyrolysis step, but rather by the fact that at high temperature and closed to equilibrium conditions the composition of the gas tends towards a sum of the gas that would be produced from bio-oil and solvent separately. This result essentially allows to trace a crude bio-oil behavior if it is diluted in a solvent.

3-4 Effect of ash

Ash is known for their catalytic effect during thermo-chemical conversion of biomass, as shown in previous works done on solid biomass. They indicated that biomass ash acted catalytically and specifically in tar steam reforming; it lowered the temperature of steam reforming reactions during gasification **[Skoulou 09] [Masek 07]**.

The aim of this part was to evaluate the potential influence of the presence of mineral matter on yields of final products from bio-oil gasification. Crude bio-oil containing 0.057% of minerals and crude bio-oil with 3% of ash were prepared to highlight effect of minerals in gasification process. The added ash was prepared by burning crushed beech wood (particle size of 300-400µm) in a furnace equipped with 3 drawers at 600°C. The choice of this temperature is designed to perform a « mild » heat treatment in order to preserve the initial properties of minerals present in the biomass, as in the case of the production of bio-oil by pyrolysis. The wood is distributed in the drawers on a thin layer of 1.5cm thickness to ensure good heat transfer and air diffusion. Air was fed to the reactor at low flow rate, 30NL/h, to avoid ignition and high temperature rapid combustion of wood.

The analysis of the elements most cited in literature was performed in the prepared ash. Silica, especially, is an important element that reacts easily with alkali metals and creates fusion and deposition problems during combustion and gasification **[Arvelakis 02]**. Calcium is present in considerable amount in wood ash, while potassium is at lower amounts quite volatile at high temperature. Trace elements Fe, Ni and Al, are known to get involved in various steam reforming reactions during gasification **[Masek 07] [Zhang 07]**. The ash components were quantified by ICP (Inductively Coupled Plasma Optical Emission Spectrometry), presented in Table 2. It can be noticed that Ca, K, Mg, and Mn are present in high concentration. Other

minority elements such as Co, Cr, Cu, Fe, Pb, Si, Zn and Cd are present in much lower concentration.

Table 2. Composition of ashes (from combustion of wood) [wt%, dry ashes]

Ca	K	Mn	Mg	P	Ni	Na	Al
11,67	3,80	1,74	1,54	1,01	0,25	0,24	0,10

The gasification temperature of 1200°C was chosen, because as demonstrated before at this temperature the equilibrium is not reached. Error bars were established by repeating each test 2 or 3 times.

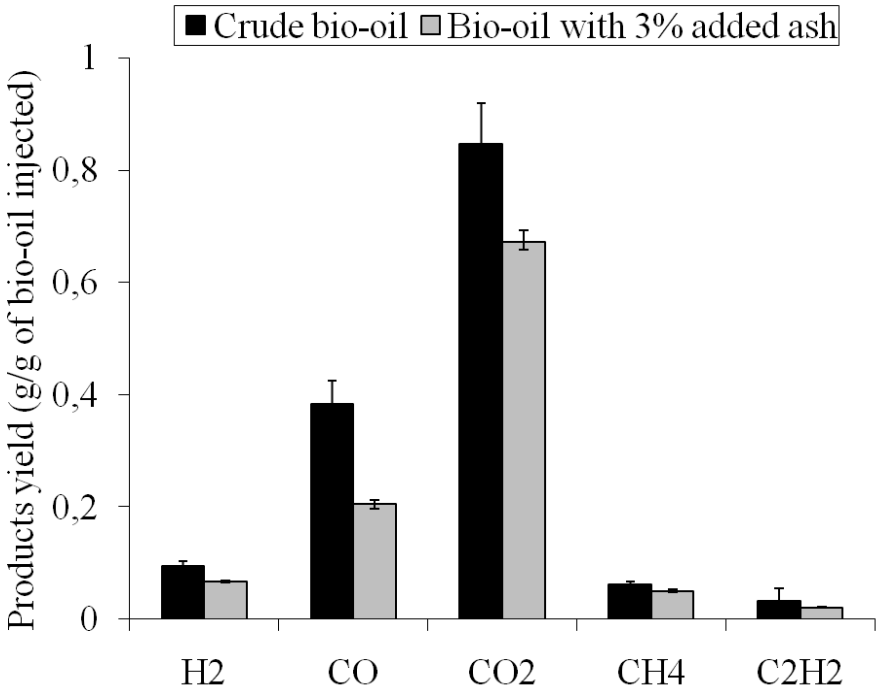

Figure 6. Yield of gas species during gasification of crude bio-oil and crude bio-oil with 3% of ash at 1200°C and S/F=4.5- effect of ash on product yield

Figure 6 shows the obtained gas yields from ‘‘crude bio-oil”, and ‘‘crude bio-oil + 3% beech ash”. Surprisingly one can notice a clear decrease in the yields of all gas species when the amount of ash is increased. The results are expressed in g of gas produced per g of ash free crude bio-oil injected. Among them, the H_2 yield decrease from 0.094 to 0.067g/g. CO and CO_2 yields decreased significantly: from 0.38 to 0.20 g/g and from 0.84 to 0.67g/g respectively. An explanation could be that added minerals favour polymerization reactions.

These reactions lead to the formation of larger quantities of carbonaceous solid residue that is not gasified, which would cause a decrease in the amount of produced gas, especially CO and CO_2.

At the high gasification temperature, volatilization of alkalis probably played a negative role on ash catalytic effect. The fact that ash did not favour gas formation at the temperature of 1200°C could also be explained by the work of Masek et al. **[Masek 07]** who pointed out ash deactivation at 950°C. Such a high temperature was shown to accelerate iron sintering leading to a loss of Fe dispersion **[Skoulou 09]**.

4- CONCLUSIONS

Crude bio-oil was successfully steam reformed in a lab-scale High Temperature Entrained Flow Reactor. The reaction temperature has a significant influence on the process. An increase in the reaction temperature implies higher hydrogen yield and higher solid carbon conversion. A thermodynamic equilibrium calculation showed that equilibrium is reached at 1400°C but not at 1300°C and below for residence times of about 3s.

The gasification of mixtures bio-oil/alcohol showed that the yields of gas follow an additivity law based on the yields of solvent and of bio-oil.

When adding ash to bio-oil, it has been observed a strong decrease in gas yield while an increase was expected as in the case of catalytic process. Ash may favour polymerization reactions, causing a decrease in the yield of gas. The volatilization of alkalies and the iron sintering at high gasification temperature may have also played a negative role on ash catalytic effect.

Experiments conducted in a high-temperature entrained flow gasifier showed the capability of this technology to obtain high gaseous product yield using non catalytic steam gasification. This work was performed without O_2 as first simplified approach. Prior to up scaling, experiments in the presence O_2 of will be required.

ACKNOWLEDGEMENTS

The authors gratefully acknowledge the financial support from EnerBio Program of Fondation Tuck France, and express their gratitude to Mr. Bernard AUDUC technician in Ecole des Mines d'Albi-Carmaux for his technical assistance, and contribution to device design and operation.

REFERENCES

[Allessio 98] Allessio, J. D.; Lazzaro, M.; Massoli, P.; Moccia, V. In: Thermo-optical investigation of burning biomass pyrolysis oil droplets. Twenty-seventh symposium (international) on combustion. Pittsburgh: The Combustion Institute 1998, 1915–22.

[Antonakou 06] Antonakou, E.; Lappas, A.; Nilsen, M.; Bouzga, A.; Stocker, M. Evaluation of various types of Al-MCM-41 materials as catalysts in biomass pyrolysis for the production of bio-fuels and chemicals. Fuel 2006, 85(14–15), 2202–12.

[Arvelakis 02] Arvelakis, S.; Koukios, E. G. Physicochemical upgrading of agroresidues as feedstocks for energy production via thermochemical conversion methods. Biomass Bioenergy 2002, 22, 331–8.

[Bimbela 09] Bimbela, F.; Oliva M.; Ruiz J.; Garcia L.; Arauzo, J. Catalytic steam reforming of model compounds of biomass pyrolysis liquids in fixed bed: Acetol and n-butanol. J. Anal. Appl. Pyrolysis Volume 85, Issues 1-2, May 2009, 204-213.

[Bridgwater 00] Bridgwater, A. V.; Peacocke, G. V. C. Fast pyrolysis processes for biomass. Renew Sust Energy Rev 2000, 4, 1–73.

[Bridgwater 01] Bridgwater, A. V.; Czernik, S.; Piskorz, J. An overview of fast pyrolysis technology. In: Bridgwater AV, editor. Progress in thermochemical biomass conversion. Oxford: Blackwell; 2001, 977–97.

[Bridgwater 04] Bridgwater, A. V.; Maniatis, K.; The production of biofuels by the thermochemical processing of biomass. In: Archer MD, Barber J, editors. Molecular to global photosynthesis. London: IC Press 2004, 521–612.

[Calabria 00] Calabria, R.; Allessio, J. D.; Lazzaro, M.; Massoli, P.; Moccia, V. Bio-fuel oil. Upgrading by hot filtration and novel physical methods. Task 5: fundamental behavior of BFO in combustion. Final report, JOR3-CT97-0253; 2000.

[Calabria 07] Calabria, R.; Chiariello, F.; Massoli, P. Combustion fundamentals of pyrolysis oil based fuels. Exp Therm Fluid Sci 2007, 31, 413–20.

[Couhert 09] Couhert, C.; Commandre, J. M.; Salvador, S. Is it possible to predict gas yields of any biomass after rapid pyrolysis at high temperature from its composition in cellulose, hemicellulose and lignin. Fuel 2009, 88, 408–417.

[Czernik 02] Czernik, S.; French, R.; Feik, C. Hydrogen by catalytic steam reforming of liquid byproducts from biomass thermoconversion processes. Ind Eng Chem Res 2002, 41,4209–15.

[factsage 09] http://www.factsage.com, 2009.

[Garcia 00] Garcia, L.; French, R.; Czernik, S.; Chornet, E. Catalytic steam reforming of bio-oils for the production of hydrogen: effects of catalyst composition. Appl. Catal. 2000, 201, 225–239.

[Goula 04] Goula, M. A.; Kontou, S. K.; Tsiakaras PE. Hydrogen production by ethanol steam reforming over a commercial Pd/γ-Al2O3 catalyst. Appl. Catal. 2004, 49, 135– 144.

[Henrich 04] Henrich, E.; Weirich, F. Pressurized Entrained Flow Gasifiers for Biomass. Environmental Engineering Science 2004, 21, 53-64.

[Levenspiel 05] Levenspiel, O. What will come after petroleum. Ind. Eng. Chem. Res. 2005, 44, 5073.

[Marda 09] Marda, J. R.; DiBenedetto, J.; McKibben, S.; Evans, R. J.; Czernik, S.; French, R.J.; Dean, A. M. Non-catalytic partial oxidation of bio-oil to synthesis gas for distributed hydrogen production. international journal o f hydrogen energy 2009, 34, 8519–8534.

[Masek 07] Masek, O.; Sonoyama, N.; Ohtsubo, E.; Hosokai, S.; Li, C. Z.; Chiba, T. Examination of catalytic roles of inherent metallic species in steam reforming of nascent volatiles from the rapid pyrolysis of brown coal. Fuel Process Technol 2007, 88, 179–85.

[Meier 99] Meier, D.; Faix, O. State of the art of applied fast pyrolysis of lignocellulosic materials – a review. Bioresource Technol 1999, 68, 71–7.

[Milne 02] Milne, T. A.; Elam, C. C.; Evans, R. J. Hydrogen from biomass, State of the art and research challenges. Golden, CO, USA: National Renewably Energy Laboratory. IEA/H2/TR-02/001.

[Mohan 06] Mohan, D.; Pittman, C. U.; Steele, P. H. Pyrolysis of wood/biomass for bio-oil: a critical review. Energy Fuel 2006, 20, 848–89.

[Ni 06] Ni, M.; Leung, D. Y. C.; Leung, M. K. H.; Sumathy, K. An overview of hydrogen production from biomass. Fuel Process Technol 2006, 87(5), 461–72.

[Oasmaa 99] Oasmaa, A.; Czernik, S. Fuel oil quality of biomass pyrolysis oils – state of the art for the ender users. Energy Fuel 1999, 13, 914–21.

[Panigrahi 03] Panigrahi, S.; Dalai, A. K.; Chaudhari, S. T.; and N. N. Bakhshi. Synthesis Gas Production from Steam Gasification of Biomass-Derived Oil. Energy Fuels 2003, 17, 637–642.

[Rioche 05] Rioche, C.; Kulkarni, S.; Meunier, F. C.; Breen, J. P.; Burch, R. Steam reforming of model compounds and fast pyrolysis bio-oil on supported noble metal catalysts. Appl. Catal. 2005, 61, 130–139.

[Rostrup-Nielsen 97] Rostrup-Nielsen, J. R. Industrial relevance of coking Catal. Today 1997, 37, 225–23.

[Sakaguchi 10] Sakaguchi, M.; Paul Watkinson A.; Naoko, E. Steam Gasification of Bio-Oil and Bio-Oil/Char Slurry in a Fluidized Bed Reactor. Energy Fuels 2010, 24, 5181–5189.

[Sharma 91] Sharma.; Bakhshi, N. N. Catalytic upgrading of biomass-derived oils to transportation fuels and chemicals. Can. J. Chem. Eng. 1991, 69, 1071–1081.

[Skoulou 09] Skoulou, V.; Kantarelis, E.; Arvelakis, S.; Yang, W.; Zabaniotou, A. Effect of biomass leaching on H_2 production, ash and tar behavior during high temperature steam gasification (HTSG) process. international journal o f hydrogen energy 2009, 34, 5666–5673.

[Trimm 97] Trimm, D. L. Coke formation and minimization during steam reforming reactions. Catal. Today 1997, 37, 233–238.

[Van de Steene 00] Van de Steene, L.; Salvador, S.; Charnay, G. Controlling powdered fuel combustion at low temperature in a new entrained flow reactor. Combustion Science and Technology 2000, 159, 255-279.

[van Rossum 07] van Rossum, G.; Kersten, S. R. A.; van Swaaij, W. P. M. Catalytic and Noncatalytic Gasification of Pyrolysis Oil. Ind. Eng. Chem. Res. 2007, 46, 3959-3967.

[Wang 97] Wang, D.; Czernik S. ; Montane, D. Biomass to hydrogen via pyrolysis and catalytic steam reforming of the pyrolysis oil and its fractions. Ind Eng Chem Res 1997, 36, 1507–18.

[Wang 98] Wang, D.; Czermik, S.; Chornet, E. Production of hydrogen from biomass by catalytic steam reforming of fast pyrolytic oils. Energy Fuels 1998, 12, 19–24.

[Zhang 07] Zhang, R.; Wang, Y.; Robert, C. Brown Steam reforming of tar compounds over Ni/olivine catalysts doped with CeO2. Energy Convers Manage 2007, 48, 68–77.

CHAPTER 6: SOOT FORMATION AND OXIDATION DURING BIO-OIL GASIFICATION: EXPERIMENTS AND MODELING

This chapter will be submitted as a research paper in the international journal Fuel.

Keywords: bio-oil, soot, pyrolysis, partial oxidation, gasification

ABSTRACT

The high temperature gasification of bio-oil in non catalytic processes leads to the formation of soot, which is an undesirable solid product. The amount of produced soot essentially depends on the reaction temperature, on the fraction of steam used for gas reforming and char conversion, and on the amount of oxygen that is necessary for the process to be autothermal. A model is proposed to describe soot formation and oxidation during gasification. It is based on the description of bio-oil heating, devolatilization, reforming of gases and conversion of both char and soot solids. Detailed chemistry (159 species and 773 reactions) is used in the gas phase. Soot production is described by a single reaction based on C_2H_2 species concentration and three heterogeneous soot oxidation reactions. To support validation of the model, three sets of experiments were carried out in lab-scale Entrained Flow Reactor (EFR) equipped with soot quantification device. The temperature was varied from 1000 to 1400°C and three gaseous atmospheres were considered: default of steam, large excess of steam (H_2O/C = 8), and presence of oxygen in the range O/C = 0.075 to 0.5. The model is shown to accurately describe the evolution of the concentration of the main gas species and to satisfactorily describe the soot concentration under the three atmospheres using a single set of identified kinetic parameters. Thanks to this model the contribution of the different mechanisms involved in soot formation and oxidation in various situations can be assessed.

1- INTRODUCTION

Due to continuous decrease in the amount and availability of conventional fossil fuels, it is becoming inevitable to search for new fuel sources. The renewable nature of biomass places it among the most attractive options. Using biomass as renewable feedstock would strongly contribute to decrease green house gas emissions due to neutral CO_2 balance. From a technical point of view, biomass feedstocks (energy crops, agricultural residues, forestry, industrial or municipal wastes) can be transformed into sustainable syngas (H_2+CO) or hydrogen by thermo chemical processes like gasification which includes several methods such as steam reforming (SR), partial oxidation (POX), and oxidative steam reforming (OSR). This last process is of interest here.

Among the various strategies for biomass collection, storage, transport and conversion, much interest was devoted in the last decade to bio-oil, liquid form of biomass with high energy content. Centralized gasification of bio-oil produced in small and dispersed units is one of the promising routes of syngas or hydrogen production from biomass.
Biomass fast pyrolysis technology for bio-oil production has been extensively studied recently. This is a thermal decomposition process that converts biomass into organic liquids (i.e., the bio-oil) by fast heating in the absence of air at around 400-600°C yields can reach 75–80% (including water) based on the original biomass weight **[Bridgwater 00]**. Bio-oil has higher energy volume density than that of solid biomass. This is particularly promising due to the high geographic dispersion of biomass which generally leads to high transportation costs.

Soot formation is a major problem to face with in biomass gasification. In combustion process soot formation results from incomplete combustion and typically occurs at fuel-rich stoichiometries. Soot formation is an active field of combustion research. This is not only because it remains a challenge from a fundamental point of view, but also because combustion-generated soot particles have serious environmental effects **[Vedal 97]**. They are also associated with health risks since both polycyclic aromatic hydrocarbons (PAHs) that are precursors of soot and soot-associated organics have been identified to be carcinogenic. More, soot may be a problem during operation of engines because it can lead to solid deposits **[Bozzano 02]**.

Thus, the control of soot emission from combustion or gasification processes is crucial issue that needs to be solved to avoid problems of deposits, to ensure syngas purity and to reduce harmful impacts to humans and the environment. Quantitative prediction of soot growth and subsequent oxidation mechanisms are critical to the development of approaches to control soot emissions.

Until now, most experimental studies of sooting processes have been focused on fossil fuel combustion in diesel engines, and more specially in diffusion flames. Thus, there are very few available data on soot formation from biomass and from bio-oil. The purpose of this paper is to propose a model able to describe as simply as possible the formation of soot and its oxidation by reaction with H_2O, O_2 and CO_2. The model is expected to describe the effect of temperature on soot formation and destruction over the range 1000-1400°C in three different kinds of atmosphere: inert, H_2O enriched and O_2 containing.

A rapid review on soot formation and oxidation is proposed below to support understanding of the work. Soot is a carbonaceous solid produced in pyrolysis and combustion/gasification systems when conditions are such as to allow gas-phase condensation reactions of the fuel. The most accepted simple theory for soot formation is well described by Haynes and Wagner **[Haynes 81]**. They assert that the pyrolysis of hydrocarbons produces smaller hydrocarbons, and in particular acetylene. The initial step is the formation of the first aromatic species from the aliphatic hydrocarbons, followed by the addition of other aromatic and alkyl species to give higher species, i.e. PolyAromatic Hydrocarbons (PAH). The continued growing of these PAHs results in the generation of small soot particles.

There is no detailed soot formation mechanism at the moment because this is a complex process that involves many chemical and physical steps. Soot generation in combustion processes needs a detailed understanding of chemical reaction pathways responsible for its formation. Nevertheless it is widely accepted that the soot formation consists of the following processes which are summarized schematically in Figure 1: particle nucleation, surface growth and particle coagulation **[Richter 05] [Balthasar 05] [Krestinin 00] [Richter 00] [Smooke 05] [Maugendre 09]**.

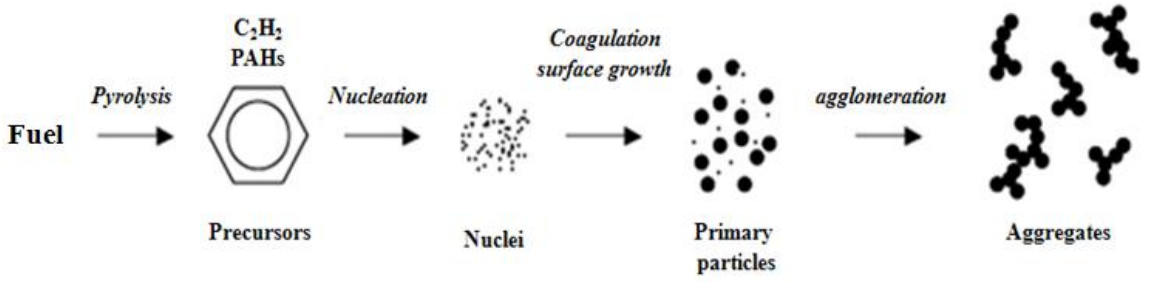

Figure 1. Mechanism of the formation and the evolution of the soot aggregates. Adapted from **[Maugendre 09]**

Soot and PAHs oxidation is a process competing with the formation of these species. It gives rise to the formation of CO and CO_2. Detailed investigations of carbon oxidation show that molecular O_2 as well as the O and OH radicals all participate in soot oxidation **[Cavaliere 94]**. OH is particularly effective **[Lee 62] [Roth 90]**. Roth et al. **[Roth 91]** showed that hydrogen peroxide (H_2O_2) assists soot oxidation at low temperatures, due to the presence of high concentrations of OH radicals.

Oxidation of soot with steam and carbon dioxide - also called gasification - was studied by de Soete **[de Soete 88]** using the same techniques as for oxygen. There was negligible reaction with H_2O below 800 K and the major product at higher temperatures was CO. The order of reaction with respect to H_2O was close to one. The gasification rates with carbon dioxide were lower than those with steam. The reaction order for CO_2 was again one, but the quantities of product CO and CO_2 were generally of the same order. Thanks to typical Arrhenius data for the gasification of soot with H_2O and CO_2, De Soete **[de Soete 88]** showed that the trends in the reaction of soot with H_2O and CO_2 are similar to those with oxygen, but at reduced rates of reaction.

In soot formation modeling, several principle proposals are known, which describe the nature of soot particle inception. According to them, different types of species are ranged as potential precursors, leading to soot particle inception e.g., polyacetylenes or polyynes **[Homann 67] [Frenklach 85] [Kiefer 90] [Krestinin 87]**, and polycyclic aromatic hydrocarbons **[Frenklach 94] [Griesheimer 98] [Appel 00] [Richter 05]**. The investigation of the role of acetylene in soot formation dates back several decades ago. The reason why many experimentalists suggested the polyacetylenes as contingent soot precursors is that several experimental investigations, performed in the 1960s and 1970s, showed the existence of hydrocarbons having molecular mass in excess of 250 g/mol. They appear at the end of the

reaction zone, before the appearance of the first particles **[Homann 67] [Haynes 81]**. Unlike the PAHs, these species rapidly disappear during the soot growth, and are no longer detected at the end of the reaction zone. Some authors suggested that such species could be polyacetylenes **[Cundall 77]**. The development of this idea can be summarized as follows: Berthelot et al. **[Berthelot 66]** and Lewes et al. **[26 Lewes 94]** emphasized the importance of C_2H_2 in thermal decomposition reactions. Keller **[Keller 00]** proposed the hypothesis of carbon formation from acetylene through its simultaneous polymerization and dehydrogenation. Haynes and Wagner **[Haynes 81]** pointed out that the investigations of the absorption profiles for "pre-soot" species in pyrolysis and oxidation of different fuels indicated the presence of species capable of absorbing in the visible and ultraviolet before soot becomes observable. Cundall et al. **[Cundall 77]** analysed the shape of some spectra and suggested that the absorbers were predominantly polyacetylenes, probably $C_{10}H_2$ and $C_{12}H_2$. These species were measured through mass-spectrometry by Kistiakowsky et al. **[Bradley 61] [29 Gay 65]** as products of C_2H_2 pyrolysis. Kistiakowsky et al and other authors **[Tanzawa 79]** concluded that the reaction proceeded as:

$$C_2H_2 \Longrightarrow C_4H_3 \Longrightarrow C_4H_2 \Longrightarrow C_6H_2 \Longrightarrow C_8H_2 \ldots \quad (1)$$

To model such a chemical process, it is desirable to use detailed chemical kinetic mechanisms including up to C6 species, for exemple the HACA-mechanism **[Frenklach 90]** and the extended HACA-mechanism **[Mauss 98]**.

An alternative approach for soot modeling is to use a semi-empirical model. The soot semi-empirical model here proposed is based on C_2H_2 as precursor. A four step soot formation and oxidation model performs the soot computations using the mechanism:

$C_2H_2 \rightarrow 2\ C(soot) + H_2$	**Soot formation**	(2)
$C(soot) + 0{,}5\ O_2 \rightarrow CO$	**Soot oxidation**	(3)
$C(soot)+H_2O \rightarrow CO+H_2$	**Soot gasification by H_2O**	(4)
$C(soot)+CO_2 \rightarrow 2CO$	**Soot gasification by CO_2**	(5)

More details about the model are given in section 2-4 of this paper.

2- MATERIALS AND METHODS

2-1 Description of experimental device

Experiments were carried out in a laboratory scale Entrained Flow Reactor (EFR). It consisted in a vertical tubular reactor electrically heated by a total of 18 kW three-zone electrical furnace, and was able to reach 1600°C in a 1m long isothermal reaction zone, as illustrated in Figure 2. The atmosphere gas was generated by feeding the controlled flows of nitrogen in a 2 kW electrical steam generator. This atmosphere gas was then preheated at 900°C using a 2.5 kW electrical battery of heating elements before reaching the isothermal reaction zone. The EFR was equipped with a specially designed bio-oil spraying feeder. The feeder consisted of a 1 m long and 14 mm o.d. probe cooled with water at 30°C. At its extremity a stainless steel nozzle was integrated, which allowed uniform distribution with fine atomization. The microscopic observation of droplets impacted on a surface indicates a size ranging between 10 and 100μm. However, the majority of the droplets were much smaller and not observable.

The oil was fed with a syringe which is pushed automatically. The expected mass flowrate of0.3 $g.min^{-1}$ was too low for direct spraying. Therefore, a 3.5 $NL.min^{-1}$ N_2 flowrate was used to entrain oil in the feeding probe and to ensure a thin spray of the oil. The spray of droplets was dispersed on the section of the 75 mm i.d. alumina reactor swept by 15 $NL.min^{-1}$ of atmosphere gas. At 1760 mm downstream of the injection point, gas and solid residue were sampled by a hot-oil cooled probe. The injected atmosphere gas flowrate and the sampled gas flowrate were accurately measured using mass flow meters/controllers. Gas and solid residue were separated using a settling box and a filter, both heated to avoid water condensation. The water and potential remaining tar were first condensed in a heat exchanger, and non-condensable gases were forwarded to a micro-chromatograph analyser (μGC) to quantify H_2, CO, CO_2, CH_4, C_2H_2, C_2H_4, C_2H_6, C_3H_8 and C_6H_6. The experimental device has been described into details in **[Chhiti 10].**

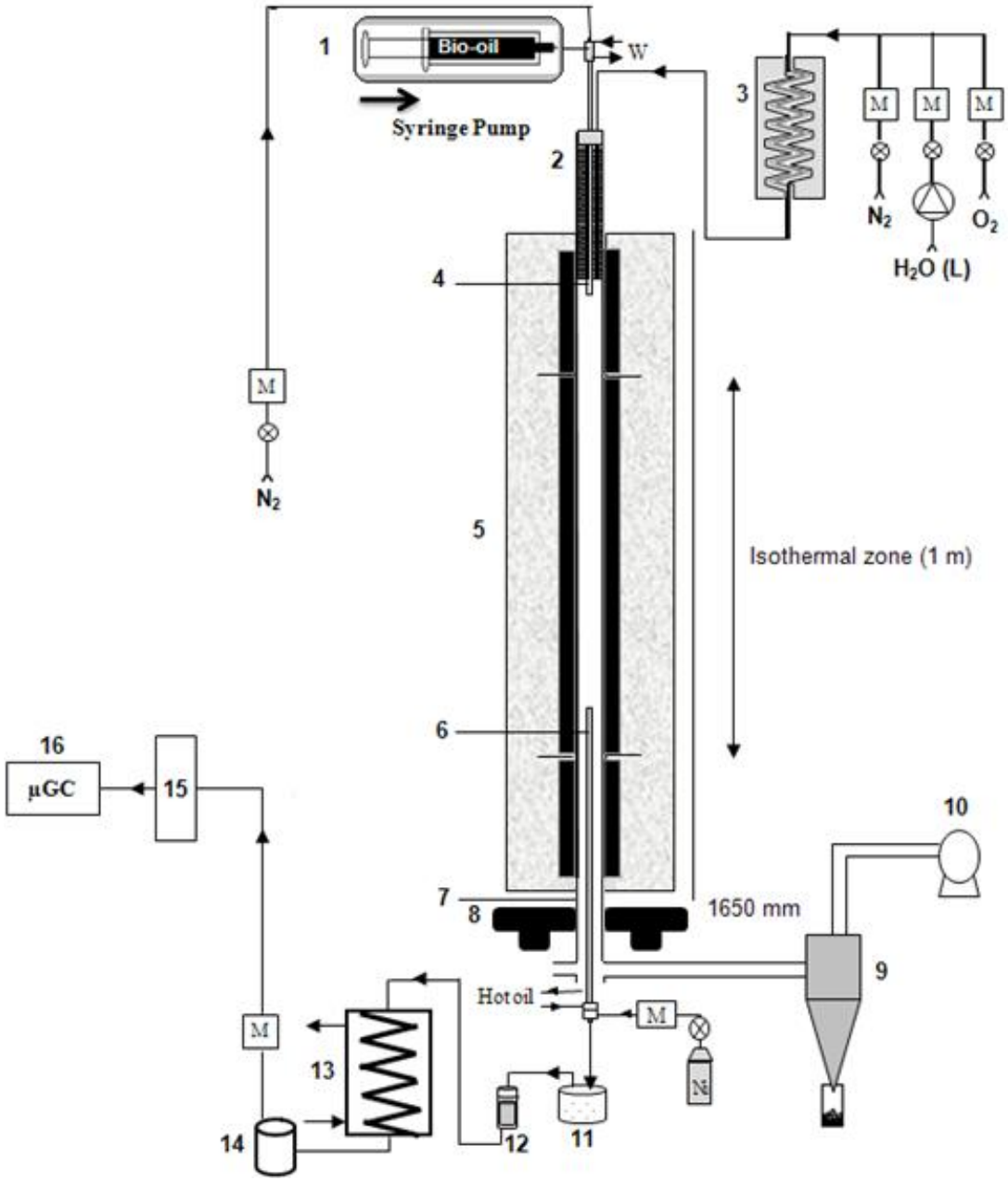

1- Injection system
2- Electrical preheater
3- Steam generator
4- Water cooled feeding probe
5- Three zones electrical furnace
6- Oil cooled sampling probe
7- 75 mm i.d. alumina reactor
8- Soot quatification device
9- Cyclone collector
10- Exhaust fan
11- Hot settling box
12- Hot particle collector (filter)
13- Water cooler
14- Condensate collector
15- Gas dryer
16- Gas analyser

M - Mass flow meters and controllers
N_2 - Nitrogen
W - Water (feeder cooling)

Figure 2. Scheme of the Entrained Flow Reactor (EFR)

2-2 Soot quantification device

Laser extinction was used to make quantitative measurements of soot content in the produced gas. The setup is shown in Figure 3. For laser extinction, a modulated 50kHz, 0.5mW, HeNe laser beam (632.8 nm) is passed through sooting region (optical path of 75 mm) and collected by an integrating sphere, narrow band pass filter, and a photodiode. This collection system accounts for beam-steering effects caused by refractive index gradients and minimizes background interference from soot luminosity **[Musculus 02, Pickett 02]**.

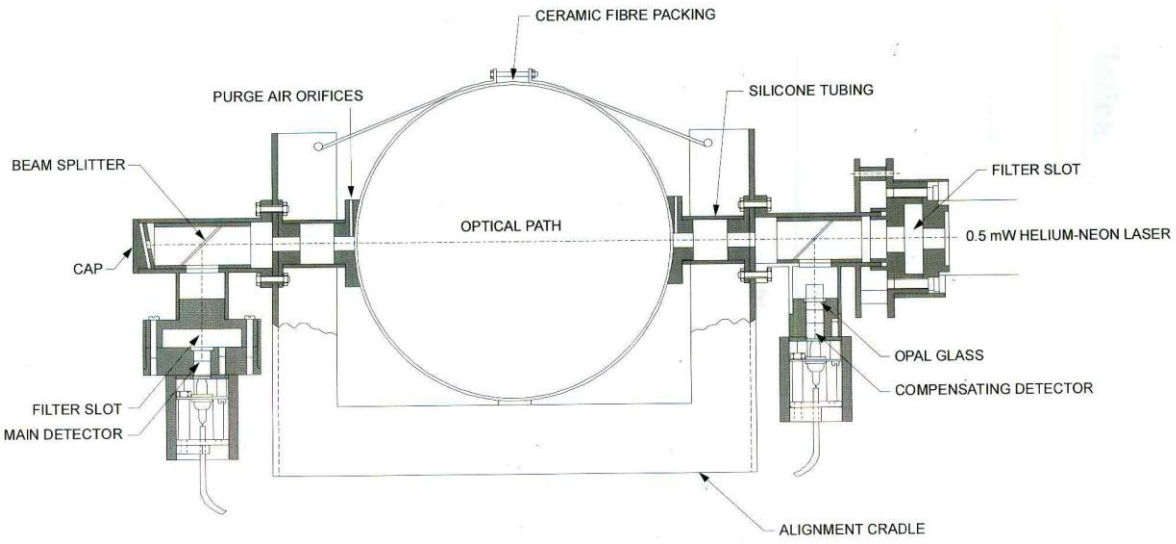

Figure 3. Schematic representation of the optical setup for soot quantification

The laser system is aligned so that the light falls on the photodetector system which has two signal outputs. Transmission is measured by splitting the laser beam at the entrance to instrument (beam splitter shown in Figure 3), and using a first photodetector to serve as a laser power reference. The rest of the beam passes through the sooting region. When light passes through a soot particle, part of the light energy is absorbed by the atoms. The amount of the absorbed light depends on the characteristics of the soot and the sooting region thickness. The transmitted laser intensities I and I_0 with and without soot, respectively, are related to optical thickness L through the relationship:

$$K= \ln (I_0/I)/L \qquad (6)$$

Where K is the extinction coefficient. The above intensities were corrected for background luminosity by turning off the modulated laser.

The optical thickness can be quantitatively related to the soot volumetric fraction through a linear relation **[Pickett 06] [Choi 94] [Cignoli 01] [Coppalle 94]**. The coefficient associated to this relation was experimentally determined, as explained below.

Bio-oil contains a large amount of water (26%), and during pyrolysis, a considerable amount of condensate species (tar+water) is produced. These species tend to condensate on the soot particles and make therefore soot become sticky. Hence the weighing of the soot collected in the sampling probe and in the filter is difficult. To face with this issue, a calibration of the measurement was performed with acetone. Acetone is considered as one of the model compounds of bio-oil. Moreover, as shown in the SEM observations of Figure 4, the soot produced by acetone and the ones produced by bio-oil have very similar size in the range of 10 to 50 nm. Chain-like aggregates composed of several tens or more of sub-units, known as monomers or spherules, can be observed in both cases.

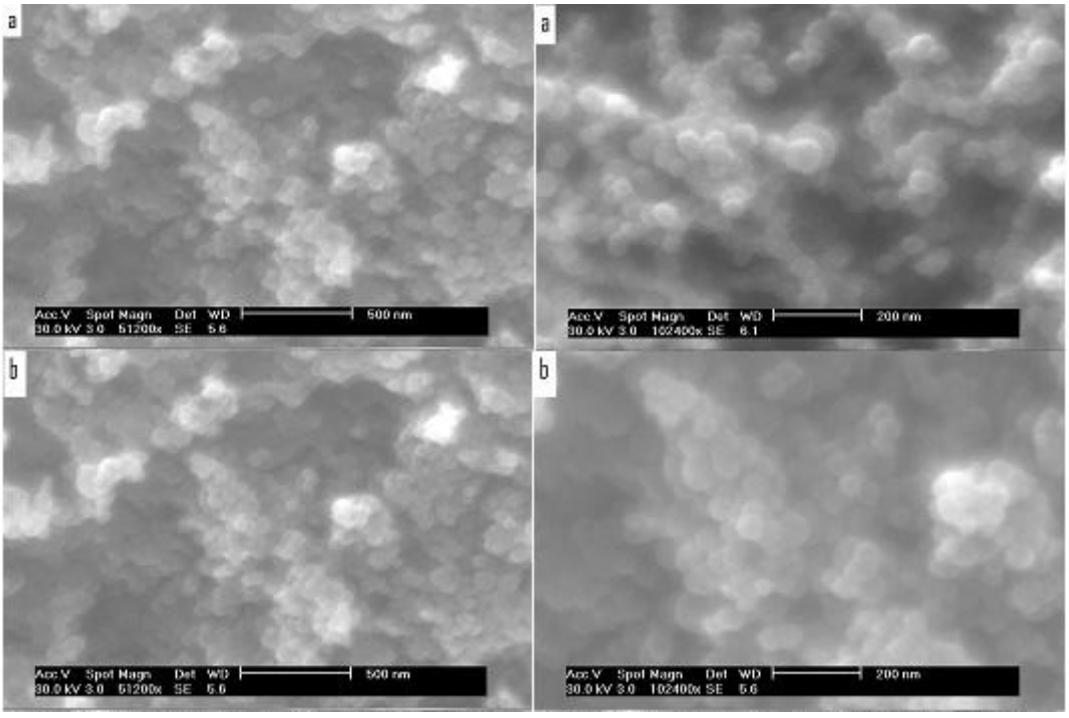

Figure 4. SEM images of the soot samples obtained from acetylene and from bio-oil pyrolysis at 1200°C. **a** - acetone; **b** - bio-oil

The acetone was pyrolyzed at different temperatures ranging from 1000 to 1400°C. Figure 5 shows the extinction coefficient measured at different temperatures. It shows that a maximum of soot is produced at 1200°C. This temperature was chosen for further calibration. Extinction

coefficient values in this sooting condition exceeded 6 m^{-1}. At this temperature, there are black clouds of soot moving and floating along the reactor; the opacity of the clouds makes the nozzle invisible from the bottom of the reactor.

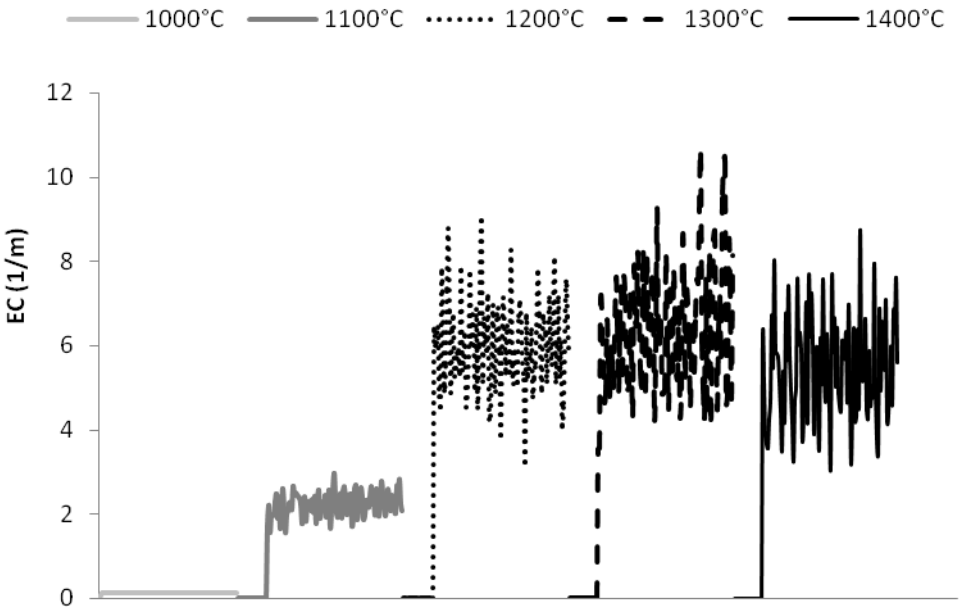

Figure 5. Extinction coefficient versus temperature – acetone pyrolysis

The pyrolysis of acetone was also carried out using different flow rates of acetone: 6, 12 and 18 ml/h. For each experiment the EC was continuously measured, as shown in Figure 6. Each experiment was then repeated with the laser device off and the sampling probe set in. After pyrolysis, soot in the sampling probe, in the settling box and in the filter was collected and accurately weighed. The soot volumetric fraction was calculated for each experiment using the relationship.

$$Fv = \frac{\text{Soot volumetric flow rate}}{\text{Total volumetric flow rate}} = \frac{Qm_s/\rho_s}{Qv_g \cdot \frac{T}{273}} \qquad (7)$$

With

Fv	Soot volumetric fraction
Qm_s	Soot mass flow rate (g/min) = mass of soot/sampling time
ρ_s	Soot density = 1800 g/l
Qv_g	Nitrogen volume flow rate sweeping the reactor ($NL.min^{-1}$)
T	Temperature (°C)

The total gas flowrate at the exit of the reactor was calculated based only on the N_2 flowrate fed to the reactor assuming that the fraction of produced gas and soot is negligible.

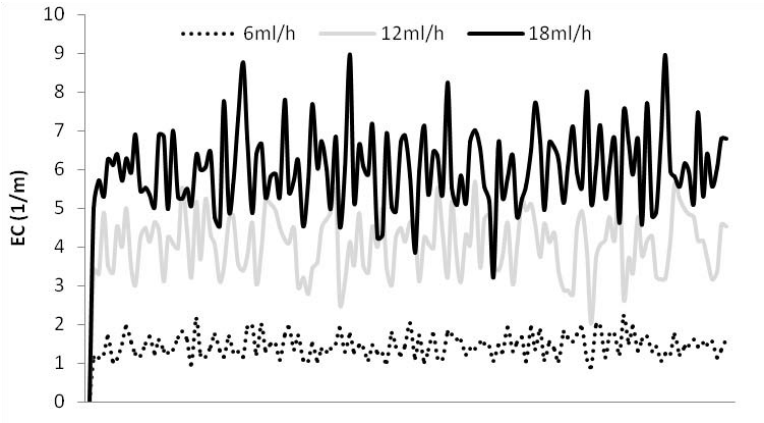

Figure 6. Extinction coefficient during acetone pyrolysis at 1200°C with different acetone flowrates

Figure 7 shows the calculated volumetric fractions (in ppb) versus the measured EC. The obtained calibration curve is a linear function (F_v=s.EC.10^{-9}) with a slope of s=16.89. This factor is subsequently used for all experiments to derive the mass yield of soot following:

$$\text{Yield} = \frac{\text{Qv}_g.\text{T.s.EC.}10^{-9}.\rho}{273.\text{Qm}_{\text{B.O}}} \quad (8)$$

With: $Qm_{B.O}$ bio-oil mass flow rate (g/min).

One should note that the value for ρ_s fixed at 1800g/l is used twice in the calculations and has finally no impact on the calculated soot mass yield.

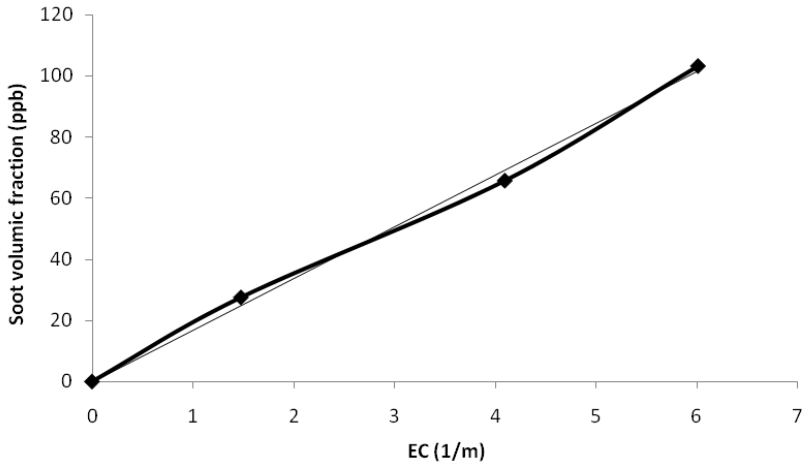

Figure 7. Soot volumetric fraction versus extinction coefficient

Note that the presence of char during the quantification of soot may impact the measurement. Previous studies **[Chhiti 10]**, have shown that the char yield during pyrolysis process is lower than 1% of the initial bio-oil at 1000°C and still lower at higher temperature. At 1000°C, the laser detects almost nothing (yield < 0.1%). This is reassuring for soot measurements in the temperature range of 1000-1400°C explored in this work.

2-3 Feedstock

The feedstock used for all experiments was bio-oil produced by fast pyrolysis of mixture of hardwood (oak, maple, ash) in an industrial-scale fluidized bed unit (Dynamotive, West Lorne, Ontario) and provided by CIRAD, France. Its physico-chemical properties have been measured (see Table 1). The water content of the bio-oil measured by Karl Fischer method (ASTM E203) is around 26 wt % which is in agreement with the average values reported in literature. It can be noticed that the solid particles content is rather high (2.3 wt.%) while the ash content remains very low (around 0.06.wt%). This confirms that the solid particles mainly consist of high-carbon content char particles. These particles were entrained during bio-oil production by the gas stream to the bio-oil condensers. Ultimate analysis and LHV of the bio-oil are very similar to those of wood. From the ultimate analysis, the chemical formula of the bio-oil can be established as $CH_{1.18}O_{0.48}.0.4H_2O$.

After the production, the bio-oil was stored at 5°C in a fridge. Before experiments, it was filtered on a 30 µm sieve to eliminate largest solid particles which represented less than 0.01 %wt of the oil.

Table 1. Ultimate analysis and physico-chemical properties of bio-oil derived from hardwood fast pyrolysis

Ultimate analysis (wt.%)				**H_2O**	**Ash**	**Solids**	**LHV**	**Kinematic viscosity**
C	H	O	N	(wt.%)	(wt.%)	(wt.%)	(MJ/kg)	at 20°C ($mm^2.s^{-1}$)
42,9	7,1	50,58	< 0,10	26,0	0,057	2,34	14,5	103

2-4 Model description and parameter setting

The GASPAR software computes the gasification of a solid spherical particle in a gaseous environment in Entrained Flow Reactor conditions. GASPAR has been developed

successively by Van de Steene, Commandré, Cancès and Peyrot **[Van de Steene 99, Commandré 02, Cancès 06, Peyrot 10]**.

A one-dimensional (1D) laminar plug flow reactor is assumed in the model based on a Lagrangian approach. The whole flow is simulated considering a single particle, with possible distribution of particles of various diameters, and the associated gas volume. This particle and the gas volume sample constitute elementary part of the EFR's flow. The model simulates the time evolution of this sample along the reactor. The model is able to predict the evolution of several variables versus gas residence, namely: gas phase temperature, particle temperature, particle mass, gas species concentrations, soot yield and tar yield.

All the differential equations are simultaneously time integrated through the Gear algorithm that can solve "stiff" ODE systems **[Radhakrishnan 93]**. The whole model is included in a FORTRAN program.

For the present contribution, bio-oil droplets gasification is simulated as if droplets were solid particles. The droplets diameter is of about 10 µm. For such size, internal heat transfer can be neglected and the particle was considered as isothermal. The slip velocity between particle and gas can also be neglected here.

The GASPAR model is used here with the aim to describe soot formation and oxidation during gasification. It is based on the description of gas phase and bio-oil heating (radiative, conductive and convective heat transfer), bio-oil devolatilization, gas reforming and conversion of both char and soot solids. Each step is described below in more details.

- **Devolatilization**

Bio-oil is decomposed following the reaction:

Bio-oil (C,H,O) → gas (CO, CO_2, H_2O, H_2, CH_4, C_2H_2, C_2H_4, C_2H_6, C_3H_8) + tar (C,H,O) + char (C) (9)

It is assumed that all the oxygen and hydrogen initially contained in the bio-oil are converted to volatile matters that are permanent gases and tar. The char residue does not contain either H or O. The distribution of bio-oil elements within the different species produced during pyrolysis is characterized by coefficients of devolatilization α_i. This is shown in the scheme of Figure 8, where C_xH_y represents hydrocarbons (CH_4, C_2H_2, C_2H_4, C_2H_6…).

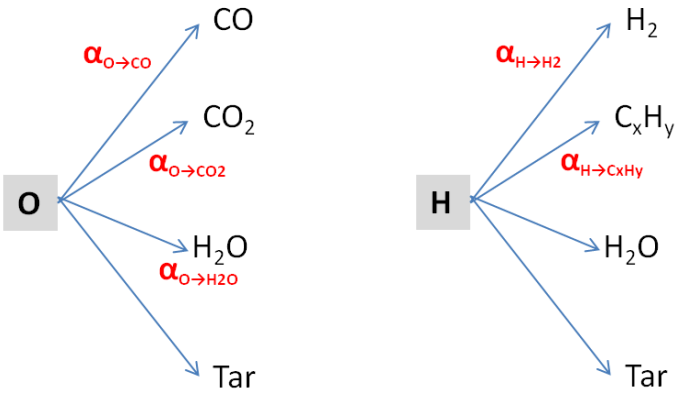

Figure 8. Devolatilization coefficients for oxygen and hydrogen elements

In the model, the coefficients of devolatilization are read from the data set. These coefficients are here first set by confrontation of the model with the experiment of bio-oil pyrolysis at 1000°C, then fitted in order to find the best data set for all simulations. Indeed these coefficients depend in reality on the reaction temperature and atmosphere. It must be emphasized that a single set of parameters was used to model all the experiments of pyrolysis, gasification and partial oxidation. The obtained values of these coefficients are given in Table 2.

Table 2. Devolatilization coefficients used in the model

$\alpha_{H\rightarrow H2} = 0.24$	$\alpha_{H\rightarrow C2H4} = 0.2$	$\alpha_{O\rightarrow CO} = 0.59$
$\alpha_{H\rightarrow CH4} = 0.25$	$\alpha_{H\rightarrow C2H2} = 0.01$	$\alpha_{O\rightarrow CO2} = 0.38$
$\alpha_{H\rightarrow C10H8} = 0.04$	$\alpha_{H\rightarrow C6H6} = 0.03$	$\alpha_{O\rightarrow H2O} = 0.02$

- **Gas phase reactions**

The gas phase reactions are computed using subroutines from the CHEMKIN II software **[Kee 90]**. For the present contribution, the chemical scheme used is the Skjoth-Rasmussen scheme (159 species, 773 reactions) **[Skjoth-Rasmussen 04].**

This model can also predict tar compounds evolution. Naphthalene has been taken as the reference compound to represent tars in devolatilization products; this compound enters in the detailed gas phase reactions.

- **Heterogeneous reactions**

In the model, char can be oxidized via three heterogeneous reactions with O_2, H_2O and CO_2. Char conversion is modelled with the into-particle diffusion model where the chemical

kinetics and the transport phenomena are taken into account through the Thiele diffusion modulus **[Villermaux 93]**.

- **Soot formation**

Acetylene is assumed to be the soot precursor through the reaction:

$$C_2H_2 \rightarrow 2\ C(soot) + H_2 \qquad (10)$$

The reaction is assumed to follow the Arrhenius law and to be of first order.

- **Soot oxidation**

Three heterogeneous soot oxidation reactions are considered in the model. For soot oxidation kinetics, Arrhenius law is used:

$C(soot)+H_2O \rightarrow CO+H_2$	Soot gasification by H_2O	(11)
$C(soot)+CO_2 \rightarrow 2CO$	Soot gasification by CO_2	(12)
$C(soot) + 0{,}5\ O_2 \rightarrow CO$	Soot oxidation	(13)

The used kinetic parameters of soot formation and oxidation reactions are shown in Table 3. Their values are obtained from literature **[Ziegler 04] [IFP 88]**.

Table 3. Kinetic coefficients of formation and oxidation of soot used in the current work

Reaction	A	E
(10)	$2.1\ 10^5$	167200
(11)	$450\ 10^5$	23500
(12)	$8100.\ 10^5$	30900
(13)	4.26	179400

The kinetic parameters associated to soot formation and soot gasification by H_2O had to be adjusted. The values of activation energy were kept equal to literature values and only the value of pre-exponential factor was changed. For soot formation, the value of A was adjusted by comparison of the model to a pyrolysis experiment (at 1200°C) during which only few soot oxidation occurred. For soot gasification by H_2O reaction, the value of A was adjusted by confrontation of the model to gasification experiment in which large excess of H_2O was used. For soot gasification by CO_2 and soot oxidation by O_2 reactions, it was found that they not contribute significantly to the process and had a very small impact on final soot yields. Therefore, the kinetic parameters were not adjusted for these two reactions.

2-5 Experimental conditions

The operating temperature was varied over the range of 1000-1400°C. Gas atmosphere was preheated at 900°C for all experiments. Bio-oil was then continuously fed by a feeding probe and injected into the reactor tube through a nozzle by a nitrogen stream. The feeding rate of feedstock was of 0,3 g/min, as explained previously.

- Firstly, the simplest situation of pyrolysis: i.e. in an inert atmosphere was studied. In this case, the reactions involved are devolatilization, cracking, and some reforming and gasification by H_2O that is present in the fed bio-oil.
- Secondly excess of H_2O, called steam gasification was studied. Gasification tests were carried out by supplying a mixed stream of nitrogen with steam. The steam to carbon molar ratio was S/C= 8.3 which was equivalent to 10 vol. % of steam in the atmosphere gas.
- Lastly the presence of O_2 was explored. The so called partial oxidation tests were carried out by supplying a mixture stream of nitrogen with O_2. The amount of O_2 was varied from very small amount to investigate a potential impact through radicals (O/C= 0.075), to large amount that may oxidize a significant part of bio-oil (O/C=0.5). This is equivalent to 0.1-0.75 vol. % of oxygen in atmosphere gas.
-

3- RESULTS AND DISCUSSIONS

In the following section, the yield of each main product is investigated separately. The experimental values are considered at first.

3-1 Profiles of product gas

Figure 9-a shows gas species molar fractions at the bottom of the reactor versus temperature for pyrolysis, steam gasification and partial oxidation processes; Figure 9-b plots gas species molar fractions at the bottom of the reactor versus O/C molar ratio for partial oxidation process at the temperature of 1200°C.

3-1-1 H_2 production

The production of H_2 increased with temperature in all cases. The yields of H_2 in the exit gas varied in the order of steam gasification > pyrolysis > partial oxidation.

In the case of pyrolysis process, H_2 is thought to be mainly generated from the dehydrogenation (through the cleavage of C–H or O–H bond) of chemical compounds of bio-oil, and from the secondary decomposition of their pyrolyzed products (tars and hydrocarbon gas). Water contained by bio-oil can cause reforming reactions and favor the increase of H_2 with temperature.

In the presence of steam excess, however, the production of H_2 can be enhanced through steam gasifications of carbon (Eq14) and condensable volatiles (Eq15). The water–gas shift reaction can also contribute to the production of H_2 (Eq16):

Carbon gasification $C + H_2O \leftrightarrow CO + H_2$ (14)

Volatiles steam reforming $C_nH_mO_k + (n - k)\, H_2O \leftrightarrow nCO + (n + m/2 - k)\, H_2$ (15)

Water gas shift $CO + H_2O \leftrightarrow CO_2 + H_2$ (16)

Both reactions (14) and (15) are endothermic, while reaction (16) is exothermic. Thus, high temperature will promote reactions (14) and (15), and low temperature will favor reaction (16) to shift towards the right.

On the other hand, the decrease in H_2 yields observed in partial oxidation runs with increasing O/C molar ratio suggests that combustion reactions predominate over steam gasification and water-gas shift reaction.

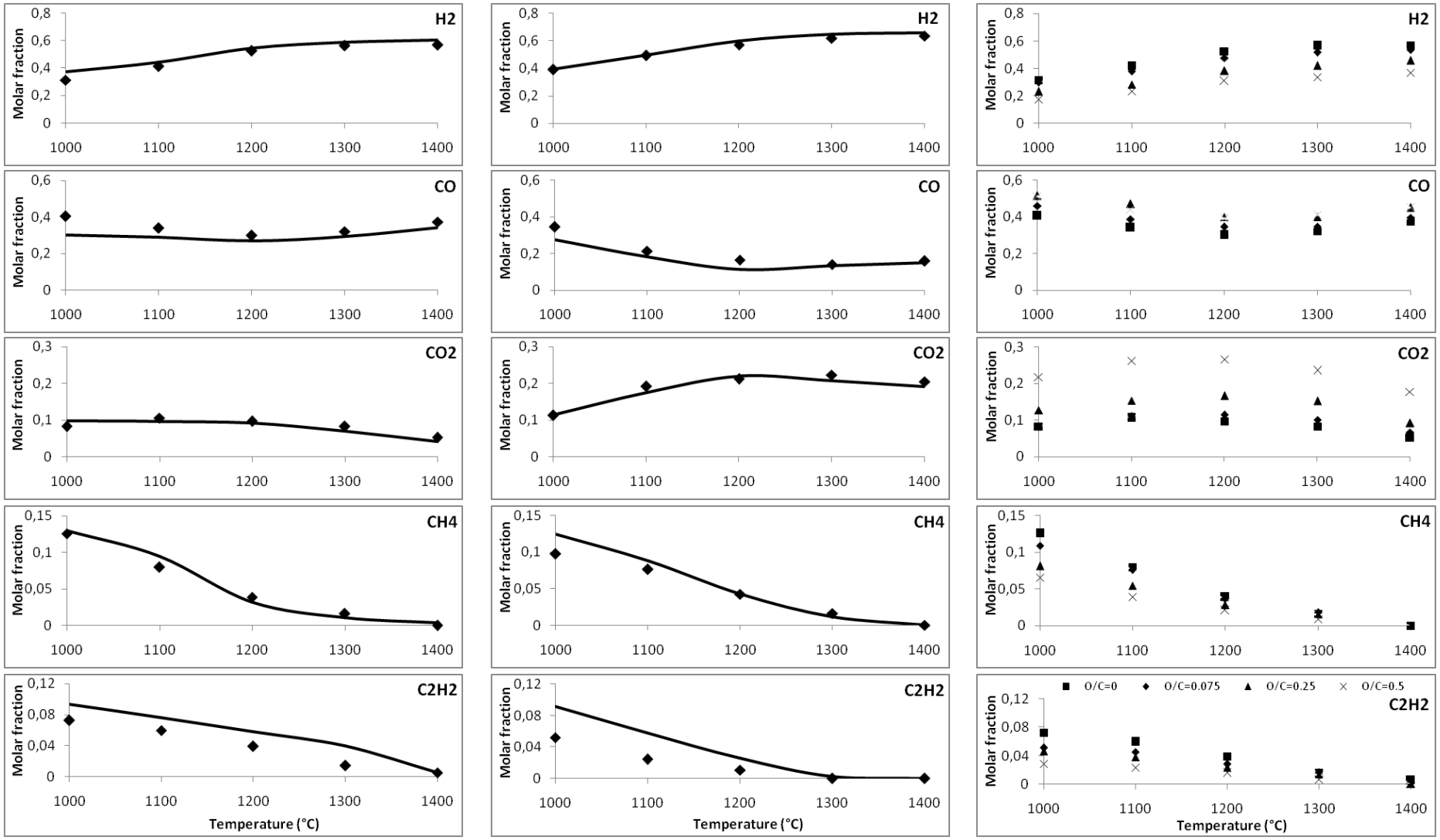

Figure 9a. Gas molar fraction versus temperature. **symbols:** experiment; **lines:** model. **a**-pyrolysis case, **b**-gasification case, **c**-partial oxidation case

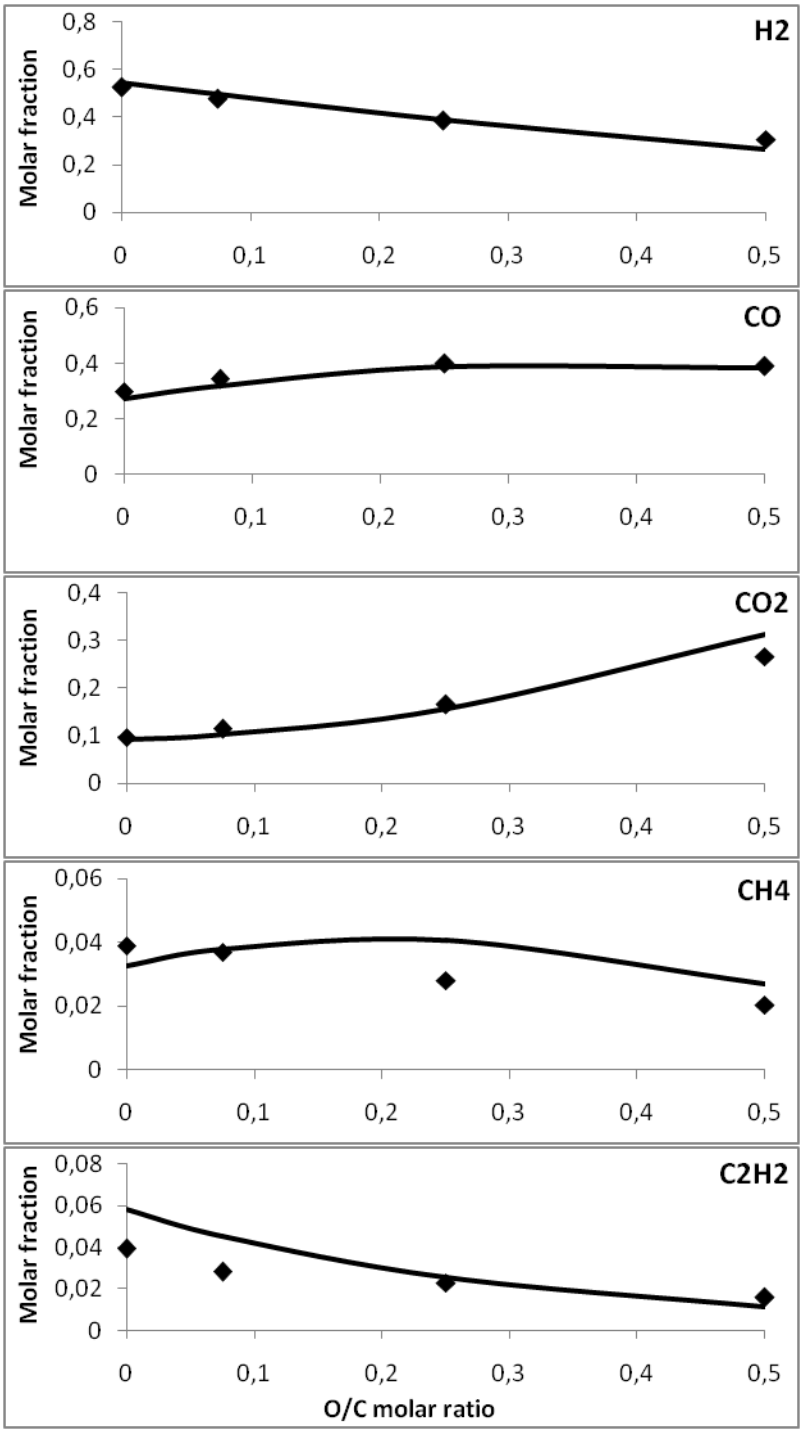

Figure 9b. Gas molar fraction versus O/C molar ratio for partial oxidation process at 1200°C.
symbols: experiment; **lines:** model

3-1-2 CO and CO_2 production

In the case of pyrolysis, CO and CO_2 yields are nearly stable between 1000 and 1200°C. At higher temperature there is a slight increase in CO in parallel with a decrease of CO_2 which may be explained by Boudouard reaction:

$$C + CO_2 \rightarrow 2CO \quad (17)$$

It is known that the production of CO in the pyrolysis process is mainly attributed to the decomposition of oxygen-containing functional groups in bio-oil.

In the steam gasification case, the water-gas shift reaction may also explain the increase of CO_2 and the decrease of CO between 1000 and 1200°C. Above 1200°C, carbon monoxide slightly increases. This may be explained by steam and CO_2 gasification of the solid carbon following the reaction (14) and the Boudouard reaction (17) which would explain the slight decrease of CO_2.

On the other hand, unlike the pyrolysis and steam gasification cases, CO and CO_2 formation was significantly enhanced during partial oxidation tests. As O/C increases the H_2 yield decreases while CO and CO_2 increase. This was caused by increased amounts of oxygen which reacted with chemical species containing carbon and hydrogen and gave rise to CO_2, CO and H_2O following the reactions:

$$C + ½\ O_2 \rightarrow CO \quad (18)$$

$$C_xH_yO_z + (x/2\text{-}z/2)O_2 \rightarrow xCO + (y/2)H_2 \quad (19)$$

$$C_xH_yO_z + (x+y/4\text{-}z/2)O_2 \rightarrow xCO_2 + (y/2)H_2O \quad (20)$$

3-1-3 Light hydrocarbon gas production

In Figures 9-a and 9-b only the major hydrocarbons CH_4 and C_2H_2 are shown. In all cases CH_4 is the most abundant species among the light hydrocarbon gases. Its production is maximal at 1000°C and then decreases with temperature. It remains in trace amounts at 1300°C and is below detection limit at 1400°C. Its yield is greatly reduced when O/C ratio increases, which shows that there is some partial oxidation. The trends are similar for C_2H_2.

The results of all simulations for the five temperatures 1000, 1100, 1200,1300 and 1400°C are shown in same Figures as experiments (Figure 9 a and b). As can be observed, the results obtained from the model are in very good agreement with experimental results, except for the specie C_2H_2. This difference will be discussed later.

3-2 Soot production

The results of soot yields obtained in the different experiments of pyrolysis, gasification, and partial oxidation are shown in Figures 10-a, 10-b and 10-c respectively.

In the case of pyrolysis (Figure 10-a), an increase in temperature results an increase in the soot yield. The increase in soot yield is accompanied by a decrease in the hydrocarbons gas yield as seen previously. This is in agreement with literature results **[Alexiou 95] [Alexiou 96] [Mendiara 05] [Fletcher 97]**.

The measured soot yield is close to zero at 1000°C, while important amounts of C_2H_2 are present at the exit of the reactor. Above 1000°C a strong increase of soot yield with temperature is observed up to 1200°C where the soot yield is 3.58 10^{-2}g/g. The soot yield measured at 1300°C and 1400°C is only slightly higher. This increase is accompanied by C_2H_2 decrease at the exit. The acetylene which is considered as the main soot precursor would react further to produce soot and hydrogen **[McEnally 06]**.

The model satisfactorily predicts the soot formation at temperatures between 1000°C and 1200°C which tends to confirm the role of C_2H_2 in soot formation. Above 1200°C the model predicts higher yields of soot than experiments. This may result from an incorrect calculation of the C_2H_2 gas phase concentration by the reaction mechanism. As can be seen in the product gas figure, the measured and calculated concentrations of acetylene show the same tendencies but with a gap.

In the gasification case, the soot yield is more than 3 times smaller than the soot yield in the pyrolysis case, as can be seen in Figure 10-b. The measured and calculated curves are both bell-shaped curves, showing that the model correctly describes the trend. At 1000°C experiment shows a low soot yield, which gets higher when reaction temperature increases and until the soot yield reaches a maximum of 1.27 10^{-2}g/g at about 1200°C. Above 1200°C, the soot yield strongly decreases. This decrease may be explained by steam and CO_2 gasification of soot following

reaction (14) and following the Boudouard reaction (17) which would explain the slight decrease of CO_2 obtained in Figure 9-a, as well as the increase of H_2 and CO.

The limited formation of soot at high temperature due to the presence of water has been reported to result from changes in the radical pool **[Skjøth-Rasmussen 04]**. Steam enhances the formation of hydroxyl radicals, through $H+H_2O \leftrightarrow OH+H_2$, and OH radicals may oxidize soot and also oxidize with C_2H_2 and therefore causes a decrease in the soot production. Water would therefore compete with C_2H_2.

In the partial oxidation case, from a thermodynamic point of view, soot formation can occur when fuel rich conditions are present i.e. when the O/C molar ratio is lower than 1. In the present experimental investigations the O/C molar ratio was varied from 0.075 to 0.5 at 1200°C, because at this temperature the production of soot is highest. As can be seen in Figure 10-c, the measured amount of soot strongly decreases with the O/C ratio under the conditions explored. This tendency is satisfactorily described by the model. According to the literature, when O/C molar ratio increases, most hydrocarbons are destroyed by oxidation or thermal decomposition, and numerous intermediate species are formed. In this way, a competition between the molecular growth and oxidative reactions occurs. Oxidative reactions lead to the formation of various oxygen-containing intermediates and products like CO, CO_2, and H_2O. As a result, the soot yield decreases compared with the case of pyrolysis.

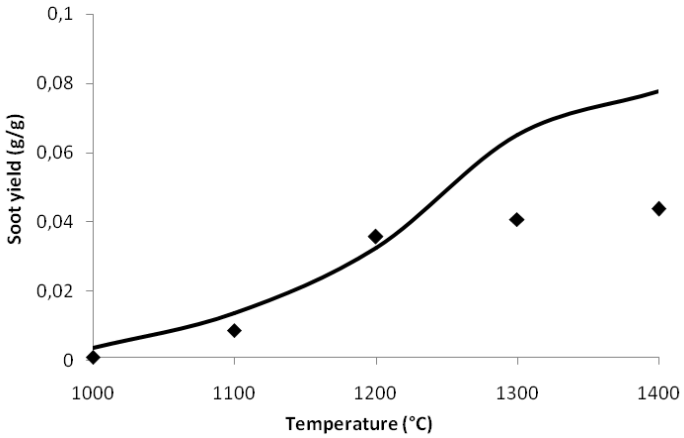

Figure 10a. Soot yields versus temperature: experiments and modeling - pyrolysis case

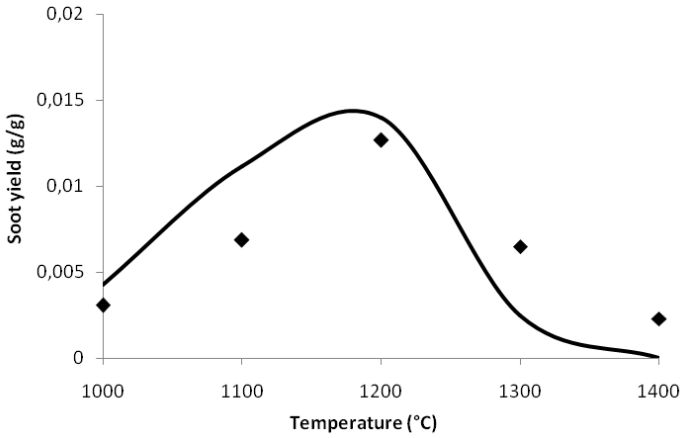

Figure 10b. Soot yields versus temperature: experiments and modeling – gasification case

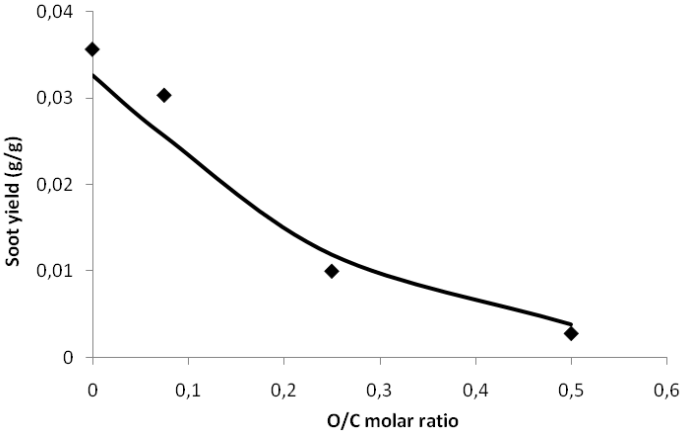

Figure 10c. Soot yields versus O/C molar ratio at 1200°C: experiments (symbols) and modeling (lines) – Partial oxidation case

3-3 Discussion: contribution of the model

In this section the model is used to discuss the results by identifying the contribution of each reaction to soot oxidation in the three situations (pyrolysis, steam gasification, partial oxidation). The prediction of the evolution of the gas species along the reactor also gives important information for understanding the transformation mechanisms.

a- Pyrolysis situation

Calculations of soot yield are shown in Figure 11 versus temperature when oxidation reaction are activated and deactivated. In pyrolysis situation we note that the activation of the reaction of oxidation by CO_2 caused a negligible decrease in the soot yield. This oxidation was of about 3% at 1400°C. Activation of the reaction with water has no effect at 1200°C. However it causes a soot yield decrease of 26% at 1400°C.

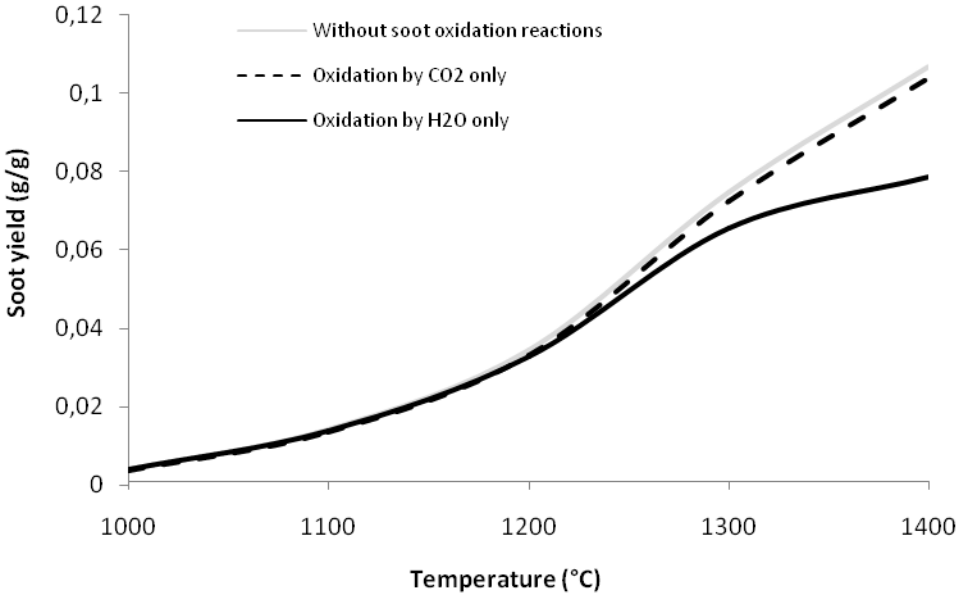

Figure 11. Soot yields versus temperature: modeling at different pyrolysis temperatures

Figure 12 shows the profile of soot yield and C_2H_2 volumetric fraction along the reactor at 1200°C. Acetylene curve shows its maximum close to the top of the reactor. This zone corresponds to the maximum of soot production rate as shown by the slope of the curve. Then the

decrease in C_2H_2 yield is logically accompanied by an increase of soot content along the reactor, in agreement with the precursor role of C_2H_2.

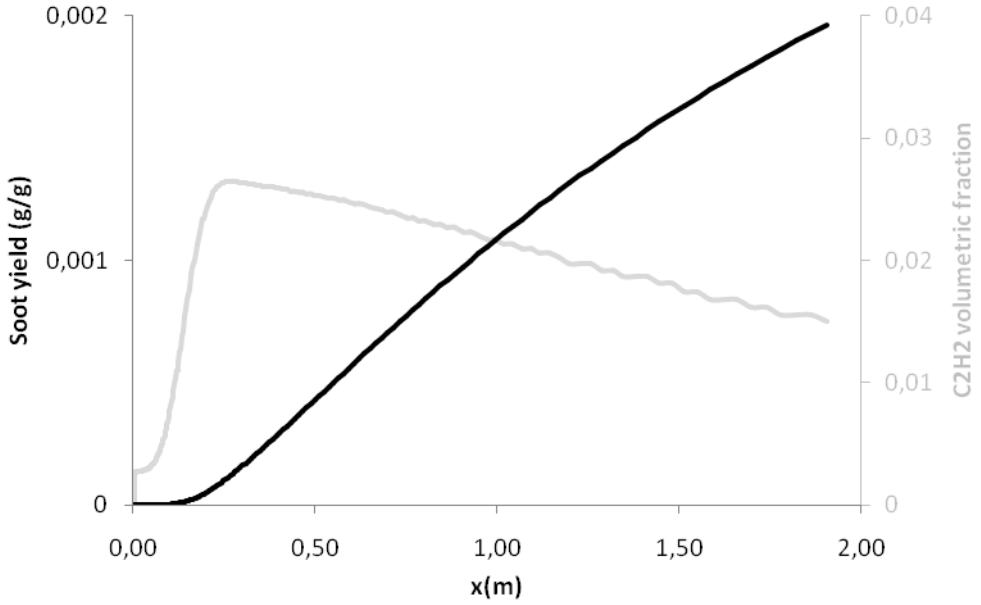

Figure 12. Profile of soot yield and C_2H_2 volumetric fraction versus the distance from nozzle during pyrolysis at 1200°C

b- Gasification situation

Calculations of soot yield are shown in Figure 13 versus temperature when oxidation reaction are activated and deactivated. We note that the activation of the reaction of oxidation with CO_2 caused a very small decrease in the soot yield. Activation of the reaction with water caused an almost complete oxidation of soot at 1300°C and 1400°C.

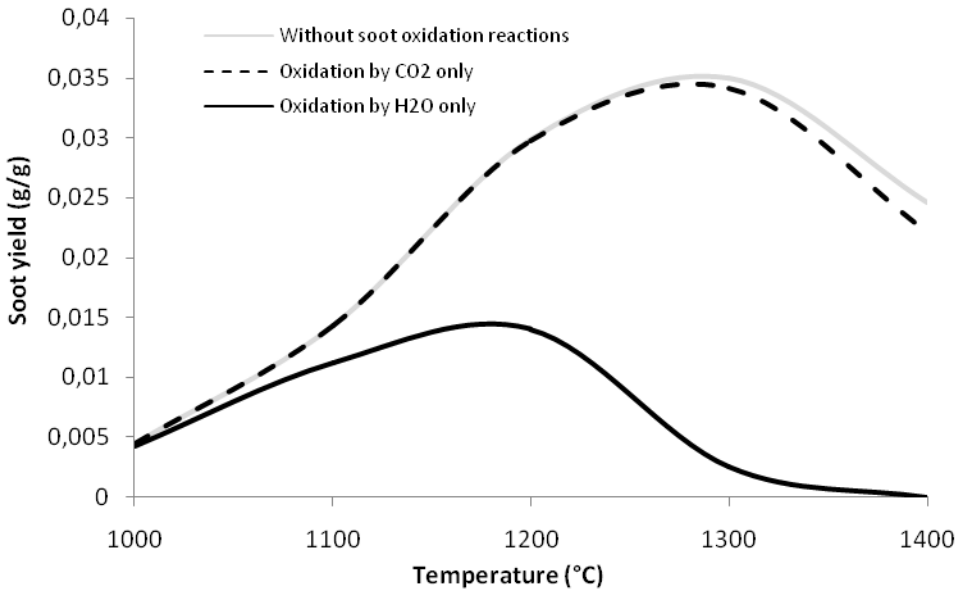

Figure 13. Soot yields versus temperature: modeling at different gasification temperatures

As previously reported steam enhances the formation of hydroxyl radicals at high temperature. These radicals may oxidize soot and also consume C_2H_2 and therefore cause a decrease in soot production. The issue here is to distinguish the effect of steam on the oxidation of soot through the reforming of C_2H_2 and through the direct oxidation by H_2O.

The profiles of C_2H_2 volumetric fraction and the soot yield through the reactor at 1200°C have been plotted in Figure 14 in three situations:

i- without steam: this corresponds to the situation in which the production of soot is at its highest level.

ii- with steam and deactivation of the steam gasification reaction: in this situation only the reforming of C_2H_2 occurs;

iii- with steam and activation of the steam gasification reaction: in this situation both the decrease of soot production through the reforming of C_2H_2 and through the direct oxidation of soot by steam may be occured.

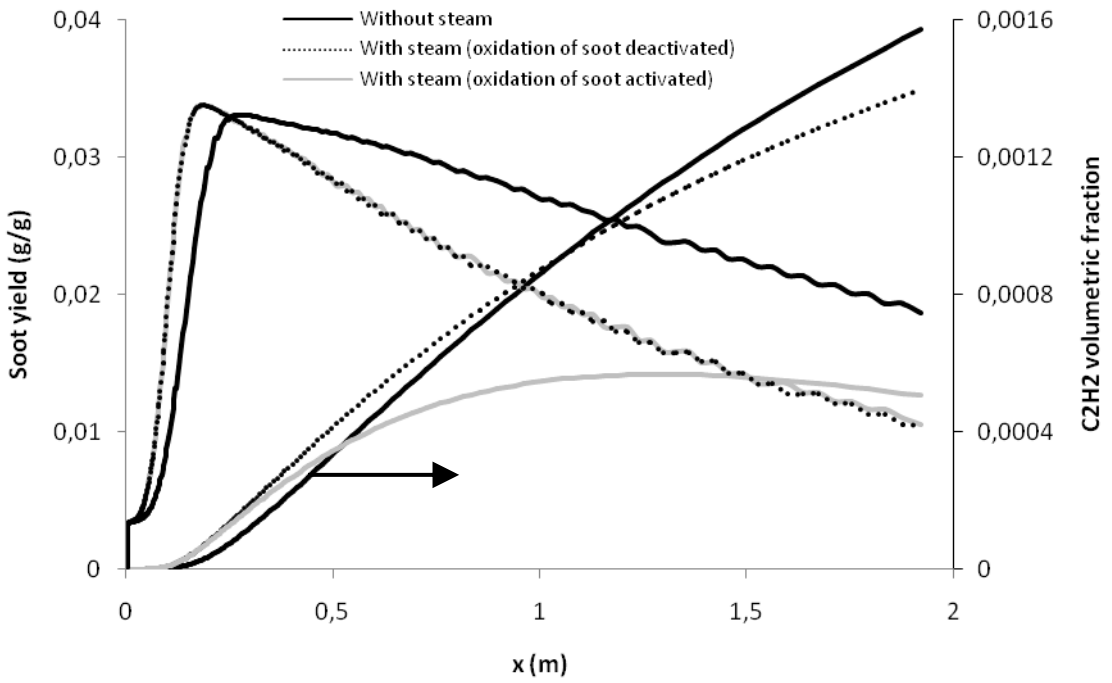

Figure 14. Profile of soot yield and C_2H_2 volumetric fraction versus the distance from nozzle during gasification at 1200°C

Comparing (i) and (ii) shows that the presence of steam leads to a slight decrease of C_2H_2, and subsequently causes a slight decrease in soot production. However the activation of steam gasification in situation (iii) causes a significant soot oxidation. This proves that the oxidation of soot is mainly due to a direct gasification of soot by steam.

c- Partial oxidation situation

Calculations of soot yield are shown in Figure 15 versus temperature when oxidation reaction are activated and deactivated. None of the three oxidation reactions has a significant effect on soot yield.

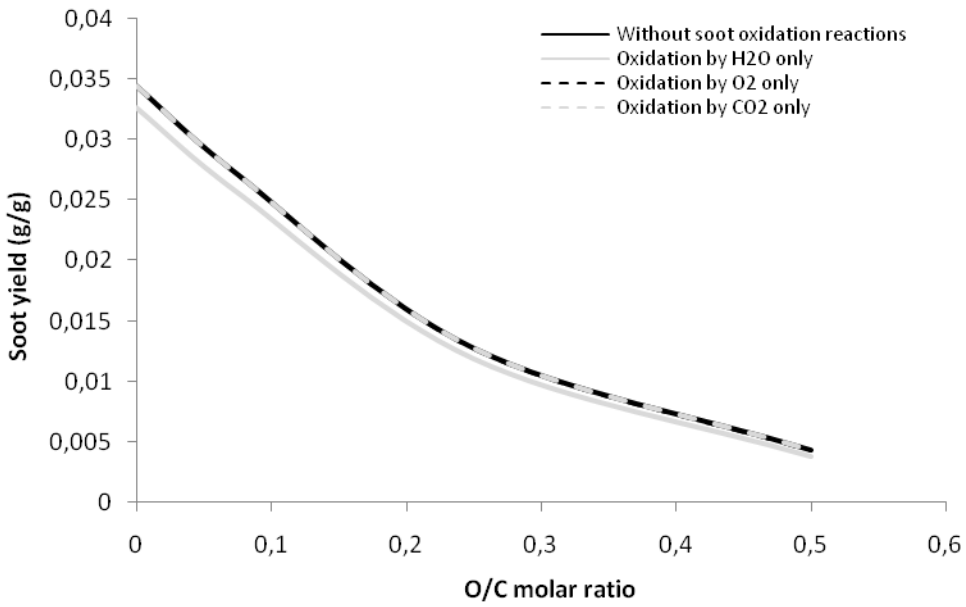

Figure 15. Soot yields versus O/C molar ratio at 1200°C

As shown in Figure 16 O_2 seems to be consumed very quickly at the top of the reactor. Figure 17 shows the soot yield and C_2H_2 volumetric fraction along the reactor at 1200°C at different O/C ratios. It can be noticed that when O/C increases C_2H_2 decreases in accordance with the O_2 consumption (Figure 16) and therefore less soot is produced. According to the model O_2 directly acts on C_2H_2 yield and thereafter on the amount of soot produced, rather than on the amount of soot consumed.

To sum up, based on the three considered situations, we found that among the three oxidation reactions only the steam gasification reaction substantially acted on soot. Gasification with CO_2 has little effect and oxidation with O_2 has no effect.

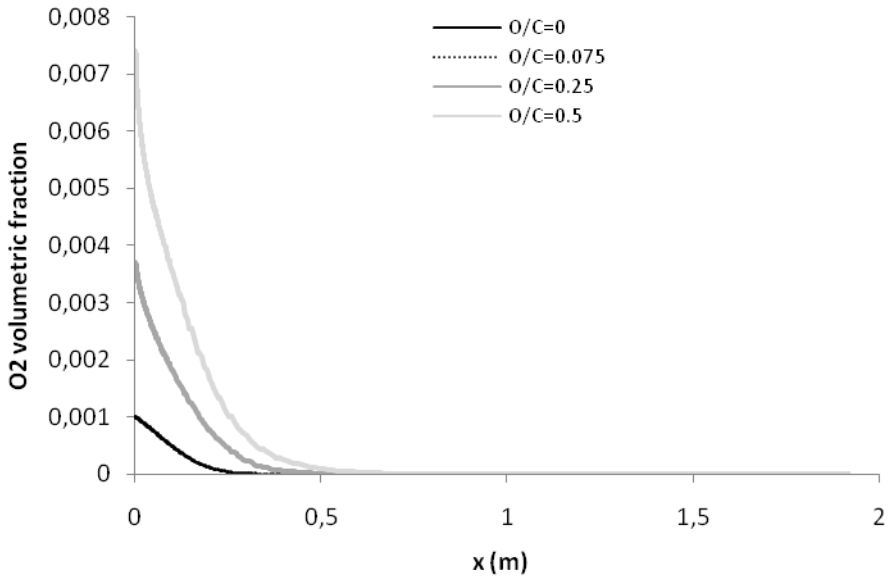

Figure 16. Profile of O_2 volumetric fraction versus a distance from nozzle at 1200°C

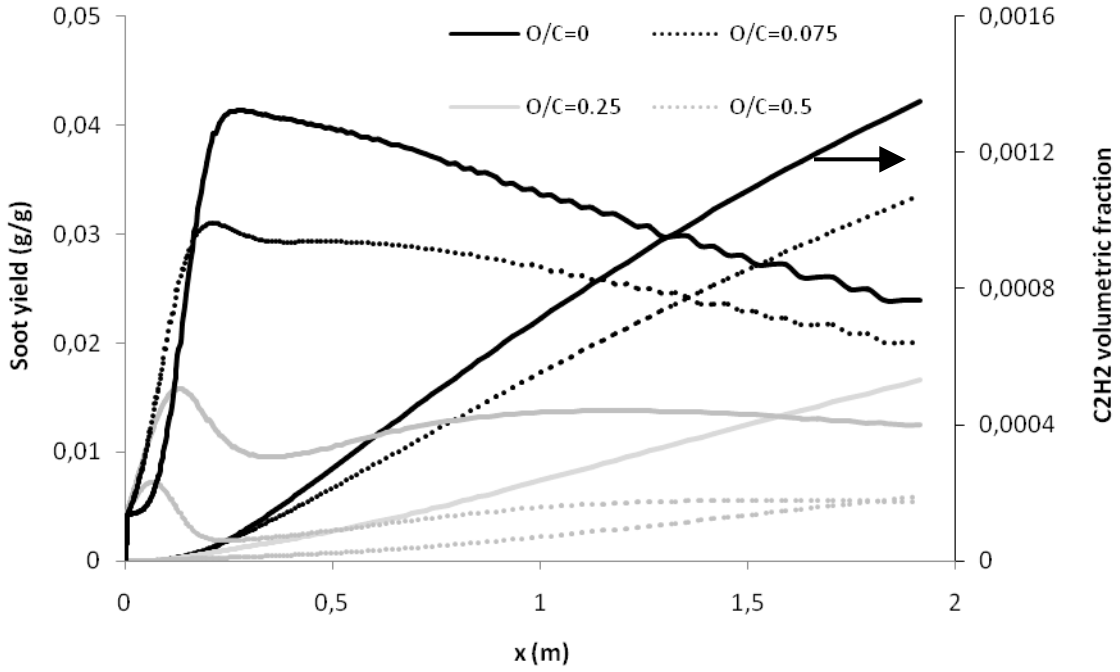

Figure 17. Profile of soot yield and C_2H_2 volumetric fraction versus the distance from nozzle during partial oxidation at 1200°C- Effect of O/C molar ratio

4- CONCLUSIONS

The mechanisms of soot formation and oxidation are investigated through experiments under three different atmospheres: inert (pyrolysis), excess of steam (gasification) and in the presence of oxygen (partial oxidation). The proposed semi-empirical model is validated. It is based on detailed chemistry to describe the gas phase, on a single reaction based on C_2H_2 concentration to describe soot formation and on three heterogeneous reactions to describe soot oxidation. The approach appears to give satisfactory results. Indeed the amount of the main gases is very accurately predicted and the soot yield is correctly predicted. It has to be highlighted that a single set of identified parameters was used for all simulations.

The study confirms a strong influence of temperature on the mechanisms of soot formation and oxidation. Emphasis was also made on the effect of gasifying agents. Water in excess causes an almost complete gasification of soot at 1300°C and 1400°C. In the partial oxidation situation, at very low concentrations of O_2, the soot yield undergoes a slight decrease; an increase of O_2 amount greatly reduces the soot yield.

The contribution of each reaction of soot oxidation in the model is identified. CO_2 is shown to reduce only small quantities of soot. O_2 has no contribution to soot oxidation because it is consumed before soot is formed. O_2 nevertheless indirectly acts by consuming C_2H_2 and therefore causes a decrease in soot production. Only steam directly oxidizes the soot and causes their decrease.

Acknowledgements

The authors gratefully acknowledge the financial support from EnerBio Program of Fondation Tuck France, and express their gratitude to Mr. Bernard AUDUC technician in Ecole des Mines d'Albi-Carmaux for his assistance and contribution to experimental device design and operation.

REFERENCES

[Alexiou 95] Alexiou A, Williams A. Soot formation in shock-tube pyrolysis of toluene-n-heptane and toluene-iso-octane mixtures. Fuel 1995:74;153-158.

[Alexiou 96] Alexiou A, Williams A. Soot formation in shock-tube pyrolysis of toluene, toluene–methanol, toluene–ethanol, and toluene–oxygen mixtures. Combust. Flame 1996 :104;51–65.

[Appel 00] Appel J, Bockhorn H, Frenklach M. Kinetic modeling of soot formation with detailed chemistry and physics: laminar premixed flames of C2 hydrocarbons. Combust. and Flame 2000;121:122–136.

[Balthasar 05] Balthasar, M. Frenklach, Detailed kinetic soot modeling of soot aggregate formation in laminar premixed flames, Comb. Flame 2005;140:130-145.

[Berthelot 66] Berthelot MPE. Theorie des corps pyrogenes. Ann. Chim. Phys. 1866;9: 469–481.

[Bozzano 02] Bozzano G, Dente M, Faravelli T, Ranzi E. Fouling phenomena in pyrolysis and combustion processes. Appl. Therm. Eng. 2002;22:919-927.

[Bradley 61] J.N. Bradley, G.B.J. Kistiakowsky. Shock wave studies by mass spectrometry. II. Polymerization and oxidation of acetylene. J. Chem. Phys. 1961;35:264–270.

[Bridgwater 00] Bridgwater AV, Peacocke GVC. Fast pyrolysis processes for biomass. Renew Sustain Energy Rev 2000;4:1–73.

[Cancès 06] Cancès J. Formation et réduction de NOx par un charbon, un lignite, un anthracite et un coke de pétrole dans les conditions d‘un précaclcinateur de cimenterie, Thèse de l‘Institut National Polytechnique de Toulouse 2006.

[Cavaliere 94] Cavaliere A, Barbella R, Ciajolo A, D’Anna A, Ragucci R. Fuel and soot oxidation in diesel-like conditions. In: Twenty fifth international symposium on combustion, Philadelphia. The Combustion Institute 1994:167–74.

[Chhiti 10] Chhiti Y, Salvador S, Commandre JM, Broust F, Couhert C. Wood bio-oil non catalytic gasification: influence of temperature, dilution by an alcohol and ash content. Energy and Fuels 2010, Online.

[Chhiti 10] Chhiti Y, Salvador S, Commandre JM, Broust F. Wood bio-oil pyrolysis: Influence of temperature, heating rate and ash content on char, gas and tar yield. Submitted to Fuel mars 2011.

[Choi 94] Choi MY, Hamins A, Mulholland GW, Kashiwagi T. Simultaneous optical measurements of soot volume fraction and temperature in premixed flames. Combust. Flame 1994;99:174-186.

[Cignoli 01] Cignoli F, DeIuliis S, Manta V, Zizak G. Two dimensional two-wavelength emission technique for soot diagnostics. Appl. Opt. 2001;40:5370-5378.

[Commandré 02] Commandré JM. Formation des oxydes d'azote lors de la combustion de cokes de pétrole dans des conditions de précalcinateur de cimenterie, Thèse de l'Institut National Polytechnique de Toulouse 2002.

[Coppalle 94] Coppalle A, Joyeux D. Temperature and soot volume fraction in turbulent diffusion flames: measurements of mean and fluctuating values. Comb. Flame 1994;96:275-285.

[Cundall 77] Cundall RB, Fussy DE, Harrison AJ, Lampard D. An investigation of the precursors to carbon particles during the pyrolysis of acetylene and ethylene. Int. Shock-tube Symp. 1977.

[de Soete 88] de Soete G. Catalysis of soot combustion by metal oxides. In: Western States section meeting. The Combustion Institute 1988.

[Fletcher97] Fletcher TH, Ma J, Rigby JR, Brown AL, Webb BW. Prog. Energy Combust. Sci. **1997 ;23 :283-**301.

[Frenklach 85] Frenklach M, Clary DW, Gardiner WC, Stein SE. Detailed kinetic modeling of soot formation in shock-tube pyrolysis of acetylene. Proc. Comb. Inst. 1985;20: 887–901.

[Frenklach 90] Frenklach, M., Wang, H. Detailed modeling of soot particles nucleation and growth. In: 23rd International Symposium on Combustion 1990:1559-1566.

[Frenklach 94] Frenklach M, Wang H. Detailed kinetic modeling of soot particle formation. Springer 1994;59: 165–192.

[Gay 65] I. D. Gay, G.B. Kistiakowsky, J.V. Michael, H. J. Niki. Thermal decomposition of acetylene in shock waves. J. Chem. Phys. 1965;43:1720-1726.

[Griesheimer 98] Griesheimer J, Homann KH. Large molecules, radicals, ions, and small soot particles in fuel-rich hydrocarbon flames. Part II: aromatic radicals and intermediate PAHs in a premixed low-pressure naphthalene/oxygen/argon flame. Proc. Comb. Inst. 1998; 27:1753–1759.

[Haynes 81] Haynes BS, Wagner HG. Soot formation. Prog. Energy Combust. Sci. 1981;7: 229 - 273.

[Homann 67] Homann HK, Wagner HG. Some new aspects of the mechanism of carbon formation in premixed flames. Proc. Comb. Inst. 1967;11:371–379.

[IFP 88] IFP. Catalysis of soot combustion by metal oxides. Paper presented at the Western States Section Meeting of the Combustion Institute 1988.

[Kee 90] Kee RJ, Rupley FM, Miller JA. The CHEMKIN thermodynamic data base, Sandia National Laboratory, Technical Report (SAND87-8215B) 1990.

[Keller 00] Keller A, Kovacs R, Homann KH. Large molecules, radicals, ions, and small soot particles in fuel-rich hydrocarbon flames. Part IV: large polycyclicaromatic hydrocarbons and their radicals in a fuel-rich benzene-oxygen flame.Phys. Chem. Chem. Phys. 2000;2: 1667–1675.

[Kiefer 90] Kiefer JH, Drasek V, William A. The mechanism of the homogeneous pyrolysis of acetylene. Int. J. Chem. Kinet. 1990;22:747–786.

[Krestinin 00] Krestinin AV. Detailed modeling of soot formation in hydrocarbon pyrolysis. Combust Flame 2000;12:513–24.

[Krestinin 87] Krestinin AV. Kinetic Model of soot formation from acetylene in different mixtures at temperatures higher then 1600 K. Chim. Phys. 1987;6:342–349.

[Lee 62] Lee KB, Thring MW, Bee´r JM. On the rate of combustion of soot in a laminar soot flame. Combust Flame 1962;6:137–45.

[Lewes 94] Lewes VB. The action of heat upon ethylene. Proc. Roy. Soc. 1894;55:90–108.

[Maugendre 09] Maugendre M. Etude des particules de suie dans les flammes de kerosene et de diester. Ph.D Thesis 2009.

[Mauss 98] Mauss, F. Development of a kinetic soot model for soot formation with fast polymerization. Ph.D Thesis, RWTH Aachen 1998.

[McEnally 06] McEnally CS, Pfefferle LD, Atakan B, Kohse-Höinghaus K. Studies of aromatic hydrocarbon formation mechanisms in flames: progress towards closing the fuel gap. Progress in Energy and Combustion Science 2006;32:247-294.

[Mendiara 05] Mendiara T, Domene MP, Millera A, Bilbao R, Alzueta MU. J. Anal. Appl. Pyrol. **2005; 74:486-**493.

[Musculus 02] Musculus MP, Dec JE, a Tree DR. Effects of Fuel Parameters and Diffusion Flame Lift-Off on Soot Formation in a Heavy-Duty Diesel Engine. SAE Paper No. 2002-01-0889.

[Peyrot 10] Peyrot M, Dupont C, Chen L, Spindler B, Valin S, Cancès J, Fast pyrolysis of millimetric wood particles between 1073K and 1273K: Modelling and experimental validation in the chemical kinetic regime. Biomass conference Lyon 2010.

[Pickett 02] Pickett LM, Siebers DL. An investigation of diesel soot formation processes using micro-orifices. Proc. Combust. Inst. 2002;29:655–662.

[Pickett 06] Pickett L M, Siebers D L. Soot Formation in Diesel Fuel Jets Near the Lift-Off Length. International Journal of Engine Research 2006;7:103-130.

[Radhakrishnan 93] Radhakrishnan, Hindmarsh AC. Description and use of LSODE, the Livermore solver for ordinary differential equations. Technical report, LLnL report (UCLR-ID113855) 1993.

[Richter 00] Richter H, Howard JB. Formation of polycyclic aromatic hydrocarbons and their growth to soot -a review of chemical reaction pathways. Progress in Energy and Combustion Science 2000; 26: 565-608.

[Richter 05] Richter H, Granata S, Green WH, Howard JB. Detailed modeling of PAH and soot formation in a laminar premixed benzen/oxygen/argon low-pressure flame. Proc. Comb. Inst. 2005;30:1397-1405.

[Roth 90] Roth P, Brandt O, von Gersum S. High temperature oxidation of suspended soot particles verified by CO and CO_2 measurements. In: Twenty-third international symposium on combustion, Pittsburgh. The Combustion Institute 1990:1485–91.

[Roth 91] Roth P, Eckhardt T, Franz B, Patschull J. H O. Assisted regeneration of diesel particulate traps at typical exhaust gas temperatures. Combust Flame 1998;115:28–37.

[Skjoth-Rasmussen 04] Skjoth-Rasmussen MS, Glarborg P, Ostberg M, Johannessen JT, Livbjerg H, Jensen AD, et al. Formation of polycyclic aromatic of methane in a laminar flow reactor. Combust Flame 2004;136:91-128.

[Skjøth-Rasmussen 04] Skjøth-Rasmussen MS, Glarborg P, Østberg M, Johaneessen JT, Livbjerg H, Jensen AD, Christensen TS. Formation of PAH and Soot in Fuel-Rich Oxidation of Methane in a Laminar Flow Reactor. Combust. Flame 2004;136:91-128.

[Smooke 05] Smooke MD, Long MB, Connelley BC, Colket MB, Hall RJ. Soot Formation in Laminar Diffusion Flames. Combust. Flame 2005;143:613-628.

[Tanzawa 79] Tanzawa T, Gardiner W C. Thermal decomposition of acetylene. Proc. Comb. Inst. 1979;17:563–573.

[Van de Steene 99] Van de Steene L. Thermochimie de la combustion à basses températures de solides pulvérises: application à un charbon, Thèse de l'Institut National Polytechnique de Toulouse 1999.

[Vedal 97] Vedal, S. 1997 Critical Review—Ambient Particles and Health: Linesthat Divide; J. Air & Waste Manage. Assoc. 1997, 47, 551-581.

[Villermaux 93] Villermaux J, Génie de la reaction chimique, conception et fonctionnement des réacteurs. 2e édition Tec & Doc Lavoisier, ISBN 1993; 2-85206-759-5.

[Ziegler 04] Ziegler I. Modélisation cinétique des dépôts de pyrocarbone obtenus par pyrolyse d'hydrocarbures. Thèse, Institut National Polytechnique de Lorraine, Nancy 2004.

GENERAL CONCLUSION

Gasification of biomass is one of the leading near-term options for renewable energy production. When large scale units are considered, bio-oil shows lots of advantages compared to solid biomass. The combination of decentralized fast pyrolysis of biomass followed by transportation and gasification of bio-oil in bio-refinery has attracted great attention.

The overall purpose of this research was to investigate the feasibility of a whole bio-oil non catalytic steam gasification process for the production of high quality syngas in entrained flow reactor.

From a chemical point of view, bio-oil gasification process is quite complex and consists of the following main stages: vaporization, thermal cracking reactions with formation of gas, tars and two solid residues - char and soot – that are considered as undesirable products. This is followed by steam reforming of gas and tars, together with char and soot oxidation. To better understand the process, the first step of gasification (pyrolysis) and thereafter, the whole process (pyrolysis+gasification) were separately studied. The objectives of this work were identified as follows.

- To better understand the pyrolysis step of bio-oil and investigate the effect of operating conditions. A temperature increase from 550°C to 1000°C greatly enhanced the gas yield, whilst solid and liquid yields decreased significantly in agreement with the literature. The heating rate of bio-oil has little impact on the gas yield, but plays a major role on the char yield. Hence the char yield decreases from 11 wt.% with a heating rate of 2°C.s^{-1} down to 1 wt.% for flash heating rate of 2000°C.s^{-1} at a final temperature of 1000°C. At very high heating rate, the final temperature has little influence on the char yield. These results show that for gasification under industrial EFR conditions, the quantity of char is very small. Thus the gasification process mainly consists in gas/tar reforming. Nevertheless, the production of clean syngas will require either complete gasification of char or its removal from the gas produced by the gasifier.
- In steam gasification process, whole bio-oil was successfully steam gasified in EFR. An increase in the reaction temperature over a wide range from 1000°C to 1400°C implies higher

hydrogen yield and higher solid carbon conversion. A thermodynamic equilibrium calculation showed that equilibrium was reached at 1400°C. At this temperature steam reforming of bio-oil leads to yield of equal 84% of theoretical maximum.

- The influence of ash on both bio-oil pyrolysis and gasification has been investigated. In the pyrolysis process, ash greatly increased the yield of solid products and decreased the yield of gaseous products. Liquid yield undergoes no dramatic change. Ash also clearly affects the gas composition. When 3% of ash was added CH_4 and CO yields decrease, while CO_2 yield increases. In gasification process, when ash is added to bio-oil, a strong decrease can be observed in gas yield, although literature results on solid biomass predict an increase. Ash seems to favor polymerization reactions leading to the formation of char, and resulting therefore in a decrease in the gas yield.

- The high temperature gasification of bio-oil in non catalytic processes leads to the formation of soot, which is an undesirable solid product. In the last part of this work, the soot formation and oxidation during bio-oil gasification have been investigated. The temperature of the reaction and the fraction of added steam were tested. Another parameter taken into account here is the amount of oxygen that is necessary when an autothermal process is envisaged. A model is proposed to describe soot formation and oxidation during gasification. It is based on the description of bio-oil heating, devolatilization, reforming of gases and conversion of both char and soot solids. Detailed chemistry is used in the gas phase. Soot production is described by a single reaction based upon C_2H_2 species concentration and one main heterogeneous reaction to describe soot oxidation. Three thermochemical situations were experimented and modeled: the lack of steam, large excess of steam (H2O/C = 8), and in the presence of oxygen in the range O/C = 0.075 to 0.5. The amount of the main gases is very accurately predicted by the model and the prediction of soot yield is correct over a wide range of temperature, water content and O_2 content of the atmosphere. Note that a single set of identified parameters is used for all situations. Hence the model may be a useful tool to support the design of a large scale gasifier.

  This study confirms the strong influence of temperature on the mechanisms of soot formation and oxidation. Emphasis was also made on the effect of soot oxidant agents during experiments. Water in excess causes an almost complete gasification of soot at 1300°C and

1400°C. In the partial oxidation situation, at very low concentrations of O_2, the soot yield undergoes a slight decrease; an increase of O_2 amount greatly reduces the soot yield.

The contribution of each reaction of soot oxidation was identified using the model. CO_2 is shown to reduce only small quantities of soot. O_2 has no contribution to soot oxidation because it is consumed before soot is formed. Nevertheless, O_2 indirectly acts, by consuming C_2H_2 and therefore causes a decrease in the soot production. Only steam oxidizes directly the soot and causes an almost complete oxidation.

Perspectives

Improvements can be made to the model by including an additional reaction involving other soot precursors such as benzene and naphthalene, that are likely to participate.

To better describe the soot formation mechanism it will be interesting to integrate in the model the different phases of the mechanism: particle nucleation, surface growth and particle coagulation.

At the industrial level, the preferred technology for production of syngas in large plants is the autothermal reforming (ATR) technology, which offers the advantage of providing the heat needed for endothermic reforming reactions. Therefore, it will be interesting to use the model for the simulation of the autothermal gasification of bio-oil.

Another point can be explored, which is the impact on the gasification process efficiency of the size of the droplets sprayed into the reactor. In the present work the bio-oil is finely pulverized, i.e. with a droplet mean diameter about 10μm. In order to approach industrial application conditions, it is important to investigate the impact of larger droplets on the effectiveness of the process.

ANNEX: The detailed chemical scheme of gas phase

ELEMENTS CONSIDERED

1.	H	1.00797
2.	O	15.9994
3.	C	12.0112
4.	N	14.0067

SPECIES CONSIDERED

		MOLECULAR WEIGHT	TEMPERATURE LOW	TEMPERATURE HIGH	ELEMENT COUNT H	O	C	N
1.	H	1.00797	300	5000	1	0	0	0
2.	H2	2.01594	300	5000	2	0	0	0
3.	C	12.01115	300	5000	0	0	1	0
4.	CH	13.01912	300	5000	1	0	1	0
5.	CH2	14.02709	300	4000	2	0	1	0
6.	CH2(S)	14.02709	300	4000	2	0	1	0
7.	CH3	15.03506	300	5000	3	0	1	0
8.	O	15.99940	300	5000	0	1	0	0
9.	CH4	16.04303	300	5000	4	0	1	0
10.	OH	17.00737	300	5000	1	1	0	0
11.	H2O	18.01534	300	5000	2	1	0	0
12.	C2H	25.03027	300	4000	1	0	2	0
13.	H2CC	26.03824	200	6000	2	0	2	0
14.	C2H2	26.03824	300	5000	2	0	2	0
15.	C2H3	27.04621	300	4000	3	0	2	0
16.	CO	28.01055	300	5000	0	1	1	0
17.	C2H4	28.05418	300	5000	4	0	2	0
18.	HCO	29.01852	300	5000	1	1	1	0
19.	N2	28.01340	300	5000	0	0	0	2
20.	C2H5	29.06215	300	4000	5	0	2	0
21.	CH2O	30.02649	300	5000	2	1	1	0
22.	C2H6	30.07012	300	4000	6	0	2	0
23.	CH2OH	31.03446	250	4000	3	1	1	0
24.	CH3O	31.03446	300	3000	3	1	1	0
25.	O2	31.99880	300	5000	0	2	0	0
26.	CH3OH	32.04243	300	5000	4	1	1	0
27.	HO2	33.00677	300	5000	1	2	0	0
28.	H2O2	34.01474	300	5000	2	2	0	0
29.	C3H	37.04142	300	5000	1	0	3	0
30.	C3H2	38.04939	150	4000	2	0	3	0
31.	H2CCCH	39.05736	300	4000	3	0	3	0
32.	AR	39.94800	300	5000	0	0	0	0
33.	C2O	40.02170	300	5000	0	1	2	0

34. C3H4	40.06533	300	4000	4	0	3	0
35. C3H4P	40.06533	300	4000	4	0	3	0
36. C3H4C	40.06533	300	5000	4	0	3	0
37. HCCO	41.02967	300	4000	1	1	2	0
38. CH2CHCH2	41.07330	300	4000	5	0	3	0
39. CH3CCH2	41.07330	300	4000	5	0	3	0
40. CH3CHCH	41.07330	300	4000	5	0	3	0
41. CH2CO	42.03764	300	5000	2	1	2	0
42. HCCOH	42.03764	300	4000	2	1	2	0
43. C3H6	42.08127	300	5000	6	0	3	0
44. C2H2OH	43.04561	300	3000	3	1	2	0
45. CH2HCO	43.04561	300	5000	3	1	2	0
46. CH3CO	43.04561	300	5000	3	1	2	0
47. CO2	44.00995	300	5000	0	2	1	0
48. CH3HCO	44.05358	300	5000	4	1	2	0
49. CH3O2	47.03386	200	6000	3	2	1	0
50. CH3OOH	48.04183	200	6000	4	2	1	0
51. C4H	49.05257	300	5000	1	0	4	0
52. C4H2	50.06054	300	5000	2	0	4	0
53. H2CCCCH	51.06851	300	4000	3	0	4	0
54. HCCHCCH	51.06851	300	4000	3	0	4	0
55. CH2CHCCH	52.07648	300	4000	4	0	4	0
56. CH2CHCCH2	53.08445	300	4000	5	0	4	0
57. CH2CHCHCH	53.08445	300	4000	5	0	4	0
58. CH3CCCH2	53.08445	300	3000	5	0	4	0
59. CH2CHCHCH2	54.09242	300	4000	6	0	4	0
60. CH2CCHCH3	54.09242	300	3000	6	0	4	0
61. CH3CCCH3	54.09242	300	3000	6	0	4	0
62. OCHCHO	58.03704	300	3000	2	2	2	0
63. C5H2	62.07169	300	5000	2	0	5	0
64. H2CCCCCH	63.07966	300	4000	3	0	5	0
65. HCCCHCCH	63.07966	300	4000	3	0	5	0
66. C5H5	65.09560	300	4000	5	0	5	0
67. C5H5(L)	65.09560	300	5000	5	0	5	0
68. C5H6	66.10357	300	5000	6	0	5	0
69. H2C4O	66.05994	300	4000	2	1	4	0
70. OC4H6	70.09182	300	5000	6	1	4	0
71. HOC4H6	71.09979	300	5000	7	1	4	0
72. C6H2	74.08284	300	5000	2	0	6	0
73. C6H4	76.09878	300	4000	4	0	6	0
74. C6H5	77.10675	300	4000	5	0	6	0
75. C5H4CH2	78.11472	300	3000	6	0	6	0
76. C6H6	78.11472	300	5000	6	0	6	0
77. C6H7	79.12269	300	2500	7	0	6	0
78. C6H813	80.13066	300	5000	8	0	6	0
79. C6H814	80.13066	300	5000	8	0	6	0
80. C5H4O	80.08703	300	5000	4	1	5	0
81. C5H4OH	81.09500	300	5000	5	1	5	0
82. C5H5O	81.09500	300	5000	5	1	5	0
83. C6H5CH2	91.13384	300	4000	7	0	7	0
84. C6H5CH3	92.14181	300	4000	8	0	7	0
85. C6H5O	93.10615	300	4000	5	1	6	0
86. C6H5OH	94.11412	300	5000	6	1	6	0
87. C6H4C2H	101.12905	300	5000	5	0	8	0
88. C6H5C2H	102.13702	300	4000	6	0	8	0
89. C6H5C2H3	104.15296	300	5000	8	0	8	0
90. CH3C6H4CH2	105.16093	300	5000	9	0	8	0

91.	CH3C6H4CH3	106.16890	300	5000	10	0	8	0
92.	C6H5C2H5	106.16890	300	5000	10	0	8	0
93.	HOC6H4CH3	108.14121	300	5000	8	1	7	0
94.	INDENYL	115.15614	300	5000	7	0	9	0
95.	INDENE	116.16411	300	5000	8	0	9	0
96.	CH3C6H4C2H3	118.18005	300	5000	10	0	9	0
97.	CH3C6H4C2H5	120.19599	300	5000	12	0	9	0
98.	PA2*	127.16729	300	5000	7	0	10	0
99.	SA2*	127.16729	300	5000	7	0	10	0
100.	A2	128.17526	300	5000	8	0	10	0
101.	C6H4C4H4	128.17526	300	5000	8	0	10	0
102.	C6H5C4H4	129.18323	300	5000	9	0	10	0
103.	H2A2*	129.18323	300	5000	9	0	10	0
104.	INDENYLCH3	129.18323	300	5000	9	0	10	0
105.	C6H5C4H5	130.19120	300	5000	10	0	10	0
106.	H2A2	130.19120	300	5000	10	0	10	0
107.	INDENECH3	130.19120	300	5000	10	0	10	0
108.	A2CH2	141.19438	300	5000	9	0	11	0
109.	A2CH3	142.20235	300	5000	10	0	11	0
110.	A2O	143.16669	300	5000	7	1	10	0
111.	A2OH	144.17466	300	5000	8	1	10	0
112.	A2R5*	151.18959	300	5000	7	0	12	0
113.	PA2*C2H*	151.18959	300	5000	7	0	12	0
114.	SA2*C2H*	151.18959	300	5000	7	0	12	0
115.	A2R5	152.19756	300	5000	8	0	12	0
116.	PA2*C2H	152.19756	300	5000	8	0	12	0
117.	SA2*C2H	152.19756	300	3000	8	0	12	0
118.	A2C2H	153.20553	300	5000	9	0	12	0
119.	C6H5C6H4	153.20553	300	5000	9	0	12	0
120.	C6H5C6H5	154.21350	300	5000	10	0	12	0
121.	A2C2H3	154.21350	300	5000	10	0	12	0
122.	HC6H5C6H5	155.22147	300	3000	11	0	12	0
123.	A2C2H5	156.22944	300	5000	12	0	12	0
124.	A2R23*	165.21668	300	5000	9	0	13	0
125.	A1L2A1*	165.21668	300	5000	9	0	13	0
126.	A2R5CH2	165.21668	300	5000	9	0	13	0
127.	A2R23	166.22465	300	5000	10	0	13	0
128.	A2R5CH3	166.22465	300	5000	10	0	13	0
129.	A1L2A1	166.22465	300	5000	10	0	13	0
130.	C6H5CHC6H5	167.23262	300	5000	11	0	13	0
131.	C6H5CH2C6H5	168.24059	300	5000	12	0	13	0
132.	(C2H)A2(C2H)	176.21986	300	3000	8	0	14	0
133.	PA3*	177.22783	300	5000	9	0	14	0
134.	S1A3*	177.22783	300	5000	9	0	14	0
135.	S2A3*	177.22783	300	5000	9	0	14	0
136.	PAL3*	177.22783	300	5000	9	0	14	0
137.	S1AL3*	177.22783	300	5000	9	0	14	0
138.	A3	178.23580	300	5000	10	0	14	0
139.	AL3	178.23580	300	5000	10	0	14	0
140.	A3C5*	189.23899	300	5000	9	0	15	0
141.	A3C5	190.24696	300	5000	10	0	15	0
142.	A3CH2	191.25493	300	5000	11	0	15	0
143.	A3CH3	192.26290	300	5000	12	0	15	0
144.	PA3O	193.22723	300	5000	9	1	14	0
145.	SA3O	193.22723	300	5000	9	1	14	0
146.	PA3OH	194.23520	300	5000	10	1	14	0
147.	SA3OH	194.23520	300	5000	10	1	14	0

148. AL3C2H*	201.25014	300	5000	9	0	16	0
149. A3C2H*	201.25014	300	5000	9	0	16	0
150. A2L2A1*	201.25014	300	5000	9	0	16	0
151. PA4*	201.25014	300	5000	9	0	16	0
152. S1A4*	201.25014	300	5000	9	0	16	0
153. S2A4*	201.25014	300	5000	9	0	16	0
154. AL3C2H	202.25811	300	5000	10	0	16	0
155. A3C2H	202.25811	300	5000	10	0	16	0
156. A3R5	202.25811	300	5000	10	0	16	0
157. A2L2A1	202.25811	300	5000	10	0	16	0
158. A4	202.25811	300	5000	10	0	16	0
159. A3C2H2	203.26608	300	3000	11	0	16	0

REACTIONS CONSIDERED

(k = A T^b exp(-E/RT))

	A	b	E
1. OH+H2<=>H2O+H	2.14E+08	1.5	3449.0
2. O+OH<=>O2+H	2.02E+14	-0.4	0.0
3. O+H2<=>OH+H	5.06E+04	2.7	6290.0
4. H+O2(+M)<=>HO2(+M)	1.50E+12	0.6	0.0
5. H+O2+AR<=>HO2+AR	2.10E+18	-1.0	0.0
6. OH+HO2<=>H2O+O2	1.91E+16	-1.0	0.0
7. H+HO2<=>2OH	1.69E+14	0.0	874.0
8. H+HO2<=>H2+O2	4.28E+13	0.0	1411.0
9. H+HO2<=>O+H2O	3.01E+13	0.0	1721.0
10. O+HO2<=>O2+OH	3.25E+13	0.0	0.0
11. 2OH<=>O+H2O	4.33E+03	2.7	-2485.7
12. 2H+M<=>H2+M	1.00E+18	-1.0	0.0
13. 2H+H2<=>2H2	9.20E+16	-0.6	0.0
14. 2H+H2O<=>H2+H2O	6.00E+19	-1.2	0.0
15. 2H+CO2<=>H2+CO2	5.49E+20	-2.0	0.0
16. H+OH+M<=>H2O+M	2.21E+22	-2.0	0.0
17. H+O+M<=>OH+M	6.20E+16	-0.6	0.0
18. 2O+M<=>O2+M	1.89E+13	0.0	-1788.0
19. 2HO2<=>H2O2+O2	4.22E+14	0.0	11982.0
20. 2HO2<=>H2O2+O2	1.30E+11	0.0	-1629.0
21. H2O2(+M)<=>2OH(+M)	3.00E+14	0.0	48500.0
22. H2O2+H<=>HO2+H2	1.69E+12	0.0	3756.0
23. H2O2+H<=>OH+H2O	1.02E+13	0.0	3576.0
24. H2O2+O<=>OH+HO2	6.62E+11	0.0	3974.0
25. H2O2+OH<=>H2O+HO2	7.83E+12	0.0	1331.0
26. CO+O+M<=>CO2+M	6.17E+14	0.0	3001.0
27. CO+OH<=>CO2+H	1.51E+07	1.3	-758.0
28. CO+O2<=>CO2+O	2.53E+12	0.0	47693.0
29. HO2+CO<=>CO2+OH	5.79E+13	0.0	22944.0
30. CH2O+OH<=>HCO+H2O	3.43E+09	1.2	-447.0
31. CH2O+H<=>HCO+H2	1.30E+08	1.6	2166.0
32. CH2O+M<=>HCO+H+M	3.31E+16	0.0	81000.0
33. CH2O+O<=>HCO+OH	1.80E+13	0.0	3066.0
34. CH2O+CH3<=>HCO+CH4	7.80E-08	6.1	1967.0
35. CH2O+HO2<=>HCO+H2O2	3.01E+12	0.0	13076.0
36. CH2O+O2<=>HCO+HO2	6.03E+13	0.0	40658.1
37. CH2O+H(+M)<=>CH3O(+M)	5.40E+11	0.5	2600.0

38.	CH2O+H(+M)<=>CH2OH(+M)	5.40E+11	0.5	3600.0
39.	CH2OH+H<=>CH3+OH	9.64E+13	0.0	0.0
40.	CH2OH+H<=>CH2O+H2	2.00E+13	0.0	0.0
41.	CH2OH+OH<=>CH2O+H2O	1.00E+13	0.0	0.0
42.	CH2OH+O<=>CH2O+OH	1.00E+13	0.0	0.0
43.	CH2OH+O2<=>CH2O+HO2	1.57E+15	-1.0	0.0
44.	CH2OH+O2<=>CH2O+HO2	7.23E+13	0.0	3577.0
45.	HCO+OH<=>H2O+CO	1.02E+14	0.0	0.0
46.	HCO+M<=>H+CO+M	1.85E+17	-1.0	17000.0
47.	HCO+H<=>CO+H2	1.19E+13	0.2	0.0
48.	HCO+O<=>CO+OH	3.00E+13	0.0	0.0
49.	HCO+O<=>CO2+H	3.00E+13	0.0	0.0
50.	HCO+O2<=>HO2+CO	7.59E+12	0.0	405.0
51.	2CH3(+M)<=>C2H6(+M)	6.77E+16	-1.2	654.0
52.	CH3+H(+M)<=>CH4(+M)	1.39E+16	-0.6	383.0
53.	CH4+O2<=>CH3+HO2	8.00E+13	0.0	56001.0
54.	CH4+H<=>CH3+H2	1.33E+04	3.0	8038.0
55.	CH4+OH<=>CH3+H2O	1.60E+06	2.1	2462.0
56.	CH4+O<=>CH3+OH	1.02E+09	1.5	8605.0
57.	CH4+HO2<=>CH3+H2O2	1.81E+11	0.0	18580.0
58.	CH3+HO2<=>CH3O+OH	8.00E+12	0.0	0.0
59.	CH3+O<=>CH2O+H	8.43E+13	0.0	0.0
60.	CH3+O2<=>CH3O+O	2.95E+13	0.0	30484.0
61.	CH3+O2<=>CH2O+OH	1.85E+12	0.0	20317.0
62.	CH3+O2(+M)<=>CH3O2(+M)	7.83E+08	1.2	0.0
63.	CH3+OH<=>CH2+H2O	7.50E+06	2.0	5000.0
64.	CH3+HCO<=>CH4+CO	1.21E+14	0.0	0.0
65.	CH3+H<=>CH2+H2	9.00E+13	0.0	15100.0
66.	CH3+OH(+M)<=>CH3OH(+M)	2.79E+18	-1.4	1330.0
67.	CH3O+H<=>CH3+OH	1.00E+14	0.0	0.0
68.	CH3O+H<=>CH2O+H2	1.99E+13	0.0	0.0
69.	CH3O+OH<=>CH2O+H2O	1.00E+13	0.0	0.0
70.	CH3O+O<=>CH2O+OH	1.00E+13	0.0	0.0
71.	CH3O+O2<=>CH2O+HO2	6.30E+10	0.0	2605.0
72.	CH3OH+OH<=>CH2OH+H2O	5.30E+04	2.5	960.0
73.	CH3OH+OH<=>CH3O+H2O	1.32E+04	2.5	960.0
74.	CH3OH+O<=>CH2OH+OH	3.88E+05	2.5	3080.0
75.	CH3OH+H<=>CH2OH+H2	1.70E+07	2.1	4868.0
76.	CH3OH+H<=>CH3O+H2	4.24E+06	2.1	4868.0
77.	CH3OH+HO2<=>CH2OH+H2O2	9.64E+10	0.0	12578.0
78.	CH3O2+H<=>CH3O+OH	9.64E+13	0.0	0.0
79.	CH3O2+O<=>CH3O+O2	3.61E+13	0.0	0.0
80.	CH3O2+OH<=>CH3OH+O2	6.03E+13	0.0	0.0
81.	CH3O2+HO2<=>CH3OOH+O2	2.47E+11	0.0	-1570.0
82.	CH3O2+H2O2<=>CH3OOH+HO2	2.41E+12	0.0	9936.0
83.	CH3O2+CH2O<=>CH3OOH+HCO	1.99E+12	0.0	11665.0
84.	CH3O2+CH4<=>CH3OOH+CH3	1.81E+11	0.0	18481.0
85.	CH3O2+CH3<=>2CH3O	2.41E+13	0.0	0.0
86.	CH3O2+CH3O<=>CH2O+CH3OOH	3.01E+11	0.0	0.0
87.	CH3O2+CH2OH<=>CH2O+CH3OOH	1.21E+13	0.0	0.0
88.	CH3O2+CH3OH<=>CH3OOH+CH2OH	1.81E+12	0.0	13712.0
89.	2CH3O2<=>2CH3O+O2	1.00E+11	0.0	300.0
90.	2CH3O2<=>CH3OH+CH2O+O2	4.00E+09	0.0	-2210.0
91.	CH3OOH<=>CH3O+OH	6.31E+14	0.0	42304.0
92.	CH3OOH+H<=>CH3O2+H2	8.80E+10	0.0	1860.0
93.	CH3OOH+H<=>CH3O+H2O	8.20E+10	0.0	1860.0
94.	CH3OOH+O<=>CH3O2+OH	1.00E+12	0.0	3000.0

95.	CH3OOH+OH<=>CH3O2+H2O	1.80E+12	0.0	-378.0
96.	C+O2<=>CO+O	1.99E+13	0.0	0.0
97.	C+OH<=>CO+H	5.00E+13	0.0	0.0
98.	C+CH3<=>C2H2+H	5.00E+13	0.0	0.0
99.	C+CH2<=>C2H+H	5.00E+13	0.0	0.0
100.	CH+O2<=>HCO+O	3.30E+13	0.0	0.0
101.	CH+O<=>CO+H	5.73E+13	0.0	0.0
102.	CH+OH<=>HCO+H	3.00E+13	0.0	0.0
103.	CH+OH<=>C+H2O	4.00E+07	2.0	3000.0
104.	CH+CO2<=>HCO+CO	3.44E+12	0.0	686.0
105.	CH+H<=>C+H2	1.50E+14	0.0	0.0
106.	CH+H2O<=>CH2O+H	5.71E+12	0.0	-755.0
107.	CH+CH2O<=>CH2CO+H	9.64E+13	0.0	-517.0
108.	CH+C2H2<=>C3H2+H	1.00E+14	0.0	0.0
109.	CH+CH2<=>C2H2+H	4.00E+13	0.0	0.0
110.	CH+CH3<=>C2H3+H	3.00E+13	0.0	0.0
111.	CH+CH4<=>C2H4+H	6.03E+13	0.0	0.0
112.	CH2+H<=>CH+H2	1.00E+18	-1.6	0.0
113.	CH2+OH<=>CH+H2O	1.13E+07	2.0	3000.0
114.	CH2+OH<=>CH2O+H	2.50E+13	0.0	0.0
115.	CH2+CO2<=>CH2O+CO	1.10E+11	0.0	1000.0
116.	CH2+O<=>CO+2H	5.00E+13	0.0	0.0
117.	CH2+O<=>CO+H2	3.00E+13	0.0	0.0
118.	CH2+O2<=>CO+H2O	2.24E+22	-3.3	2867.0
119.	CH2+O2<=>CO2+2H	3.29E+21	-3.3	2867.0
120.	CH2+O2<=>CH2O+O	3.29E+21	-3.3	2867.0
121.	CH2+O2<=>CO2+H2	2.63E+21	-3.3	2867.0
122.	CH2+O2<=>CO+OH+H	1.65E+21	-3.3	2867.0
123.	CH2+CH4<=>2CH3	4.30E+12	0.0	10039.0
124.	2CH2<=>C2H2+2H	4.00E+13	0.0	0.0
125.	CH2+HCCO<=>C2H3+CO	3.00E+13	0.0	0.0
126.	CH2+CH3<=>C2H4+H	4.00E+13	0.0	0.0
127.	CH2+C2H2<=>H2CCCH+H	1.20E+13	0.0	6621.0
128.	CH2(S)+M<=>CH2+M	1.00E+13	0.0	0.0
129.	CH2(S)+H<=>CH2+H	2.00E+14	0.0	0.0
130.	CH2(S)+H2O<=>CH2+H2O	3.00E+13	0.0	0.0
131.	CH2(S)+C2H2<=>CH2+C2H2	4.00E+13	0.0	0.0
132.	CH2(S)+N2<=>CH2+N2	1.26E+13	0.0	430.0
133.	CH2(S)+AR<=>CH2+AR	1.45E+13	0.0	884.0
134.	CH2(S)+C6H6<=>CH2+C6H6	7.00E+13	0.0	0.0
135.	CH2(S)+CH4<=>2CH3	4.30E+13	0.0	0.0
136.	CH2(S)+C2H6<=>CH3+C2H5	1.20E+14	0.0	0.0
137.	CH2(S)+O2<=>CO+OH+H	7.00E+13	0.0	0.0
138.	CH2(S)+H2<=>CH3+H	7.00E+13	0.0	0.0
139.	CH2(S)+H2O<=>CH3+OH	3.01E+15	-0.6	0.0
140.	CH2(S)+O<=>CO+2H	3.00E+13	0.0	0.0
141.	CH2(S)+OH<=>CH2O+H	3.00E+13	0.0	0.0
142.	CH2(S)+H<=>CH+H2	3.00E+13	0.0	0.0
143.	CH2(S)+CO2<=>CH2O+CO	3.00E+12	0.0	0.0
144.	CH2(S)+CH3<=>C2H4+H	2.00E+13	0.0	0.0
145.	CH2(S)+CH2CO<=>C2H4+CO	1.60E+14	0.0	0.0
146.	CH2(S)+C2H2<=>H2CCCH+H	1.80E+14	0.0	0.0
147.	CH2(S)+C6H6<=>C6H5+CH3	1.70E+14	0.0	0.0
148.	C2H6+CH3<=>C2H5+CH4	5.50E-01	4.0	8295.0
149.	C2H6+H<=>C2H5+H2	5.41E+02	3.5	5210.0
150.	C2H6+O<=>C2H5+OH	3.00E+07	2.0	5115.0
151.	C2H6+OH<=>C2H5+H2O	7.22E+06	2.0	864.0

152.	C2H6+O2<=>C2H5+HO2	5.00E+13	0.0	55000.1
153.	C2H6+HO2<=>C2H5+H2O2	1.32E+13	0.0	20468.0
154.	C2H5+H<=>2CH3	4.89E+12	0.3	0.0
155.	C2H5+H(+M)<=>C2H6(+M)	5.20E+17	-1.0	1580.0
156.	C2H5+O2<=>C2H4+HO2	1.02E+10	0.0	-2186.0
157.	C2H5+O<=>CH3+CH2O	4.20E+13	0.0	0.0
158.	C2H5+O<=>CH3HCO+H	5.30E+13	0.0	0.0
159.	C2H5+O<=>C2H4+OH	3.00E+13	0.0	0.0
160.	C2H5+OH<=>C2H4+H2O	2.42E+13	0.0	0.0
161.	C2H5+HCO<=>C2H6+CO	1.21E+14	0.0	0.0
162.	C2H5+CH2O<=>C2H6+HCO	5.50E+03	2.8	5862.0
163.	C2H5+CH3<=>C2H4+CH4	1.15E+12	0.0	0.0
164.	2C2H5<=>C2H6+C2H4	1.45E+12	0.0	0.0
165.	C2H4+H<=>C2H3+H2	5.42E+14	0.0	14902.0
166.	C2H4+O<=>CH3+HCO	8.10E+06	1.9	180.0
167.	C2H4+O<=>CH2HCO+H	4.70E+06	1.9	180.0
168.	C2H4+O<=>CH2CO+H2	6.80E+05	1.9	180.0
169.	C2H4+OH<=>C2H3+H2O	2.02E+13	0.0	5936.0
170.	C2H4+O2<=>CH2HCO+OH	2.00E+08	1.5	39000.1
171.	C2H4+HO2<=>CH3HCO+OH	2.20E+12	0.0	17200.0
172.	C2H4+CH3<=>C2H3+CH4	5.01E+11	0.0	15057.0
173.	C2H4+H(+M)<=>C2H5(+M)	1.08E+12	0.5	1822.0
174.	C2H4+M=C2H2+H2+M	3.49E+16	0.0	71539.0
175.	C2H3+O2=C2H2+HO2	1.34E+06	1.6	-383.5
176.	C2H3+C2H3=C2H4+C2H2	6.30E+13	0.0	0.0
177.	C2H3+H(+M)<=>C2H4(+M)	6.10E+12	0.3	280.0
178.	C2H3+H<=>C2H2+H2	4.00E+13	0.0	0.0
179.	C2H3+O<=>CH2CO+H	3.00E+13	0.0	0.0
180.	C2H3+O2<=>CH2O+HCO	4.57E+16	-1.4	1013.0
181.	C2H3+O2<=>CH2HCO+O	3.03E+11	-0.3	10.7
182.	C2H3+OH<=>C2H2+H2O	2.00E+13	0.0	0.0
183.	C2H3+CH2<=>C3H4+H	3.00E+13	0.0	0.0
184.	C2H3+C2H<=>2C2H2	3.00E+13	0.0	0.0
185.	C2H3+C2H<=>H2CCCCH+H	3.00E+13	0.0	0.0
186.	C2H3+CH3<=>C2H2+CH4	2.05E+13	0.0	0.0
187.	C2H3+CH2O<=>C2H4+HCO	5.43E+03	2.8	5862.0
188.	C2H3+HCO<=>C2H4+CO	9.04E+13	0.0	0.0
189.	C2H3+CH<=>CH2+C2H2	5.00E+13	0.0	0.0
190.	2C2H3<=>CH2CHCCH2+H	9.00E+12	0.0	0.0
191.	2C2H3<=>H2CCCH+CH3	1.80E+13	0.0	0.0
192.	C2H2+O<=>CH2+CO	6.10E+06	2.0	1900.0
193.	C2H2+O<=>HCCO+H	1.43E+07	2.0	1900.0
194.	C2H2+O<=>C2H+OH	3.16E+15	-0.6	15000.0
195.	C2H2+H(+M)<=>C2H3(+M)	3.11E+11	0.6	2589.0
196.	C2H2+OH<=>C2H+H2O	3.37E+07	2.0	14000.0
197.	C2H2+OH<=>HCCOH+H	5.04E+05	2.3	13500.0
198.	C2H2+OH<=>CH3+CO	4.83E-04	4.0	-2000.0
199.	C2H2+OH<=>CH2CO+H	2.18E-04	4.5	-1000.0
200.	C2H+CH4<=>CH3+C2H2	7.23E+12	0.0	976.0
201.	C2H2+O2<=>HCO+HCO	4.00E+07	1.5	30100.0
202.	H+C2H(+M)<=>C2H2(+M)	1.00E+17	-1.0	0.0
203.	C2H2+HO2<=>CH2O+HCO	1.00E+12	0.0	10000.0
204.	H2CC+C2H2(+M)<=>CH2CHCCH(+M)	3.50E+05	2.1	-2400.0
205.	H2CC+C2H4<=>CH2CHCHCH2	1.00E+12	0.0	0.0
206.	H2CC+O2<=>2HCO	1.00E+13	0.0	0.0
207.	C2H+H2<=>C2H2+H	4.10E+05	2.4	864.3
208.	C2H+O2<=>2CO+H	2.52E+13	0.0	0.0

209.	C2H+C2H2<=>C4H2+H	2.47E+12	0.5	-391.0
210.	HCCOH+H<=>HCCO+H2	3.00E+07	2.0	1000.0
211.	HCCOH+OH<=>HCCO+H2O	1.00E+07	2.0	1000.0
212.	HCCOH+O<=>HCCO+OH	2.00E+07	3.0	1900.0
213.	C2H2OH+H<=>CH2HCO+H	5.00E+13	0.0	0.0
214.	C2H2OH+O<=>OCHCHO+H	5.00E+13	0.0	0.0
215.	C2H2OH+O2<=>OCHCHO+OH	1.00E+12	0.0	5000.0
216.	CH2HCO+H<=>CH3+HCO	1.00E+14	0.0	0.0
217.	CH2HCO+H<=>CH3CO+H	3.00E+13	0.0	0.0
218.	CH2HCO+O<=>CH2O+HCO	5.00E+13	0.0	0.0
219.	CH2HCO+OH<=>CH2CO+H2O	2.00E+13	0.0	0.0
220.	CH2HCO+OH<=>CH2OH+HCO	1.00E+13	0.0	0.0
221.	CH2HCO+CH3<=>C2H5+HCO	5.00E+13	0.0	0.0
222.	CH2HCO+CH2<=>C2H4+HCO	5.00E+13	0.0	0.0
223.	CH2HCO+CH<=>C2H3+HCO	1.00E+14	0.0	0.0
224.	CH2HCO+O2<=>OH+OCHCHO	2.22E+11	0.0	1500.0
225.	CH2HCO+M<=>CH3+CO+M	2.00E+16	0.0	42000.1
226.	OCHCHO+M<=>2HCO+M	1.00E+17	0.0	58000.1
227.	OCHCHO+H<=>CH2O+HCO	3.00E+13	0.0	0.0
228.	CH3HCO+OH<=>CH3CO+H2O	2.35E+10	0.7	-1113.0
229.	CH3HCO+H<=>CH3CO+H2	4.08E+09	1.2	2409.0
230.	CH3HCO+CH3<=>CH3CO+CH4	2.00E-06	5.6	2464.0
231.	CH3HCO<=>CH3+HCO	7.10E+15	0.0	81280.0
232.	CH3HCO+O<=>CH3CO+OH	5.80E+12	0.0	1800.0
233.	CH3HCO+O2<=>CH3CO+HO2	3.00E+13	0.0	39000.1
234.	CH3HCO+HO2<=>CH3CO+H2O2	3.00E+12	0.0	12000.0
235.	CH2+CO(+M)<=>CH2CO(+M)	8.10E+11	0.5	4510.0
236.	CH2CO+O<=>CO2+CH2	1.76E+12	0.0	1349.0
237.	CH2CO+H<=>CH3+CO	5.93E+06	2.0	1300.0
238.	CH2CO+H<=>HCCO+H2	3.00E+07	2.0	10000.0
239.	CH2CO+O<=>HCCO+OH	2.00E+07	2.0	10000.0
240.	CH2CO+OH<=>HCCO+H2O	1.00E+07	2.0	3000.0
241.	CH2CO+OH<=>CH2OH+CO	7.20E+12	0.0	0.0
242.	CH2CO+OH<=>CH3+CO2	3.00E+12	0.0	0.0
243.	CH3CO(+M)<=>CH3+CO(+M)	2.80E+13	0.0	17150.0
244.	CH3CO+H<=>CH3+HCO	2.10E+13	0.0	0.0
245.	CH3CO+H<=>CH2CO+H2	1.20E+13	0.0	0.0
246.	CH3CO+O<=>CH3+CO2	1.50E+14	0.0	0.0
247.	CH3CO+O<=>CH2CO+OH	4.00E+13	0.0	0.0
248.	CH3CO+OH<=>CH2CO+H2O	1.20E+13	0.0	0.0
249.	CH+CO(+M)<=>HCCO(+M)	5.00E+13	0.0	0.0
250.	HCCO+C2H2<=>H2CCCH+CO	1.00E+11	0.0	3000.0
251.	HCCO+H<=>CH2(S)+CO	1.21E+14	0.0	0.0
252.	HCCO+O<=>H+2CO	1.00E+14	0.0	0.0
253.	HCCO+O2<=>CO2+CO+H	1.40E+07	1.7	1000.0
254.	HCCO+O2<=>2CO+OH	2.88E+07	1.7	1000.0
255.	HCCO+OH<=>C2O+H2O	6.00E+13	0.0	0.0
256.	HCCO+CH<=>C2H2+CO	5.00E+13	0.0	0.0
257.	2HCCO<=>C2H2+2CO	1.00E+13	0.0	0.0
258.	C2O+H<=>CH+CO	1.00E+13	0.0	0.0
259.	C2O+O<=>2CO	5.00E+13	0.0	0.0
260.	C2O+OH<=>2CO+H	2.00E+13	0.0	0.0
261.	C2O+O2<=>2CO+O	2.00E+13	0.0	0.0
262.	C2H3+CH3<=>C3H6	4.46E+56	-13.0	13865.0
263.	C3H6<=>C2H2+CH4	2.50E+12	0.0	70000.0
264.	C3H6<=>C3H4+H2	3.00E+13	0.0	80000.0
265.	CH2CHCH2+H<=>C3H6	1.88E+26	-3.6	5468.0

266.	C3H6+HO2<=>CH2CHCH2+H2O2	9.64E+03	2.6	13910.0
267.	C3H6+OH+O2<=>CH3HCO+CH2O+OH	3.00E+10	0.0	-8280.0
268.	C3H6+OH<=>CH2CHCH2+H2O	3.12E+06	2.0	-298.0
269.	C3H6+OH<=>CH3CCH2+H2O	1.11E+06	2.0	1451.0
270.	C3H6+OH<=>CH3CHCH+H2O	2.11E+06	2.0	2778.0
271.	C3H6+O<=>C2H5+HCO	1.58E+07	1.8	-1216.0
272.	C3H6+O<=>CH2CHCH2+OH	5.24E+11	0.7	5884.0
273.	C3H6+O<=>CH3CHCH+OH	1.20E+11	0.7	8959.0
274.	C3H6+O<=>CH3CCH2+OH	6.03E+10	0.7	7632.0
275.	C3H6+H<=>C2H4+CH3	7.23E+12	0.0	1302.0
276.	C3H6+H<=>CH2CHCH2+H2	1.73E+05	2.5	2492.0
277.	C3H6+H<=>CH3CCH2+H2	4.09E+05	2.5	9794.0
278.	C3H6+H<=>CH3CHCH+H2	8.04E+05	2.5	12284.0
279.	C3H6+CH3<=>CH2CHCH2+CH4	2.22E+00	3.5	5675.0
280.	C3H6+CH3<=>CH3CCH2+CH4	8.43E-01	3.5	11656.0
281.	C3H6+CH3<=>CH3CHCH+CH4	1.35E+00	3.5	12848.0
282.	C3H6+HCO<=>CH2CHCH2+CH2O	1.08E+07	1.9	17010.0
283.	C3H6+C2H3<=>CH2CHCHCH2+CH3	7.23E+11	0.0	5000.0
284.	CH2(S)+C2H4<=>CH2CHCH2+H	1.30E+14	0.0	0.0
285.	C2H3+CH3<=>CH2CHCH2+H	4.73E+02	3.7	5677.0
286.	CH3CHCH+H<=>C3H6	1.00E+14	0.0	0.0
287.	CH3CHCH+HO2<=>C3H6+O2	2.00E+12	0.0	0.0
288.	CH3CHCH+O2<=>CH3HCO+HCO	1.09E+23	-3.3	3892.0
289.	CH3CHCH+H<=>C3H4P+H2	2.00E+13	0.0	0.0
290.	CH3CHCH+OH<=>C3H4P+H2O	1.00E+13	0.0	0.0
291.	CH3CHCH+H<=>CH2CHCH2+H	1.00E+14	0.0	0.0
292.	CH3CCH2+HO2<=>C3H6+O2	1.00E+12	0.0	0.0
293.	CH3CCH2+H<=>C3H6	5.00E+13	0.0	0.0
294.	CH3CCH2+H<=>CH2CHCH2+H	1.00E+14	0.0	0.0
295.	CH3CCH2+O2<=>CH3CO+CH2O	1.09E+22	-3.3	3892.0
296.	CH3CCH2+O<=>CH2CO+CH3	1.00E+14	0.0	0.0
297.	CH3CCH2+H<=>C3H4P+H2	4.00E+13	0.0	0.0
298.	CH3CCH2+OH<=>C3H4P+H2O	2.00E+13	0.0	0.0
299.	CH3CCH2+CH3<=>C3H4P+CH4	1.00E+11	0.0	0.0
300.	CH2CHCH2+HO2<=>C3H6+O2	3.00E+12	0.0	0.0
301.	CH2CHCH2+O2<=>C3H4+HO2	4.99E+15	-1.4	22428.0
302.	CH2CHCH2+O2<=>CH2HCO+CH2O	1.06E+10	0.3	12838.0
303.	CH2CHCH2+O2<=>C2H2+CH2O+OH	2.78E+25	-4.8	15468.0
304.	CH2CHCH2+OH<=>C3H4+H2O	1.00E+13	0.0	0.0
305.	CH2CHCH2+H<=>C3H4+H2	5.00E+13	0.0	0.0
306.	CH2CHCH2+CH3<=>C3H4+CH4	3.02E+12	-0.3	-131.0
307.	2CH2CHCH2<=>C3H6+C3H4	1.02E+13	0.0	0.0
308.	CH3+C2H2<=>C3H4+H	5.14E+09	0.9	22153.0
309.	C3H4+H<=>C3H4P+H	1.00E+13	0.0	5000.0
310.	C3H4+H<=>H2CCCH+H2	3.00E+07	2.0	5000.0
311.	C3H4+OH<=>H2CCCH+H2O	2.00E+07	2.0	1000.0
312.	C3H4P+H<=>H2CCCH+H2	3.00E+07	2.0	5000.0
313.	C3H4P+H<=>CH3+C2H2	1.00E+14	0.0	4000.0
314.	C3H4P+OH<=>H2CCCH+H2O	2.00E+07	2.0	1000.0
315.	C3H4P+H(+M)<=>CH3CCH2(+M)	6.50E+12	0.0	2000.0
316.	C3H4+H(+M)<=>CH2CHCH2(+M)	1.20E+11	0.7	3007.0
317.	C3H4+H(+M)<=>CH3CCH2(+M)	8.49E+12	0.0	2000.0
318.	C3H4C<=>C3H4	1.51E+14	0.0	50400.0
319.	C3H4C<=>C3H4P	1.20E+15	0.0	43730.0
320.	C3H4+O<=>C2H4+CO	2.00E+07	1.8	1000.0
321.	C3H4+CH3<=>H2CCCH+CH4	1.30E+12	0.0	7700.0
322.	C3H4P+O<=>HCCO+CH3	2.04E+13	0.0	2250.0

323.	C3H4P+O<=>C2H4+CO	5.80E+12	0.0	2250.0
324.	C3H4P+CH3<=>H2CCCH+CH4	1.80E+12	0.0	7700.0
325.	H2CCCH+H(+M)<=>C3H4(+M)	1.00E+17	-0.8	315.0
326.	H2CCCH+H(+M)<=>C3H4P(+M)	1.00E+17	-0.8	315.0
327.	H2CCCH+O2<=>CH2CO+HCO	3.00E+10	0.0	2868.0
328.	H2CCCH+O<=>CH2O+C2H	1.40E+14	0.0	0.0
329.	H2CCCH+H<=>C3H2+H2	5.00E+13	0.0	1000.0
330.	H2CCCH+OH<=>C3H2+H2O	2.00E+13	0.0	0.0
331.	H2CCCH+CH2<=>CH2CHCCH+H	4.00E+13	0.0	0.0
332.	H2CCCH+CH<=>HCCHCCH+H	7.00E+13	0.0	0.0
333.	H2CCCH+CH<=>H2CCCCH+H	7.00E+13	0.0	0.0
334.	2H2CCCH<=>C6H5+H	5.00E+12	0.0	0.0
335.	2H2CCCH<=>C5H4CH2	4.50E+12	0.0	0.0
336.	2H2CCCH<=>HCCCHCCH+CH3	5.00E+11	0.0	0.0
337.	H2CCCH+CH2CHCH2<=>C5H4CH2+2H	5.56E+20	-2.5	1692.0
338.	H2CCCH+C2H3<=>C5H5+H	9.63E+40	-7.8	28820.0
339.	H2CCCH+C2H2<=>C5H5	7.39E+53	-12.5	57313.1
340.	H2CCCH+C2H2<=>C5H5(L)	5.62E+32	-7.3	6758.0
341.	H2CCCH+HO2<=>C3H4+O2	9.00E+11	0.0	0.0
342.	H2CCCH+HO2<=>C3H4P+O2	1.10E+12	0.0	0.0
343.	C3H2+O2<=>HCCO+CO+H	2.00E+12	0.0	1000.0
344.	C3H2+O<=>C2H2+CO	1.00E+14	0.0	0.0
345.	C3H2+OH<=>C2H2+HCO	5.00E+13	0.0	0.0
346.	C3H2+CH2<=>H2CCCCH+H	3.00E+13	0.0	0.0
347.	C3H2+CH3<=>CH2CHCCH+H	2.00E+13	0.0	0.0
348.	C3H2+C2H2<=>HCCCHCCH+H	5.00E+12	0.0	5000.0
349.	C3H2+H2CCCH<=>C6H4+H	1.00E+13	0.0	0.0
350.	C3H2+HCCO<=>HCCHCCH+CO	3.00E+13	0.0	0.0
351.	C3H2+CH2(S)<=>H2CCCCH+H	5.00E+13	0.0	0.0
352.	C3H2+H<=>C3H+H2	1.00E+13	0.0	0.0
353.	C3H+O2<=>HCCO+CO	1.00E+13	0.0	0.0
354.	C3H+O<=>C2H+CO	1.00E+13	0.0	0.0
355.	H2C4O+OH<=>C2H2+CO+HCO	1.00E+13	0.0	0.0
356.	C4H2+OH<=>H2C4O+H	6.66E+12	0.0	-410.0
357.	C4H2+CH2<=>H2CCCCCH+H	1.30E+13	0.0	4326.0
358.	C4H2+CH2(S)<=>H2CCCCCH+H	3.00E+13	0.0	0.0
359.	C4H2+CH<=>C5H2+H	1.00E+14	0.0	0.0
360.	C4H2+O<=>C3H2+CO	1.20E+12	0.0	0.0
361.	C4H2+OH<=>C4H+H2O	1.00E+07	2.0	1000.0
362.	C4H2+H<=>C4H+H2	2.00E+07	2.0	2000.0
363.	C4H2+C2H<=>C6H2+H	4.00E+13	0.0	0.0
364.	C4H+O2<=>2CO+C2H	1.20E+12	0.0	0.0
365.	HCCHCCH+H<=>H2CCCCH+H	1.00E+14	0.0	0.0
366.	HCCHCCH+C2H2<=>C6H5	1.67E+10	0.4	7719.3
367.	HCCHCCH(+M)<=>C4H2+H(+M)	1.00E+14	0.0	36000.0
368.	H2CCCCH(+M)<=>C4H2+H(+M)	1.00E+14	0.0	55000.1
369.	HCCHCCH+C2H3<=>C5H4CH2	4.00E+12	0.0	0.0
370.	HCCHCCH+C2H3<=>C6H5+H	1.60E+13	0.0	0.0
371.	HCCHCCH+C2H3<=>C4H2+C2H4	1.00E+12	0.0	5000.0
372.	HCCHCCH+C2H3<=>CH2CHCCH+C2H2	2.00E+12	0.0	5000.0
373.	H2CCCCH+O2<=>CH2CO+HCCO	1.00E+12	0.0	0.0
374.	H2CCCCH+OH<=>C4H2+H2O	3.00E+13	0.0	0.0
375.	H2CCCCH+O<=>CH2CO+C2H	2.00E+13	0.0	0.0
376.	H2CCCCH+O<=>H2C4O+H	2.00E+13	0.0	0.0
377.	H2CCCCH+H<=>C4H2+H2	5.00E+13	0.0	0.0
378.	H2CCCCH+CH2<=>C3H4+C2H	2.00E+13	0.0	0.0
379.	H2CCCCH+C2H3<=>C5H4CH2	1.00E+13	0.0	0.0

380.	H2CCCCH+C2H3<=>C6H5+H	6.00E+12	0.0	0.0
381.	H2CCCCH+C2H3<=>2H2CCCH	4.00E+12	0.0	0.0
382.	H2CCCCH+C2H3<=>C4H2+C2H4	1.00E+12	0.0	5000.0
383.	H2CCCCH+C2H3<=>CH2CHCCH+C2H2	2.00E+12	0.0	5000.0
384.	C2H4+C2H<=>CH2CHCCH+H	1.20E+13	0.0	0.0
385.	C2H3+C2H2<=>CH2CHCCH+H	2.00E+12	0.0	5000.0
386.	CH2CHCCH+OH<=>H2CCCCH+H2O	1.00E+07	2.0	2000.0
387.	CH2CHCCH+H<=>H2CCCCH+H2	3.00E+07	2.0	5000.0
388.	CH2CHCCH+OH<=>HCCHCCH+H2O	7.50E+06	2.0	5000.0
389.	CH2CHCCH+H<=>HCCHCCH+H2	2.00E+07	2.0	15000.0
390.	CH2CHCCH+H2CCCH<=>C6H5CH2	9.25E+11	-1.3	-14295.0
391.	2CH2CHCCH<=>C6H5C2H3	5.47E+40	-8.0	51241.1
392.	CH2CHCCH2+H<=>CH3+H2CCCH	1.00E+14	0.0	0.0
393.	CH2CHCCH2+OH<=>CH2CHCCH+H2O	3.00E+13	0.0	0.0
394.	CH2CHCCH2(+M)<=>CH2CHCCH+H(+M)	1.00E+14	0.0	50000.0
395.	CH2CHCCH2+C2H<=>C5H4CH2	1.00E+13	0.0	0.0
396.	CH2CHCCH2+C2H<=>C6H5+H	6.00E+12	0.0	0.0
397.	CH2CHCCH2+C2H<=>2H2CCCH	4.00E+12	0.0	0.0
398.	CH2CHCCH2+C2H<=>CH2CHCCH+C2H2	3.00E+12	0.0	5000.0
399.	CH2CHCHCH+OH<=>CH2CHCCH+H2O	2.00E+07	2.0	1000.0
400.	CH2CHCHCH+H<=>CH2CHCCH+H2	3.00E+07	2.0	1000.0
401.	CH2CHCHCH+H<=>CH2CHCCH2+H	1.00E+14	0.0	0.0
402.	CH2CHCHCH(+M)<=>CH2CHCCH+H(+M)	1.00E+14	0.0	37000.0
403.	CH2CHCHCH+CO<=>C5H5O	6.11E-01	1.9	31067.0
404.	CH2CHCHCH+C2H2<=>C6H6+H	8.21E+08	0.8	6348.0
405.	CH2CHCHCH+C2H<=>C5H4CH2	4.00E+12	0.0	0.0
406.	CH2CHCHCH+C2H<=>C6H5+H	1.60E+13	0.0	0.0
407.	CH2CHCHCH+C2H<=>CH2CHCCH+C2H2	3.00E+12	0.0	5000.0
408.	CH2CHCHCH+C2H2<=>C6H7	1.96E+19	-3.4	4910.0
409.	CH2CHCHCH+C2H3<=>C6H813	5.50E+15	-1.7	1470.0
410.	CH2CHCHCH+C4H2<=>C6H5C2H+H	3.16E+11	0.0	1800.0
411.	CH2CHCHCH+C3H4<=>C6H5CH3+H	2.00E+11	0.0	3700.0
412.	CH2CHCHCH+C3H4P<=>C6H5CH3+H	3.16E+11	0.0	3700.0
413.	CH2CHCHCH+CH2CHCCH<=>C6H5C2H3+H	3.16E+11	0.0	600.0
414.	CH3CCCH2<=>CH2CHCCH2	1.50E+67	-16.9	59100.1
415.	CH3CCCH2+HO2<=>OH+C2H2+CH3CO	8.00E+11	0.0	0.0
416.	CH3CCCH2+O2<=>CH3CO+CH2CO	2.16E+10	0.0	2500.0
417.	CH2CHCHCH2+O2=CH2CHCCH2+HO2	1.40E+13	0.0	50600.0
418.	CH2CHCHCH2+HO2<=>CH2CHCHCH+H2O2	2.00E+11	0.0	12600.0
419.	CH2CHCHCH2+HO2<=>CH2CHCCH2+H2O2	1.00E+11	0.0	9920.0
420.	C2H3+C2H4<=>CH2CHCHCH2+H	5.00E+11	0.0	7304.0
421.	2C2H3<=>CH2CHCHCH2	7.23E+13	0.0	0.0
422.	CH2CHCHCH2+H<=>C3H4P+CH3	2.00E+12	0.0	7000.0
423.	CH2CHCHCH2+H<=>C3H4+CH3	2.00E+12	0.0	7000.0
424.	CH2CHCHCH2+O<=>HCO+CH2CHCH2	6.02E+08	1.4	-858.0
425.	CH2CHCHCH2<=>CH2CHCCH2+H	5.70E+36	-6.3	112353.2
426.	CH2CHCHCH2+CH3<=>CH2CHCCH2+CH4	1.00E+14	0.0	19800.0
427.	CH2CHCHCH2+C2H3<=>CH2CHCCH2+C2H4	2.50E+13	0.0	19800.0
428.	CH2CHCHCH2+CH2CHCH2<=>CH2CHCCH2+C3H6	5.00E+12	0.0	19500.0
429.	CH2CHCHCH2+CH3<=>CH2CHCHCH+CH4	2.00E+14	0.0	22800.0
430.	CH2CHCHCH2+C2H3<=>CH2CHCHCH+C2H4	5.00E+13	0.0	22800.0
431.	CH2CHCHCH2+H2CCCH<=>CH2CHCHCH+C3H4	1.00E+13	0.0	22500.0
432.	CH2CHCHCH2+CH2CHCH2<=>CH2CHCHCH+C3H6	1.00E+13	0.0	22500.0
433.	CH2CHCHCH2<=>CH2CHCCH+H2	2.50E+15	0.0	94700.1
434.	CH2CHCHCH2+C2H3<=>C6H813+H	1.14E+12	-0.2	9920.0
435.	CH2CHCHCH2+C2H3<=>C6H814+H	1.14E+12	-0.2	9920.0
436.	CH2CHCHCH2+C2H2<=>C6H814	2.30E+12	0.0	35000.0

437.	CH2CHCHCH2+H<=>CH2CHCCH2+H2	5.00E+15	0.0	22800.0
438.	CH2CHCHCH2+O<=>CH2CHCCH2+OH	4.53E+15	-0.5	7028.0
439.	CH2CHCHCH2+OH<=>CH2CHCCH2+H2O	1.74E+06	2.0	3744.0
440.	CH2CHCHCH2<=>CH2CHCHCH+H	1.58E+16	0.0	110000.0
441.	CH2CHCHCH2+H<=>CH2CHCHCH+H2	5.00E+15	0.0	22800.0
442.	CH2CHCHCH2+O<=>CH2CHCHCH+OH	2.27E+15	-0.5	7028.0
443.	CH2CHCHCH2+OH<=>CH2CHCHCH+H2O	2.29E+07	2.0	7253.0
444.	H2CCCH+CH3(+M)<=>CH2CCHCH3(+M)	1.50E+12	0.0	0.0
445.	CH2CCHCH3+H<=>CH2CHCHCH2+H	2.00E+13	0.0	4000.0
446.	CH2CCHCH3+CH3<=>CH2CHCCH2+CH4	7.00E+13	0.0	18500.0
447.	CH2CCHCH3+O<=>CH2CO+C2H4	1.20E+08	1.6	327.0
448.	CH2CCHCH3+OH<=>CH2CHCCH2+H2O	3.10E+06	2.0	-298.0
449.	CH2CCHCH3<=>CH2CHCHCH2	3.00E+13	0.0	65000.1
450.	CH3CCCH3+H<=>CH3+C3H4P	2.60E+05	2.5	1000.0
451.	CH2CHCHCH2+OH<=>HOC4H6	3.50E+12	0.0	-994.0
452.	HOC4H6=>OC4H6+H	5.00E+14	0.0	28000.0
453.	CH2CHCHCH2+O<=>OC4H6	1.40E+13	0.0	80.0
454.	OC4H6<=>C3H6+CO	2.00E+13	0.0	57000.0
455.	OC4H6<=>C2H4+CH2CO	1.00E+16	0.0	73000.0
456.	OC4H6+OH<=>CH2CO+C2H3+H2O	2.03E+13	0.0	5955.0
457.	C5H6+HO2<=>C5H5+H2O2	1.99E+12	0.0	11660.0
458.	C5H6+O2<=>C5H5+HO2	2.00E+13	0.0	37000.0
459.	C5H6+O2<=>C5H5O+OH	1.00E+13	0.0	20712.0
460.	C5H6+O<=>C5H5+OH	1.81E+13	0.0	3080.0
461.	C5H6+OH<=>C5H5+H2O	3.43E+09	1.2	-447.0
462.	C5H6+H<=>C5H5+H2	2.19E+08	1.8	3000.0
463.	C5H6+H<=>CH2CHCH2+C2H2	1.00E+13	0.0	12000.0
464.	C5H5+H<=>C5H6	2.92E+29	-4.7	6148.0
465.	C5H5<=>C5H5(L)	4.09E+47	-10.4	54874.1
466.	C5H5+O<=>CH2CHCHCH+CO	1.00E+14	0.0	0.0
467.	C5H5+HO2<=>C5H5O+OH	3.00E+13	0.0	0.0
468.	C5H5+O<=>C5H5O	1.24E+25	-3.7	4763.0
469.	C5H5+O<=>C5H4O+H	1.00E+14	0.0	0.0
470.	C5H5+OH<=>C5H4OH+H	3.00E+13	0.0	0.0
471.	C5H5+CH3<=>C6H7+H	2.44E+41	-8.0	39259.1
472.	C5H5+C2H2<=>C6H5CH2	1.73E+17	-1.9	10231.0
473.	2C5H5<=>A2+2H	2.00E+12	0.0	4000.0
474.	C5H4O+H<=>C5H4OH	5.27E+27	-4.2	10863.0
475.	C5H4O<=>CO+2C2H2	1.00E+15	0.0	78000.1
476.	H2CCCCCH+H<=>C5H2+H2	1.00E+13	0.0	0.0
477.	H2CCCCCH+CH3<=>C5H4CH2	1.40E+13	0.0	0.0
478.	H2CCCCCH+CH3<=>C6H5+H	6.00E+12	0.0	0.0
479.	H2CCCCCH+CH3<=>C5H2+CH4	3.00E+12	0.0	5000.0
480.	HCCCHCCH+H<=>C5H2+H2	1.00E+13	0.0	0.0
481.	HCCCHCCH+H<=>H2CCCCCH+H	1.00E+13	0.0	0.0
482.	HCCCHCCH+CH3<=>C5H4CH2	1.00E+13	0.0	0.0
483.	HCCCHCCH+CH3<=>C6H5+H	1.00E+13	0.0	0.0
484.	HCCCHCCH+CH3<=>C5H2+CH4	3.00E+12	0.0	5000.0
485.	C6H5+H<=>C6H6	5.00E+13	0.0	0.0
486.	C6H5+H<=>C6H4+H2	2.00E+07	2.0	1000.0
487.	C6H5+OH<=>C6H4+H2O	1.00E+07	2.0	1000.0
488.	C6H5+O<=>C5H5+CO	9.00E+13	0.0	0.0
489.	C6H5+O2<=>C6H5O+O	2.60E+13	0.0	6120.0
490.	C6H5+O2<=>C6H5O+O	3.00E+13	0.0	8981.0
491.	C6H5+C2H2<=>C6H5C2H+H	2.47E+06	1.8	2289.0
492.	C6H5+C2H<=>C6H5C2H	2.54E+17	-1.5	1541.0
493.	C6H5+C4H2<=>C6H5C2H+C2H	2.00E+13	0.0	0.0

494.	C6H5+CH2CHCCH<=>C6H5C2H+C2H3	3.20E+11	0.0	1350.0
495.	C6H5+CH3<=>C6H5CH3	2.00E+22	-3.0	2304.0
496.	C6H5+OH<=>C6H5O+H	5.00E+13	0.0	0.0
497.	C6H5+CH3<=>C6H5CH2+H	5.00E+13	0.0	0.0
498.	C6H5+C2H3<=>C6H5C2H3	2.67E+19	-2.1	2187.0
499.	C6H5+CH2CHCCH<=>C6H5C2H3+C2H	3.20E+11	0.0	1900.0
500.	C6H5+CH2CHCHCH2<=>C6H5C2H3+C2H3	3.20E+11	0.0	1900.0
501.	C6H5+HCCHCCH<=>A2	2.22E+43	-9.1	14810.0
502.	C6H5+HCCHCCH<=>PA2*+H	1.36E+22	-2.3	18485.0
503.	C6H6+H<=>C6H5+H2	3.00E+07	2.0	8000.0
504.	C6H6+OH<=>C6H5+H2O	7.50E+06	2.0	5000.0
505.	C6H6+O<=>C6H5+OH	2.40E+13	0.0	4700.0
506.	C6H6+C2H<=>C6H5C2H+H	1.00E+12	0.0	0.0
507.	C6H5O<=>C5H5+CO	7.40E+11	0.0	43853.1
508.	C6H5O+H<=>C5H6+CO	1.06E+42	-7.6	35349.0
509.	C6H5O+CH3<=>HOC6H4CH3	1.00E+12	0.0	0.0
510.	C5H4CH2<=>C6H6	7.59E+13	0.0	73853.1
511.	C5H4CH2+H<=>C6H6+H	3.00E+12	0.5	2000.0
512.	C6H7<=>C6H6+H	6.64E+46	-11.1	34478.0
513.	C6H7+H<=>C6H6+H2	1.00E+13	0.0	0.0
514.	C6H7+C6H5<=>2C6H6	1.00E+12	0.0	0.0
515.	2C6H7<=>C6H813+C6H6	2.82E+13	0.0	0.0
516.	2C6H7<=>C6H814+C6H6	1.39E+13	0.0	0.0
517.	C6H813<=>C6H7+H	2.42E+59	-13.3	96147.1
518.	C6H813+O2<=>C6H7+HO2	8.13E+11	0.0	24840.0
519.	C6H813<=>C6H6+H2	4.39E+37	-7.3	71949.1
520.	C6H814<=>C6H7+H	1.21E+59	-13.3	96147.1
521.	C6H814+H<=>C6H7+H2	4.00E+13	0.0	3000.0
522.	C6H814<=>C6H6+H2	1.28E+28	-4.9	49309.1
523.	C6H5C2H+H<=>C6H4C2H+H2	2.50E+14	0.0	16000.0
524.	C6H5C2H+OH<=>C6H4C2H+H2O	2.10E+13	0.0	4600.0
525.	C6H5C2H+CH3<=>C6H4C2H+CH4	1.67E+12	0.0	15057.0
526.	C6H4C2H+C2H2<=>SA2*	3.98E+13	0.0	10100.0
527.	C6H5CH2+H<=>C6H5CH3	4.81E+20	-2.1	1986.0
528.	C6H5CH2+C6H5OH<=>C6H5CH3+C6H5O	1.05E+11	0.0	9500.0
529.	C6H5CH2+OH<=>C6H5O+CH3	2.33E+59	-13.0	35964.0
530.	C6H5CH2+HO2<=>C6H5+CH2O+OH	5.00E+12	0.0	0.0
531.	C6H5CH2+CH3<=>C6H5C2H5	2.10E+37	-7.4	12269.0
532.	C6H5CH2+CH3<=>C6H5C2H3+H2	4.68E+24	-3.2	27018.0
533.	C6H5CH2+C2H2<=>INDENE+H	3.20E+11	0.0	7000.0
534.	C6H5CH2+H2CCCH<=>A2+2H	6.03E+11	0.0	0.0
535.	C6H5CH3+O2<=>C6H5CH2+HO2	3.00E+14	0.0	41400.1
536.	C6H5CH3+OH<=>C6H5CH2+H2O	1.26E+13	0.0	2583.0
537.	C6H5CH3+H<=>C6H5CH2+H2	1.20E+14	0.0	8235.0
538.	C6H5CH3+H<=>C6H6+CH3	1.20E+13	0.0	5148.0
539.	C6H5CH3+CH3<=>C6H5CH2+CH4	3.16E+11	0.0	9500.0
540.	C6H5CH3+C2H3<=>C6H5CH2+C2H4	3.98E+12	0.0	8000.0
541.	C6H5CH3+C6H5<=>C6H5CH2+C6H6	2.10E+12	0.0	4400.0
542.	HOC6H4CH3+H<=>C6H5CH3+OH	2.21E+13	0.0	7910.0
543.	HOC6H4CH3+H<=>C6H5OH+CH3	1.20E+13	0.0	5148.0
544.	C6H5C2H5<=>C6H5C2H3+H2	5.01E+12	0.0	64000.1
545.	C6H5C2H5+H<=>C6H6+C2H5	1.20E+13	0.0	5100.0
546.	C6H5C2H5+H<=>C6H5C2H3+H2+H	8.00E+13	0.0	8235.0
547.	C6H5C2H5+OH<=>C6H5C2H3+H2O+H	8.34E+12	0.0	2583.0
548.	C6H5C2H5+O2<=>C6H5C2H3+HO2+H	2.00E+14	0.0	41400.1
549.	C6H5C2H3+H<=>C6H5C2H+H2+H	6.92E+14	0.0	14500.0
550.	SA2*+O2<=>A2O+O	1.00E+13	0.0	0.0

551.	SA2*+OH<=>A2O+H	5.00E+13	0.0	0.0
552.	SA2*+H<=>A2	1.00E+14	0.0	0.0
553.	PA2*+O2<=>A2O+O	1.00E+13	0.0	0.0
554.	PA2*+OH<=>A2O+H	5.00E+13	0.0	0.0
555.	PA2*+H<=>A2	1.00E+14	0.0	0.0
556.	A2O<=>INDENYL+CO	7.40E+11	0.0	43850.0
557.	A2O+H<=>A2OH	2.53E+14	0.0	0.0
558.	A2OH+H<=>A2O+H2	1.15E+14	0.0	12400.0
559.	A2OH+H<=>A2+OH	2.23E+13	0.0	7929.0
560.	A2OH+OH<=>A2O+H2O	6.00E+12	0.0	0.0
561.	INDENE+H<=>INDENYL+H2	2.19E+08	1.8	3000.0
562.	INDENE+OH<=>INDENYL+H2O	3.43E+09	1.2	-447.0
563.	INDENE+O<=>INDENYL+OH	1.81E+13	0.0	3080.0
564.	INDENYL+H<=>INDENE	2.00E+14	0.0	0.0
565.	A2+H<=>PA2*+H2	2.50E+14	0.0	16000.0
566.	A2+H<=>SA2*+H2	2.50E+14	0.0	16000.0
567.	A2+OH<=>PA2*+H2O	2.10E+13	0.0	4600.0
568.	A2+OH<=>SA2*+H2O	2.10E+13	0.0	4600.0
569.	A2+C2H<=>PA2*+C2H2	5.00E+13	0.0	16000.0
570.	A2+C2H<=>SA2*+C2H2	5.00E+13	0.0	16000.0
571.	A2+C2H3<=>PA2*+C2H4	5.00E+13	0.0	16000.0
572.	A2+C2H3<=>SA2*+C2H4	5.00E+13	0.0	16000.0
573.	CH3CCCH2+CH3CCCH2<=>CH3C6H4CH2+H	1.00E+08	0.0	0.0
574.	CH3C6H4CH3+OH<=>CH3C6H4CH2+H2O	2.95E+13	0.0	2623.0
575.	CH3C6H4CH3+O<=>CH3C6H4CH2+OH	5.00E+08	1.5	8000.0
576.	CH3C6H4CH3+H<=>CH3C6H4CH2+H2	3.98E+02	3.4	3120.0
577.	CH3C6H4CH2+C2H2<=>H2A2+H	3.20E+11	0.0	7000.0
578.	CH3C6H4CH2+C2H2<=>INDENECH3+H	3.20E+11	0.0	7000.0
579.	CH3C6H4CH2+H<=>CH3C6H4CH3	7.46E+13	0.0	78.0
580.	CH3C6H4CH2+CH3<=>CH3C6H4C2H5	6.00E+12	0.0	221.0
581.	CH3C6H4C2H5+OH<=>CH3C6H4C2H3+H2O+H	8.43E+12	0.0	2583.0
582.	CH3C6H4C2H5+H<=>CH3C6H4C2H3+H2+H	8.00E+13	0.0	8235.0
583.	CH3C6H4C2H3+OH<=>INDENE+H+H2O	1.26E+13	0.0	2583.0
584.	CH3C6H4C2H3+H<=>INDENE+H+H2	3.98E+02	3.4	3120.0
585.	C6H5CH2+H2CCCH<=>C6H5C4H4+H	2.00E+12	0.0	0.0
586.	C6H5C4H5+OH<=>C6H5C4H4+H2O	5.00E+06	2.0	0.0
587.	C6H5C4H5+O<=>C6H5C4H4+OH	7.00E+11	0.7	6000.0
588.	C6H5C4H5+H<=>C6H5C4H4+H2	2.00E+05	2.5	2500.0
589.	C6H5C4H4+H<=>C6H5C4H5	1.00E+14	0.0	0.0
590.	C6H4C4H4+H<=>C6H5C4H4	2.00E+13	0.0	1500.0
591.	C6H4C4H4+H<=>A2+H	3.00E+12	0.5	0.0
592.	C6H4C4H4<=>A2	5.00E+37	-7.4	76979.0
593.	H2A2+OH<=>H2A2*+H2O	5.00E+06	2.0	0.0
594.	H2A2+O<=>H2A2*+OH	7.00E+11	0.7	6000.0
595.	H2A2+H<=>H2A2*+H2	2.00E+05	2.5	2500.0
596.	H2A2*+H<=>H2A2	1.00E+14	0.0	0.0
597.	A2+H<=>H2A2*	5.00E+14	0.0	5000.0
598.	INDENECH3+OH<=>INDENYLCH3+H2O	3.43E+09	1.2	-447.0
599.	INDENECH3+O<=>INDENYLCH3+OH	1.81E+13	0.0	3080.0
600.	INDENECH3+H<=>INDENYLCH3+H2	2.19E+08	1.8	3000.0
601.	INDENECH3+H<=>INDENE+CH3	1.20E+13	0.0	5200.0
602.	INDENYLCH3+H<=>INDENECH3	2.00E+14	0.0	0.0
603.	INDENYLCH3+C5H5<=>A3CH3+2H	1.00E+13	0.0	8000.0
604.	PA2*+CH3<=>A2CH3	5.00E+12	0.0	0.0
605.	PA2*+CH3<=>A2CH2+H	5.00E+12	0.0	0.0
606.	SA2*+CH3<=>A2CH3	5.00E+12	0.0	0.0
607.	SA2*+CH3<=>A2CH2+H	5.00E+12	0.0	0.0

608.	A2CH3+OH<=>A2CH2+H2O	1.27E+13	0.0	2583.0
609.	A2CH3+O<=>A2CH2+OH	5.00E+08	1.5	8000.0
610.	A2CH3+H<=>A2CH2+H2	3.98E+02	3.4	3120.0
611.	A2CH3+H<=>A2+CH3	1.20E+13	0.0	5148.0
612.	A2CH2+O<=>PA2*+CH2O	1.00E+14	0.0	0.0
613.	A2CH2+CH3<=>A2C2H5	1.19E+13	0.0	221.0
614.	A2CH2+H<=>A2CH3	1.00E+14	0.0	0.0
615.	A2CH2+HO2<=>PA2*+CH2O+OH	1.00E+13	0.0	0.0
616.	SA2*+C2H2<=>A2R5+H	3.98E+13	0.0	10100.0
617.	A2R5+H<=>A2R5*+H2	2.50E+14	0.0	16000.0
618.	A2R5+OH<=>A2R5*+H2O	2.10E+13	0.0	4600.0
619.	A2R5*+CH3<=>A2R5CH2+H	5.00E+13	0.0	0.0
620.	A2R5CH2+H<=>A2R5CH3	1.00E+14	0.0	0.0
621.	A2R5CH3+H<=>A2R5+CH3	1.20E+13	0.0	5148.0
622.	A2R5*+H(+M)<=>A2R5(+M)	1.00E+14	0.0	0.0
623.	A2C2H3+OH<=>A2C2H+H2O	1.00E+07	2.0	2000.0
624.	A2C2H3+H<=>A2C2H+H2	2.00E+07	2.0	6000.0
625.	A2C2H5+H<=>A2C2H3+H2+H	8.00E+13	0.0	8235.0
626.	A2C2H5+OH<=>A2C2H3+H2O+H	8.44E+12	0.0	2583.0
627.	PA2*+C2H2<=>PA2*C2H+H	3.98E+13	0.0	10100.0
628.	PA2*C2H+H<=>SA2*C2H*+H2	2.50E+14	0.0	16000.0
629.	PA2*C2H+H<=>PA2*C2H*+H2	2.50E+14	0.0	16000.0
630.	PA2*C2H+OH<=>SA2*C2H*+H2O	2.10E+13	0.0	4600.0
631.	PA2*C2H+OH<=>PA2*C2H*+H2O	2.10E+13	0.0	4600.0
632.	A2+C2H<=>PA2*C2H+H	5.00E+13	0.0	0.0
633.	A2+C2H<=>SA2*C2H+H	5.00E+13	0.0	0.0
634.	PA2*+C2H2<=>A2C2H	1.70E+43	-9.1	21100.0
635.	PA2*C2H+H<=>A2C2H	5.90E+46	-10.0	19100.0
636.	A2C2H+H<=>PA2*C2H+H2	1.50E+13	0.0	0.0
637.	A2C2H+OH<=>PA2*C2H+H2O	2.50E+12	0.0	0.0
638.	SA2*C2H+H<=>SA2*C2H*+H2	2.50E+14	0.0	16000.0
639.	SA2*C2H+OH<=>SA2*C2H*+H2O	1.60E+08	1.4	1450.0
640.	SA2*C2H*+H(+M)<=>SA2*C2H(+M)	1.00E+14	0.0	0.0
641.	PA2*C2H*+H(+M)<=>PA2*C2H(+M)	1.00E+14	0.0	0.0
642.	PA2*C2H*+C2H2<=>S1A3*	5.50E+61	-14.6	33100.0
643.	PA2*C2H*+C2H2<=>S2A3*	5.50E+61	-14.6	33100.0
644.	PA2*C2H+OH<=>PA2*+CH2CO	2.18E-04	4.5	-1000.0
645.	SA2*C2H+OH<=>SA2*+CH2CO	2.18E-04	4.5	-1000.0
646.	PA2*C2H+OH<=>C6H5C2H+H2C4O+H	1.30E+13	0.0	10600.0
647.	SA2*C2H+OH<=>C6H5C2H+H2C4O+H	1.30E+13	0.0	10600.0
648.	A3+OH<=>SA2*C2H+CH2CO+H	6.50E+12	0.0	10600.0
649.	A3+OH<=>PA2*C2H+CH2CO+H	6.50E+12	0.0	10600.0
650.	PA2*C2H+O<=>HCCO+PA2*	2.04E+07	2.0	1900.0
651.	SA2*C2H+O<=>HCCO+SA2*	2.04E+07	2.0	1900.0
652.	A3+O<=>PA2*C2H+CH2CO	1.10E+13	0.0	4530.0
653.	A3+O<=>SA2*C2H+CH2CO	1.10E+13	0.0	4530.0
654.	PA2*C2H*+O2<=>PA2*+CO+CO	2.10E+12	0.0	7470.0
655.	SA2*C2H*+O2<=>SA2*+CO+CO	2.10E+12	0.0	7470.0
656.	S1A3*+O2<=>SA2*C2H+HCO+CO	6.05E+11	0.0	7470.0
657.	S2A3*+O2<=>SA2*C2H+HCO+CO	6.05E+11	0.0	7470.0
658.	PA3*+O2<=>PA2*C2H+HCO+CO	2.10E+12	0.0	7470.0
659.	C6H5+C6H5<=>C6H5C6H5	5.00E+12	0.0	0.0
660.	C6H5+C6H6<=>C6H5C6H5+H	4.00E+11	0.0	4000.0
661.	C6H6+C6H5<=>HC6H5C6H5	3.70E+32	-6.7	9870.0
662.	C6H5+C6H5<=>C6H5C6H4+H	2.30E-01	4.6	28950.0
663.	C6H5C6H5+H<=>C6H5C6H4+H2	2.50E+14	0.0	16000.0
664.	C6H5C6H5+OH<=>C6H5C6H4+H2O	2.10E+13	0.0	4600.0

665.	C6H5C6H4+C2H2<=>A3+H	3.98E+13	0.0	10100.0
666.	HC6H5C6H5<=>C6H5C6H5+H	3.80E+37	-8.0	27880.0
667.	C6H5C6H5<=>C6H5C6H4+H	1.10E+25	-2.7	114270.0
668.	C6H6+C6H5CH2<=>C6H5CH2C6H5+H	1.20E+12	0.0	15940.0
669.	C6H5+C6H5CH2<=>C6H5CH2C6H5	2.00E+22	-3.0	2304.0
670.	C6H5CH2C6H5+H<=>C6H5CHC6H5+H2	2.50E+14	0.0	16000.0
671.	C6H5CH2C6H5+OH<=>C6H5CHC6H5+H2O	2.10E+13	0.0	4600.0
672.	A2CH2+C2H2<=>A2R23+H	3.20E+11	0.0	7000.0
673.	A2R23*+H<=>A2R23	2.00E+14	0.0	0.0
674.	A2R23+OH<=>A2R23*+H2O	3.43E+09	1.2	-447.0
675.	A2R23+O<=>A2R23*+OH	1.81E+13	0.0	3080.0
676.	A2R23+H<=>A2R23*+H2	2.19E+08	1.8	3000.0
677.	PA3O<=>A2R23*+CO	7.40E+11	0.0	43850.0
678.	C6H5CHC6H5<=>A1L2A1+H	4.00E+11	0.0	4000.0
679.	A1L2A1+OH<=>A1L2A1*+H2O	3.43E+09	1.2	-447.0
680.	A1L2A1+O<=>A1L2A1*+OH	1.81E+13	0.0	3080.0
681.	A1L2A1+H<=>A1L2A1*+H2	2.19E+08	1.8	3000.0
682.	A1L2A1*+H<=>A1L2A1	2.00E+14	0.0	0.0
683.	SA3O<=>A1L2A1*+CO	7.40E+11	0.0	43850.0
684.	PA2*C2H*+C2H2<=>(C2H)A2(C2H)+H	1.80E+19	-1.7	18800.0
685.	SA2*C2H*+C2H2<=>(C2H)A2(C2H)+H	1.80E+19	-1.7	18800.0
686.	(C2H)A2(C2H)+H<=>PA3*	6.90E+63	-14.6	29900.0
687.	(C2H)A2(C2H)+H<=>S1A3*	6.90E+63	-14.6	29900.0
688.	PA2*C2H+C2H<=>(C2H)A2(C2H)+H	5.00E+13	0.0	0.0
689.	SA2*C2H+C2H<=>(C2H)A2(C2H)+H	5.00E+13	0.0	0.0
690.	AL3<=>A3	8.00E+12	0.0	65000.0
691.	PA2*C2H*+C2H2<=>S1AL3*	3.98E+13	0.0	10100.0
692.	S1AL3*+H<=>AL3	5.00E+13	0.0	0.0
693.	AL3+H<=>S1AL3*+H2	2.50E+14	0.0	16000.0
694.	AL3+OH<=>S1AL3*+H2O	2.10E+13	0.0	4600.0
695.	AL3+H<=>PAL3*+H2	2.50E+14	0.0	16000.0
696.	AL3+OH<=>PAL3*+H2O	2.10E+13	0.0	4600.0
697.	PAL3*+H<=>AL3	5.00E+13	0.0	0.0
698.	INDENYL+C5H5<=>A3+2H	1.00E+13	0.0	8000.0
699.	SA2*C2H*+C2H2<=>S1A3*	3.98E+13	0.0	10100.0
700.	S1A3*+H<=>A3	5.00E+13	0.0	0.0
701.	A3+OH<=>PA3*+H2O	2.10E+13	0.0	4600.0
702.	A3+OH<=>S1A3*+H2O	2.10E+13	0.0	4600.0
703.	A3+OH<=>S2A3*+H2O	2.10E+13	0.0	4600.0
704.	A3+H<=>PA3*+H2	2.50E+14	0.0	16000.0
705.	A3+H<=>S1A3*+H2	2.50E+14	0.0	16000.0
706.	A3+H<=>S2A3*+H2	2.50E+14	0.0	16000.0
707.	PA3*+H(+M)<=>A3(+M)	1.00E+14	0.0	0.0
708.	S1A3*+H(+M)<=>A3(+M)	1.00E+14	0.0	0.0
709.	S2A3*+H(+M)<=>A3(+M)	1.00E+14	0.0	0.0
710.	PA2*+CH2CHCCH<=>A3+H	3.30E+33	-5.7	25500.0
711.	SA2*+CH2CHCCH<=>A3+H	3.30E+33	-5.7	25500.0
712.	C6H4C2H+C6H6<=>A3+H	1.10E+23	-2.9	15890.0
713.	C6H5+C6H5C2H<=>A3+H	1.10E+23	-2.9	15890.0
714.	PA3*+CH3<=>A3C5+H+H	5.00E+13	0.0	0.0
715.	A3CH3+OH<=>A3C5+H2O+H	1.27E+13	0.0	2583.0
716.	A3CH3+H<=>A3C5+H2+H	3.98E+02	3.4	3120.0
717.	A3C5+OH<=>A3C5*+H2O	3.43E+09	1.2	-447.0
718.	A3C5+O<=>A3C5*+OH	1.81E+13	0.0	3080.0
719.	A3C5+H<=>A3C5*+H2	2.19E+08	1.8	3000.0
720.	A3C5*+H<=>A3C5	2.00E+14	0.0	0.0
721.	S2A3*+CH3<=>A3CH2+H	5.00E+13	0.0	0.0

722.	A3CH2+H<=>A3CH3	1.00E+14	0.0	0.0
723.	A3CH3+H<=>A3CH2+H2	1.20E+14	0.0	8235.0
724.	A3CH3+H<=>A3+CH3	1.20E+13	0.0	5148.0
725.	A3CH3+OH<=>A3CH2+H2O	1.26E+13	0.0	2583.0
726.	A3CH2<=>A3C5+H	1.20E+12	0.0	15940.0
727.	A3+OH<=>PA3OH+H	9.00E+12	0.0	10592.0
728.	A3+OH<=>SA3OH+H	9.00E+12	0.0	10592.0
729.	PA3*+O2<=>PA3O+O	1.00E+13	0.0	0.0
730.	S1A3*+O2<=>SA3O+O	1.00E+13	0.0	0.0
731.	PA3OH+OH<=>PA3O+H2O	2.95E+06	2.0	-1310.0
732.	PA3OH+H<=>PA3O+H2	1.59E+13	0.0	6100.0
733.	PA3O+H<=>PA3OH	1.00E+14	0.0	0.0
734.	SA3OH+OH<=>SA3O+H2O	2.95E+06	2.0	-1310.0
735.	SA3OH+H<=>SA3O+H2	1.59E+13	0.0	6100.0
736.	SA3O+H<=>SA3OH	1.00E+14	0.0	0.0
737.	PA3*+C2H2<=>A3C2H+H	3.98E+13	0.0	10100.0
738.	A3C2H+H<=>A3C2H*+H2	2.50E+14	0.0	16000.0
739.	A3C2H+OH<=>A3C2H*+H2O	2.10E+13	0.0	4600.0
740.	PAL3*+C2H2<=>AL3C2H+H	3.98E+13	0.0	10100.0
741.	AL3C2H+H<=>AL3C2H*+H2	2.50E+14	0.0	16000.0
742.	AL3C2H+OH<=>AL3C2H*+H2O	2.10E+13	0.0	4600.0
743.	A3+C2H<=>A3C2H+H	5.00E+13	0.0	0.0
744.	S2A3*+C2H2<=>A3C2H2	8.00E+61	-14.5	34800.0
745.	S2A3*+C2H2<=>A3C2H+H	1.20E+26	-3.4	30200.0
746.	A3C2H+H<=>A3C2H2	1.90E+64	-15.1	29300.0
747.	A3C2H+OH<=>PA2*C2H+H2C4O+H	6.50E+12	0.0	10600.0
748.	A3C2H+OH<=>SA2*C2H+H2C4O+H	6.50E+12	0.0	10600.0
749.	A3C2H+O<=>PA2*C2H+H2C4O	1.10E+13	0.0	4530.0
750.	A3C2H+O<=>SA2*C2H+H2C4O	1.10E+13	0.0	4530.0
751.	A3C2H+OH<=>S2A3*+CH2CO	2.11E-04	4.5	-1000.0
752.	SA2*+C6H5<=>A2L2A1+2H	5.00E+12	0.0	0.0
753.	SA2*+C6H6<=>A2L2A1+H+H2	4.00E+11	0.0	4000.0
754.	A2L2A1+H<=>A2L2A1*+H2	2.50E+14	0.0	16000.0
755.	A2L2A1+OH<=>A2L2A1*+H2O	2.10E+13	0.0	4600.0
756.	S1A3*+C2H2<=>A3R5+H	3.98E+13	0.0	10100.0
757.	A3R5<=>A2L2A1	8.51E+12	0.0	62860.0
758.	S2A3*+C2H2<=>A4+H	3.98E+13	0.0	10100.0
759.	A4+H<=>PA4*+H2	2.50E+14	0.0	16000.0
760.	A4+H<=>S1A4*+H2	2.50E+14	0.0	16000.0
761.	A4+H<=>S2A4*+H2	2.50E+14	0.0	16000.0
762.	A4+OH<=>PA4*+H2O	2.10E+13	0.0	4600.0
763.	A4+OH<=>S1A4*+H2O	2.10E+13	0.0	4600.0
764.	A4+OH<=>S2A4*+H2O	2.10E+13	0.0	4600.0
765.	A4+OH<=>S1A3*+CH2CO	1.30E+13	0.0	10600.0
766.	A4+OH<=>S2A3*+CH2CO	1.30E+13	0.0	10600.0
767.	A4+O<=>S1A3*+HCCO	2.20E+13	0.0	4530.0
768.	A4+O<=>S2A3*+HCCO	2.20E+13	0.0	4530.0
769.	S1A4*+O2<=>S2A3*+2CO	2.10E+12	0.0	7470.0
770.	S2A4*+O2<=>S2A3*+2CO	2.10E+12	0.0	7470.0
771.	A3C2H+H<=>A4+H	9.00E+38	-7.4	20700.0
772.	A3C2H2<=>A4+H	2.00E+63	-15.3	43200.0
773.	C6H5C2H+C6H4C2H<=>A4+H	1.10E+23	-2.9	15890.0